U.PORTO

DOUTORAMENTO

BIOLOGIA MOLECULAR E CELULAR

Regulation of the KtrAB cation channel

Celso Duarte

D

2021

U.PORTO

Celso Duarte. Regulation of the KtrAB cation channel

Regulation of the KtrAB cation channel

Celso Moura Teixeira Duarte

D.ICBAS **2021**

SEDE ADMINISTRATIVA

INSTITUTO DE CIÊNCIAS BIOMÉDICAS ABEL SALAZAR

FACULDADE DE CIÊNCIAS

Celso Moura Teixeira Duarte

Regulation of the KtrAB cation channel

Tese de Candidatura ao grau de Doutor em Biologia Molecular e Celular;

Programa Doutoral da Universidade do Porto (Instituto de Ciências Biomédicas de Abel Salazar e Faculdade de Ciências)

Orientador – Doutor João Morais Cabral

Categoria – Investigador Principal

Afiliação – Instituto de Biologia Molecular e Celular

FUNDING

In this work, I was financed by a PhD Fellowship from FCT - Fundação para a Ciência e a Tecnologia (SFRH/BD/123761/2016). The work was also supported by FLAD- Fundação Luso-Americana para o Desenvolvimento through FLAD Life Science 2020, by FEDER - Fundo Europeu de Desenvolvimento Regional funds through COMPETE 2020 - Operational Program for Competitiveness and Internationalization (POCI), Portugal 2020, and by Portuguese funds through FCT - Fundação para a Ciência e a Tecnologia/ Ministério da Ciência, Tecnologia e Inovação in the framework of the project "Institute for Research and Innovation in Health Sciences" (POCI-01-0145-FEDER-007274) and project FCOMP-01-0124-FEDER-028115 (PTDC/BBB-BEP/2017/2012), and by the National Institutes of Health - NS081320.

Para a minha mãe,

ACKNOWLEDGEMENTS

First I would like to express my utmost gratitude to my supervisor João Morais Cabral. Thank you for nurturing my development as a scientist and for opening my horizons. For the support with funding and for providing me with strong foundations with your training and discussions. For the many opportunities to improve, including going to international meetings. For always lending a helping hand and for all the emotional support. Thank you for trusting in me every step of the way, even in my first plane trip, and for all the advice and encouragement. I could not have asked for a better mentor.

I am especially grateful to Carol for playing a vital role in my growth as a scientist and as a person throughout all these years. I will always value all the training and meaningful discussions. Thank you for always being available for a chat, for making it easy to work in the lab and for helping me to uncomplicate situations with a practical approach.

I would like to thank everyone that worked with me in the Structural Biochemistry group during these years. You provided a great environment with all the companionship and leisure moments outside of the lab. I treasure all of you and will leave with very fond memories.

To all my other friends and colleagues from the institute, thank you for your support and fun moments.

I am thankful to Rita for all the training, advice and especially for our friendship. Thank you for all the support, even in the toughest times. Your cheerfulness, unwavering commitment and contagious motivation were vital to propel me forward.

I thank Tatiana for the friendship and all the support and encouragement. Thank you for understanding my struggles, always cheering me up and for all the fun leisure moments that I will always cherish.

To my long-time friends, thank you for the love, unwavering friendship, support and understanding over the years. For giving me strength, cheering me up and always adjusting to my crazy schedules. You made my path easier.

I thank my family for all the unconditional love and support.

To my mother, thank you for all the effort that allowed me to reach this stage, the unconditional love, care, support, guidance and always being there for me.

CONTENTS

PUBLICATION LIST

Teixeira-Duarte, C. M., Fonseca, F., & Morais-Cabral, J. H. (2019). Activation of a nucleotide-dependent RCK domain requires binding of a cation cofactor to a conserved site. eLife, 8, e50661. https://doi.org/10.7554/eLife.50661

Rocha, R., Teixeira-Duarte, C. M., Jorge, J. M. P., & Morais-Cabral, J. H. (2019). Characterization of the molecular properties of KtrC, a second RCK domain that regulates a Ktr channel in Bacillus subtilis. J Struct Biol, 205(3), 34-43. https://doi.org/10.1016/j.jsb.2019.02.002

ABBREVIATIONS

ACMA - 9-amino-6-chloro-2-methoxyacridine
ADA - N-(2-acetamide)iminodiacetic acid
ADP - Adenosine diphosphate
AMP - Adenosine monophosphate
AMS - Ammonium sulphate
ANTS - 8-aminonaphthalene-1,3,6-trisulfonic acid
ATP - Adenosine triphosphate
B.subtilis - *Bacillus subtilis*
cAMP - Cyclic adenosine monophosphate
CCCP - Carbonyl cyanide m-chlorophenyl hydrazone
CCP4 - Collaborative computational project 4
c-di-AMP - Cyclic dimeric adenosine monophosphate
c-di-IMP - Cyclic dimeric inosine monophosphate
c-di-GMP - Cyclic dimeric guanosine monophosphate
cGAMP - Cyclic guanosine monophosphate-adenosine monophosphate
cGMP - Cyclic guanosine monophosphate
ChCl - Choline chloride
CPS - Counts per second
Cryo-EM - Cryo-electron microscopy
Cymal-6 - 6-cyclohexyl-1-hexyl-β-D-maltoside
DDM - n-dodecyl-β-D-maltoside
DM - n-decyl-β-D-maltoside
DMSO - Dimethylsulfoxide
DTT - Dithiothreitol
E.coli - *Escherichia coli*
EDTA - Ethylenediaminetetraacetic acid
GMP - Guanosine monophosphate
GTP - Guanosine triphosphate
HEPES - 4-(2-hydroxyethyl)piperazine-1-ethanesulfonic acid
IPTG - Isopropyl β-D-1-thiogalactopyranoside
ITC - Isothermal titration calorimetry
KCl - Potassium chloride
kDa - Kilodalton
KTN domain - K^+ transport nucleotide binding domain
LB - Lysogeny broth

LLG - Log-of-likelihood gain

MES - 2-(N-morpholine)ethanesulfonic acid

MPD - 2-methyl-2,4-pentanediol

NaCl - Sodium chloride

NAD^+ - Nicotinamide adenine dinucleotide (oxidized)

NADH - Nicotinamide adenine dinucleotide (reduced)

NMG - N-methyl-D-glucamine

OD - Optical density

pApA - 5'-phosphoadenylyl-(3',5')-adenosine

pGpG - 5'-phosphoguanylyl-(3',5')-guanosine

PCR - Polimerase chain reaction

PDB - Protein Data Bank

PEG - Polyethylene glycol

P-helix - Pore helix

P-loop - Pore loop

PMF - Proton motive force

PMSF - Phenylmethylsulfonyl fluoride

RCK domain - Regulator of conductance of K^+ domain

RNA - Ribonucleic Acid

SDS-PAGE - Sodium dodecyl sulfate polyacrylamide electrophoresis

SKT - Superfamily of K^+ transporters

STING - Stimulator of interferon genes

TBA - Tetrabutylammonium

TCEP - Tris(2-carboxyethyl)phosphine

TFZ - Translation function Z-score

Tm - Melting temperature

TM - Transmembrane helix

Tris-HCl - Tris(hydroxymethyl)aminomethane hydrochloride

WT - Wild-type

ABSTRACT

KtrAB is a cation channel involved in the homeostasis of potassium in many bacterial species. This channel is a complex composed by KtrB, the ion conduction membrane protein, and KtrA, an RCK cytosolic regulatory protein. KtrA binds ATP and ADP and assembles as an octameric ring that adopts different conformations upon nucleotide binding, regulating channel function. ATP binding induces the adoption of a square-conformation of the ring and increased K^+ flux activity through the channel; ADP binding results in a non-square conformation and decreased K^+ flux. However, it was not clear how ATP binding induced the adoption of the square-activated conformation by the KtrA octameric ring. We employed X-ray crystallography and a proteoliposome K^+ flux assay to study the mechanism of nucleotide-dependent activation in KtrA. In particular, we identified residues in the KtrA intra-dimer interface that are vital for activation in the presence of ATP and demonstrated that divalent cations are cofactors in the activation process.

Recently, the cyclic dinucleotide c-di-AMP was shown to be involved in the regulation of potassium homeostasis in many bacteria. Particularly, c-di-AMP regulates the activity of potassium channels and transporters by binding directly to their regulatory domains and/or by controlling the protein expression level through interaction with a riboswitch and modulation of transcription. We used differential scanning fluorimetry and ITC to characterize the binding of c-di-AMP to the two *B. subtilis* RCK regulatory subunits, KtrA and KtrC. Furthermore, we also explored the role of this cyclic dinucleotide in the function of the KtrCB-ATP channel and used X-ray crystallography to obtain a structure of KtrCB-ATP in complex with c-di-AMP.

RESUMO

KtrAB é um canal catiónico que está envolvido na regulação da homeostase de potássio em várias espécies bacterianas. Este canal é um complexo composto por KtrB, a proteína membranar que facilita a passagem de iões, e por KtrA, uma proteína RCK citosólica com funções reguladoras. KtrA liga ATP e ADP e organiza-se num anel octamérico que adota conformações diferentes consoante o nucleótido, regulando a função do canal. A ligação de ATP promove a adoção de uma conformação quadrada do anel e induz um fluxo elevado de K^+; a ligação de ADP promove uma conformação "não-quadrada" que resulta num fluxo de K^+ diminuto. No entanto, a forma como a ligação de ATP promove a adoção da conformação quadrada pelo anel octamérico de KtrA ainda não era evidente. Utilizámos cristalografia de raios-X e um ensaio funcional de medição de fluxo de K^+ com recurso a proteolipossomas, para estudar a dependência nucleotídica do mecanismo de ativação de KtrA. Em particular, identificámos resíduos na interface entre as subunidades do dímero de KtrA que são vitais para a ativação na presença de ATP e demonstramos que catiões divalentes são cofatores no processo de ativação.

Recentemente, foi demonstrado que o dinucleótido cíclico c-di-AMP está envolvido na regulação da homeostase de potássio em várias bactérias. Em particular, c-di-AMP regula a atividade de canais e transportadores de potássio, ligando-se diretamente aos seus domínios reguladores e/ou controlando o nível de expressão proteica através da interação com uma riboswitch e modulação da transcrição. Fizemos uma caracterização da interação de c-di-AMP com as duas subunidades reguladoras RCK de *B.subtilis*, KtrA e KtrC, utilizando técnicas de fluorescência e ITC. Explorámos também o papel desempenhado por este dinucleótido cíclico na função do canal KtrCB-ATP e determinamos uma estrutura de KtrCB-ATP em complexo com c-di-AMP utilizando cristalografia de raios-X.

I. INTRODUCTION

This work addresses the molecular details of the mechanism of regulation of the KtrAB cation channel from *B. subtilis*. This channel is involved in potassium uptake and was proposed to have evolved from potassium channels. As such, this introductory section includes segments regarding the physiological importance of potassium, as well as insights about ion channels. In particular, potassium channel structure and mechanisms of regulation are discussed, with examples for specific channels being provided. A detailed analysis of the current knowledge regarding the TrkAH and KtrAB cation channels is also included. On another note, the *B. subtilis* potassium homeostasis machinery was recently shown to be regulated by c-di-AMP, a cyclic dinucleotide. The role of this nucleotide in the regulation of the *B. subtilis* Ktr channel proteins is also studied in this thesis. Therefore, an overview of the currently known cyclic dinucleotides and their roles in the regulation of physiological processes, with emphasis on c-di-AMP, is presented in this section.

With these segments, I hope to introduce important concepts that will result in a better understanding of this thesis.

Physiological role of the potassium (K^+) ion

Potassium (K^+) is an essential macro element for all living organisms. In fact, potassium is the most abundant inorganic cation in the cytosol of both prokaryotic and eukaryotic cells, with estimated concentrations of ~ 140 mM in mammalian cells (Voet et al., 2006), 50 to 250 mM in plants and fungi (Rodriguez-Navarro, 2000) and 200 to 500 mM in bacteria (Schultz & Solomon, 1961). Potassium is therefore accumulated inside the cells against a large concentration gradient that reaches up to 10^3 to 10^5-fold difference in bacteria, fungi and plant cells (Rodriguez-Navarro, 2000; Schultz & Solomon, 1961).

Since sodium is generally more abundant in the environment than potassium, the preferential accumulation of potassium inside the cell poses an interesting question. In the 1920's Macallum described the principles of evolutionary chemistry (paleochemistry) of living organisms, where he addressed the evolutionary importance of K^+ prevalence in the cytosol (Macallum, 1926). Regarding eukaryotic cells, Macallum noted that, even though the cation content of fluids such as the blood and lymph was very similar to that of sea water, the cytosolic cation content was remarkably different.

He pointed out that the cytosolic content of the cell is more conservative to changes than its surrounding environment and must be older than the media that constitutes its current environment. Therefore, the relative proportions of the inorganic elements contained in the cytosol are of more ancient origin than the relative proportions of the same elements in the surrounding media. A possible hypothesis advanced by the author is that the first cells emerged in a primordial K^+-rich environment (Macallum, 1926). This hypothesis has been supported in recent studies that show a potassium prevalence over sodium in the vapour of inland geothermal systems, and suggests that the first cells would have emerged in primordial anoxic geothermal fields, where the elementary composition of the condensed vapour would resemble the current internal cell content (Mulkidjanian et al., 2012). Potassium would then have evolved as an essential cation used by the cell machinery for physiological processes.

K^+ has been shown to be compatible with protein structures even at high concentrations (D T Clarkson & Hanson, 1980), and to contribute to the electrical neutralization of anionic groups inside the cell, while also being required for modulation of enzyme activity (H J Evans & Sorger, 1966; Suelter, 1970). This monovalent cation is essential for protein synthesis (Lubin & Ennis, 1964), enabling a proper ribosomal functional activity (Naslund & Hultin, 1970, 1971) by playing a role in ribosomal conformation stabilization. Particularly, K^+ has been shown to be present throughout the large subunit of the ribosome, interacting with both RNA and protein molecules (Klein et al., 2004; Nissen et al., 2000; Rozov et al., 2019). In this way, K^+ helps to ensure ribosomal integrity and architecture. Absence of the monovalent cation results in the destabilization of ribosomal structure, with denaturation and loss of proteins and RNA integrity, which leads to loss of function.

K^+ also plays a central role in several physiological processes such as osmoregulation, pH homeostasis and establishment of the transmembrane electrical potential.

Regarding osmoregulation, the intracellular K^+ concentration is adjusted according to the osmotic conditions of the external media in order to maintain the turgor pressure stable and enable cell division and growth (Meury, 1988). Prokaryotes, for instance, are subjected to changes in the external environment that result in osmotic stress. The osmoregulation process has been extensively studied in organisms like *Escherichia coli* (Epstein & Schultz, 1965; Meury et al., 1985) and *Bacillus subtilis* (Whatmore et al., 1990; Whatmore & Reed, 1990). K^+ uptake is the initial response used by these organisms in order to cope with exposure to a hyperosmotic environment, followed by

production of glutamate to counterbalance the positive charges (Cayley et al., 1991; Epstein & Schultz, 1965; Larsen et al., 1987; McLaggan et al., 1994). Potassium glutamate provides a transient adaptation to osmotic stress, but the high ionic strength is detrimental for cellular metabolism during prolonged stress, due to the inhibitory effect in enzyme activity (Cayley, et al., 1991). Therefore, the potassium glutamate increase in the cytosol acts as a signal to promote protein expression of transport systems and uptake of compatible solutes such as proline (Brill et al., 2011; Whatmore, et al., 1990), glycine betaine (Boch et al., 1994; Holtmann & Bremer, 2004; Prince & Villarejo, 1990; L. Sutherland et al., 1986) and threalose (Dinnbier et al., 1988; Larsen, et al., 1987) that function as osmoprotectants.

In the 1960's, Mitchell published the Chemiosmotic Hypothesis, shedding light on the role played by the proton flux in microbial energetics (Mitchell, 1966). His work showed that the energy transduction required for ATP synthesis, solute transport and cell motility is regulated by a transmembrane electrochemical potential of protons designated proton motive force (PMF). The PMF (Δp) is composed by two interchangeable components: the membrane potential (Δψ) and the pH gradient (ΔpH), being described by: $\Delta p=\Delta\psi+\Delta pH$. K^+ uptake has been shown to regulate these two components. Most microbes control their pH homeostasis in order to have a near neutral intracellular pH, despite fluctuations of external pH. Organisms like *Escherichia coli* and *Bacillus subtilis* for instance, maintain their intracellular pH between 7.4 and 7.8, while being exposed to external pH's in the 5.0 to 9.0 range (Padan et al., 1976; Shioi et al., 1980; Slonczewski et al., 1981). K^+ uptake is used as a mechanism to alkalinize the cytosol when the cells are exposed to an acidic pH. The influx of K^+ modulates Δψ by depolarizing the cells due to the increase in positive charges, allowing efflux of protons and therefore increasing ΔpH and maintaining a near neutral intracellular pH (Bakker & Mangerich, 1981; Kroll & Booth, 1981). When these organisms are exposed to an alkaline pH, K^+/H^+ transporters modulate proton influx in order to adjust the intracellular pH to near neutral (Kroll & Booth, 1983).

More recently, K^+ has been proposed to be involved in cell communication between bacterial communities through signalling in biofilms. Biofilms are organized bacterial communities that typically form under environmental stress conditions, such as nutrient limitation (Branda et al., 2001; Vlamakis et al., 2008). Recent studies of *Bacillus subtilis* biofilms by Suel and colleagues revealed the existence of a metabolic oscillation that results from a co-dependence between cells in the interior and at the periphery of the biofilm (J. Liu et al., 2015). As the biofilm grows in size, cells in the interior and at the

periphery compete for nutrients. This metabolic oscillation causes a periodic halt in biofilm growth, until nutrients are made available to the interior cells (J. Liu, et al., 2015). Coordination of the metabolism between distant cells in the biofilm is conveyed through electrical signalling (Prindle et al., 2015). It was proposed that this signal results from a K^+ flux from the cytosol to the extracellular media, which produces electrical waves that propagate through the biofilm and coordinate metabolic states.

Ion channels

The cellular membrane is a phospholipid bilayer that envelopes and defines the cell, by separating the aqueous media inside the cell from the surrounding environment. This membrane creates a barrier for the passage of hydrophilic compounds and allows the cell to create electrical charge differences by controlling the intracellular and extracellular ion concentrations. These charge differences establish an electrical potential across the membrane (membrane potential), inside negative at the resting state, which enables the cell to store and use energy. The main inorganic ions involved in this membrane potential are K^+, Na^+, Ca^{2+} and Cl^- and their transport is mediated by specialized membrane-embedded proteins, namely ion channels and ion pumps (Bertil Hille, 2001). Ion channels are involved in the passive diffusion of ions down their electrochemical gradient while ion pumps transport ions against their gradient, at the cost of energy (in the form of ATP, for example).

The study of ion channels can be traced back to the 19th century, when Ringer demonstrated that a specific proportion of sodium, potassium and calcium was required in order to enable the contraction of the frog cardiac muscle for several hours (Ringer, 1882a, 1882b, 1883a, 1883b). In the beginning of the 20th century, Julius Bernstein suggested the “membrane hypothesis”. In his studies of excitable cells from nerve and muscle, he proposed that, in the resting state, the cellular membrane is selectively permeable to K^+, with the resting potential being set by the movement of K^+ ions across the membrane according to their concentration gradient. When a stimulus occurs, the membrane would become non-selective and therefore permeable to other ions as well, short-circuiting the diffusion potential of K^+ and transiently increasing the membrane potential to 0 mV and generating what is known as the action potential (Bernstein, 1902) (English translation in: Boylan JW (ed) Founders of experimental physiology. JF Lehmanns Verlag, München 1971, pp 258–299]).

In the 1950s, Hodgkin and Huxley provided a breakthrough in ion channel understanding (Hodgkin & Huxley, 1952a, 1952b, 1952c, 1952d). They recorded intracellularly an action potential for the first time and showed that it exceeded 0 mV, adjusting Bernstein's hypothesis. In fact they demonstrated, along with Katz, that this overshoot is due to an increased permeability of the membrane to Na^+ ions during the action potential and not to non-selective permeability (Hodgkin & Katz, 1949). In 1955, Hodgkin and Keynes provided the first experimental evidence for channel mediated ion flux, by measuring directional K^+ flow using the $^{42}K^+$ isotope. They suggested that the ions move in a single file and that several ions cross the membrane at the same time (Hodgkin & Keynes, 1955). Later on, Armstrong and Hille demonstrated that K^+ and Na^+ flux across the membrane is mediated by unique protein pores (Na^+ channels and K^+ channels) (Armstrong, 1971, 1981; B. Hille, 1970).

Potassium channels

Potassium channels are ubiquitous in all living organisms and kingdoms of life including archaea (Jiang et al., 2002a; Parfenova et al., 2007), bacteria (Milkman, 1994; Schrempf et al., 1995), yeast (Ketchum et al., 1995; X. L. Zhou et al., 1995), plants (Anderson et al., 1992; Sentenac et al., 1992) and animals (Atkinson et al., 1991; Dworetzky et al., 1994; Papazian et al., 1987; Tempel et al., 1988), making them the most widely distributed type of ion channel. Attesting to their physiological importance, K^+ channels are present in most cell types, including cells from electrically inexcitable tissues such as the liver (Pearson et al., 1999) and also in organellar membranes, including mitochondria (Siemen et al., 1999; Szabo et al., 2005) and chloroplasts (Carraretto et al., 2013; Tempel, et al., 1988; Tester & Blatt, 1989).

The first K^+ channel to be cloned was the Shaker channel from *Drosophila melanogaster* (Kamb et al., 1987; Papazian, et al., 1987; Pongs et al., 1988). This revealed for the first time the sequence of a K^+ channel and led to subsequent biochemical and functional studies, using pore blockers and mutagenesis, in order to map the channel pore and selectivity filter, as well as the gating region (Aggarwal & MacKinnon, 1996; Heginbotham et al., 1994; Hidalgo & MacKinnon, 1995; Roderick MacKinnon, 1991; R. MacKinnon & Miller, 1989; Ranganathan et al., 1996; Yellen et al., 1991). These studies allowed important inferences about the general architecture of K^+ channels.

K^+ channels usually assemble as tetramers, with four subunits surrounding a central pore, through which K^+ flows. Each of these subunits can have two, four or six

transmembrane helices, as well as associated cytoplasmic regulatory domains. The hallmark of K^+ channels is their ability to conduct K^+ at high rates (10^7-10^8 per second), while also being able to select for K^+ ions (1.33 Å radius) over the smaller Na^+ ions (0.95 Å radius) by a factor of over 1000. Remarkably, this high selectivity for K^+ does not compromise the conduction rates that are very similar to the rates of unrestricted diffusion of ions in water (Bertil Hille, 2001; R. MacKinnon, 2004). K^+ channel selectivity occurs in the selectivity filter, a region that forms the coordination shell for K^+ ions inside the channel pore. The K^+ channel selectivity filter contains a highly conserved sequence (TVGYG or TVGFG) and mutation of these residues impairs the ability of the channel to discriminate between K^+ and Na^+ (Heginbotham, et al., 1994).

The determination of the high resolution potassium channel structures of the *Streptomyces lividans* KcsA (Doyle et al., 1998; Y. Zhou et al., 2001) and the *Methanobacterium thermoautotrophicum* MthK (Jiang, et al., 2002a; Jiang et al., 2002b) was a major contribution to the study of potassium channels. These structures confirmed many of the previous predictions and provided a better understanding of K^+ conduction, by revealing molecular details regarding the pore and selectivity filter structure and the mechanisms of permeation and gating.

Selectivity and permeation

KcsA assembles as a tetramer of identical subunits, with four-fold symmetry around the pore. Each subunit adopts the TM1-P-loop-TM2 architecture that consists of two transmembrane helices (TM1 and TM2) and a pore loop (P-loop) region that includes the pore helix (P-helix) and the selectivity filter sequence (Figure 1a). The intracellular end of the channel presents a constriction known as the cytoplasmic gate, formed by the packing of the TM2 helices in a bundle. This gate leads to a water filled cavity at the centre of the membrane that contains a hydrated K^+ ion, stabilized by its hydration shell (the oxygen atoms of eight water molecules) and the negative charges provided by the C-terminus of the four P-helices. The selectivity filter constitutes the narrowest region of the pore, around 4.5 Å wide, and contains four evenly spaced K^+ binding sites (S1 to S4) that allow ion permeation in a single file. Each K^+ ion is coordinated by eight oxygen atoms from the main chain carbonyl and threonine hydroxyl groups of the conserved TVGYG sequence (Doyle, et al., 1998; Y. Zhou, et al., 2001) (Figure 1b). This oxygen coordination results in a cage-like structural configuration surrounding the K^+ ion, with four oxygens on a plane above the ion and another four on a plane below; this

configuration mimics the K^+ hydration shell and therefore compensates the dehydration energy cost, helping to explain the high flux rates and selectivity for K^+.

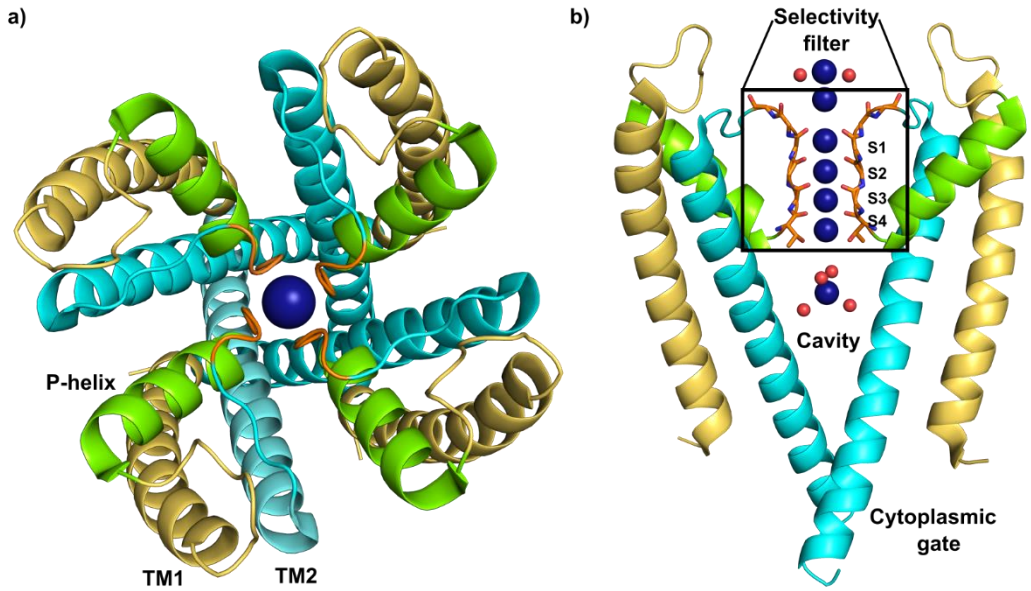

Figure 1: KcsA potassium channel structure (PDB: 1K4C). a) Top view of the tetramer forming the ion pore. TM1, P-helix and TM2 are colored yellow, green and cyan, respectively. The selectivity filter is highlighted in orange and K^+ ions are shown as blue spheres. **b)** Side view of two channel subunits, depicting the selectivity filter (orange sticks), the water filled cavity and the cytoplasmic gate formed by the TM2 helix bundle. K^+ ions and water molecules are shown as blue and red spheres, respectively. The ion binding sites S1 to S4 are indicated. The structure shows an average K^+ occupation in the S1, S3 and S2, S4 configurations.

It was also shown that the selectivity filter contains more than one ion at a time and proposed that K^+ adopts two distinct configurations, occupying two sites at a time (S1, S3 or S2, S4), while the remaining sites are occupied by water molecules (Morais-Cabral et al., 2001). Ion conduction is propelled by electrostatic repulsions, but the number of actual K^+ ions inside the filter is a subject that is still being explored. The conduction model described above, with two K^+ ions intercalated with water molecules at a time in the filter, is called the soft knock-on model. Recently, the hard or direct knock-on model has been proposed, in which all four sites of the filter contain K^+ ions and there are no water molecules present (Kopfer et al., 2014). This model arose from re-refinement of available KcsA structures using different approaches, as well as molecular dynamics simulations. The conclusion was that direct contact between the ions is not energetically prohibitive and Coulomb repulsion between the ions drives ion conduction. Other techniques have been employed to understand this issue, including two-dimensional infrared spectroscopy (Kopec et al., 2018; Kratochvil et al., 2016), and

results have been obtained that support both models. Further studies will be required to reach a consensus regarding the mechanism of ion permeation through the selectivity filter.

Gating

Ion flux through a potassium channel pore is regulated by a process called gating, which allows the channel to go from a closed non-active state to an open active state in response to different stimuli. These stimuli can be ligands (ligand-gated channels), changes in the membrane potential (voltage-gated channels), membrane pressure (mechanosensitive channels) or temperature (temperature-gated channels). A channel can encompass several gates that obstruct ion conductance, such as the cytoplasmic gate shown in Figure 1b. For instance, the KcsA cytoplasmic gate is regulated by pH. At low pH, binding of protons at the cytoplasmic gate, disrupts the hydrogen bonds that stabilize the TM2 helix bundle and results in channel opening (Cuello et al., 1998; Heginbotham et al., 1999; Takeuchi et al., 2007; Thompson et al., 2008).

In other channels, such as MthK, the gating process is regulated by ligand binding to cytoplasmic regulatory domains. MthK is a ligand-gated K^+ channel that assembles as a tetramer and displays a four-fold symmetry around the pore. Each subunit is composed by two transmembrane helices (TM1 and TM2) linked by the pore loop (P-loop) region, and an attached cytosolic regulatory domain at the C terminus of TM2. Four additional copies of this cytosolic domain are expressed via an alternative starting codon initiated at methionine 107. These additional domains assemble in the cytosol with the four domains attached to the channel to form an octameric gating ring (Figure 2) (Jiang, et al., 2002a, 2002b). The MthK selectivity filter contains the canonical TVGYG sequence characteristic of K^+ channels.

The MthK channel has been extensively studied and was shown to be activated by Ca^{2+} and inhibited by pH (H^+) (Jiang, et al., 2002a; M. M.-C. Kuo et al., 2007; Li et al., 2007; Parfenova et al., 2006; Pau et al., 2010; Zadek & Nimigean, 2006). Several full-length and transmembrane (pore) channel structures (Fan et al., 2020; Jiang, et al., 2002a, 2002b; Sheng Ye et al., 2010), along with several structures of the gating ring in different conformations (Dong et al., 2005; Pau et al., 2011; Smith et al., 2013; S. Ye et al., 2006) were obtained. Recently, cryo-electron microscopy (Cryo-EM) structures of different MthK functional states have also been determined (Fan, et al., 2020). These structures provided molecular details regarding channel regulation.

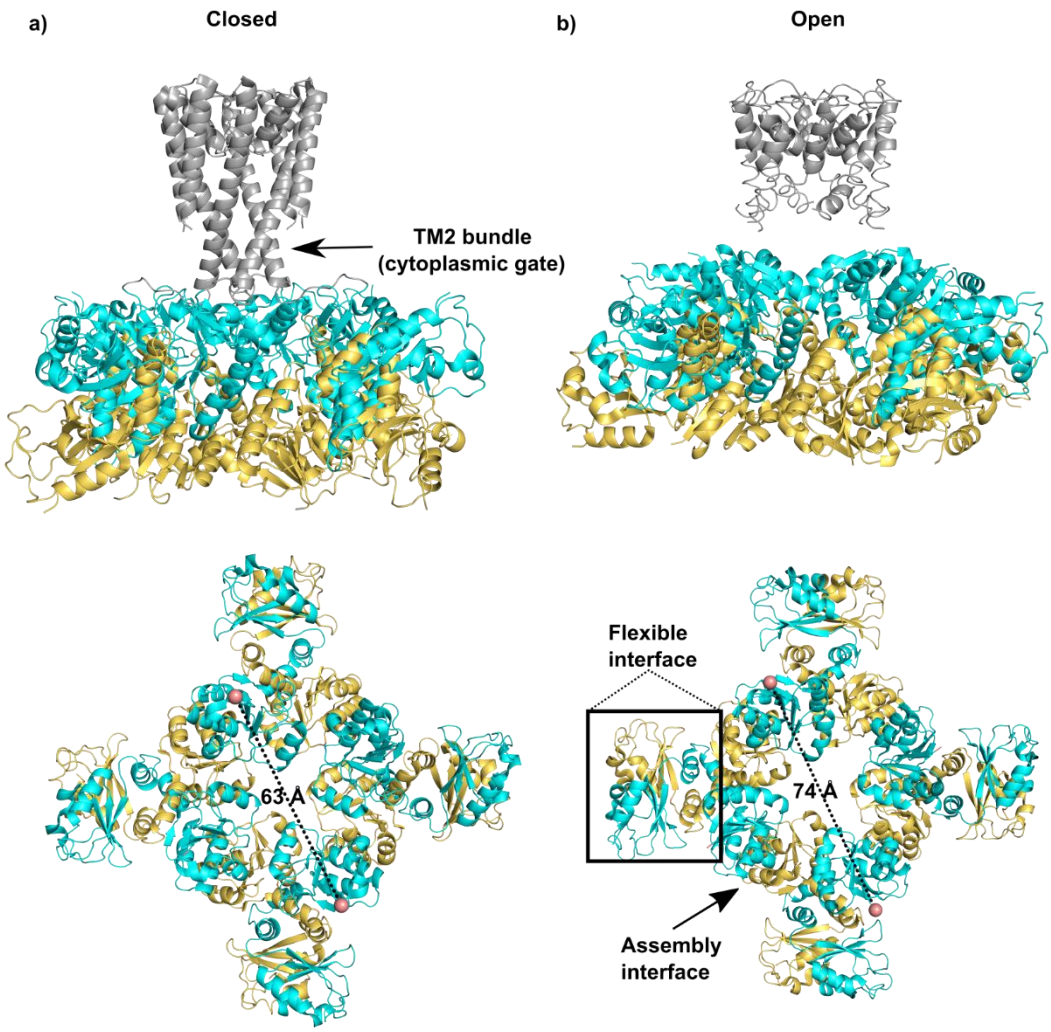

Figure 2: MthK potassium channel structures. a) Top- Side view of a closed MthK channel (PDB: 6U6D), depicting the obstruction to ion conduction created by the TM2 bundle. Bottom- gating ring in the absence of calcium. **b)** Top- Side view of an open MthK channel (PDB: 1LNQ), depicting the bending of the TM2 helices and opening of the pore. The linkers between the TM2 helices and their C-terminal cytosolic domains are not observed in the structure. Bottom- gating ring with bound calcium. The assembly and flexible ring interfaces are highlighted for one set of dimers in the gating ring. Expansion of the ring in the open state compared to the closed state is illustrated by the distances between the Cα of R116 residues in opposite sides of the rings. Pore domains are shown in in grey. In the octameric ring, the domains depicted in cyan are covalently attached to the pore domain and the domains depicted in yellow are expressed separately and assemble with the cyan ones in the cytosol.

In the closed state, the pore inner helices (TM2) that make up the cytoplasmic gate are straight and create a constriction at the intracellular side, forming a bundle that impairs ion conduction (Figure 2a). Upon Ca^{2+} binding, the octameric gating ring expands and pulls on the C-linker that attaches the gating ring to the C-terminus of the TM2 helices,

causing them to bend just below the selectivity filter. The bent helices splay open and create a wide entryway that allows for ion conduction (open state) (Figure 2b).

K^+ channels are also known to be inactivated shortly after activation, going from an open active state to an open inactivate state. Inactivation consists in the stoppage of ion conduction while the activating stimulus is still present. There are currently two mechanisms proposed for inactivation of K^+ channels: C-type inactivation and N-type inactivation.

The C-type inactivation mechanism is usually slow and results from conformational changes at the selectivity filter that impair K^+ binding and abolish ion conduction (Toshinori Hoshi et al., 1991). This mechanism provides an example of gating at the selectivity filter. In the KcsA channel, the structure of the selectivity filter was shown to depend on the number of K^+ ions that are present inside the filter. In the presence of a $[K^+]$ below 20 mM, only one K^+ ion was detected inside the filter and a conformational change occurs that causes the filter to collapse, closing in the middle (Y. Zhou, et al., 2001). Furthermore, functional studies revealed that E71, a residue that establishes contacts with the selectivity filter sequence, is essential for the inactivation process (Cordero-Morales et al., 2006).

The N-type inactivation mechanism is a fast, auto-inhibitory process in which an N-terminal portion of the channel goes through the open cytoplasmic gate into the pore and blocks ion conduction (T Hoshi et al., 1990; Zagotta et al., 1990). This process is often referred to as the ball and chain mechanism, originally described for Na^+ channels (Bezanilla & Armstrong, 1977). The ball consists of a cytoplasmic region at the channel N terminus, with hydrophobic residues at the beginning that establish interactions within the pore and a few hydrophilic residues at the end that interact with residues at the intracellular gate region. The chain is a stretch of residues that confers mobility. A recent Cryo-EM structure of the open-inactivated state of the MthK channel presents an example of N-type inactivation. The structure displays an elongated density inside the pore corresponding to the first 17 residues of the N-terminal domain, modelled as an α-helix (Fan, et al., 2020). Molecular dynamics simulations indicate that the binding of this α-helix inside the pore is energetically favourable and functional studies showed that a MthK mutant lacking residues 2-17 is no longer inactivated (Fan, et al., 2020; M. M. Kuo et al., 2008). Furthermore, an open state Cryo-EM structure determined for this mutant does not have an extended density inside the pore (Fan, et al., 2020).

RCK domains

RCK (regulator of conductance of K^+) domains are cytosolic regulatory domains that modulate the activity of K^+ channels and transporters (Jiang et al., 2001), with one example being the gating ring described above for the MthK K^+ channel (Jiang, et al., 2002a). A sequence analysis of 270 prokaryotic genomes showed that more than half of the identified potassium channels (127 of 217) contain RCK domains, demonstrating their importance in prokaryotic K^+ homeostasis (M. M. Kuo et al., 2005; Loukin et al., 2005).

RCK domains have a characteristic structural feature, the Rossman-fold (Rossmann et al., 1974). The classical Rossman-fold is composed by two β-α-β-α-β motifs linked by an α-helix. The motifs are arranged so that the six β-strands are parallel and form an extended β-sheet with both faces surrounded by the α-helices. In some RCK domains, the Rossman-fold contains the classical nucleotide binding motif (GxGxxGx[n]E/D; where G is glycine, E glutamate, D aspartate, x any amino acid and n is the number of residues until E/D, usually ~16) (Bellamacina, 1996), which enables them to bind nucleotides. Domains that contain this nucleotide binding motif are sometimes referred to as KTN domains (K^+ transport and nucleotide binding) (Jiang, et al., 2001; Roosild et al., 2002). RCK domains form dimeric or pseudo-dimeric units that assemble as a functional octameric ring (Albright et al., 2006; Cao et al., 2013; Deller et al., 2015; Dong, et al., 2005; Jiang, et al., 2002a; Jiang, et al., 2001; Kong et al., 2012; Vieira-Pires et al., 2013; Wu et al., 2010). The KefC K^+ transporter presents an exception in which the dimer is the functional unit (Roosild et al., 2009). The majority of RCK domains include an N-terminal domain, that adopts the Rossman-fold, and a C-terminal domain that is less conserved. However, it is possible to find RCK domains that lack the C-terminal domain.

RCK domains have been found in K^+ channels with two or six transmembrane helices per subunit (2TM and 6TM, respectively). Interestingly, while in 2TM K^+ channels RCK domains with and without the nucleotide binding motif have been found, none of the RCK domains found in 6TM K^+ channels contain this motif and these are regulated by cations (M. M. Kuo, et al., 2005). In general, RCK domains are classified as either nucleotide- or cation-dependent (Cao, et al., 2013). RCK domains are also known to display different arrangements and interactions with the effector membrane protein. In some prokaryotic RCK-containing K^+ channels, each channel subunit contains a single RCK domain attached to the C terminus of the membrane protein. Additional copies of

the domain are expressed as separate proteins via an alternative starting codon, enabling the assembly of the functional octameric gating ring, as seen in the MthK channel (Jiang, et al., 2002a, 2002b). In the Slo K^+ channel family, each channel subunit contains two tandem RCK domains attached to the C terminus of the membrane protein, enabling the formation of the gating ring without the need for a separate RCK domain protein (Wu, et al., 2010; Yuan et al., 2010). Single or two tandem RCK domains can also be expressed as soluble proteins that form an independent octameric ring and assemble in a complex with the membrane protein (Cao, et al., 2013; Vieira-Pires, et al., 2013). Prokaryotic genome sequencing analysis also revealed that at least five 2TM K^+ channels have an RCK attached to both the N-terminal and C-terminal domains (M. M. Kuo, et al., 2005) but, to the date, none of these channels has been studied.

RCK domains regulate K^+ flux through rearrangements of the dimer unit upon binding of signalling molecules, which ultimately results in a conformational change in the effector membrane protein. In the MthK channel, which contains a cation-dependent RCK gating ring, the mechanisms that underlie these conformational changes have been explained by thorough functional and structural analyses. The eight RCK domains that compose the MthK octameric gating ring are arranged in a tetramer of dimers, with the N-terminal domains forming the ring and the C-terminal domains at the periphery (Figure 2). In each dimer, only one subunit is attached to the C terminus of the membrane protein; the attached subunits of different dimers are disposed on a higher plane than the ones coming from solution and do not interact with each other. The ring displays two unique protein interfaces termed assembly interface and flexible interface (Jiang, et al., 2002a; S. Ye, et al., 2006).The assembly interface is formed by the inter-dimer contacts of N-terminal helices αD and αE and the flexible interface is formed by intra-dimer contacts involving the RCK C-terminal domains and helices αF and αG (Figure 2).

Three distinct Ca^{2+} binding sites (C1, C2 and C3) have been identified in each RCK domain, totalling six sites per dimer (Pau, et al., 2011). The C1 site is located in the N-terminal domain of each dimer subunit, while sites C2 and C3 are located at intra-dimer interfaces in the C-terminal domains (Figure 3). All the sites are involved in channel activation and sites C1 and C3 are allosterically coupled (Pau, et al., 2011; Smith, et al., 2013).

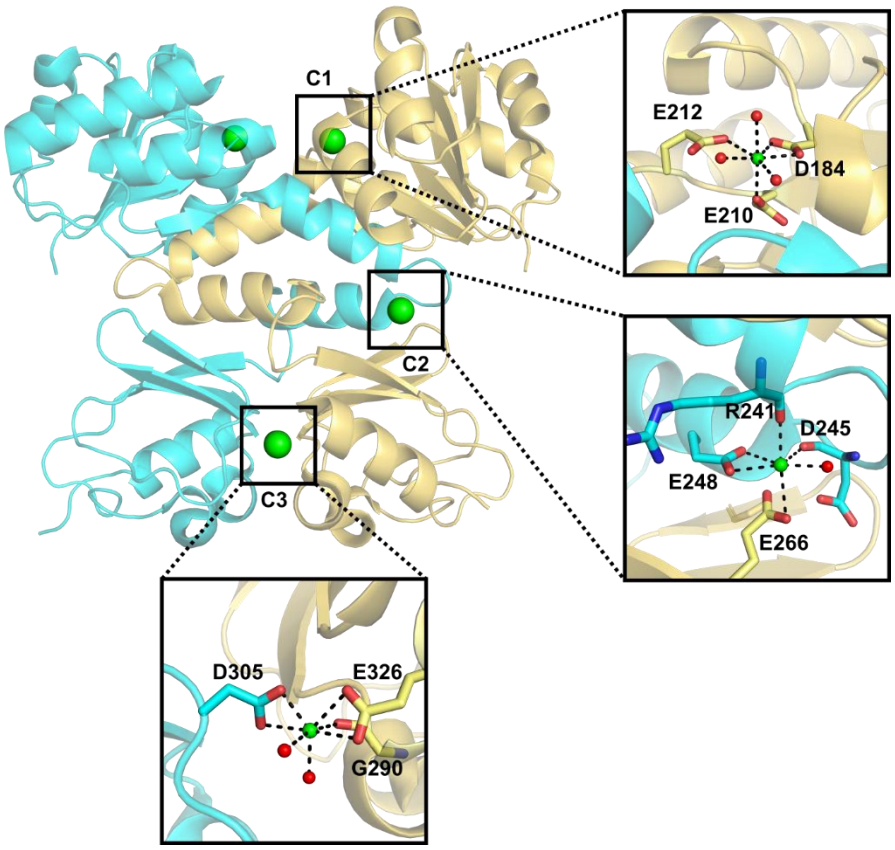

Figure 3: MthK RCK dimer calcium binding sites. Cartoon representation of a MthK RCK dimer with one subunit in cyan and another in yellow (PDB: 4L73). The three calcium binding sites C1, C2 and C3 are shown in close-up detail. Residues involved in interactions with calcium ions are depicted using stick representation. Calcium ions and water molecules are shown as green and red spheres, respectively.

Ca^{2+} binding activates the MthK channel by stabilizing the octameric gating ring in an expanded conformation that is propagated to the pore domain, opening the gate. The ligand induced conformational changes in the octameric ring are achieved by rigid body movements of the individual RCK dimer subunits, occurring across the flexible and assembly ring interfaces. Interestingly, in the absence of Ca^{2+}, the gating ring is able to adopt different conformations (S. Ye, et al., 2006).

MthK can also be activated by other divalent cations including Cd^{2+}, Ba^{2+} and Sr^{2+}, but not Mg^{2+} (Dvir et al., 2010; M. M.-C. Kuo, et al., 2007; F. J. Smith et al., 2012). Like Ca^{2+}, these cations also bind to the RCK gating ring, sharing at least the C1 binding site, although other sites have been reported depending on the cation. Interestingly, the ability of Ba^{2+} to activate MthK led to the suggestion that, in physiological conditions, K^{+} might also activate the channel. In these conditions, the cytosolic concentration of K^{+} is

around 150 mM or higher. Moreover, the ionic radius of K^+ is very similar to that of Ba^{2+} (1.33 and 1.38 Å radius, respectively) and, in two of the described Ba^{2+} binding sites, the interaction of the divalent cation with the protein is suggested to also be compatible with a K^+ ion (Smith, et al., 2012).

MthK has been shown to be inhibited by pH. A pH lower than 7.5 inhibits ion conduction through the channel by impairing calcium binding to the RCK domains and disrupting the assembly of the octameric gating ring (Dong, et al., 2005; M. M.-C. Kuo, et al., 2007; Pau, et al., 2010; Smith, et al., 2012; S. Ye, et al., 2006). The increased concentration of protons (H^+) at lower pH alters the RCK oligomerization state by destabilizing the inter-dimer interactions at the assembly interfaces of the ring, breaking the RCK octameric ring into dimers.

The Trk and Ktr cation channels

Trk and Ktr are multimeric complexes formed by an ion-conducting transmembrane subunit (TrkH, G or I in Trk systems and KtrB or D in Ktr systems), and a cytosolic regulatory subunit (TrkA or E and KtrA, C or E, respectively). Some of these cytosolic regulatory proteins are RCK domains that, unlike in K^+ channels with RCK domains, are not covalently bonded to the transmembrane channel region.

These cation channels play key roles in the regulation of pH homeostasis, adjustment of membrane potential, osmoregulation, resistance to antibiotics and bacterial pathogenicity (Berry et al., 2003; Gries et al., 2013; Holtmann et al., 2003; Kraegeloh et al., 2005; Matsuda et al., 2004; Nanatani et al., 2015; Ochrombel et al., 2011; Prindle, et al., 2015; J. Su et al., 2009). Particularly, they are essential for resistance to osmotic stress and high salinity, by mediating an early K^+ uptake (Price-Whelan et al., 2013).

Trk is a constitutively expressed protein system with an estimated K^+ K_M of 1 mM. This system has been extensively studied in *Escherichia coli*. The *E.coli* K12 strain contains two ion conduction subunits (TrkH and TrkG) and one RCK cytosolic regulatory subunit, TrkA. TrkA establishes functional complexes with both ion conduction subunits and has been reported to be required for a high-flux Trk-mediated K^+ transport (Bossemeyer et al., 1989; Rhoads et al., 1976; Schlosser et al., 1991; Schlosser et al., 1995). Halophilic bacteria such as *Halomonas elongata* rely on Trk-mediated K^+ transport to avoid Na^+ intake in saline environments and cope with salt stress. In this organism TrkI is the ion conduction subunit and TrkA is the regulatory subunit (Kraegeloh, et al., 2005).

The Ktr protein system has been described and characterized in *Vibrio alginolyticus* (Nakamura et al., 1998), in the cyanobacterium *Synechocystis* and in the Gram-positive bacteria *Bacillus subtilis*. In *Synechocystis*, there is only one ion-conducting subunit, KtrB, previously known as NtpJ (Berry, et al., 2003). KtrB assembles in a functional complex with the regulatory subunits KtrA and KtrE. While KtrA is an RCK domain, KtrE displays amino acid sequence similarity with glycosyl transferases (Matsuda, et al., 2004). In *Baciilus subtilis* there are two ion conducting subunits, KtrB and KtrD, and two RCK cytosolic regulatory subunits, KtrA and KtrC. KtrA and KtrB are in the same operon while KtrC and KtrD are encoded separately. This has led to the proposal that two K^+ transport systems exist in this organism: KtrAB and KtrCD. The two systems differ in K^+ affinity; KtrAB has a K_M for K^+ of 1 mM as opposed to 10 mM in KtrCD (Holtmann, et al., 2003). Glutamate has been suggested to increase the KtrCD K^+ affinity (Krüger et al., 2020a). Recently, we showed that each ion conduction subunit can assemble in a functional complex with KtrA or KtrC (Rocha et al., 2019).

The initial functional studies of the Trk and Ktr systems suggested that they were transporters, coupling influx of K^+ with H^+ (Harms et al., 2001; Stewart et al., 1985) and Na^+ (Tholema et al., 1999; Zulkifli et al., 2010), respectively. However, recent structural and functional studies showed that these proteins are cation channels (Cao et al., 2011; Cao, et al., 2013; Mikusevic et al., 2019; Szollosi et al., 2016; Vieira-Pires, et al., 2013; H. Zhang et al., 2020). Trk and Ktr channels belong to the superfamily of K^+ transporters (SKT). In this superfamily, each transmembrane subunit (protomer) is typically composed by four homologous non-identical repeats, adopting the same TM1-P-loop-TM2 architecture present in K^+ channels. These domains are termed D1-D4 and create an ion permeation pathway. SKT protomers are proposed to have evolved from a 2TM K^+ channel ancestor by multiple gene duplication and fusion (Durell et al., 1999), nonetheless, these proteins also reveal differences in comparison to K^+ channels. The TM1-P-loop-TM2 domains have variable sequences and are connected by cytoplasmic loops of different lengths (Durell, et al., 1999). Furthermore, the selectivity filter of SKT proteins is less conserved than in K^+ channels: instead of the canonical TVGYG sequence, only the first glycine residue is conserved in SKT protomers, conferring less selectivity for K^+ (Tholema, et al., 1999; Tholema et al., 2005) (Figure 4).

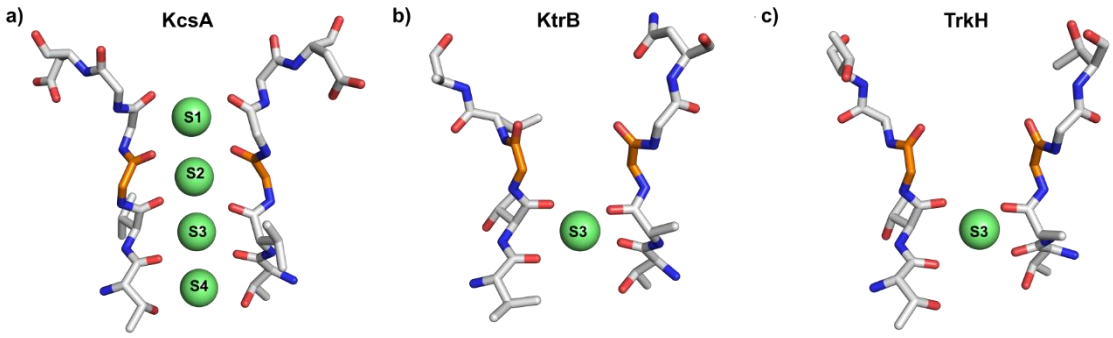

Figure 4: Selectivity filter comparison between KcsA, KtrB and TrkH. a) KcsA selectivity filter (PDB: 1K4C). **b)** KtrB selectivity filter (PDB: 4J7C). **c)** TrkH selectivity filter (PDB: 3PJZ). Selectivity filter residues are shown as sticks. K^+ ions are shown as green spheres and ion binding sites are labelled S1 to S4. Conserved glycine is highlighted in orange.

The determined structures of the *Vibrio parahaemolyticus* TrkAH (Cao, et al., 2011; Cao, et al., 2013; H. Zhang, et al., 2020) and of the *Vibrio alginolyticus* and *Bacillus subtilis* KtrAB (Diskowski et al., 2017; Szollosi, et al., 2016; Vieira-Pires, et al., 2013) channels confirmed that each TrkH and KtrB protomer is composed by four TM1-P-loop-TM2 segments (D1-D4), with TrkH also containing two additional transmembrane helices at the N terminus (D0). Interestingly, the ion conducting subunits organize as homodimers, with each protomer forming an ion permeation pathway. Furthermore, these homodimers assemble in a complex with an octameric gating ring formed by RCK cytosolic regulatory proteins.

TrkAH channel structure and regulation

TrkAH is a nucleotide regulated cation channel, upregulated by ATP and downregulated by ADP (Cao, et al., 2013). The structures of the *Vibrio parahaemolyticus* TrkH, TrkA and TrkAH complexes, contributed to the understanding of the regulation mechanism of this channel (Cao, et al., 2011; Cao, et al., 2013; H. Zhang, et al., 2020).

The TrkH dimer assembles in a complex with a gating ring formed by the nucleotide-dependent RCK regulatory protein TrkA (Figure 5a). The TrkH dimer interface between the two protomers is formed by helices from the D3 and D4 domains. A large portion of this extensive interface is formed by the second half of the broken M2 helix from the D3 domain (D3M2b), which is sharply tilted in relation to the membrane (Figure 5b). As

described above, the ion permeation pathway is formed by the assembly of domains D1 to D4 and has two important features: the selectivity filter and the intramembrane loop.

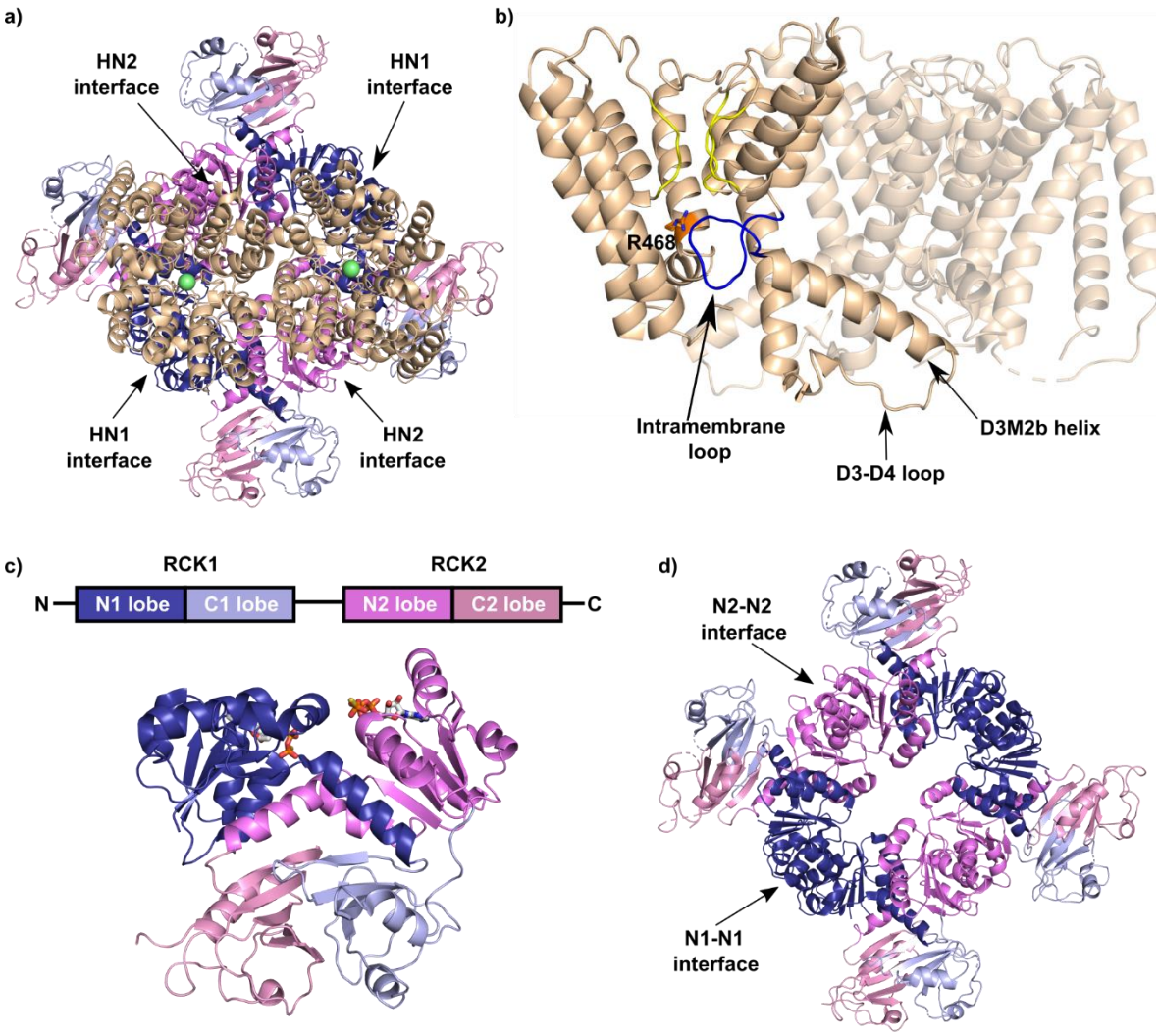

Figure 5: TrkAH structure. a) Extracellular view of the TrkAH complex. TrkH dimer, shown in wheat, sits on top of a TrkA octameric ring formed by four TrkA protomers. In each TrkA protomer, the N and C-terminal domains are shown in blue and grey, respectively, for RCK1 and in violet and pink for RCK2. K^+ ion is shown as green sphere. HN1 and HN2 contact regions between TrkH and TrkA are indicated. **b)** Membrane view of the TrkH dimer with relevant structural elements discussed in the text highlighted in one subunit. D2 domain is omitted in this subunit for clarity. Selectivity filter is shown in yellow and intramembrane loop in blue. R468 is shown in orange stick. **c)** Top- Scheme showing RCK domain organization in the TrkA protomer. Bottom- Cartoon representation of a nucleotide bound TrkA protomer (PDB: 4J9V). ATPγS is shown in stick representation. **d)** Cartoon representation of a TrkA ring with the inter-protomer N1-N1 and N2-N2 interfaces indicated. Color scheme for c) and d) is the same stated in a).

The intramembrane loop, together with R468, forms a barrier for cation permeation and is positioned close to the selectivity filter (Figure 5b). R468 is positioned in the second transmembrane segment of D4 and is highly conserved in bacterial SKT proteins. The intramembrane circular loop connects the two helical sections of TM2 in D3 and is present in TrkH, TrkG and KtrB. The intramembrane loop is rich in glycine and other small residues such as serine and alanine, which are well conserved across different sequences (Cao, et al., 2011). These two elements form a narrow constriction that needs to widen in order to allow cation permeation, possibly acting as a gate, and are a feature that has not been observed in the structure of any K^+ channel to date. Mutations of R468 in TrkH result in an increased channel activity and the intramembrane loop is required for TrkH interaction with the regulatory protein TrkA (Cao, et al., 2013).

Each TrkA protomer contains two tandem RCK domains, RCK1 and RCK2, and both have a nucleotide binding site (Figure 5c). Therefore, the TrkA ring is formed by a tetramer of protomers and contains eight nucleotide binding sites. In the case of TrkA, the flexible interface described for K^+ channels RCK domains is equivalent to the intramolecular interface between RCK1 and RCK2 in a TrkA protomer. The gating ring shows two assembly interfaces between TrkA protomers: one between the N-terminal lobes of RCK1 (N1-N1 interface) and another between the N-terminal lobes of RCK2 (N2-N2 interface) (Figure 5d). These interactions give the ring a 2-fold symmetry that matches the TrkH dimer (Cao, et al., 2013). The X-ray structure of a closed state TrkAH bound to NADH revealed that each TrkH monomer interacts with the TrkA N2 domains. The structure of an isolated TrkA in solution showed a gating ring with a substantial conformational change compared to the complex structure. In this structure, the N2-N2 interfaces rotate and slide past each other, converting TrkA from a planar to a twisted conformation. It was suggested that this conformational change may be regulated by nucleotide-binding and act as a mechanism for activating the TrkAH complex.

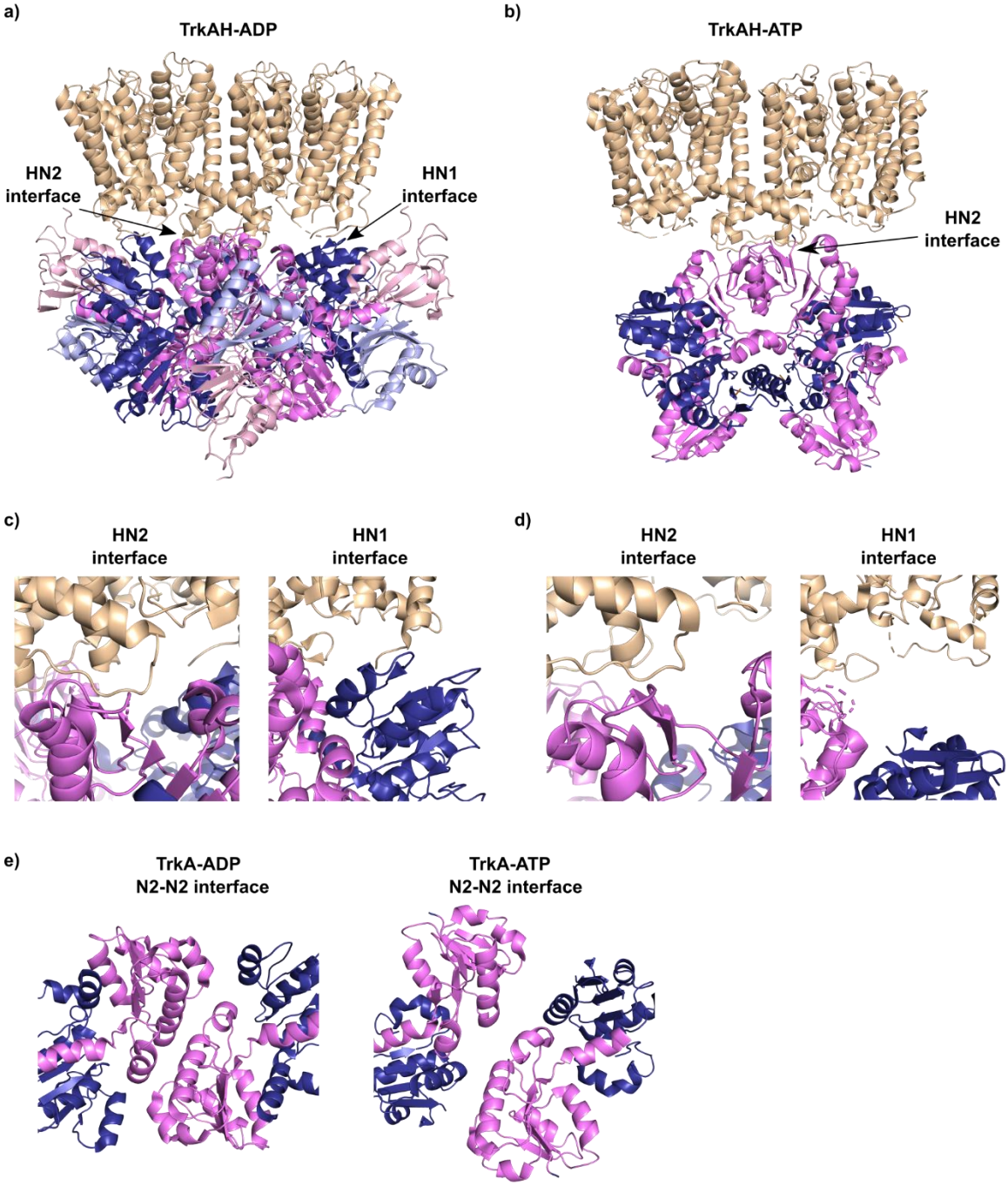

Figure 6: ADP and ATP-bound TrkAH structures. Membrane views of the TrkAH complexes **a)** ADP-bound and **b)** ATP-bound, depicting conformational changes in the TrkH-TrkA contacts and disruption of the HN1 interface in the ATP-bound TrkAH. Close-up views are shown for the HN1 and HN2 interfaces for **c)** TrkAH-ADP and **d)** TrkAH-ATP, showing no major changes in the HN2 interface. **e)** Close-up view of the ADP (left) and ATP-bound (right) TrkA N2-N2 interfaces, depicting the disruption of the N2-N2 interface in the ATP bound state. TrkH is shown in wheat. In each TrkA protomer, the N and C-terminal domains are shown in blue and grey, respectively, for RCK1 and in violet and pink for RCK2. In b), TrkA C-terminal domains are absent in the ring, since they were not modelled in the structure due to poor density in these regions.

A Cryo-EM structure of TrkAH bound to ATP and an X-ray crystallography structure of TrkAH bound to ADP have recently been solved (H. Zhang, et al., 2020), providing new insights on the regulatory mechanism of this channel. In the ADP-bound structure the channel is in a closed conformation, similar to the one previously obtained in the NADH-bound TrkAH structure. This structure revealed that each TrkH monomer interacts with both the N1 and N2 domains of TrkA (HN1 and HN2 interfaces, respectively), and not only with the N2 domain as previously described (Figure 6a and 6c). The ATP-bound structure provides a new perspective of TrkAH regulation. In this structure, TrkH is partially open and only interacts with TrkA through the HN2 interface (Figure 6b and 6d). ATP appears to bind in the TrkA N1 and N2 domains. Binding of ATP leads to conformational changes in the TrkA gating ring that involve a rotation of the N2 domains relative to the N1 domains. This rotation disrupts the N2-N2 interface, resulting in the breaking of the TrkA tetramer into two dimers and forcing the N1 domains to move away from TrkH, eliminating the HN1 interaction (Figure 6b, 6d and 6e). However, in this structure TrkA is poorly resolved at the level of the N1 domains and the C-terminal domains could not be modelled. Functional studies performed by the authors support that the HN1 interaction is required to close the channel and that mobility at the N2-N2 interface is required for TrkA-induced opening of TrkH. Nonetheless, the ATP-bound TrkAH channel is only in a partially open state and further studies are required to understand the conformational changes that the channel undergoes to reach a fully-open state.

The mechanism of TrkAH activation proposed by the authors is the following: ADP binding to TrkA stabilizes the TrkA tetrameric gating ring and keeps the channel closed, by promoting interactions with TrkH at the HN1 and HN2 interfaces. Upon ATP binding to TrKA, the N2-N2 interfaces of the ring are disrupted, breaking it into two dimers. The conformational changes that result from this breakage eliminate the HN1 interaction and lead to the opening of TrkH. The opening of the ion permeation pathway results from dilation of the pore-lining helices and movement of the intramembrane loop towards the cytoplasmic side.

KtrAB structure and regulation

KtrAB is a cation channel regulated by nucleotide-dependent conformational changes of its RCK domain KtrA. Binding of ATP to KtrA results in high ion flux, while binding of ADP decreases the flux activity (Kroning et al., 2007; Vieira-Pires, et al., 2013). This channel has been extensively studied, with structures being determined for KtrAB

complexes from *Vibrio alginolyticus* and *Bacillus subtilis*, as well as for KtrA alone bound to different nucleotides (Albright, et al., 2006; Diskowski, et al., 2017; Roosild, et al., 2002; Szollosi, et al., 2016; Vieira-Pires, et al., 2013).

Like TrkH, KtrB assembles as a homodimer in the membrane (Albright et al., 2007; Vieira-Pires, et al., 2013), with each protomer forming an ion permeation pathway. Only one canonical cation binding site in the selectivity filter is confirmed, with the possibility of two others being available (Figure 4b). A recent study of KtrB form *Vibrio algynoliticus* revealed that KtrB is able to bind different cations with similar affinities, in the low milimolar range (K_d of 1.6-3 mM). Interestingly, in the presence of Na^+ or Li^+, the binding affinity for K^+ increased by ten-fold (K_d of 96-260 µM) (Mikusevic, et al., 2019).

As described for TrkH, below the selectivity filter there is an intramembrane loop in repeat D3. Together with the highly conserved arginine residue (R417), this loop blocks access between the selectivity filter and the cytoplasmic pore (Figure 7b). Electron paramagnetic resonance studies revealed movement of the loop in the presence of K^+; point mutations and truncations in the intramembrane loop also showed an increased K^+ flux (Hanelt, Lochte, et al., 2010; Hanelt, Wunnicke, et al., 2010; Vieira-Pires, et al., 2013).

The most striking difference between KtrB and TrkH resides in the C terminus. TrkH has a short C terminus that does not establish any contacts; KtrB has a long C terminus that runs from one protomer to the other, interacting with KtrA, entering the pore of the neighbouring subunit and finishing just below the intramembrane loop (Figure 7b and 7c) (Vieira-Pires, et al., 2013). A highly conserved C-terminal glycine (G445) is positioned close to the intramembrane loop so that its C-terminal carboxylate group interacts with the side chain of a lysine that is part of the intramembrane loop and is conserved in both KtrB (K315) and TrkH (K357) (Figure 7b). This C-terminal glycine does not exist in TrkH. The glycine carboxylate by itself does not appear to have a substantial effect in channel regulation, as shown by truncation studies. However, removal of the last four residues of the KtrB C terminus results in a non-functional channel and impairs the KtrAB complex assembly (Vieira-Pires, et al., 2013); Furthermore, removal of the last 10 or 15 residues of the KtrB C terminus destabilizes the KtrB dimer (Albright, et al., 2007).

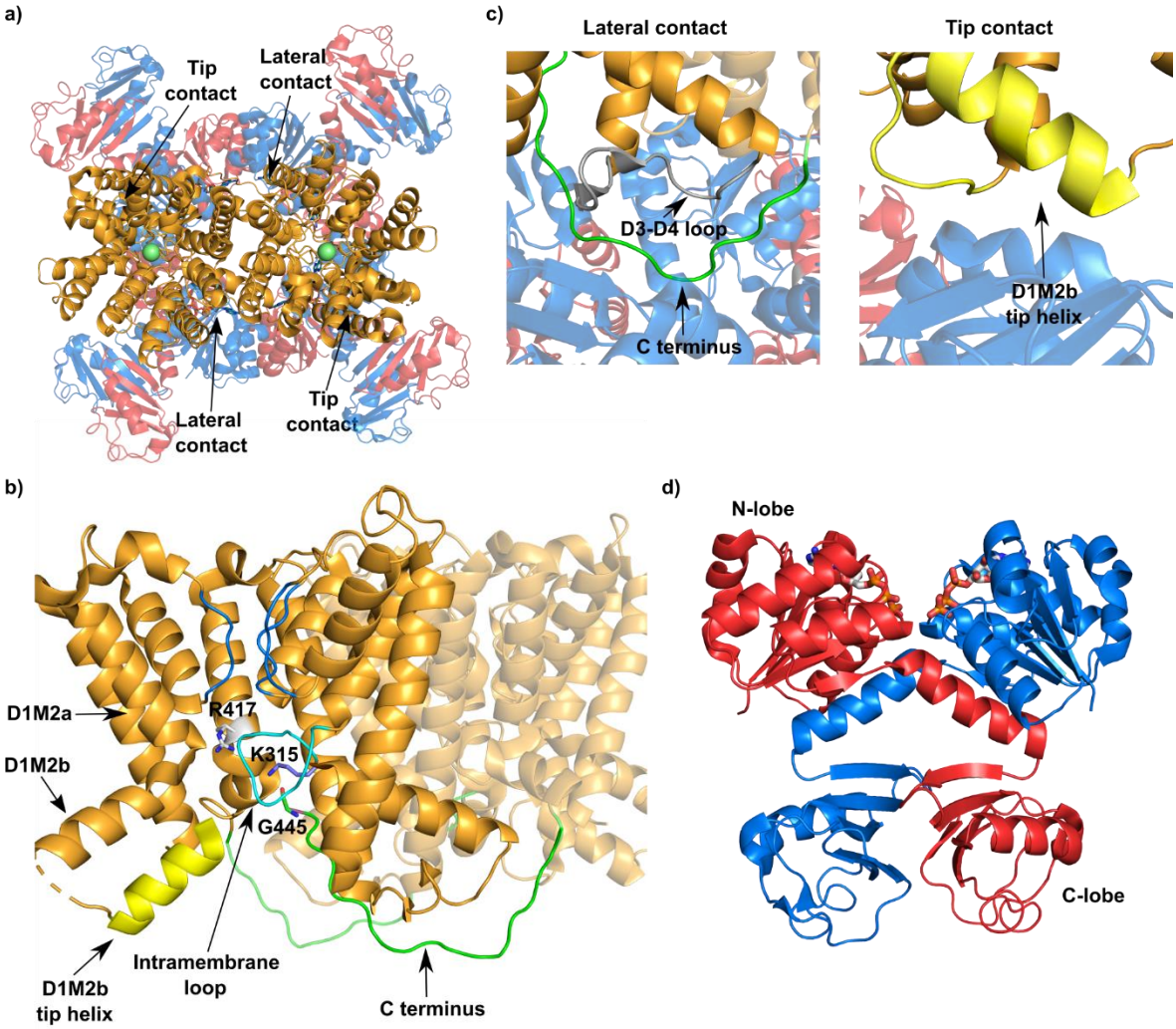

Figure 7: KtrAB structure. a) Extracellular view of the KtrAB complex. A KtrB dimer, shown in orange, sits on top of a KtrA octameric ring formed by four KtrA dimers. KtrA subunits in the ring are alternately colored blue and red. Lateral and tip contact interfaces between KtrB and KtrA are indicated. K^+ ion is shown as green sphere. **b)** Membrane view of the KtrB dimer with relevant structural elements discussed in the text highlighted in one subunit. D2 domain is omitted in this subunit for clarity. Selectivity filter is shown in blue and intramembrane loop in cyan. KtrB long C terminus that protrudes into the opposite subunit is shown in green. D1M2b tip helix is shown in yellow. R417 is shown in white stick, K315 is shown in purple stick and G445 is shown in green stick. **c)** Close-up views of a lateral and a tip contact interface. D3-D4 KtrB loop is shown in grey. KtrB C terminus and D1M2b helix are shown in green and yellow, respectively. **d)** Cartoon representation of an ATP-bound KtrA dimer. Subunits are colored blue and red and ATP is shown in stick representation. N and C-lobe domains are indicated for a KtrA protomer.

The KtrB dimer assembles in a complex with a KtrA octameric gating ring to form the KtrAB channel (Figure 7a). Unlike TrkA, each KtrA protomer only contains one nucleotide-binding RCK domain (Figure 7d). Since the basic KtrA structural unit is a

dimer, the KtrA octameric ring is composed by a tetramer of dimers, with eight N-terminal nucleotide binding sites.

Earlier crystal structures of a C-terminal truncated version of KtrA (KtrAΔc) from *Bacillus subtilis* were obtained with several bound nucleotides, including ATP, ADP, NAD^+ and NADH (Albright, et al., 2006; Roosild, et al., 2002). These structures revealed that the KtrA octameric gating ring is able to adopt different conformations. Three distinct conformations were described: a four-fold symmetric square conformation and two two-fold symmetric conformations (a diamond and a rectangle), that result from diagonal expansions of two opposing KtrA dimers. Curiously, the same conformation was adopted with different ligands. The square conformation was observed with ATP and NADH, the diamond conformation was observed with ADP, NADH and NAD^+ and the rectangle conformation was only obtained with NADH. Biochemical studies showed that both the full-length and the C-terminal truncated versions of KtrA bind ATP and ADP even more tightly than NAD^+ or NADH, suggesting that these two nucleotides are involved in the regulation of KtrAB (Albright, et al., 2006; Kroning, et al., 2007).

Crystal structures of the ATP-bound KtrAB channel and of the native full-length KtrA alone from *Bacillus subtilis*, bound to both ATP and ADP were determined (Vieira-Pires, et al., 2013). Additionally, a crystal structure of the KtrAΔcB bound to ADP and a Cryo-EM structure of the *Vibrio alginolyticus* KtrAB bound to ADP were also obtained (Diskowski, et al., 2017). These structures helped to gain some understanding about the KtrAB regulation mechanism.

The KtrA full-length structures clearly show a different ring conformation for each ligand: a two-fold diamond conformation with ADP and a four-fold square conformation with ATP (Vieira-Pires, et al., 2013) (Figure 11). The conformation of the KtrA ring in the ATP-bound KtrAB complex is very similar to the isolated KtrA ring with ATP. This indicates that, unlike the truncated form where ligand binding is not coupled to ring conformation, in the full-length isolated KtrA the binding of either ATP or ADP determines the conformation of the ring. These results reinforced the essential role played by the C-terminal domain of the RCK protein in the conformation adopted by the octameric ring upon ligand binding.

The ATP-bound KtrAB channel structure revealed that the KtrB dimer sits directly on the face of the KtrA ring, establishing two types of contacts with it through cytoplasmic loops: a lateral contact and a tip contact (Figure 7a and 7c) (Vieira-Pires, et al., 2013).

The lateral contact is established by the D3-D4 loop of a KtrB subunit, a section of the KtrB C terminus of the neighbouring KtrB subunit and the KtrA N-terminal domain. The tip contact occurs at the apexes of the cytoplasmatic face of KtrB, where the D1M2b tip helix interacts with two opposing KtrA subunits (Figure 7c). However, even though ATP binding leads to the activation of the KtrAB channel (Szollosi, et al., 2016; Vieira-Pires, et al., 2013), the ATP-bound KtrAB structure captured a state where the channel pores are closed, with the intramembrane loop occluding the ion permeation pathway, possibly because the protein was crystallized in detergent.

The ADP-bound KtrAΔcB crystal structure and KtrAB Cryo-EM structure revealed details of the low activity state of the channel (Diskowski, et al., 2017; Szollosi, et al., 2016). In these structures, the KtrB homodimer displays a similar conformation to that observed in the ATP-bound state. The KtrB protomers interaction involves their C-termini, which also establishes lateral contacts with the KtrA octameric ring. However, the RCK ring adopts a non-square conformation and is asymmetrically expanded along the diagonal defined by the tip contacts. The most interesting feature observed in the Cryo-EM structure of the low activity state is related to the KtrB D1M2 helix. In the ATP-bound state the D1M2 helix is divided in three regions: M2a, M2b and the M2b tip helix, with the tip helix bent towards the membrane (Figure 7b). In the ADP-bound state, D1M2b forms a continuous helix that is fully extended towards the cytoplasmic side, poking through the inner hole of the KtrA ring (Figure 8). Furthermore, the KtrB D4M2 helix also seems to straighten in the ADP bound state compared to the bending observed in the ATP bound state in the vicinity of the conserved R417. Unfortunately, the resolution of the structure does not allow mapping of the specific contacts established by the KtrB D1M2b helix and KtrA, but the interaction is likely to occur with residues in the vicinity of the ADP binding site. For the same reason, the conformation of the gate composed by the intramembrane loop and R417 could not be analysed.

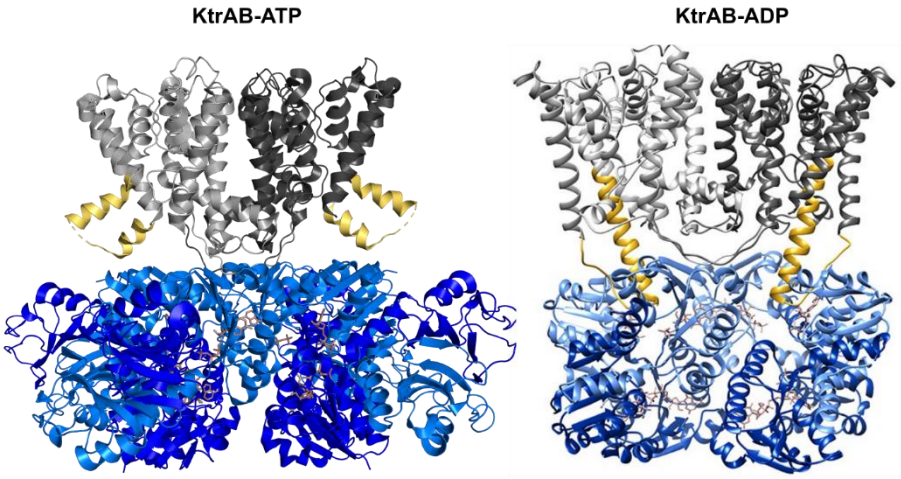

Figure 8: ATP and ADP-bound KtrAB structures. Side view of the KtrAB complex bound to ATP or ADP, showing the conformational rearrangement of the D1M2b helix, protruding into the KtrA ring in the ADP-bound state. KtrB subunits are shown in light and dark grey and KtrA ring subunits are alternately colored light and dark blue. D1M2b helix is shown in yellow. KtrAB-ADP structure image was adapted from (Diskowski, et al., 2017) due to the lack of an available model in the PDB.

An activation mechanism was proposed in which, in the ADP-bound state, the KtrAB channel is in a closed state with the KtrB D1M2 helix fully extended and interacting with the KtrA gating ring. This D1M2 conformation, together with the straightening of the D4M2 helix, stabilizes the occlusion of the permeation pathway by the intramembrane loop/R417 gating region. Upon ADP replacement by ATP, the KtrA octameric ring contracts and adopts a square conformation. This conformational change causes the KtrB D1M2b helix to retract towards the membrane and bend forming a tip helix. This conformational change is accompanied by alterations in the KtrB D4M2 helix and at the level of the intramembrane loop/R417 that lead to channel opening.

Nonetheless, as previously stated, the ATP-bound KtrAB structure does not display an open pore and the intramembrane loop occludes the ion conduction pathway. In addition, the mechanistic details that induce KtrA ring conformational changes upon ATP binding are not yet well understood. On another note, the ATP-bound KtrA octameric ring shows no evidence of ring breakage upon ATP binding, as reported for TrkA. This indicates that the TrkAH and KtrAB activation mechanisms differ. Therefore, more structural and functional studies are needed in order to discern the nucleotide-dependent activation mechanism of KtrAB.

Physiological role of cyclic nucleotides

Recently, c-di-AMP, a cyclic dinucleotide, was shown to bind to the C-terminal domain of a KtrA ortholog (R. M. Corrigan et al., 2013) and to regulate KtrAB expression in *B.subtilis* (Nelson et al., 2013). As such, this molecule has been suggested to play a role in the regulation of the cation channel.

All organisms rely on nucleotide-based signal transduction to respond to diverse cellular stimuli. Cyclic mono and dinucleotides have been known to act as second messengers, regulating signalling pathways that control many physiological processes in both prokaryotic and eukaryotic cells in response to external stimuli (Kalia et al., 2013). In microorganisms, such as bacteria, this signal amplification and relay becomes especially important in order for them to adapt to environmental changes.

To date, cyclic nucleotide second messengers include the mononucleotides cyclic adenosine monophosphate (cAMP) and cyclic guanosine monophosphate (cGMP), as well as the dinucleotides cyclic dimeric adenosine monophosphate (c-di-AMP), cyclic dimeric guanosine monophosphate (c-di-GMP) and cyclic guanosine monophosphate-adenosine monophosphate (cGAMP). Recently, the synthesis of cyclic dimeric uridine monophosphate (c-di-UMP) and cyclic uridine monophosphate-adenosine monophosphate (cUMP-AMP) have also been reported in bacteria, however their physiological role needs to be further explored (Whiteley et al., 2019).

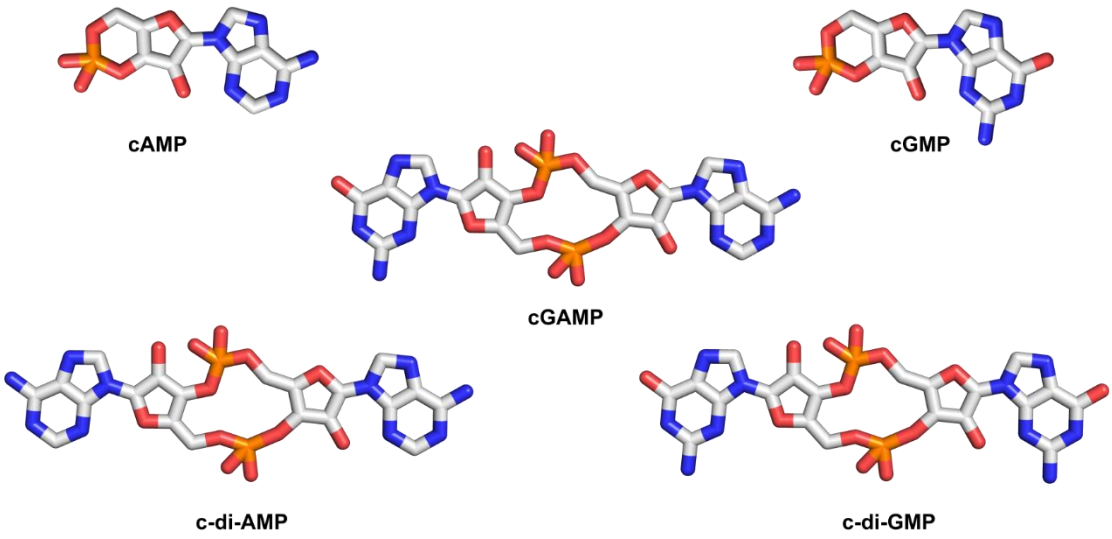

Figure 9: Structural representation of cyclic mono and dinucleotide second messengers.

Among these nucleotides, the first second messenger to be described was cAMP (Makman & Sutherland, 1965; Okabayashi et al., 1963; Rall & Sutherland, 1958; E. W. Sutherland & Rall, 1958). This molecule is produced from ATP by adenylate cyclases and degraded to AMP by phosphodiesterases. cAMP binds to protein targets and induces conformational changes that relay the signal downstream. This nucleotide functions as a major gene expression regulator, being involved in several biological processes in both eukaryotes and prokaryotes. In eukaryotes, cAMP binds mainly to protein kinase A (PKA) (Walsh et al., 1968), cyclic nucleotide-gated ion channels (Nakamura & Gold, 1987) and the Epac guanine-nucleotide exchange factors (de Rooij et al., 1998; Kawasaki et al., 1998), playing a role in processes such as metabolism regulation (Berthet et al., 1957), cell growth, division and differentiation (Burgering et al., 1993; Cook & McCormick, 1993; A. Y. Liu, 1982; Schwartz & Rubin, 1983; Withers et al., 1995), memory formation (Pittenger et al., 2002), ion channel conductivity (Li et al., 1993) and immunity (Torgersen et al., 2002). In bacteria this molecule is involved in carbon catabolite repression (glucose preference) (Botsford & Drexler, 1978; Peterkofsky & Gazdar, 1971), biofilm formation (Liang et al., 2007) and virulence control (Lowrie et al., 1975; Petersen & Young, 2002; Rickman et al., 2005), among other processes.

The other mononucleotide second messenger, cGMP, was firstly isolated from rat urine (Ashman et al., 1963) and has been extensively studied in eukaryotes, but less so in prokaryotes. This nucleotide is formed from GTP by guanylate cyclases and degraded to GMP by phosphodiesterases. In eukaryotes, cGMP is involved in photoreception by regulation of cation channel conduction (Fesenko et al., 1985). It also plays a role in smooth muscle relaxation (Ignarro et al., 1987; Rapoport & Murad, 1983), neurotransmission (Stone & Taylor, 1977) and cellular apoptosis (Garthwaite & Garthwaite, 1988); furthermore, this nucleotide regulates cAMP production through interaction with cAMP phosphodiesterases and is involved in some of the same signalling pathways, such as glycogenolysis (Brass & Vetter, 1993) and olfactory regulation (Pietrobon et al., 2011), being essential to the correct functioning of vital organs. The role of cGMP in bacteria is less understood but this molecule was already shown to be involved in UV-B stress response (Cadoret et al., 2005) and cyst development (Marden et al., 2011), as well as in biofilm formation and virulence (An et al., 2013).

Cyclic dimeric guanosine monophosphate (c-di-GMP) was the first cyclic dinucleotide to be reported and has emerged as a ubiquitous bacterial second messenger. This cyclic dinucleotide is obtained from the condensation of 2 molecules of GTP by the action of diguanylate cyclases, and degraded to either 5'-Phosphoguanylyl-(3',5')-guanosine (pGpG) or GMP by phosphodiesterases (Galperin et al., 1999; Merkel et al., 1998; Tal et al., 1998). c-di-GMP was first discovered in 1987 as an allosteric activator of a cellulose synthase in *Gluconoacetobacter xylinus* (Ross et al., 1987). Several years later, this cyclic dinucleotide has been shown to be involved in several bacterial physiological processes, with a prominent role in virulence and in the shift from a motile to a sessile biofilm associated lifestyle (Kulesekara et al., 2006; Simm et al., 2004; Tischler & Camilli, 2004, 2005). Some of these processes include: cell cycle regulation (Abel et al., 2013; Hecht & Newton, 1995; Lori et al., 2015; R. Paul et al., 2004), synthesis of exopolysaccharides (Merighi et al., 2007; Ross, et al., 1987; Tagliabue et al., 2010), production of toxins and virulence factors (McKee et al., 2013), quorum sensing (Deng et al., 2012) and chemotaxis (K. Paul et al., 2010; Russell et al., 2013). c-di-GMP is also able to bind to the stimulator of interferon genes (STING) and stimulate the mammalian immune response (McWhirter et al., 2009) and its first case of eukaryotic production was detected in *Dictyostelium* amoebas, where it triggers stalk cell differentiation (Chen & Schaap, 2012). The central role of c-di-GMP in bacterial lifestyle and the fact that it is not produced in mammalian cells made this molecule and associated signalling pathways an interesting target for the development of novel antimicrobial therapies (Karaolis et al., 2007; B. Kim et al., 2018; Ogunniyi et al., 2008; Sambanthamoorthy et al., 2012).

cGAMP is one of the most recently explored cyclic dinucleotides, being first discovered as a signalling molecule in *Vibrio cholera* (Davies et al., 2012). This nucleotide is synthesized from ATP and GTP by a subset of dinucleotide cyclases containing SMODS domains (Second Messenger Oligonucleotide or Dinucleotide Synthetase) in bacteria and by cGAS synthases in eukaryotes (Ablasser et al., 2013; Hallberg et al., 2016). Two structural versions of this cyclic nucleotide have currently been reported: a canonical 3'-3'-cGAMP is synthesized in bacteria and a non-canonical 2'-3'-cGAMP has been reported in eukaryotes. Both forms of cGAMP are involved in the STING immune response pathway in eukaryotes (Ablasser, et al., 2013; Davies, et al., 2012; Diner et al., 2013; Gao et al., 2013; Sun et al., 2013). In bacteria, cGAMP has been shown to play a role in chemotaxis and virulence (Davies, et al., 2012), extracellular electron transfer or exoelectrogenesis (Kellenberger et al., 2015; Nelson et al., 2015),

phospholipase activity (Severin et al., 2018) and resistance to phage infection (Cohen et al., 2019),

c-di-AMP

Cyclic dimeric adenosine monophosphate (c-di-AMP) is the second cyclic dinucleotide shown to be produced by bacteria, after c-di-GMP. c-di-AMP is synthesised through the condensation of 2 ATP molecules by diadenylate cyclases and degraded to 5'-Phosphoadenylyl-(3',5')-adenosine (pApA) or AMP by phosphodiesterases. This nucleotide was first obtained *in vitro* in 1985, in an attempt to find RNA polymerase inhibitors (Jenny et al., 1985). However, evidence for its biological production only arose in 2008, when c-di-AMP was identified in the crystal structure of the *Thermotoga maritima* DisA, whose homolog in *Bacillus subtilis* acts as a sporulation checkpoint by scanning the DNA integrity for double-stranded breaks (Oppenheimer-Shaanan et al., 2011; G. Witte et al., 2008). Later on, this nucleotide was detected in the cytosol of *Listeria monocytogenes* and shown to be secreted into the cytosol of the eukaryotic cell harbouring the bacteria, resulting in IFN-β production (Woodward et al., 2010). Since then, it has also been found in archaea (Braun et al., 2019) and in numerous bacteria, including *Streptococcus pneumoniae* (Y. Bai et al., 2013), *Streptococcus pyogenes* (Kamegaya et al., 2011), *Bacillus subtilis* (Oppenheimer-Shaanan, et al., 2011; G. Witte, et al., 2008), *Chlamydia trachomatis* (Barker et al., 2013), *Staphylococcus aureus* (Rebecca M. Corrigan et al., 2011), *Borrelia burgdorferi* (Savage et al., 2015), *Mycobacterium tuberculosis* (Yinlan Bai et al., 2012), *Mycobacterium smegmatis* (L. Zhang & He, 2013), *Lactococcus lactis* (W. M. Smith et al., 2012; Zhu et al., 2016) and *Mycoplasma pneumoniae* (Blötz et al., 2017). Interestingly, a phylogenetic survey of the c-di-AMP turnover machinery revealed that the majority of the bacterial species that do not possess the domains required to produce this nucleotide are subdivisions of the phylum Proteobacteria. Furthermore, these encode multiple c-di-GMP regulatory enzymes and are the group where signalling by this cyclic dinucleotide has been more extensively studied (He et al., 2020).

<u>c-di-AMP signalling pathways</u>

c-di-AMP is the only second messenger known to the date which is both essential and toxic for many of the organisms that produce it, being coined as an “essential poison”

(Gundlach et al., 2015). It regulates multiple physiological processes by binding to target receptors, proteins and RNA molecules, namely riboswitches.

These processes include: monitoring DNA integrity (Oppenheimer-Shaanan, et al., 2011; G. Witte, et al., 2008), sporulation (Oppenheimer-Shaanan, et al., 2011; C. Zheng et al., 2015), peptidoglycan and fatty acids biosynthesis (Luo & Helmann, 2012; Tang et al., 2015; Zhu, et al., 2016), biofilm formation (Gundlach et al., 2016; Peng et al., 2016), regulation of cell size, growth, competence and central metabolism (Y. Bai, et al., 2013; Rebecca M. Corrigan, et al., 2011; Sureka et al., 2014; Whiteley et al., 2017; M. Ye et al., 2014; Zarrella et al., 2020), resistance to acid stress and cold shock (Bowman et al., 2016; S. Liu et al., 2006; L. Zhang et al., 2013), antibiotic susceptibility (Cho & Kang, 2013; Luo & Helmann, 2012) and regulation of light-dark cycle in cyanobacteria (Rubin et al., 2018). This cyclic dinucleotide has also been shown to be involved in the virulence of multiple pathogens and in the eukaryotic immune response upon being released into the cytosol (Abdul-Sater et al., 2013; Y. Bai, et al., 2013; Cho & Kang, 2013; McFarland et al., 2017; C. E. Witte et al., 2013; Woodward, et al., 2010; Xia et al., 2018; Yang et al., 2014; M. Ye, et al., 2014). This role in the immune response and the fact that c-di-AMP is not produced in eukaryotes led to attempts to use this cyclic dinucleotide as an adjuvant for vaccination (I. Quintana et al., 2018; Volckmar et al., 2019). Finally, c-di-AMP was shown to play a central role in osmoregulation by regulating both potassium and compatible solute homeostasis (Y. Bai et al., 2014; Commichau & Stülke, 2018; R. M. Corrigan, et al., 2013; Gibhardt et al., 2019; Gundlach et al., 2017; Gundlach et al., 2019; Huynh et al., 2016; Krüger et al., 2020b; Moscoso et al., 2016; Pham et al., 2018; I. M. Quintana et al., 2019; Schuster et al., 2016).

c-di-AMP regulation of the *B.subtilis* potassium homeostasis

Bacillus subtilis is one of the organisms where c-di-AMP is an important second messenger (Gundlach, et al., 2015). The crucial role of c-di-AMP in potassium homeostasis is highlighted by the fact that this nucleotide's intracellular levels are tuned according to the internal potassium concentration and, furthermore, the *B.subtilis* potassium uptake and export machinery is directly regulated by c-di-AMP. In this Gram-positive bacteria, potassium uptake is mediated by the KimA potassium transporter and by the Ktr cation channel system composed by the ion conducting membrane proteins KtrB and KtrD and the cytosolic regulatory proteins KtrA and KtrC (Gundlach, et al., 2017; Holtmann, et al., 2003; Tascón et al., 2020). On the other hand, potassium export is mediated by the KhtTU transporter, composed by the membrane protein KhtU and

the cytosolic regulatory protein KhtT (Makoto Fujisawa et al., 2004), by the YugO potassium channel (Lundberg et al., 2013) and by the NhaK transporter (M. Fujisawa et al., 2005). YjbQ, a putative cation/proton antiporter, is also present in *B.subtilis* and was recently shown to bind c-di-AMP (Gundlach, et al., 2019). An *S.aureus* ortholog as already been shown to transport K^+ and to be activated by c-di-AMP (Chin et al., 2015) however, the function of this transporter and the role of c-di-AMP in its regulation still need to be characterized in *B.subtilis*.

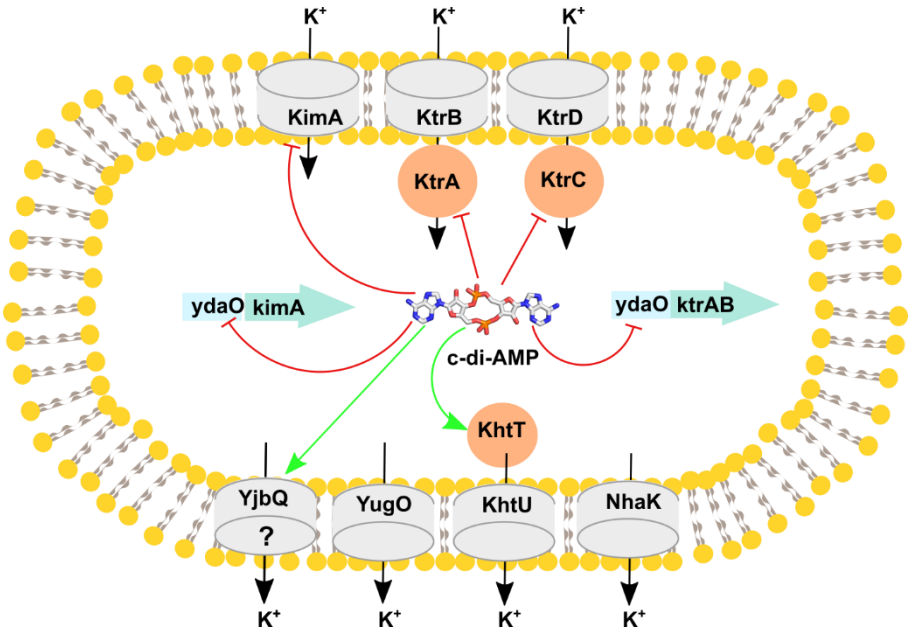

Figure 10: Regulation of the *B.subtilis* K^+ homeostasis machinery by c-di-AMP. The scheme illustrates the currently proposed mechanism of K^+ uptake and efflux systems regulation by c-di-AMP. Proposed enhanced activity or inhibition of the channels or transporters upon binding of c-di-AMP is indicated by green or red arrows, respectively. Inhibition of *kimA* and *ktrAB* transcription through binding of c-di-AMP to the ydaO riboswitch is also shown.

Regulation of potassium homeostasis in *B.subtilis* by this cyclic dinuleotide has been extensively studied. The currently proposed mechanism is the following: Accumulation of potassium inside the cell stimulates c-di-AMP production and leads to the inhibition of the Ktr and KimA K^+ uptake systems, both by binding directly to the proteins and by reducing transcription. Transcription of the *ktrAB* and *kimA* operons is regulated by the *ydaO* riboswitch that responds to c-di-AMP (Nelson, et al., 2013). c-di-AMP has also been proposed to bind and activate the K^+ export systems, allowing potassium efflux and leading to c-di-AMP degradation (Gundlach, et al., 2017; Gundlach, et al., 2019; Nelson, et al., 2013; Rocha, et al., 2019). However, there is little or no data demonstrating a direct functional effect of c-di-AMP on any of these proteins.

II. AIMS OF THE WORK

The main aim of this work is to gain further insights into the molecular mechanisms of regulation of the KtrAB cation channel from *Bacillus subtilis*. Two major aspects were addressed: 1) the mechanism of ATP-dependent activation in KtrA, particularly the characterization of crucial residues and cation binding in the N-terminal nucleotide binding pocket, and 2) binding of c-di-AMP to the two Ktr cytosolic regulatory subunits of *Bacillus subtilis*, KtrA and KtrC, and analysis of the role of this cyclic dinucleotide in Ktr channel function.

We are interested in understanding how binding of nucleotide molecules to the regulatory subunits promotes conformational changes that are propagated to KtrB and regulate the activation of the channel. In order to do this, a biochemical, functional and structural characterization of the role of divalent cations in the ATP-bound KtrA and of c-di-AMP binding to KtrA and KtrC was performed. Biophysical techniques such as isothermal titration calorimetry and x-ray crystallography were employed. Functional characterization was conducted by using an *E.coli* phenotype complementation assay and an *in vitro* fluorescence-based K^+ flux assay.

III. ACTIVATION OF THE KtrA RCK DOMAIN REQUIRES BINDING OF A CATION COFACTOR TO A CONSERVED SITE

The work presented in this chapter has been published in:

Teixeira-Duarte, C. M., Fonseca, F., & Morais-Cabral, J. H. (2019). Activation of a nucleotide-dependent RCK domain requires binding of a cation cofactor to a conserved site. *eLife*, 8, e50661. https://doi.org/10.7554/eLife.50661

INTRODUCTION

The KtrAB channel activity is regulated by KtrA, a cytosolic nucleotide-dependent RCK domain. KtrA binds to ATP and ADP and assembles as an octameric ring that adopts different conformations upon nucleotide binding. ATP binding induces the adoption of a square-conformation and increased K^+ flux activity through the channel; ADP binding results in a non-square conformation and decreased K^+ flux. However, the molecular mechanisms that underlie ligand-dependent conformational changes in nucleotide-dependent RCK domains are still not well understood. Therefore, it is still not clear how ATP binding induces the adoption of the square-activated conformation by the KtrA octameric ring.

In this chapter, the mechanism of nucleotide-dependent activation in KtrA was explored. In particular, we sought to identify residues in the KtrA intra-dimer interface that are vital for activation in the presence of ATP and to demonstrate the role of these residues.

MATERIALS AND METHODS

Cloning

N-terminal Strep-tagged KtrB was cloned in a pRSFDuet-1 expression vector. Tag-less wild-type KtrA and respective site-directed mutants were cloned in a pET-24d expression vector. The mutants were created with the QuikChange Site-Directed Mutagenesis Kit (Agilent), using the following oligonucleotide primers:

KtrA mutant	Primers
R16A	Forward: 5'-ATCGGGCTGGGCGCCTTTGGCGGCAGCATTTG-3' Reverse: 5'-CAAATGCTGCCGCCAAAGGCGCCCAGCCCGATC-3'
R16K	Forward: 5'-GATCGGGCTGGGCAAGTTTGGCGGCAGCATTTG-3' Reverse: 5'-CAAATGCTGCCGCCAAACTTGCCCAGCCCGATC-3'
A80P	Forward: 5'-GTGATTGTTGCCATCGGACCAAATATTCAAGCGAGTA-3 Reverse: 5'-TACTCGCTTGAATATTTGGTCCGATGGCAACAATCAC-3'
E125Q	Forward: 5'-GCTGACCGCATTATTCATCCTCAGAAAGATATGGGGGTTAAAATC-3' Reverse: 5'-GATTTTAACCCCCATATCTTTCTGAGGATGAATAATGCGGTCAGC-3'

Protein Expression and Purification

Tag-less wild-type KtrA and respective mutants were over-expressed in the *Escherichia coli* BL21 (DE3) strain. Cells transformed with an expression vector were grown at 37 ºC with agitation in LB medium supplemented with 50 mg/L of kanamycin to an optical density at 600 nm (OD_{600}) of 0.6-0.8. At this point, the cultures were placed in ice for 30 min (to induce cold-shock chaperones). Ethanol was then added dropwise to a final concentration of 2% (v/v) (to induce expression of heat-shock chaperones); IPTG was added to a final concentration of 0.5 mM for overnight induction at 20 ºC (14-16 h) and

cells were harvested by centrifugation. Cell lysis was done in Buffer A (50 mM Tris-HCl pH 7.5, 50 mM KCl, 5 mM DTT) supplemented with protease inhibitors (1 mM PMSF, 1 µg/mL leupeptin, 1 µg/mL pepstatin A) using a cooled cell cracker Emulsiflex-C5 (Avestin). Lysate was cleared by centrifugation and the supernatant was loaded into an anion exchange column Hi-Trap Sepharose Q-HP (GE Healthcare). KtrA was eluted with a 50-1000 mM KCl gradient. Protein-containing fractions were pooled and incubated with an ATP-agarose resin (Immobilized γ-Aminophenyl-ATP C10-spacer from Jena Bioscience) overnight at 4 °C with gentle agitation. The resin was then washed thoroughly with Buffer B (50 mM Tris-HCl pH 8.0, 150 mM KCl, 1 mM TCEP) and protein was eluted in Buffer B supplemented with 5 mM ADP or ATP (sodium salts). Protein was concentrated to ~5 mg/ml and further purified by size-exclusion chromatography in a Superdex-S200 (GE Healthcare) column using Buffer C (50 mM Tris-HCl pH 7.5, 150 mM KCl, 5 mM DTT). Eluted KtrA was supplemented with 1 mM ATP or ADP. Protein concentration was determined using with a colorimetric assay (Bio-Rad). For complex assembly with KtrB and reconstitution in proteoliposomes, all buffers throughout the purification contained 1 mM Ethylenediaminetetraacetic acid (EDTA) in order to prevent contamination with divalent cations. In this case, the final size-exclusion chromatography step contained 0.2 mM EDTA.

N-terminal Strep-tagged KtrB was over-expressed in the *Escherichia coli* BL21 (DE3) strain. Cells transformed with an expression vector were grown at 37 ºC with agitation in LB medium supplemented with 50 mg/L of kanamycin to an optical density at 600 nm (OD_{600}) of 0.9-1.0. Protein expression was induced at 37 °C for 2.5 h with the addition of 0.5 mM IPTG and 1 mM $BaCl_2$. Cells were lysed in Buffer D (50 mM Tris-HCl pH 8.0, 120 mM NaCl, 30 mM KCl, 1 mM EDTA) supplemented with protease inhibitors (1 mM PMSF, 1 µg/mL leupeptin, 1 µg/mL pepstatin A) using a cooled cell cracker Emulsiflex-C5 (Avestin). KtrB was extracted with 40 mM n-dodecyl-β-D-maltoside (DDM) (Sol-grade from Anatrace) overnight at 4 °C with gentle agitation. Spin-cleared lysate was loaded into a Strep-Tactin Sepharose resin (IBA Lifesciences) and washed with Buffer E (50 mM Tris-HCl pH 8.0, 120 mM NaCl, 30 mM KCl, 1 mM DDM, 5 mM DTT, 1 mM EDTA, 1 mM ATP or ADP).

To assemble the KtrAB complex, purified KtrA-ATP or ADP was added to the resin and incubated for 30 min at 4 ºC with gentle agitation. The resin was thoroughly washed with Buffer E and KtrAB was eluted with Buffer E supplemented with 5 mM desthiobiotin. The eluted protein was dialysed overnight at 4 ºC against Buffer F (50 mM Tris-HCl pH 8.0; 120 mM NaCl; 30 mM KCl; 0.5 mM DDM; 5 mM DTT), in the presence of thrombin for KtrB tag cleavage. For proteoliposome reconstitution, Buffer F was replaced by

Buffer G (10 mM HEPES, 7 mM N-methyl-D-glucamine (NMG) (pH 8.0), 150 mM KCl, 0.5 mM DDM, 5 mM DTT, 1mM EDTA). Protein was further purified by size-exclusion chromatography in a Superdex-S200 (GE Healthcare) column using Buffer F or Buffer G containing 0.2 mM EDTA. Eluted fractions corresponding to KtrAB were pooled, concentrated to 1 mg/ml and used for proteoliposome preparation when required. No nucleotide was added during dialysis and size-exclusion chromatography. Protein concentration was estimated by measuring absorbance at 280 nm on a NanoDrop ND-1000 Spectrophotometer (NanoDrop Technologies). KtrB alone was purified in the same manner as the KtrAB complexes without the KtrA addition step.

Crystallization

KtrA-ATP and KtrA-ADP (wild-type and mutants) were purified in buffer C and supplemented with 1 mM ATP or ADP, respectively. Crystals were grown using the sitting-drop vapour diffusion method at 20 ºC.

$KtrA_{WT}$-ATP-Ca^{2+} crystals were obtained by supplementing KtrA-ATP with 5 mM $CaCl_2$ after size-exclusion chromatography. Crystals grew in 100 mM HEPES-NaOH pH 8.0, 5% PEG 6000, 2.5% MPD (2-Methyl-2,4-pentanediol). Before being flash-cooled in liquid nitrogen, crystals were cryoprotected by sequential transfer to 100 mM HEPES pH 8.0, 6% PEG 6000, 2.5% MPD, 0.5 mM ATP, 2.5 mM $CaCl_2$, supplemented with 15% and 30% glycerol.

$KtrA_{R16K}$-ATP crystals grew in 100 mM Tris-HCl pH 8.5, 8% PEG 8000. Before being flash-cooled in liquid nitrogen, crystals were cryoprotected using 20% glycerol by adding 100 mM Tris-HCl pH 8.5, 10% PEG 8000, 0.5 mM ATP, 25% glycerol solution directly to the drop and equilibrating before freezing.

$KtrA_{R16K}$-ADP crystals grew in 100 mM HEPES-NaOH pH 7.5, 6 to 8% PEG 8000, 20% ethylene glycol and were directly flash-cooled in liquid nitrogen.

$KtrA_{R16A}$-ATP crystals grew in 100 mM HEPES-NaOH pH 7.5, 2% PEG 6000, 1% MPD. Before being flash-cooled in liquid nitrogen, crystals were cryoprotected with 100 mM HEPES-NaOH pH 7.5, 6% PEG 6000, 25% ethylene glycol solution.

$KtrA_{R16A}$-ADP crystals grew in a solution optimized from solution number 2-30 of the Morpheus crystallization kit (Molecular Dimensions), containing 5% PEG 8000 and 20%

ethylene glycol. Before being flash-cooled in liquid nitrogen, crystals were cryoprotected by transferring to mother liquor containing 12% PEG 8000.

$KtrA_{E125Q}$-ATP crystals grew in 100 mM MES pH 6.5, 6% PEG 4000, 20% glycerol. Before being flash-cooled in liquid nitrogen, crystals were cryoprotected with 100 mM MES pH 6.5, 12% PEG 4000, 20% glycerol solution.

$KtrA_{E125Q}$-ADP crystals grew in 100 mM ADA pH 6.5, 4% PEG 4000, 20% glycerol. Before being flash-cooled in liquid nitrogen, crystals were cryoprotected by transferring to 100 mM ADA pH 6.5, 12% PEG 4000, 20% glycerol solution.

$KtrA_{A80P}$-ATP crystals grew in 100 mM HEPES-NaOH pH 7.5, 1% PEG 6000, 2% MPD. Before being flash-cooled in liquid nitrogen, crystals were cryoprotected with 100 mM HEPES-NaOH pH 7.5, 6% PEG 6000, 2% MPD, 25% ethylene glycol solution.

$KtrA_{A80P}$-ADP crystals grew in 100 mM HEPES-NaOH pH 7.5, 2% PEG 4000, 20% glycerol. Crystals were cryoprotected with to 100 mM HEPES-NaOH pH 7.5, 12% PEG 4000, 20% glycerol solution, before being flash-cooled in liquid nitrogen.

Data processing and structure determination

Diffraction data were collected at ALBA Synchrotron, Barcelona, Spain; European Synchrotron Radiation Facility (ESRF), Grenoble, France, and French National Synchrotron Source (SOLEIL), Gif-sur-Yvette, France. Data were processed using XDS (Kabsch, 2010) and AIMLESS (Evans & Murshudov, 2013) from the CCP4 program suite (Winn et al., 2011). $KtrA_{R16K}$-ATP and $KtrA_{WT}$-ATP-Ca^{2+} structures were determined by molecular replacement with Phaser (McCoy et al., 2007) using a $KtrA_{WT}$-ATP dimer (PDB: 4J90) and a $KtrA_{R16K}$-ATP dimer (PDB: 6S2J) as search models, respectively. Final models were obtained after several manual model building rounds in Coot (Emsley et al., 2010) and refinement with Phenix (Adams et al., 2010). The lower resolution structures were solved by molecular replacement with Phaser using a $KtrA_{WT}$-ATP dimer as template (PDB: 4J90). Refinement was limited to an initial rigid body and TLS single group refinement in Phenix (Adams, et al., 2010)(Adams, et al., 2010), followed by minimal adjustments to resolve stereo-chemical violations in Coot and refinement with secondary structure and non-crystallographic restraints in Phenix. Figures were created using PyMOL (Delano, 2002).

E.coli phenotype complementation assay

The complementation assay with the *E.coli* TK2420 strain (Δ(*kdpFAB*)5 Δ(*trkA-mscL'*) *trkD1*) was performed as previously described (Albright, et al., 2007; Vieira-Pires, et al., 2013) with a few modifications. Wild-type KtrB and KtrA (wild-type or mutants) were cloned into a dicistronic constitutive expression plasmid (pKCe). Empty pKCe plasmid was used as a negative control. Transformed cells were plated on LBK (Lysogeny broth where NaCl is replaced by KCl) agar plates containing 100 µg/mL Ampicillin. Three individual colonies for each protein version were picked and grown separately in 5 mL pre-cultures of minimal media containing 30 mM K^+, supplemented with 100 µg/mL Ampicillin, overnight at 37 °C, with agitation. A 5 µL aliquot of the overnight cultures was then used to inoculate 5 mL of minimal media, supplemented with 100 µg/mL Ampicillin, prepared with different K^+ concentrations (0.1, 0.3, 1, 2, 6, 10, 30 or 115 mM) and incubated at 37 °C with agitation. Optical density at 595 nm was measured after 16 h.
The minimal media contained the following composition: 8 mM $(NH_4)_2S0_4$, 400 µM $MgSO_4$, 6 µM $FeSO_4$, 6 µM ferric chloride, 1 mM sodium citrate, 1 mg/L thiamine-HCl, 2 g/L glucose, 10 mg/L $CaCl_2$, 69 mM phosphate buffer and 115 mM (K^+ + Na^+). A fixed ratio of hydrogen phosphate to dihydrogen phosphate was used to maintain the pH and overall phosphate concentration constant, even as the K^+:Na^+ ratios varied. Phosphate component concentrations (K_2HPO_4, KH_2PO_4, Na_2HPO_4, NaH_2PO_4, respectively) used for the various final K^+ concentrations were: 0 mM K^+ (46 mM Na_2HPO_4 and 23 mM NaH_2PO_4); 0.1 mM K^+ (40 µM, 20 µM, 46 mM, and 23 mM); 0.3 mM K^+ (120 µM, 60 µM, 45.9 mM, and 22.9 mM); 1 mM K^+ (400 µM, 200 µM, 45.6 mM, and 22.8 mM); 2 mM K^+ (800 µM, 400 µM, 45.2 mM, and 22.6 mM); 6 mM K^+ (2.4 mM, 1.2 mM, 43.6 mM, and 21.8 mM); 10 mM K^+ (4 mM, 2 mM, 42 mM, and 21 mM); 30 mM K^+ (12 mM, 6 mM, 34 mM, and 17 mM); and 115 mM K^+ (46 mM K_2HPO_4 and 23 mM KH_2PO_4).

Preparation of proteoliposomes

Proteoliposome preparation followed previously described methods with some modifications (Szollosi, et al., 2016; Vieira-Pires, et al., 2013). *E. coli* polar lipids (Avanti) suspended in chloroform were dried by hand in a round flask using an Argon gas stream, in order to create a thin lipid film. The lipid film was then resuspended at 10 mg/mL lipid concentration in Swelling Buffer (150 mM KCl, 10 mM HEPES, 7 mM NMG (pH 8.0), 0.2 mM EDTA) using 4-6 cycles of sonication (15 s ON/ 15 s OFF in ice) in a ultrasonic bath Sonorex Digitec (Bandelin) and further solubilized by adding 40 mM n-Decyl-β-D-maltoside (DM) (Sol-Grade from Anatrace) and doing again 4-6 cycles of sonication.

The lipid suspension was then incubated at 25 ºC for 2 h with gentle agitation. KtrB alone and KtrAB complexes were purified as described above, just before the reconstitution, and supplemented with ATP or ADP to reach a final concentration of 0.1 mM inside the proteoliposomes after reconstitution. Protein was added to solubilized lipids at 1:100 (w:w) protein-to-lipid ratio and incubated for 30 min at room temperature. In control liposomes (empty), Swelling Buffer was added to the lipids instead of protein solution. Detergent was removed using adsorbing SM-2 Biobeads (Bio-Rad): the protein-lipid mix was incubated twice with fresh Biobeads at 10:1 (w:w) bead-to-detergent ratio at room temperature for 1 h and then incubated overnight at 4 ºC at a 20:1 (w:w) bead-to-detergent ratio. Proteoliposomes were then flash-frozen in liquid nitrogen and stored at -80 ºC.

ACMA-fluorescence-based K^+ flux assay

The assay was adapted from a previously described method (Z. Su et al., 2016). Proteoliposomes were thawed in a 37 ºC water bath for 15 min, briefly sonicated (3x5 s) in an ultrasound bath Sonorex Digitec (Bandelin) and kept at room temperature until the experiment. In assays with the sorbitol external solution, proteoliposomes were diluted 100-fold (10 µL sample in 1 mL final volume) in Flux Buffer (10 mM HEPES and 7 mM NMG (pH 8.0), 150 mM sorbitol, 0.1 mM ATP; 0.2 mM EDTA) to establish the K^+ gradient. Magnesium ($MgCl_2$) and calcium ($CaCl_2$) were added to the Flux Buffer when needed. The pH-sensitive dye 9-amino-6-chloro-2-methoxyacridine (ACMA) was then added to the proteoliposomes to a final concentration of 550 nM, from a 111 µM stock in DMSO. Fluorescence was monitored every 2 s (λ_{Ex}=410 nm, λ_{Em}=480 nm), using a 104F-QS 10 mm quartz cuvette (Hellma) with a small magnet in a Horiba FluoroMax 4 spectrofluorometer (Horiba Scientific). After measuring the initial baseline fluorescence during 100 s, the assay was initiated by adding 1 µM of the H^+ ionophore carbonyl cyanide m-chlorophenyl hydrazone (CCCP) from a 200 µM stock in HNE Buffer (10 mM HEPES, 7 mM NMG (pH 8.0), 1 mM EDTA). CCCP enables H^+ entry into the liposomes to counterbalance the negative potential created upon K^+ efflux, leading to ACMA fluorescence signal quenching. The flux signal was monitored for 400 s. For each experimental condition, one additional replica was performed in which, after baseline fluorescence measurement and CCCP addition, 296 nM of the K^+ ionophore valinomycin was quickly added from a 60 µM stock in DMSO and flux signal was monitored for an additional 100 s. This was performed to avoid valinomycin contamination of the cuvette between sample measurements and was done every day for each proteoliposome preparation and external solution used. Valinomycin

incorporates into all liposomes and mediates K^+ efflux, indicating the total flux of the liposome population. The maximum value of fluorescence quenching change obtained was used to normalize the data. For assays with the choline or lithium external solution, the 150 mM sorbitol in the Flux Buffer was partially or totally replaced by choline chloride, choline acetate or lithium chloride.

Fluorescence quenching curves were normalized individually as follows:

$$NF = \frac{F - F_{val}}{F_{ini} - F_{val}}$$

NF is the normalized fluorescence, F is the measured fluorescence in arbitrary units, F_{ini} corresponds to the last baseline point measured before CCCP addition and F_{val} corresponds to the lowest point measured after valinomycin addition. For magnesium and choline titrations, normalization was performed taking into account the steady-state of each curve instead of the maximum value of fluorescence quenching change obtained with valinomycin. In these cases, F_{val} was replaced in the previous expression by F_{ss} that corresponds to the average of the last 50 s of the assay (450-500 s).

Determination of magnesium ion concentration in flux assay solutions

For several of the flux assay mixtures used for the magnesium titration, we collected the assay mixture after running the assay. Proteoliposomes were removed from these samples by centrifuging 800 µL at 267,000 g for 25 min at 4 ºC. 700 µL of the resulting supernatant were used for determination of magnesium ion concentration by flame ionization spectroscopy analysis at the FCUP|DQB-Lab&Services (University of Porto). Buffer solutions used in the flux assay were also tested for magnesium contamination.

Quantification of flux rate constants

Individual fluorescence quenching curves (after CCCP addition) were fitted with a one-phase exponential equation: $y = y0 + A1 \times e^{-(x-x0)/\tau}$ or a two-phase exponential equation $y = y0 + A1 \times e^{-(x-x0)/\tau fast} + A2 \times e^{-(x-x0)/\tau slow}$ using the Origin software (OriginLab), where A1 and A2 are amplitudes, x0 is the initial fit point, y0 corresponds to the plateau and τ is the time constant. In each case, the simplest model that explained the data was chosen. The first point measured immediately after CCCP addition was not considered in this fit due to uncertainty in the fluorescence measurement after compound addition. Flux rate constants were determined by inverting the respective time constants (rate constant= 1/τ).

RESULTS

Impact of intra-dimer interface mutants on KtrA structure

The full-length KtrA structures determined with ATP (PDB: 4J90) and ADP (PDB: 4J91) show the RCK octameric rings arranged in different conformations: square and non-square, respectively (Figure 11a and 11b) (Vieira-Pires, et al., 2013). The adoption of the square conformation upon ATP binding involves a change in the intra-dimer hinge angle (Figure 12). This change brings closer together the two nucleotide-binding sites in the KtrA dimeric units, as seen in the D36-D36 Cα intra-dimer distance, a conserved residue in the nucleotide binding site (Figure 12 and Table 2).

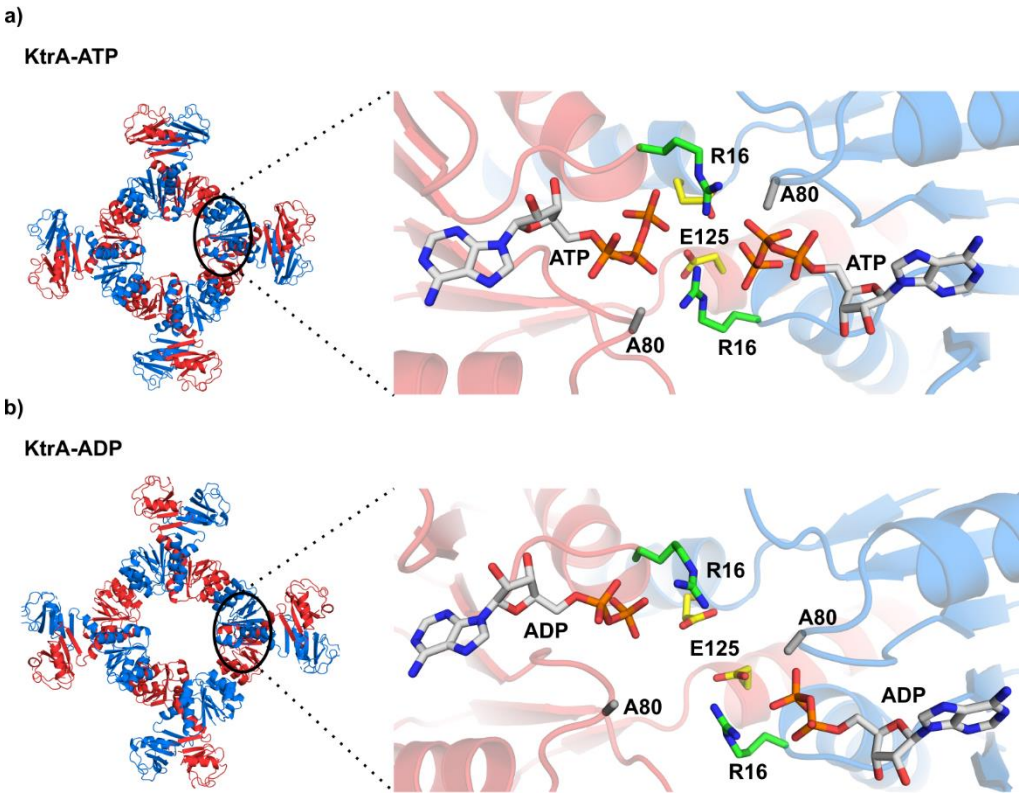

Figure 11: KtrA bound to ATP and ADP. a) Left- square conformation of the KtrA octameric ring bound to ATP. Right- view of the ATP binding pockets in a KtrA dimer showing dimer subunits and nucleotides positioned close together. **b)** Left- non-square conformation of the KtrA octameric ring bound to ADP. Right- view of the ADP binding pockets showing dimer subunits and nucleotides positioned farther apart relative to a). Intra-dimer interface residues discussed in the text are shown as stick and labeled. KtrA octameric ring subunits are colored alternately blue and red.

Narrowing of the intra-dimer space with bound ATP allows the establishment of interactions between the phosphate groups and residues in both the same and opposite subunits of the KtrA dimer. In particular, the R16 residues are positioned between the two nucleotides and appear to stabilize the closely positioned negatively-charged phosphate groups. In contrast, in the ADP-bound structure the nucleotide molecules do not establish interactions with opposing subunit residues (Figure 11a and 11b). Based on this evidence, it was previously proposed that bridging interactions mediated by R16 and ATP stabilize the square or high-flux conformation of the KtrA octameric ring (Vieira-Pires, et al., 2013).

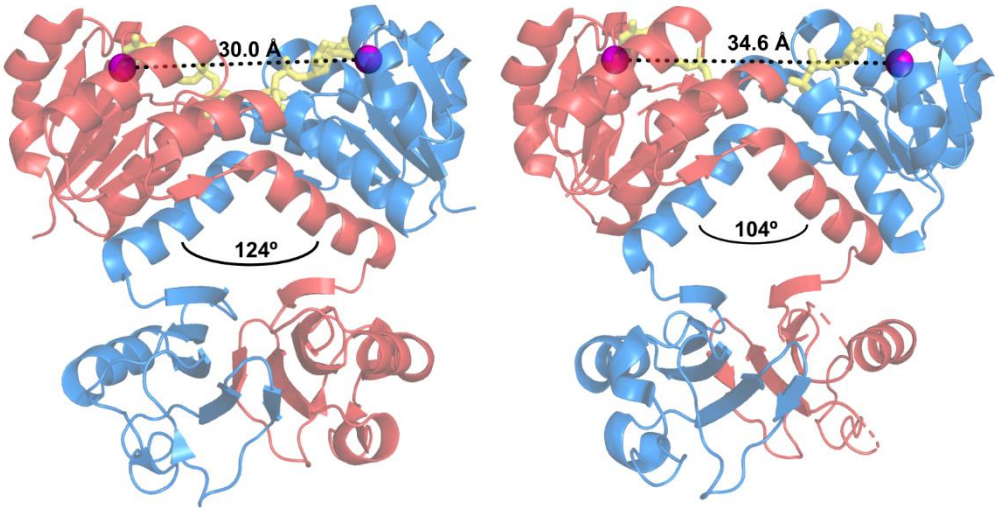

Figure 12: Intra-dimer hinge angle in wild-type KtrA. Cartoon representation of ATP-bound (left) and ADP-bound (right) KtrA dimers, depicting the intra-dimer hinge angle measured between αF helices (black arc) and the D36-D36 intra-dimer distances. Dimer subunits are colored blue and red, D36 Cα are shown as purple spheres and nucleotides as yellow stick.

In order to explore the role of intra-dimer interface residues in the KtrA octameric ring conformation, we created the KtrA single-point mutants R16A, R16K, A80P and E125Q. Like R16, E125 is located in the KtrA dimer interface and close to the ATP phosphate groups, as depicted in Figure 11. The A80P mutant was created as a control, to evaluate the impact of mutating A80, since substitution of the small alanine side-chain with a bulkier side-chain was expected to cause a distortion of the nucleotide-binding site.

We started by verifying that the mutants retained the same basic properties of the wild-type KtrA. All the mutants assembled as octamers bound to either ATP or ADP, as revealed by size-exclusion chromatography (Figure 13).

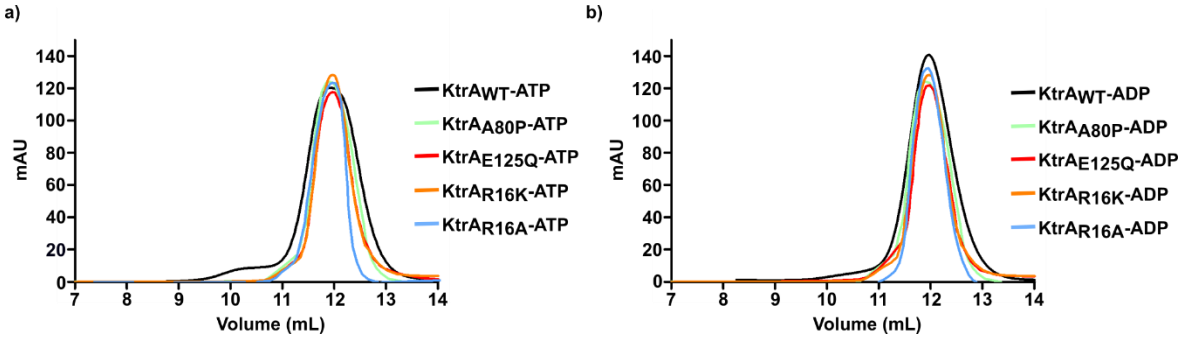

Figure 13: Size-exclusion chromatography elution profiles of KtrA proteins bound to a) ATP and b) ADP.

We then determined the structures of all KtrA mutants with bound ATP or ADP (Figure 14 and Table 1).The structures of R16K (at 2.7 Å resolution) and R16A (at 3.4 Å resolution) with ATP are very similar to that of the previously determined wild-type KtrA-ATP (WT-ATP) (Figure 14a), adopting the square conformation. A simple indicator of ring conformation is the pair of distances (L1/L2) separating the Cα of N38 residues located in opposite subunits across a ring face (Figure 14a and Table 3). In the ATP-bound rings, these distances are similar in the R16K (30.8/30.8 Å), R16A (29.9/29.9 Å) mutants and wild-type (30.0/30.0 Å) structures. Like in the wild-type protein, the ADP-bound R16K (at 3.0 Å resolution) and R16A (at 3.7 Å resolution) rings adopt a non-square conformation (Figure 14a). However, the ADP-bound ring conformations are different from each other and from the wild-type, with L1/L2 distances for the wild-type of 40.7/30.7 Å and for R16K of 52.0/21.9 Å (Table 3). In the ADP-bound R16A mutant there are eight KtrA dimers present in the asymmetric unit, corresponding to two different rings with L1/L2 distances of 34/30 Å and 37/28 Å.

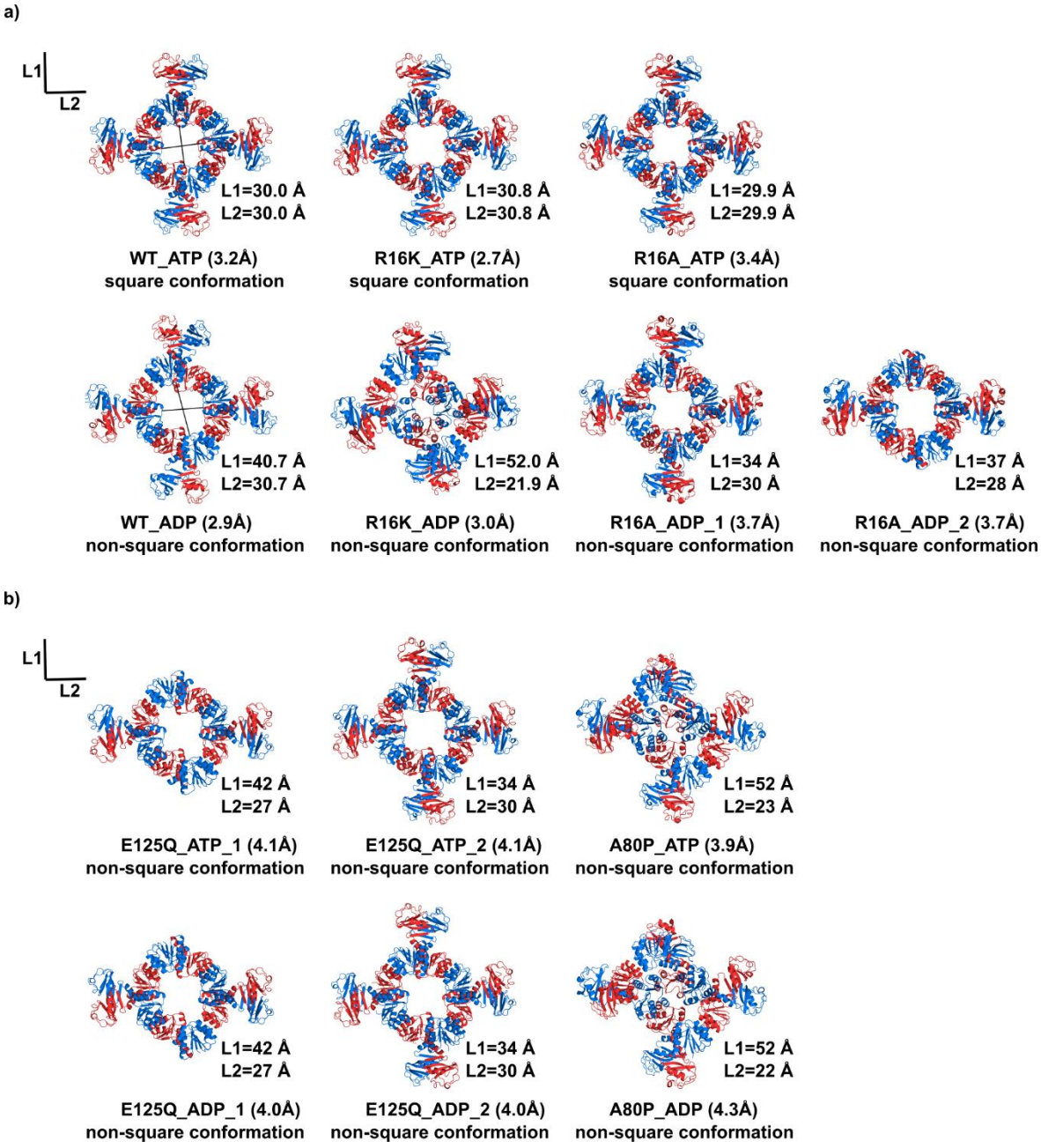

Figure 14: KtrA ring structures. Views of crystal structures of wild-type and mutant KtrA that **a)** adopt an ATP-bound square conformation or **b)** do not adopt an ATP-bound square conformation. Top rows show structures with bound ATP and bottom rows show structures with bound ADP. KtrA octameric rings are displayed with subunits colored alternately blue and red. L1 and L2 are the pair of distances between the Cα of N38 residues located in opposite subunits across the ring. In three of these rings (R16A_ADP_2, E125Q_ATP_1 and E125Q_ADP_1), poor electron-density prevented modelling of C-terminal domains.

The crystal structures of the A80P and E125Q mutants revealed a different picture (Figure 14b). The ATP-bound structures do not adopt a square conformation, displaying L1/L2 distances for A80P (at 3.9 Å resolution) of 52/23 Å and for E125Q (at 4.1 Å resolution and with two different half-rings in the asymmetric unit) of 34/30 Å and 42/27 Å. The ADP-bound structures are also non-square, showing ring conformations that are very similar to those observed with ATP. A80P (at 4.3 Å resolution) has L1/L2 distances of 52/22 Å and E125Q (at 4.0 Å resolution and with two rings) of 34/30 Å and 42/27 Å.

It is apparent that the square conformation adopted by the KtrA octameric rings is unique and stable (Figure 15 and Table 2). In contrast, there is a large structural variability between rings adopting the non-square conformation. This variability is shown in the D36-D36 distances and L1/L2 distances (Tables 2 and 3), allowing the clustering of these structures in four groups (Table 3). It is worthwhile pointing out that, besides variations between rings, we also found variation in the D36-D36 distance within individual non-square rings (Table 2).

Importantly, these structures show that A80 and E125 are crucial residues for the adoption of the square conformation by the KtrA octameric ring. On the other hand, R16 does not play a major role in the conformational arrangement of the RCK ring.

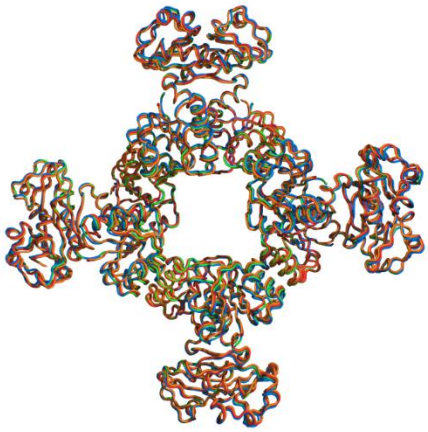

Figure 15: KtrA square conformation. Superposition of KtrA-ATP octameric rings that adopt the square conformation. $KtrA_{WT}$ (red), $KtrA_{R16K}$ (marine), $KtrA_{R16A}$ (orange), $KtrA_{WT}$ with bound calcium (green).

Table 1: Data collection and refinement statistics for the KtrA mutant structures

Data collection statistics				
Crystal	R16K_ATP	R16K_ADP	R16A_ATP	R16A_ADP
PDB ID	6S2J	6S5B	6S5D	6S7R
Space group	I4	$P2_12_12_1$	I4	P1
Unit-cell dimensions **a, b, c (Å)** **α, β, γ (°)**	 123.3, 123.3, 84.4 90, 90, 90	 85.8, 137.4, 202.6 90, 90, 90	 121.6, 121.6, 83.7 90, 90, 90	 93.0, 97.9, 144.6 90.4, 97.1, 110.3
Protomers in the asymmetric unit	2	8	2	16
Wavelength (Å)	0.954240	0.979480	0.978570	0.978570
Resolution (Å)	46.16-2.67 (2.80-2.67)	49.51-3.05 (3.16-3.05)	45.60-3.39 (3.66-3.39)	48.80-3.73 (3.86-3.73)
No. of reflections (measured/unique)	85203/17872	383771/46032	76213/8535	161349/46426
Multiplicity	4.8 (4.5)	8.3 (4.2)	8.9 (8.5)	3.5 (3.0)
Completeness (%)	99.0 (96.5)	99.2 (91.6)	99.8 (99.0)	94.0 (51.2)
Rmerge (all I) (%)	5.5 (86.8)	14.8 (47.4)	4.7 (182.9)	9.5 (96.6)
Rmeasure (all I) (%)	6.2 (98.1)	15.8 (53.8)	5.0 (194.6)	11.2 (116.0)
Mean I / σ(I)	13.9 (1.7)	15.9 (0.2)	17.1 (1.3)	7.4 (1.1)
$CC_{1/2}$	0.999 (0.541)	0.995 (0.886)	1.000 (0.573)	0.996 (0.494)
Refinement statistics				
Resolution range (Å)	46.16-2.67	48.17-3.05	45.60-3.39	48.80-3.73
R_{work}/R_{free} (%)	18.96/23.57	20.93/24.29	23.83/27.90	24.57/30.04
No. of reflections	17870	46032	8535	46426
Total No. of atoms	6969	13784	3459	25028
No. of waters	2	-	2	-
No. of ATP	2	-	2	-
No. of ADP	-	8	-	16
No. of Mg	1	-	1	-
Wilson B factor($Å^2$)	90.2	97.4	194.2	152.9
r.m.s.d. bond lengths (Å)	0.013	0.003	0.003	0.003
r.m.s.d. bond angles (°)	1.086	0.760	0.745	0.824
Ramachandran plot				
Residues in favored/allowed regions (%)	98 / 2	99 / 1	97 / 3	98 / 2

Data collection statistics				
Crystal	E125Q_ATP	E125Q_ADP	A80P_ATP	A80P_ADP
PDB ID	6S5N	6S5O	6S5E	6S5G
Space group	$C222_1$	$C222_1$	$P2_12_12_1$	$P2_12_12_1$
Unit-cell dimensions **a, b, c (Å)** **α, β, γ (°)**	 109.1, 156.5, 286.4 90, 90, 90	 108.2, 155.2, 285.9 90, 90, 90	 85.7, 133.9, 205.1 90, 90, 90	 85.3, 132.9, 203.3 90, 90, 90
Protomers in the asymmetric unit	8	8	8	8
Wavelength (Å)	0.978570	0.978570	0.978570	0.978570
Resolution (Å)	48.24-4.09 (4.48-4.09)	48.07-3.98 (4.36-3.98)	49.63-3.89 (4.20-3.89)	49.28-4.33 (4.84-4.33)
No. of reflections (measured/unique)	131430/19704	274868/ 20970	146620/22230	100662/14674
Multiplicity	6.7 (6.8)	13.1 (13.0)	6.6 (6.6)	6.9 (4.7)
Completeness (%)	99.5 (98.3)	99.4 (97.9)	99.5 (98.0)	91.9 (79.1)
Rmerge (all I) (%)	12.7 (113.5)	11.2 (132.6)	8.1 (133.9)	19.1 (56.8)
Rmeasure (all I) (%)	13.7 (122.9)	11.7 (138.1)	8.8 (145.4)	20.5 (62.9)
Mean I / σ(I)	9.5 (1.7)	12.0 (1.9)	10.3 (1.3)	7.9 (2.6)
$CC_{1/2}$	0.999 (0.835)	0.999 (0.771)	0.999 (0.830)	0.995 (0.873)
Refinement statistics				
Resolution range (Å)	48.24-4.09	47.66-3.98	47.88-3.89	49.28-4.33
R_{work}/R_{free} (%)	27.91/31.99	24.96/28.62	26.02/31.72	25.37/31.43
No. of reflections	19704	20970	22230	14674
Total No. of atoms	12594	12426	13912	13744
No. of waters	-	-	-	-
No. of ATP	8	-	8	-
No. of ADP	-	8	-	8
No. of Mg	-	-	-	-
Wilson B factor($Å^2$)	183.9	201.8	188.6	135.7
r.m.s.d. bond lengths (Å)	0.003	0.003	0.003	0.003
r.m.s.d. bond angles (°)	0.804	0.791	0.883	0.729
Ramachandran plot				
Residues in favored/allowed regions (%)	98 / 2	97 / 3	98 / 2	97 / 3

R.m.s.d is the root-mean-square deviation; values in parenthesis correspond to the highest resolution shell.

Table 2: Cα D36-D36 intra-dimer distances in KtrA octameric rings.

ATP	**D36-D36 (Å)**			
Structure	**Dimer 1**	**Dimer 2**	**Dimer 3**	**Dimer 4**
WT-ATP	30.0	30.0	30.0	30.0
R16K-ATP	30.7	30.7	30.7	30.7
R16A-ATP	31.0	31.0	31.0	31.0
WT-ATP-Ca	30.7	30.7	30.7	30.7
A80P-ATP	32	31	31	32
E125Q-ATP (1)[$]	33	34	33	34
E125Q-ATP (2)[$]	31	32	31	32
ADP	**D36-D36 (Å)**			
Structure	**Dimer 1**	**Dimer 2**	**Dimer 3**	**Dimer 4**
WT-ADP	34.6	34.8	34.6	34.8
R16K-ADP	31.5	31.4	31.0	32.1
R16A-ADP (1)[$]	31	32	30	32
R16A-ADP (2)[$]	31	38	31	32
A80P-ADP	32	32	32	33
E125Q-ADP (1)[$]	34	35	34	35
E125Q-ADP (2)[$]	34	34	34	34

$ R16A-ADP, E125Q-ATP and E125Q-ADP have two different octameric rings in the crystal, indicated by (1) or (2).

Table 3: Cα N38 distances (L1/L2) in KtrA octameric rings.

	L1/L2 (Å)	
Octameric Ring	Front face*	Back face*
Square conformation		
WT-ATP	30.0/30.0	29.0/29.0
R16K-ATP	30.8/30.8	30.3/30.3
R16A-ATP	29.9/29.9	29.0/29.0
WT-ATP-Ca	30.5/30.5	29.6/29.6
Non-square conformation 1#		
WT-ADP	40.7/30.7	40.1/29.5
Non-square conformation 2#		
E125Q-ATP (1) $	42/27	36/30
E125Q-ADP (1) $	42/27	36/30
Non-square conformation 3#		
R16A-ADP (1) $	34/30	34/30
R16A-ADP (2) $	37/28	34/32
E125Q-ATP (2) $	34/30	34/30
E125Q-ADP (2) $	34/30	34/30
Non-square conformation 4#		
R16K-ADP	52.0/21.9	51.3/22.5
A80P-ATP	52/23	51/22
A80P-ADP	52/22	52/21

*Distances measured on the two faces of the ring are slightly different and we have named the front face as the one with the larger individual distance value. Values mentioned in the main text correspond to front face. # Non-square conformations were clustered in four groups according to L1/L2. $ R16A-ADP, E125Q-ATP and E125Q-ADP have two different octameric rings in the crystal, indicated by (1) or (2).

Impact of A80P and E125Q mutations on the nucleotide-binding site

The ATP-bound octameric rings formed by the A80P and E125Q KtrA mutants are not able to adopt a square conformation. Therefore, in order to understand the molecular basis of the impact of A80P and E125Q, we analysed the nucleotide binding sites in these mutant ATP-bound structures. In this analysis, we took in consideration the low resolution of the structures and focused only on the impact of the mutations in the main-chain trace. It is worthwhile explaining that refinement of the low-resolution structures (worse than 3.5 Å) involved only rigid-body refinement of the molecular replacement model (wild-type KtrA), followed by all-atom refinement with non-crystallographic and secondary structure restraints. We performed minimal manual adjustments.

In the A80P-ATP structure, the main-chain atoms of residue P80 are positioned outside the 2Fo-Fc and Fo-Fc electron-density maps in all eight proteins in the asymmetric unit (Figure 16). Importantly, this offset was not the result of the refinement procedure, since the position of the residue is very similar to the one in the wild-type structure. It is obvious from the maps that adjustment of the main-chain position of the residue into the density would impinge on the ATP molecule, requiring a shift in the nucleotide position to avoid steric-clashes. Unfortunately, at this low resolution it is not clear how to adjust the position of the nucleotide in the electron-density map. We concluded therefore that the A80P mutation causes a distortion of the main-chain and leads to an alteration in the position of the ATP, impeding the adoption of the square conformation.

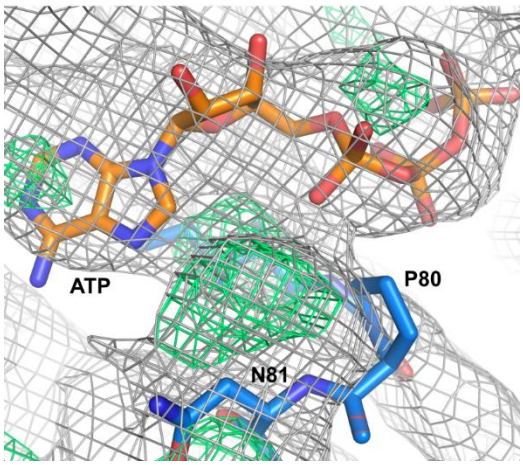

Figure 16: Nucleotide-binding site of the ATP-bound $KtrA_{A80P}$ mutant. Electron density maps 2Fo-Fc (in gray) and Fo-Fc (in green), contoured at 1.0 and 3.0 σ, respectively, are shown in mesh. ATP and two residues are shown as sticks. Residue P80 is outside the electron density in the eight KtrA subunits in the asymmetric unit.

In contrast, in the maps for the E125Q-ATP structure we do not observe obvious changes in the main-chain trace that might explain the impact of the mutation in the conformation of the octameric ring.

Divalent cation binding site

A clue for the role of E125 was revealed by the 2.7 Å structure of the ATP-bound R16K KtrA mutant. In this structure, there was a distinct additional electron-density in the KtrA intra-dimer interface, between the γ-phosphates of the nucleotide (Figure 17a).

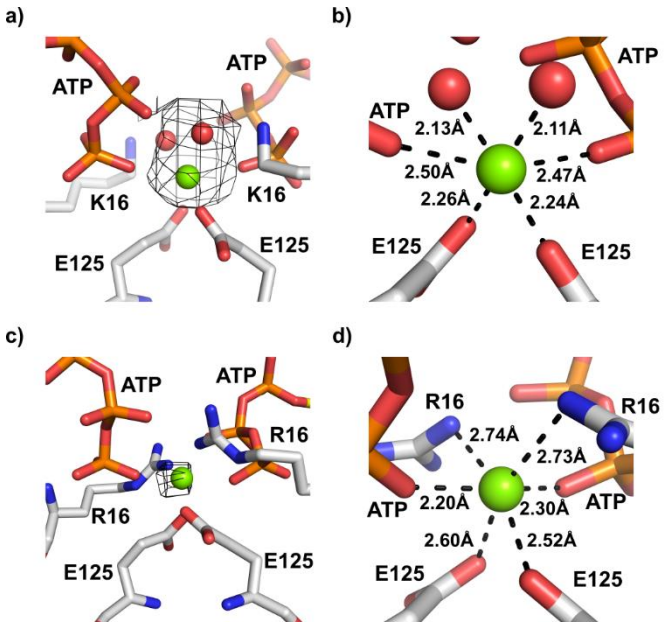

Figure 17: Magnesium ion binding site in the interface of KtrA dimers. a) View of the intra-dimer interface of R16K-ATP with unexplained electron density in Fo-Fc map (contoured at 3.0 σ and calculated at a refinement stage when the structural model did not yet include Mg^{2+} or coordination waters) superposed on final refined model. **b)** Close-up of the magnesium binding site depicted in a), showing the octahedral geometry of cation coordination. **c)** View of the intra-dimer interface of wild-type KtrA-ATP (PDB: 4J90) with Fo-Fc electron density (contoured at 3.0 σ and calculated from deposited structure, which does not include Mg^{2+}) superposed on refined model. **d)** Close-up of the magnesium binding site shown in c), highlighting the interactions established by the cation. Magnesium ion and water molecules are shown as green and red spheres, respectively. Residues and nucleotides coordinating ions are shown as stick with coordination distances indicated.

After careful crystallographic refinement, we concluded that the density likely corresponds to a magnesium ion (Figure 17a and 17b). The ion is coordinated by six oxygen atoms, adopting octahedral geometry. The coordinating atoms are provided by the γ-phosphate of both ATP molecules, by two water molecules and by the carboxylic groups of the two E125 residues. In this structure, the K16 side-chain is well defined in the electron density, interacting with one of the Mg^{2+} coordinating water molecules, with the carbonyl group of Q105 from the opposite subunit and with the γ-phosphate from the ATP in the same subunit. The octahedral coordination of the ion along with the majority of the coordination distances fit well with the expected coordination of a magnesium ion; however, the interaction distances with the oxygen atoms in the phosphate groups are longer than expected (Bock et al., 1994; Harding, 2001; H. Zheng et al., 2008). Calcium could also be a possible solution for the density but calcium ions are often coordinated by seven oxygen atoms in crystal structures (Harding, 2001), acquiring preferentially a pentagonal bipyramidal geometry according to the MetalPDB server (http://metalweb.cerm.unifi.it). In addition, the ideal coordination distances established by calcium ions are longer than for magnesium ions (H. Zheng, et al., 2008). Refinement of Ca^{2+} at the site showed the same interactions and very similar distances to Mg^{2+}. Importantly, the temperature factor of Ca^{2+} became larger than for the atoms forming its coordination shell (Table 4), suggesting that the density corresponds to a less electron-dense cation.

Overall, we conclude that the ion bound to the intra-dimer interface site is a magnesium ion. It is worthwhile mentioning that magnesium was not added to the protein or crystallization mixture and so the ion was sequestered during protein preparation or crystallization.

Table 4: *B* factors of divalent cation and coordinating atoms in R16K-ATP and WT-ATP KtrA structures after refinement with magnesium or calcium.

	***B* factor (Å^2)**			
	R16K-ATP		**WT-ATP(4J90)**	
Atom	Magnesium refinement	Calcium refinement	Magnesium refinement	Calcium refinement
Divalent cation	74.32	109.75	125.14	165.00
O from H_2O (1)	68.41	77.03	-	-
O from H_2O (2)	66.67	76.92	-	-
OE2 from E125 chain A	84.88	92.19	90.83	89.69
OE2 from E125 chain B	92.66	102.90	103.50	102.36
O2G from ATP 1	54.58	71.41	141.91	144.43
O2G from ATP 2	90.22	105.68	157.40	151.27
NH2 from R16 chain A	-	-	93.14	100.24
NH2 from R16 chain B	-	-	93.62	91.41

We also revisited the electron-density maps of the previously resolved wild-type KtrA structure bound to ATP (at 3.2 Å, PDB code: 4J90), which also adopts a square-conformation, looking for unexplained density in the intra-dimer interface. It is possible to detect density that could also be accounted by a coordinated Mg^{2+} (Figure 17c). Re-refinement of the structure with Mg^{2+} does not cause great adjustments in the intra-dimer interface. The cation has a similar octahedral coordination to that seen in the R16K mutant structure, interacting with the oxygen atoms in the γ-phosphate of both ATP molecules and the carboxylic groups of the E125 residues. However, instead of water molecules, nitrogen atoms of the R16 guanidinium group appear to complete the coordination shell of the divalent cation (Figure 17d). Magnesium coordination by an arginine side-chain has been reported for at least two high-resolution structures (better than 2.0 Å) with PDB codes 1NUW and 3OS4.

In addition, we crystallized wild-type KtrA-ATP in the presence of 5 mM of Ca^{2+} and determined the structure at 3.0 Å resolution (Figure 18a and Table 5). The structure shows an octameric ring adopting a square conformation with L1/L2 distances of 30.5/30.5 Å that are similar to those of the WT-ATP structure (Table 3 and Figure 15). The intra-dimer interface shows a bound calcium ion (Figure 18b). After refinement, we defined a coordination shell formed by oxygens from the carboxylic groups of the E125 side chains and the oxygen atoms of the ATP γ-phosphates. Unlike what we had observed in the wild-type structure with Mg^{2+}, the R16 side-chains are not in position to

coordinate the divalent cation. The coordination distances are consistent with a calcium ion but the coordination number (4 ligands) is unusual and there could be additional interactions, with water molecules for example, which we are not currently able to model due to the limited resolution.

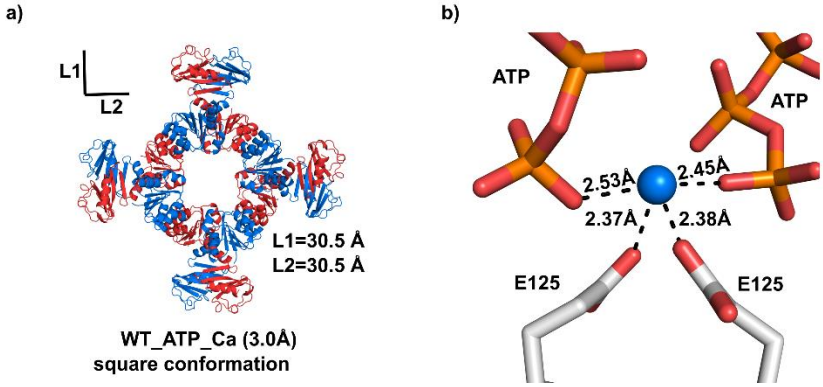

Figure 18: KtrA structure with calcium. a) Structure of wild-type KtrA octameric ring with bound ATP supplemented with 5mM $CaCl_2$. Subunits of the octameric ring are colored alternately blue and red. L1 and L2 correspond to the distances between the Cα of N38 residues located in opposite subunits across the ring. **b)** Calcium-binding site showing cation coordination. Calcium ion is shown as blue sphere. Residues and nucleotides coordinating calcium are shown as stick with coordination distances indicated.

Altogether, these structural results reveal that E125 coordinates a divalent cation at the KtrA intra-dimer interface. Importantly, the γ-phosphates of the ATP molecules complete the coordination of the divalent cation. In this arrangement, the divalent cation bridges the ligand molecules in two KtrA dimer subunits, suggesting that the cation stabilizes the two subunits in the RCK dimers close together, favoring the adoption of the square conformation. Mutation to glutamine likely affects the coordination of the divalent cation binding site, disturbing the stability of the square conformation.

Table 5: Data collection and refinement statistics for the KtrA WT structure with calcium

Data collection statistics	
Crystal	WT_ATP_Ca
PDB ID	6S5C
Space group	I4
Unit-cell dimensions	
a, b, c (Å)	122.7, 122.7, 84.0
α, β, γ (º)	90, 90, 90
Protomers in the asymmetric unit	2
Wavelength (Å)	0.978570
Resolution (Å)	45.94-3.00 (3.18-3.00)
No. of reflections (measured/unique)	123606/12614
Multiplicity	9.8 (9.8)
Completeness (%)	99.8 (98.9)
Rmerge (all I) (%)	4.3 (141.8)
Rmeasure (all I) (%)	4.6 (149.6)
Mean I / σ(I)	24.5 (1.6)
$CC_{1/2}$	0.999 (0.658)
Refinement statistics	
Resolution range (Å)	37.81-3.00
R_{work}/R_{free} (%)	20.70/25.88
No. of reflections	12614
Total No. of atoms	3475
No. of waters	-
No. of ATP	2
No. of ADP	-
No. of Ca	1
Wilson B factor($Å^2$)	135.1
r.m.s.d. bond lengths (Å)	0.004
r.m.s.d. bond angles (°)	0.697
Ramachandran plot	
Residues in favored/allowed regions (%)	98 / 2

Influence of KtrA mutants in KtrAB function

In order to evaluate the role of KtrA intra-dimer interface residues in KtrAB activity we employed an *E.coli* phenotype complementation assay. In this complementation assay, low-level constitutive expression of an active potassium channel in the K^+-transport deficient-strain TK2420 rescues bacterial growth in a media containing low amounts of K^+ (Albright, et al., 2007; Buurman et al., 2004). While empty vector-containing cells require a minimum of 30 mM K^+ to grow, expression of wild-type KtrAB allows growth of *E.coli* TK2420 with only 1 mM K^+ (Figure 19a).

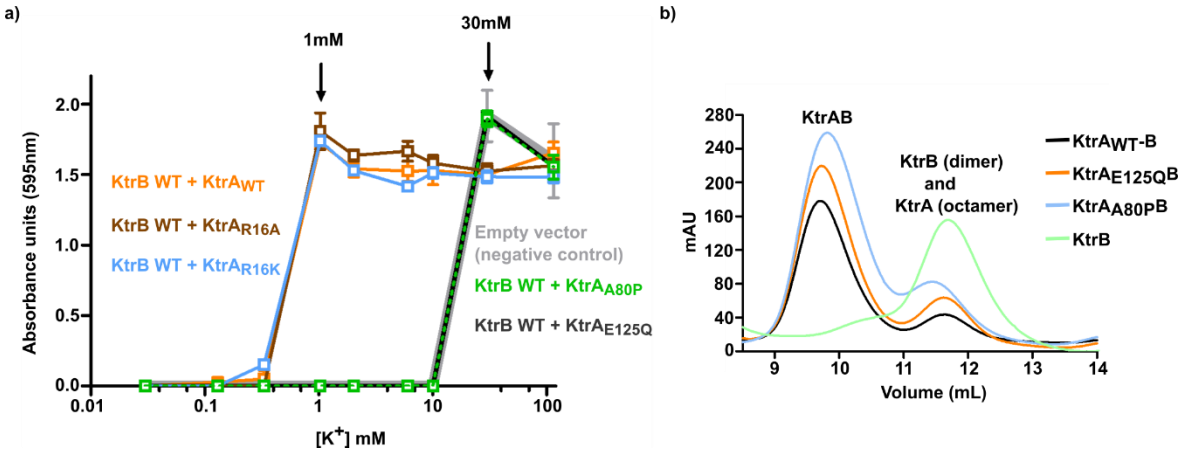

Figure 19: Functional impact of KtrA intra-dimer interface residues. a) Optical density of overnight *E.coli* TK2420 cultures (expressing different KtrAB constructs) as a function of K^+ concentration in the growth media. Mean ± SD (n=6) from two independent experiments. **b)** Elution profiles of KtrB and KtrAB complexes assembled with wild-type or mutant KtrA in the presence of ATP.

We tested the KtrA single-point mutants in the presence of wild-type KtrB and evaluated their impact in the complementation assay. None of the R16 mutations had an impact on the growth phenotype. R16A and R16K behave like wild-type KtrA and result in a KtrAB mediated growth rescue with 1 mM K^+. On the other hand, the A80P and E125Q mutations resulted in an apparently inactive KtrAB (Figure 16). Importantly, we confirmed by size-exclusion chromatography that these mutants are able to assemble in a stable complex with KtrB (Figure 19b).

Our phenotype rescue assay fits well with the structural analysis. KtrA mutants that show a wild-type protein function (R16K and R16A) in the complementation assay are able to adopt a square conformation with ATP. In contrast, mutants that do not rescue

growth (A80P and E125Q) also do not adopt the square conformation in the ATP-bound structures.

These structural and functional results confirm that KtrAB activation requires the adoption of a stable KtrA-ATP ring square conformation. Furthermore, unlike what had been previously proposed, R16 is not essential for the adoption of this conformation. Instead, E125 is a crucial residue in the KtrA-intradimer interface that stabilizes the active square-conformation of the octameric ring by coordinating a divalent cation.

Functional effect of divalent cations in KtrAB activity

To establish the importance of a divalent cation in the function of KtrAB we adapted the fluorescence based ACMA-liposome K^+ flux assay (Z. Su, et al., 2016). In this assay, KtrAB was reconstituted into liposomes in the presence of 150 mM KCl and a K^+ gradient was established by dilution of the proteoliposomes into a low K^+ concentration solution. The assay was initiated by addition of carbonyl cyanide m-chlorophenylhydrazone (CCCP, a H^+-ionophore), which builds-up a H^+ gradient across the membrane as potassium ions efflux through KtrAB. Formation of an H^+ gradient results in quenching of 9-amino-6chloro-2-methoxyacridine (ACMA) fluorescence (Figure 20).

We have found that using 2 µM ACMA in the flux assay, as others have described, causes inhibition of KtrAB. We have therefore reduced the concentration of fluorescence probe to 550 nM. In these conditions, we observe a fluorescence quenching window of ~80% in our functional assays. One- or two-phase exponential equations were fitted to the fluorescence quenching curves and flux rate constants were determined as the inverse of time constants extracted from the fit (Appendix- Figure 27 and Table 6). The fast component of the majority of double-exponential fits was the dominant term (larger amplitude) and is used in the analysis below. Exceptions are noted in the figure legends.

In many of the experiments below we compared the activity of proteoliposomes reconstituted with different protein combinations, for example KtrB assembled with KtrA-ATP, KtrA-ADP or E125Q KtrA with bound ATP. Reconstitutions with different assemblies show similar amounts of protein associated with liposomes (Appendix-Figure 28).

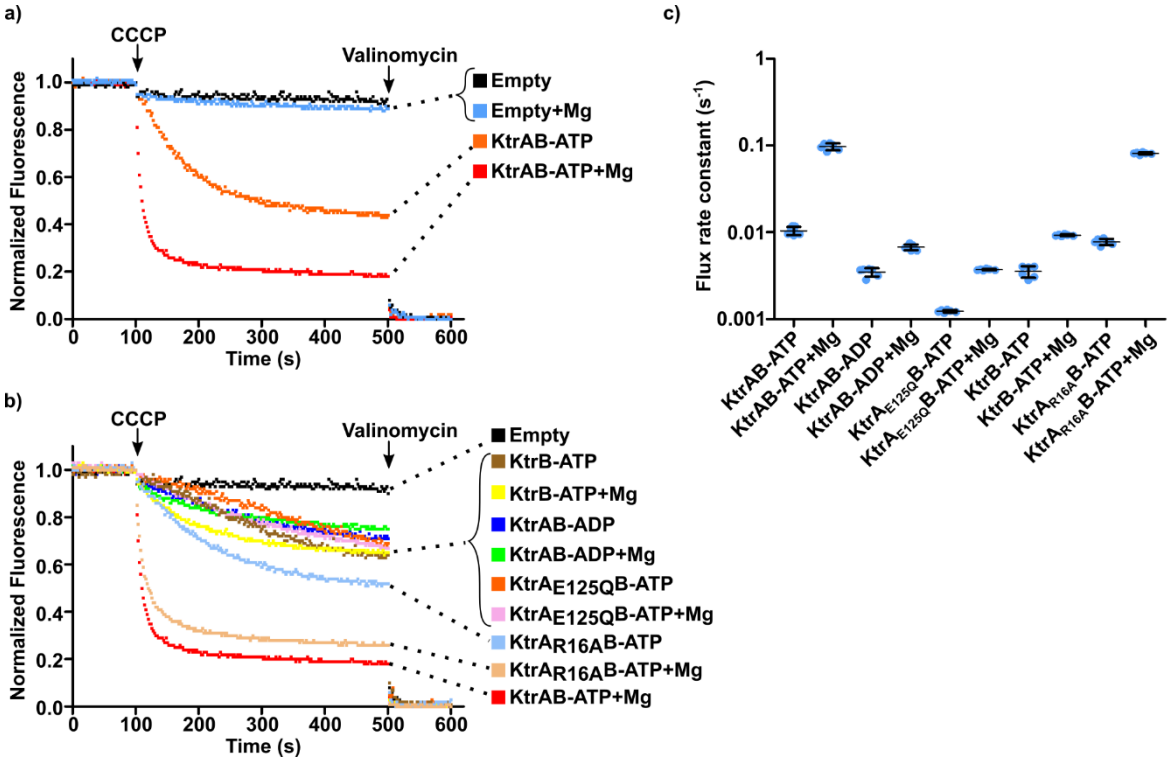

Figure 20: Impact of magnesium ion on KtrAB activity. a) and **b)** Proteoliposome flux assay performed with wild-type KtrB and wild-type and mutant KtrAB with ATP or ADP, in the presence or absence of 2 mM magnesium, as indicated. All assays were performed with sorbitol in the external solution. Panels show representative fluorescence quenching curves. Empty liposomes were used as control. **c)** Plot of flux rate constants for conditions in a) and b). Mean ± SD as well as individual rate constants (blue dots) are shown for n=6-7 from at least two different proteoliposome preparations.

We first compared the differences in the flux of KtrAB-ATP with and without Mg^{2+}, in proteoliposomes resuspended in an external solution containing 150 mM sorbitol and 1.5 mM KCl (Figure 20a). Flux is ~10-fold faster in the presence of Mg^{2+}, with the rate constant increasing from 0.011 ± 0.001 to 0.096 ± 0.008 s^{-1} (Figure 20c).

Next, we removed the chemical groups that coordinate Mg^{2+} in the KtrA R16K and WT-ATP structures (Figure 17b and 17d) by substituting ATP for ADP or mutating E125 to a glutamine (E125Q) and measured flux (Figure 20b). Relative to KtrAB-ATP with Mg^{2+}, flux was 14-fold and 24-fold slower for KtrAB-ADP and $KtrA_{E125Q}B$-ATP with Mg^{2+}, respectively (Figure 20c). For the same protein forms without divalent cation, the impact of Mg^{2+} on KtrAB-ADP and $KtrA_{E125Q}B$-ATP is only a 2- to 4-fold rate increase. This difference is also observed with KtrB alone (Figure 20b and 20c), indicating that the Mg^{2+} effect in the ADP and E125Q protein forms is most likely not related to the

mechanism of RCK activation. Like for wild-type KtrAB-ATP, Mg^{2+} also activates the complex with the R16A KtrA mutant (Figure 20b and 20c).

Despite the clear impact of Mg^{2+} in KtrAB activation, it is noticeable that absence of added divalent cation does not abolish KtrAB-ATP activity and that its flux is larger than for KtrB or KtrAB-ADP (Figure 20a and 20c). This observation is explained in the discussion. The functional data supports the proposal that Mg^{2+} is a cofactor in the nucleotide-dependent activation of KtrAB, by binding at the intra-dimer RCK interface site and being coordinated by both the ATP γ-phosphates and the KtrA E125 residues.

Our structural studies also suggest that calcium is able to bind at the KtrA intra-dimer interface. Therefore, in order to understand if the intra-dimer interface site is selective for Mg^{2+}, we performed flux experiments with addition of Ca^{2+} and Mg^{2+} to an external solution containing 20 mM choline chloride and sorbitol (Figure 21). We chose to include choline chloride in this assay because we wanted to minimize any non-specific effect of divalent cations on the liposomes by increasing the ionic strength of the assay solution and because choline is an organic cation that does not permeate KtrAB.

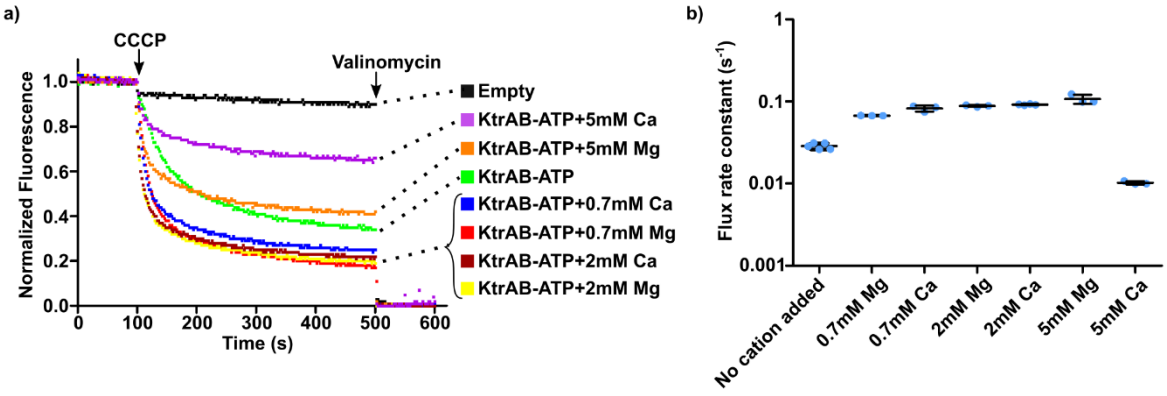

Figure 21: Impact of calcium ion on KtrAB activity. a) Proteoliposome flux assay with KtrAB-ATP in an external solution with 20 mM choline chloride and sorbitol. The panel shows representative fluorescence quenching curves. Empty liposomes were used as control. **b)** Plot of flux rate constants for conditions shown in a). Mean ± SD as well as individual flux rate constants (blue dots) are shown with n=3-5 of the same proteoliposome preparation. For KtrAB-ATP + 5 mM Mg^{2+} the amplitude of the fast component in the double-exponential fit is slightly lower than of the slow component. Nevertheless, we plotted the rate constant of the fast component as it represents the initial decay phase of the curve, allowing comparison with other rate constants (Appendix- Table 6).

Relative to the condition without divalent cation, adding 0.7 or 2 mM Ca^{2+} or Mg^{2+} increases flux up to 4-fold. Rate constants become similar to those measured in the sorbitol/Mg^{2+} condition (0.088 ±.0.002 s^{-1} for 2 mM Mg^{2+} and 0.092 ± 0.001 s^{-1} for 2 mM Ca^{2+}) (Figure 21a and 21b). Addition of 5 mM Ca^{2+} or Mg^{2+} resulted in a reduction in steady-state fluorescence at 500 s to ~60% for Mg^{2+} and ~35% for Ca^{2+} (Figure 21a). No changes in total fluorescence quenching were observed when valinomycin was added to these conditions, indicating that the high concentrations of divalent cations are not affecting the structure of the proteoliposomes. However, while the flux rate constant with 5 mM Mg^{2+} is unchanged, it decreases 9-fold with 5 mM Ca^{2+} (Figure 21b), suggesting that, at high concentrations, Ca^{2+} inhibits flux by blocking the KtrAB channel.

These functional experiments establish that the intra-dimer interface site binds both Mg^{2+} and Ca^{2+}, further supporting the idea that divalent cations stabilize the square conformation of the RCK domain ring and activate the KtrAB channel.

Monovalent cation effect in KtrAB function

While establishing the flux assay using choline chloride we tested an assay solution containing 150 mM choline chloride and 1.5 mM KCl, without any Mg^{2+} included. We were surprised to observe that fluorescence quenching was comparable to the sorbitol/Mg^{2+} condition, with steady-state values of ~80% and a rate constant of 0.062 ± 0.007 s^{-1} (Figure 22a and 22c).

Addition of Mg^{2+} had little or no effect in the rate constant (0.058 ± 0.003 or 0.079 ± 0.010 s^{-1} with addition of 0.7 mM or 2 mM Mg^{2+} , respectively), confirming that KtrAB is fully active in the presence of 150 mM choline chloride (Figure 22a and 22c). Lowering the concentration of choline to 20 mM decreased the flux rate by ~2-fold and, as shown above, addition of 0.7 or 2 mM Mg^{2+} re-established maximum activity (Figure 21a and 21c).

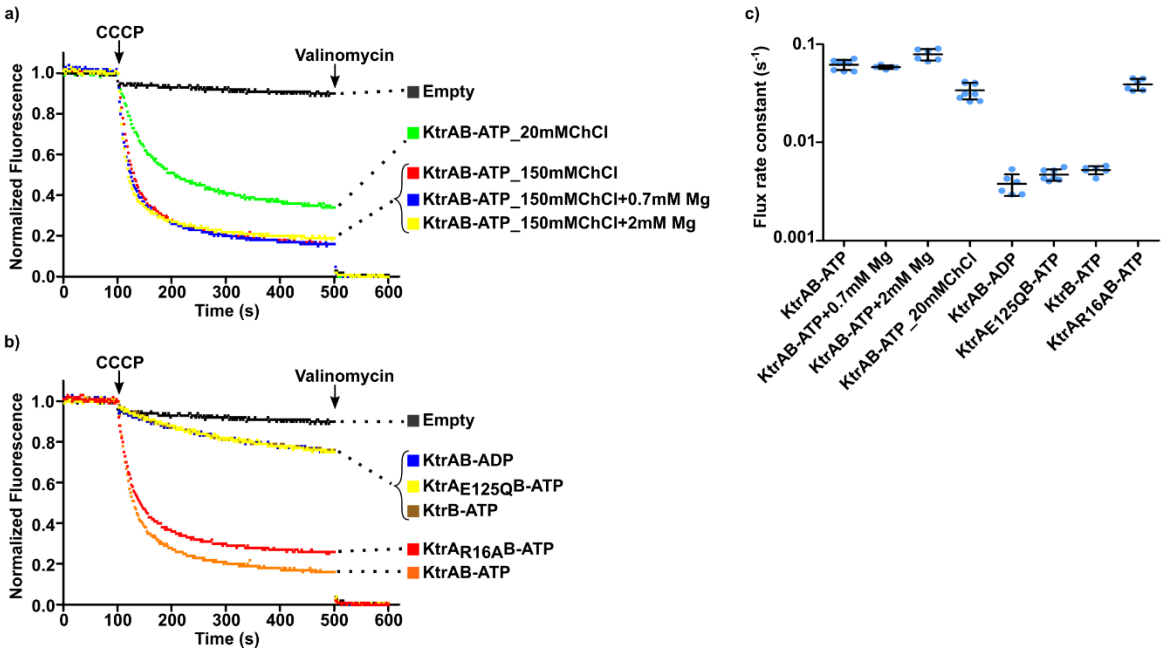

Figure 22: Impact of choline on KtrAB flux. a) and **b)** Proteoliposome flux assay performed with KtrB and wild-type and mutant KtrAB with ATP or ADP with choline chloride (ChCl) in the external solution. Panels show representative fluorescence quenching curves. Empty liposomes were used as control. **c)** Plot of flux rate constants for conditions shown in a) and b). Mean ± SD as well as individual flux rate constants (blue dots) are shown for n=5-9 from at least two different proteoliposome preparations. Conditions correspond to 150 mM choline chloride external solution except where stated otherwise.

The dependence of flux on the concentration of choline chloride raised the possibility that the choline cation and/or the chloride anion are also activators of KtrAB.

To explore the role of Cl^- we performed the functional assay with 150 mM choline acetate (Figure 23) and concluded that KtrAB is active in the absence of Cl^- as the rate constants in choline acetate (0.043 ± 0.002 s^{-1}) and choline chloride (0.062 ± 0.007 s^{-1}) are similar.

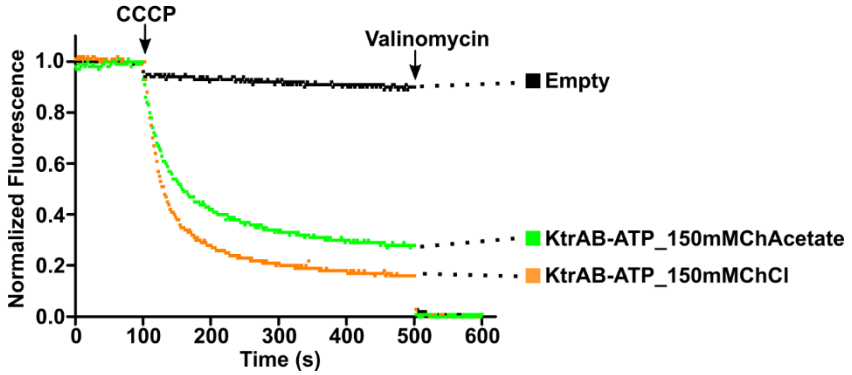

Figure 23: Impact of chloride ion on KtrAB activity. KtrAB-ATP proteoliposome flux assays with choline chloride or choline acetate in the external solution. Representative fluorescence quenching curves obtained for each condition. Empty liposomes were used as controls.

To explore the possibility that choline is an activator, we analysed the impact of the E125Q KtrA mutation and of ADP in the presence of 150 mM choline. Both $KtrA_{E125Q}B$-ATP and KtrAB-ADP display low ion flux, with rates that are 12- and 16-fold slower than for KtrAB-ATP (Figure 22b and 22c). Flux observed in these conditions is similar to that of liposomes reconstituted with KtrB alone (Figure 22b and 22c). In contrast, $KtrA_{R16A}B$-ATP is also active in the choline condition without added Mg^{2+} (Figure 22b and 22c). Importantly, using flame ionization spectroscopy, we determined that the contaminating levels of Mg^{2+} in the choline solution are undetectable (less than 2 µM) which, as shown further down, is well below the activating concentrations for this divalent cation.

Overall, these data suggest that choline is able to activate KtrAB and that the effect is exerted through the RCK domain ring, involving the same intra-dimer interface site previously identified for the divalent cations.

If choline is able to activate KtrAB-ATP, we asked whether the same happens with inorganic monovalent cations. We explored this possibility with Li^+ added to the outside solution, as it is likely that KtrAB is more selective for K^+ than for Li^+ (as demonstrated for KtrB from *V. alginolyticus* and the related cation channel TrkHA (Cao, et al., 2013; Mikusevic, et al., 2019)), allowing us to observe flux. In the presence of 5 and 20 mM Li^+, flux is higher than in sorbitol alone (~2- and ~5-fold, respectively) (Figure 24, confront (cf.) with Figure 20c).

Addition of Mg^{2+} to either one of these conditions results in a 3- and 1.5-fold increase in the rate constants (0.069 ± 0.001 and 0.070 ± 0.002 s^{-1}, respectively), similar to the maximum observed above (cf. Figure 20c). Importantly, $KtrA_{E125Q}B$-ATP or KtrB-ATP in the presence of 20 mM Li^+ display rates that are ~12- and ~15-fold lower than KtrAB-ATP in the same condition, suggesting that the Li^+ effect is mediated by the RCK domain (Figure 24).In 150 mM Li^+ there is a clear decrease in flux rate, down to values that are similar to KtrB-ATP, most likely because in this concentration range Li^+, as a permeant ion, affects the build-up of the H^+-gradient in the assay (Figure 24).

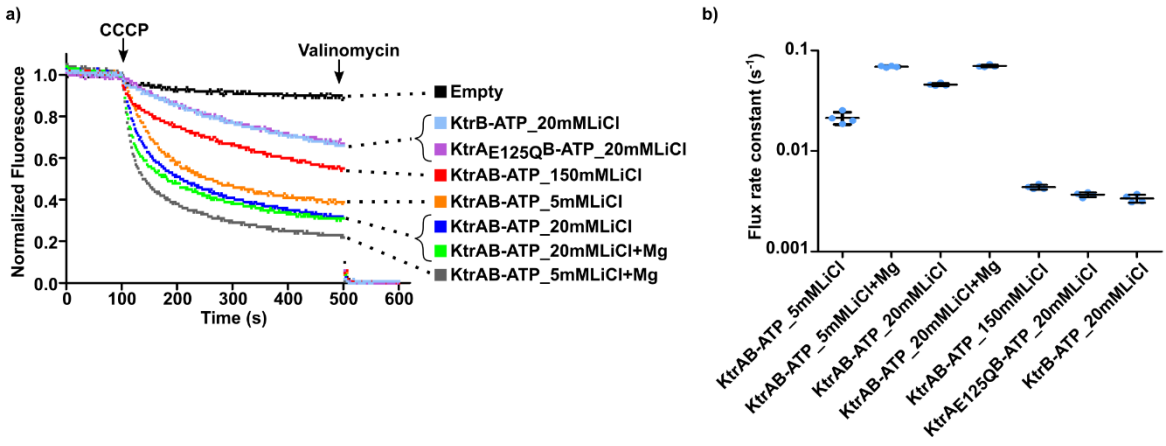

Figure 24: Impact of Li^+ on KtrAB flux. a) Proteoliposome flux assay performed with KtrB and wild-type and mutant KtrAB with ATP with lithium chloride (LiCl) in the external solution. Osmolarity differences were partially compensated with inclusion of sorbitol in the solution. Panels shows representative fluorescence quenching curves. Empty liposomes were used as control. **b)** Plot of flux rate constants for conditions shown in a). Mean ± SD as well as individual flux rate constants (blue dots) are shown for n=4 from one proteoliposome preparation. For conditions in 20 mM Li^+ (with and without Mg^{2+}) and in 5 mM (Li^+ (without Mg^{2+}) the amplitude of the fast component of the double-phase exponential fit is either equal or smaller than of the slow component. However, we plot the "fast" rate constant as it represents the initial decay phase of the curve, allowing comparison with other rate constants (see Appendix- Table 6).

Overall, our data suggests that monovalent cations (both Li^+ and choline) are able to activate KtrAB through a mechanism that involves the intra-dimer interface of the RCK domain.

We decided to compare the impact of monovalent and divalent cations on the activation mechanism of KtrAB. To do so, we performed titrations of choline and Mg^{2+} using the flux assay (Figure 25 and Appendix- Figure 29). Although osmolarity differences did not affect flux (Appendix- Figure 30), we matched the osmolarity of the conditions in the two titration experiments to directly compare results. In addition, we verified that the free concentration of Mg^{2+} in the assay solutions is similar to the added concentration. For this, we spun-down proteoliposomes after running the assay and measured Mg^{2+} in the supernatant using flame ionization spectroscopy. For example, for conditions with 25, 107 and 1156 µM added Mg^{2+}, the determined free concentrations were 34 ± 0, 126 ± 8 and 1210 ± 9 µM, respectively.

The titrations show that increasing concentrations of both Mg^{2+} and choline result in increased flux rate (Figure 25a and 25c). Fitting the titration curves with a Hill equation yielded a $K_{1/2}$ of activation for Mg^{2+} of 155 ± 17 µM (Hill coefficient 1.8 ± 0.0) and for choline, 25 ± 2 mM for choline with a Hill coefficient 1.9 ± 0.2 (Figure 25b and 25d).

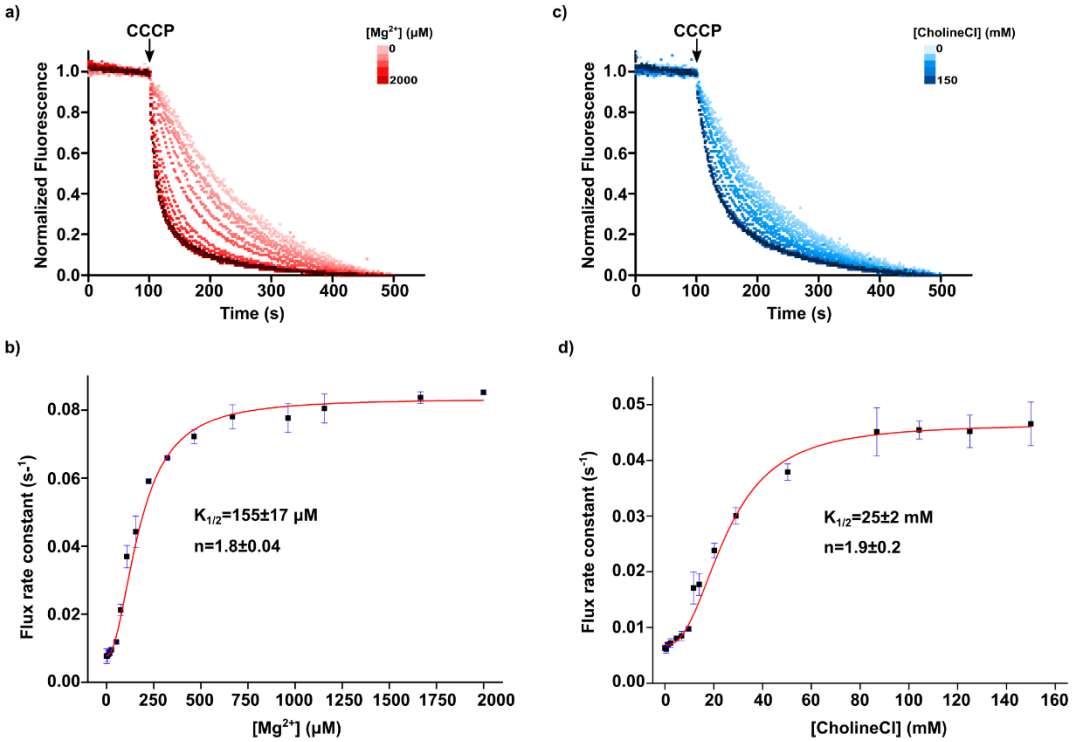

Figure 25: Mg^{2+} and Choline titrations. a) Magnesium ion titration of KtrAB-ATP using a proteoliposome flux assay performed with increasing amounts of $MgCl_2$ added to a 300 mM sorbitol external solution. Panel shows representative fluorescence quenching titration curves normalized to their steady-state. Magnesium ion concentration increases with red color intensity from 0 to 2000 µM **b)** Plot of flux rate constants (mean ± SD, from 3 separate titrations) as a function of magnesium ion concentration. **c)** Choline titration of KtrAB-ATP using a proteoliposome flux assay performed with increasing amounts of choline chloride in the external solution while compensating the change in osmolarity with sorbitol. Panel shows representative fluorescence quenching titration curves normalized to their steady-state. Choline chloride concentration increases with blue color intensity from 0 to 150 mM **d)** Plot of flux rate constants (mean ± SD, from 3 separate titrations) as a function of choline concentration. Titrations were fitted with a Hill equation, $y = Start + (End - Start) \times \frac{x^n}{K1/2^n + x^n}$. Mean ± SD of $K_{1/2}$ and of Hill coefficients (n) determined from fits to separate titrations are shown. EDTA was not added to the external solution in these assays.

Overall, these data strongly suggest that monovalent cations, including an organic monovalent, are able to activate the KtrAB complex and that this effect is ATP dependent and dependent on an intact intra-dimer interface binding site. Nevertheless, we clearly show that the KtrAB activation mechanism is ~160-fold more sensitive to Mg^{2+} than choline.

Conserved divalent cation binding site in other nucleotide-dependent RCK domains

Nucleotide-dependent RCK domains are associated with different families of bacterial K^+ or cation transporters and we wondered if the intra-dimer interface divalent cation-binding site is conserved in those proteins. More specifically, we verified the conservation of a glutamate (equivalent to the KtrA E125) in the intra-dimer interface.

For this we analysed structures of RCK domains which are known to be nucleotide-dependent by having a bound nucleotide like KtrA or having the classical nucleotide binding site motif associated with a Rossmann fold (GxGxxG[17-18]xE/D; where G is glycine, E glutamate, D aspartate and x any amino acid) (Bellamacina, 1996). In this analysis, we did not consider the RCK domain from GsuK since only one of the domains in the RCK dimeric unit binds nucleotides (Kong, et al., 2012).

First, we analysed the structure of the KtrA protein from the thermophilic archaean *Methanocaldococcus jannaschii* (PDB: 1LSS) (Figure 26a). The structure clearly shows a glutamate residue in the same position as E125 in KtrA from *B. subtilis*. We generated a sequence alignment of KtrA orthologs by randomly selecting 2-3 species from all phyla of bacteria and archaea that have Ktr cation channels. We cured the alignment to retain only proteins that show the nucleotide binding site sequence motif (Figure 26b and Appendix- Figure 31). The final alignment has 15 sequences, including KtrA from *B. subtilis*, of which 13 have a glutamate coincident with E125, corresponding to 87% sequence identity. Interestingly, a neighbouring proline is also highly conserved, forming the motif PE.

We also inspected the TrkA protein from *Vibrio parahaemolyticus* (PDB: 4J9V); this protein assembles with the membrane protein TrkH to form the non-selective TrkAH cation channel (Figure 26c). TrkA has two RCK domains in tandem (RCK1 and RCK2), forming a pseudo-dimeric unit, and both domains bind nucleotide. In the intra-dimer interface there is a glutamate in RCK1 in a position similar to that of E125 in KtrA. In

contrast, in RCK2 there is a glutamine. A sequence alignment of TrkA orthologs, generated using the approach described above, shows that the PE sequence motif noted in KtrA is highly conserved in RCK1 (80% sequence identity) (Figure 26d and Appendix- Figure 32). However, there are no glutamates or aspartates in the E125 position of RCK2 in any of the orthologs (Appendix- Figure 33); instead, arginine and lysine residues are common, suggesting that in TrkA the activation mechanism is not dependent on a divalent cation cofactor.

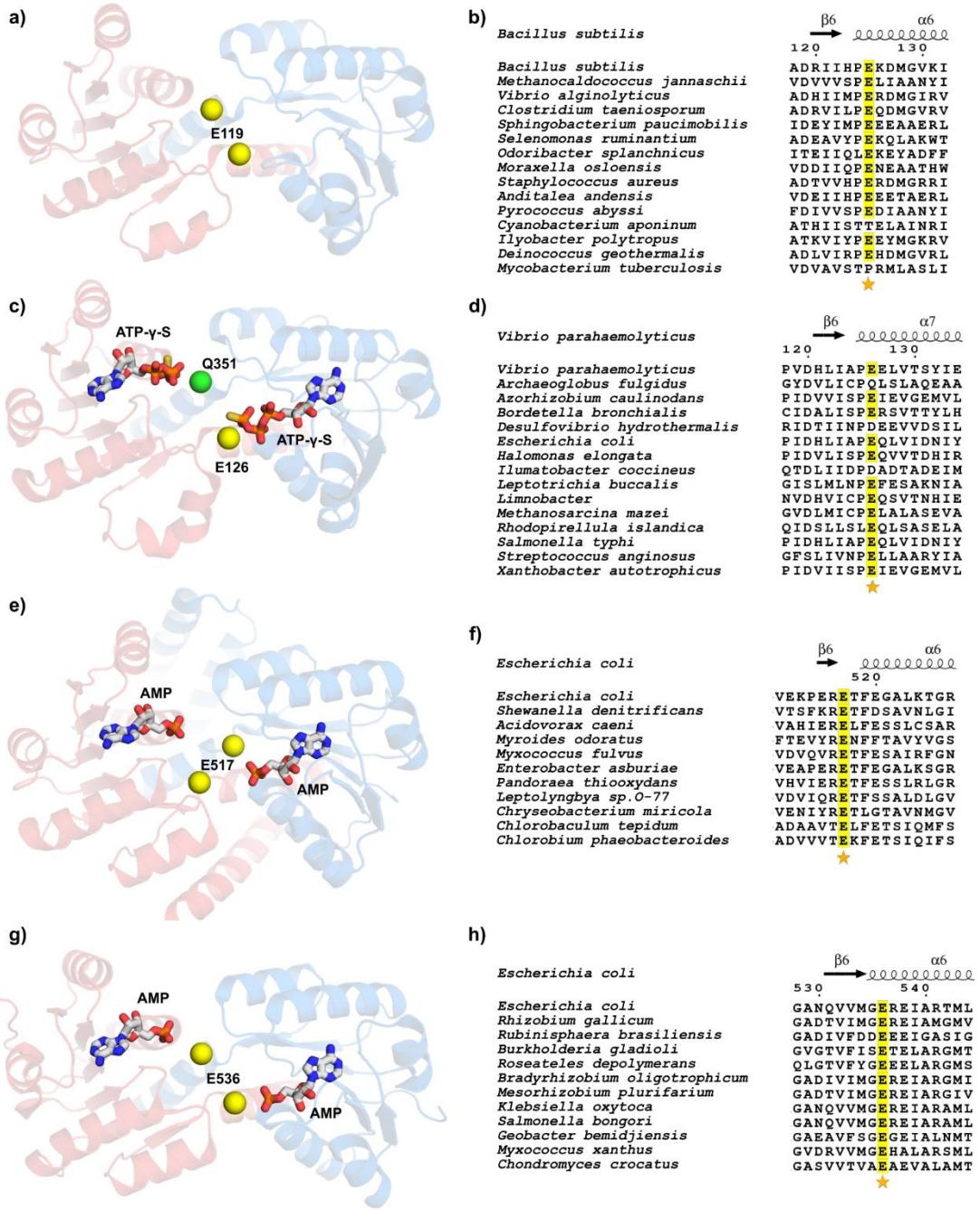

Figure 26: Conservation of glutamate residue in the intra-dimer interface of nucleotide-dependent RCK domains. a) View of nucleotide binding sites in *M.jannaschii* KtrA dimer (PDB: 1LSS). **b)** Partial view of sequence alignment of KtrA orthologs with conserved glutamate in yellow. Numbering and secondary structure elements are from *B. subtilis* KtrA. **c)** View of nucleotide binding sites in *V. parahaemolyticus* TrkA pseudo-dimer (PDB: 4J9V). The RCK2 glutamine in an equivalent position to KtrA E125 is shown as a green sphere. **d)** Partial view of sequence alignment of TrkA orthologs with conserved glutamate in RCK1 in yellow. Numbering and secondary structure elements are from the *V.parahaemolyticus* TrkA. **e)** View of nucleotide binding sites in *E.coli* KefC C-terminal dimer (PDB: 3L9W). **f)** Partial view of sequence alignment of Kef orthologs with conserved glutamate in yellow. Numbering and secondary structure elements are from the *E.coli* KefC C-terminal. **g)** View of nucleotide binding sites in *E.coli* YbaL C-terminal dimer (PDB: 3FWZ). **h)** Partial view of sequence alignment of YbaL orthologs with conserved glutamate in yellow. Numbering and secondary structure elements are from the *E.coli* YbaL C-terminal. Dimer subunits are colored red and blue and conserved glutamates are shown as yellow spheres. Sequence alignments were obtained with MEGA software (Tamura et al., 2013) and figures made using ESPript (Robert & Gouet, 2014). In all alignments, the position corresponding to KtrA E125 or equivalent is marked with a star.

We also found the structure of an RCK octameric ring formed by two different RCK proteins (TM1088A/TM1088B) (Deller, et al., 2015). Each protein assembles as a homo-dimeric unit and the ring includes two pairs of each dimeric unit, with identical pairs positioned across each other in the ring. As in TrkA, the RCK pair that binds nucleotide does not have the conserved divalent cation site, showing a PA sequence motif, instead of PE, in the intra-dimer interface.

Another nucleotide-dependent RCK family for which there are available structures is that of the regulatory domain of the Kef K^+/H^+ antiporters (Munro et al., 1991; Pliotas et al., 2017; Roosild et al., 2010; Roosild, et al., 2009). Unlike the Ktr and Trk channels where the RCK domain is a separate protein, in Kef antiporters the membrane protein and the RCK domain are in the same polypeptide. In addition, their C-terminal regions lack the C lobe observed in the RCK domains of MthK and KtrA. Despite these differences, the structure of the C-terminal domain of KefC from E. coli shows the homo-dimeric unit arrangement and an AMP molecule bound in a similar binding site to KtrA (Figure 26e). Strikingly, the KefC structure shows a glutamate at the intra-dimer interface, shifted one residue in the sequence relative to KtrA. However, this is a position where the glutamate can still potentially coordinate a divalent cation, as E125 in KtrA.

While analysing sequences of KefC proteins it became apparent that there are three groups of Kef-related proteins: the KefC proteins (with at least 580 amino acids), the KefC-like group (less than 580 amino acids long) and the YbaL orthologs (Appendix-Figure 34). A sequence alignment of the C termini of 11 KefC proteins shows that the glutamate at the intra-dimer interface is 100% conserved (Figure 26f and Appendix-Figure 35). The sequence motif is RE or TE, and not PE as seen in KtrA. In contrast, in the sequence alignment of KefC-like proteins the glutamate is substituted by a conserved tyrosine or phenyalanine (Appendix- Figure 36).

Finally, we analyzed the structure of the nucleotide-dependent RCK domain of YbaL (PDB: 3FWZ), a putative *E.coli* cation antiporter. As stated above, YbaL proteins are related to KefC. This structure also shows the presence of a glutamate in the intra-dimer interface in an equivalent position to that of E125 in KtrA (Figure 26g). A sequence alignment reveals that the glutamate is strongly conserved (100% conserved among the 12 sequences) but the sequence motif is primarily GE instead of PE (Figure 26h and Appendix- Figure 37).

This analysis reveals a striking conservation of glutamates in the intra-dimer interface of many homodimeric nucleotide-dependent RCK domains. These glutamates occupy similar positions to E125 in KtrA, strongly suggesting that the cation-binding site is present in many nucleotide-dependent RCK domains and in particular, that divalent cations are essential cofactors for the activation of these RCK proteins.

DISCUSSION

We have established that the activation mechanism of KtrA, a nucleotide-dependent RCK domain, involves divalent cations, Mg^{2+} or Ca^{2+}, as cofactors. The divalent cation binds to the intra-dimer interface site of a KtrA dimer, coordinated by E125 and the γ-phosphates from two ATP molecules. This results in the tethering of the two ATP molecules, stabilizing the active state square conformation of the octameric ring.

Our data also strongly suggests that monovalent cations like Li^{+} and choline, an organic monovalent cation, are able to activate KtrAB. This effect is dependent on the RCK domain having bound ATP and an intact intra-dimer interface site, as either ADP or mutation of E125 disrupt activation. This suggests that, like Mg^{2+} or Ca^{2+}, monovalent cations bind to the intra-dimer interface site. Although not demonstrated here, it is likely that K^{+} will also activate KtrAB-ATP, providing an explanation for the partial activity of

KtrAB-ATP in the absence of Mg^{2+} (Figure 20a). In those experiments, the lumen of the liposomes contains 150 mM K^+ and therefore the fraction of KtrAB-ATP molecules that are oriented with KtrA facing the lumen will be activated by K^+, giving rise to a flux curve that is intermediate between KtrAB-ADP and KtrAB-ATP-Mg^{2+}.

The dimensions of the intra-dimer interface binding site as well as the chemical groups that line this site are ideal for divalent cation binding, as reflected in the KtrA structures with Mg^{2+} and Ca^{2+} and the $K_{1/2}$ of activation ~150 μM, corresponding to 160-fold higher sensitivity of the activation mechanism for Mg^{2+} over choline. Nevertheless, it is easy to imagine that several lithium ions will bind in the intra-dimer interface site, compensating the intense negative electrostatics of the site and stabilizing the close positioning of the ATP γ-phosphate groups in the active conformation. It is harder to imagine how choline binds to the same site but the quaternary ammonium group in choline might adopt the flattened configuration seen in the TBA (tetrabutylammonium) molecule bound in the pore of the KcsA K^+ channel (Lenaeus et al., 2014). In this configuration, the group might be able to slide into the intra-dimer crevice in the non-square conformation and stabilize, at least, a partial closure of the site around the cation, giving rise to activation.

What cation functions as the activation cofactor in the cell?

We determined that the $K_{1/2}$ for Mg^{2+} activation is ~150 μM. Mg^{2+} is often found associated with ATP molecules and is by far the most abundant divalent cation in the cytosol of bacteria, with a total concentration of ~100 mM (Moncany & Kellenberger, 1981) and a free concentration of ~2 mM (Alatossava et al., 1985), 13-fold higher than the determined $K_{1/2}$. In contrast, the concentration of free calcium in bacteria has been estimated at 100-300 nM (Gangola & Rosen, 1987; Jones et al., 1999). It is therefore reasonable to think that in the cell, the active conformation of the RCK domain ring in KtrAB will involve Mg^{2+} and not Ca^{2+}. We have not been able to determine the $K_{1/2}$ of activation for Li^+ or K^+ using the flux assay and determination of their binding affinity for the intra-dimer interface site by isothermal titration calorimetry (ITC) is likely to be complicated by all the interactions established between the cation and other protein chemical groups. However, the reported K^+ concentration in the cytosol of *B. subtilis* is ~300 mM, rising to 600-700 mM in certain environmental conditions (Whatmore, et al., 1990; Whatmore & Reed, 1990). It is therefore likely that the free concentration of the monovalent cation in the cytosol is sufficient to make a contribution to the activation of KtrAB.

We have determined multiple structures of the KtrA octameric ring. A comparison of the ring structures with bound-ATP and adopting the square conformation revealed that they are very similar to each other, with little differences in the Cα N38 L1/L2 distances and low RMSDs for Cα atoms: 0.56 Å for R16K-ATP and 0.83 Å for R16A-ATP, when compared to WT-ATP (PDB: 4J90). In contrast, we found a large structural variability in the non-square structures, with four different conformational groups based on Cα N38 L1/L2 distances. This indicates that there is a single well defined square or active conformation for KtrA, while the ring in the non-active (or non-square) conformation is most likely more flexible, giving rise to different ring conformations in the crystals of isolated KtrA.

Although our understanding of the conformational changes occurring in the KtrA ring during activation is well established, the same cannot be said of the membrane protein KtrB. The non-active conformation (ADP-bound) seems well represented by the structure of KtrAB-ADP from *V. alginolyticus* (Diskowski, et al., 2017), where the flexible KtrA ring appears to adapt its conformation to that of the KtrB dimer, favouring the formation of interactions between the two proteins. In particular, the long transmembrane helix D1M2 from the KtrB subunits interacts with the inner surface of the ring. Binding of ATP and of the cation cofactor to the RCK domain stabilizes the rigid square conformation of the octameric ring. This appears to cause the release of D1M2 from its interaction site on KtrA and bending of the C-terminal end into a short helix, parallel to the membrane surface. This change must be propagated to the intramembrane loop region of KtrB, opening the pore gate. However, we do not have a good molecular understanding of the activated-state of KtrB since the ion pore of the membrane protein remains closed in the available KtrAB-ATP structure despite the adoption of the square conformation by KtrA (Vieira-Pires, et al., 2013). We do not know the reason for this “incomplete” activation but it is possible that KtrAB-ATP does not adopt the fully active conformation in detergent.

It is worthwhile pointing out that a $^{86}Rb^{+}$-uptake assay had previously been used to characterize KtrAB function (Szollosi, et al., 2016; Vieira-Pires, et al., 2013). With that assay, very low levels of activity for KtrAB-ATP were observed, taking ~60 minutes to reach 20% of valinomycin signal (total signal), that were only 2-fold faster than for KtrAB-ADP. Those values contrast with the levels of activity described here, using the fluorescence based ACMA-liposome K^{+} flux assay. We now understand that the low KtrAB-ATP activity recorded in those early reports is partly due to a lack of cations in the assay solution, so that many KtrAB-ATP molecules were not in an activated state.

Importantly, analysis of structures and amino acid sequences of nucleotide-dependent RCK domains from several different channel and transporter families demonstrated the presence of a strongly conserved glutamate in the intra-dimer interface, at a position that is equivalent to E125 in KtrA. These conserved glutamates are available for interaction with cations, divalent cations in particular, strongly suggesting that the cation-binding site is conserved and that cations are cofactors in the regulatory mechanism of many nucleotide-dependent RCK domains.

APPENDIX

Table 6: Parameters extracted from fits of fluorescence quenching curves with one-phase (τ) or two-phase exponential equations (τ_{fast} and τ_{slow}).

Sorbitol external solution								
[Sorbitol]	**Proteoliposomes**	**Amplitude**	**τ (s)**	**Amplitude (fast)**	**τ_{fast} (s)**	**Amplitude (slow)**	**τ_{slow} (s)**	**Plateau**
150mM	KtrAB-ATP	0.44±0.06	97.32±9.51	-	-	-	-	0.50±0.06
	KtrAB-ATP 2mM Mg	-	-	0.39±0.03	10.40±0.88	0.12±0.02	110.34±25.17	0.25±0.06
	KtrAB-ADP	0.31±0.01	291.42±33.11	-	-	-	-	0.64±0.01
	KtrAB-ADP 2mM Mg	0.18±0.01	149.38±10.26	-	-	-	-	0.75±0.01
	$KtrA_{E125Q}B$-ATP	0.80±0.00	813.33±25.51	-	-	-	-	0.2*
	$KtrA_{E125Q}B$-ATP 2mM Mg	0.39±0.01	270.00±4.85	-	-	-	-	0.59±0.01
	$KtrA_{R16A}B$-ATP	0.45±0.01	129.77±9.95	-	-	-	-	0.51±0.01
	$KtrA_{R16A}B$-ATP 2mM Mg	-	-	0.35±0.01	12.34±0.31	0.18±0.01	92.83±4.33	0.25±0.01
	KtrB-ATP	0.44±0.07	288.96±41.69	-	-	-	-	0.54±0.07
	KtrB-ATP 2mM Mg	0.28±0.01	108.33±2.21	-	-	-	-	0.66±0.01
Choline Chloride external solution								
[CholineCl]	**Proteoliposomes**	**Amplitude**	**τ (s)**	**Amplitude (fast)**	**τ_{fast} (s)**	**Amplitude (slow)**	**τ_{slow} (s)**	**Plateau**
150mM	KtrAB-ATP	-	-	0.45±0.04	16.42±1.88	0.24±0.02	115.19±11.09	0.16±0.06
	KtrAB-ATP 0.7mM Mg	-	-	0.43±0.04	17.17±0.64	0.24±0.02	126.36±5.40	0.17±0.04
	KtrAB-ATP 2mM Mg	-	-	0.43±0.06	12.91±1.57	0.20±0.03	106.19±7.34	0.18±0.01
	KtrAB-ADP	0.24±0.02	276.83±56.71	-	-	-	-	0.72±0.01
	$KtrA_{E125Q}B$-ATP	0.27±0.02	216.77±25.83	-	-	-	-	0.70±0.02
	KtrB-ATP	0.25±0.04	193.01±19.11	-	-	-	-	0.72±0.05
	$KtrA_{R16A}B$-ATP	-	-	0.38±0.02	26.10±3.22	0.28±0.05	134.27±21.72	0.24±0.02
20mM	KtrAB-ATP	-	-	0.38±0.06	30.55±5.55	0.25±0.07	153.07±25.75	0.32±0.02
	KtrAB-ATP 0.7mM Mg	-	-	0.43±0.06	13.40±1.51	0.25±0.03	129.19±9.78	0.18±0.02
	KtrAB-ATP 2mM Mg	-	-	0.39±0.02	10.57±0.80	0.17±0.04	116.49±11.33	0.20±0.01
	KtrAB-ATP 5mM Mg	-	-	0.20±0.02	9.46±0.93	0.24±0.01	116.26±4.36	0.41±0.01
	KtrAB-ATP 0.7mM Ca	-	-	0.33±0.01	11.81±1.03	0.24±0.01	120.28±7.69	0.24±0.01
	KtrAB-ATP 2mM Ca	-	-	0.38±0.02	10.93±0.14	0.21±0.01	130.42±5.24	0.21±0.01
	KtrAB-ATP 5mM Ca	0.19±0.01	97.99±3.69	-	-	-	-	0.66±0.01

Table 6 (continued)

Choline Acetate external solution								
[Choline Acetate]	**Proteoliposomes**	**Amplitude**	**τ (s)**	**Amplitude (fast)**	**τ_{fast} (s)**	**Amplitude (slow)**	**τ_{slow} (s)**	**Plateau**
150mM	KtrAB-ATP	-	-	0.33±0.01	23.54±1.09	0.31±0.01	143.83±8.73	0.26±0.01
Lithium Chloride external solution								
[LiCl]	**Proteoliposomes**	**Amplitude**	**τ (s)**	**Amplitude (fast)**	**τfast (s)**	**Amplitude (slow)**	**τslow (s)**	**Plateau**
150mM	KtrAB-ATP	0.39±0.03	229.34±10.39	-	-	-	-	0.50±0.03
5mM	KtrAB-ATP	-	-	0.31±0.04	47.56±5.33	0.31±0.03	222.95±30.3	0.34±0.01
	KtrAB-ATP 0.7mM Mg	-	-	0.35±0.04	14.47±0.24	0.31±0.03	149.63±5.32	0.21±0.01
20mM	KtrAB-ATP	-	-	0.31±0.03	21.85±0.63	0.36±0.04	178.09±5.70	0.27±0.01
	KtrAB-ATP 0.7mM Mg	-	-	0.25±0.02	14.28±0.37	0.37±0.01	164.03±3.75	0.28±0.01
	KtrB-ATP	0.38±0.03	298.46±23.10	-	-	-	-	0.60±0.04
	KtrAE125QB-ATP	0.39±0.01	272.15±13.48	-	-	-	-	0.58±0.01

Values shown are the mean ± SD values calculated from parameters from individual fits. Rate constants referred to in the text and figures were calculated as the mean of the inverse of τ extracted from individual fits. * For KtrAE125QB-ATP in 150mM sorbitol the plateau had to be fixed during fitting since the signal is closer to a linear decay.

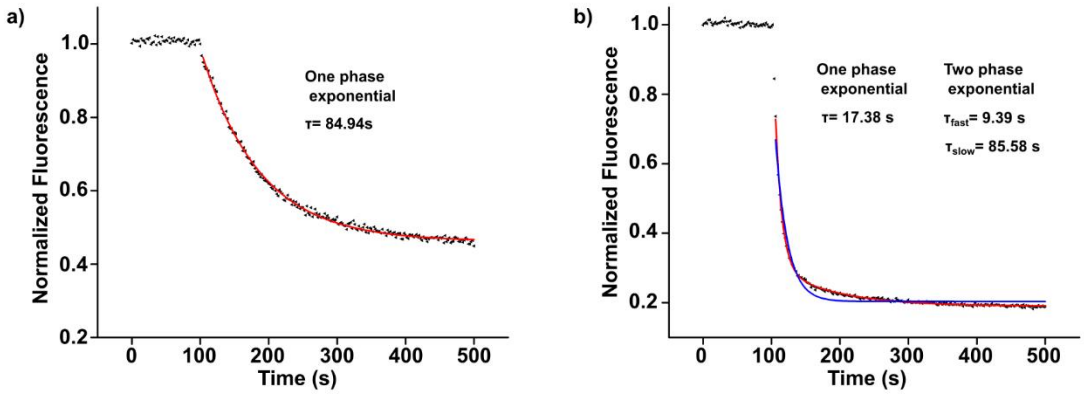

Figure 27: Examples of fluorescence quenching fits with exponential equations. a) KtrAB-ATP flux assay representative curve with sorbitol in the external solution. Fit was performed using a one-phase exponential equation: $y = y0 + A1e^{-(x-x0)/\tau}$ (red line). **b)** KtrAB-ATP flux assay representative curve with sorbitol in the external solution and in the presence of 2 mM magnesium. Fit was performed using a two-phase exponential equation: $y = y0 + A1e^{-(x-x0)/\tau fast} + A2e^{-(x-x0)/\tau slow}$ (red line). Attempt of fitting with a one phase exponential equation is shown as a blue line.

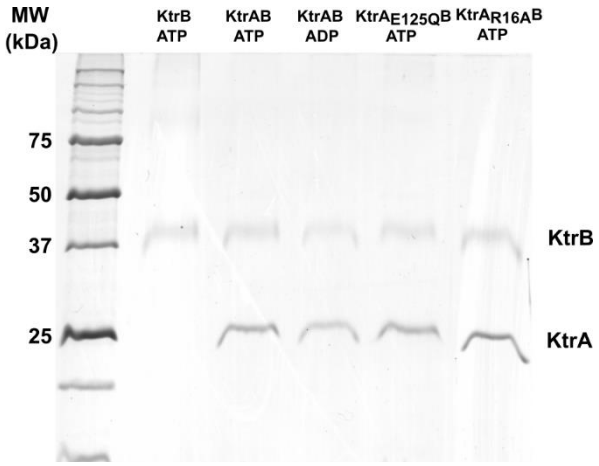

Figure 28: SDS-PAGE gel analysis of proteoliposomes. 5 µl of proteoliposomes reconstituted with KtrB or KtrAB assemblies were loaded in each well. Molecular weight markers (MW) are shown on the left. Bands corresponding to KtrB and KtrA are indicated.

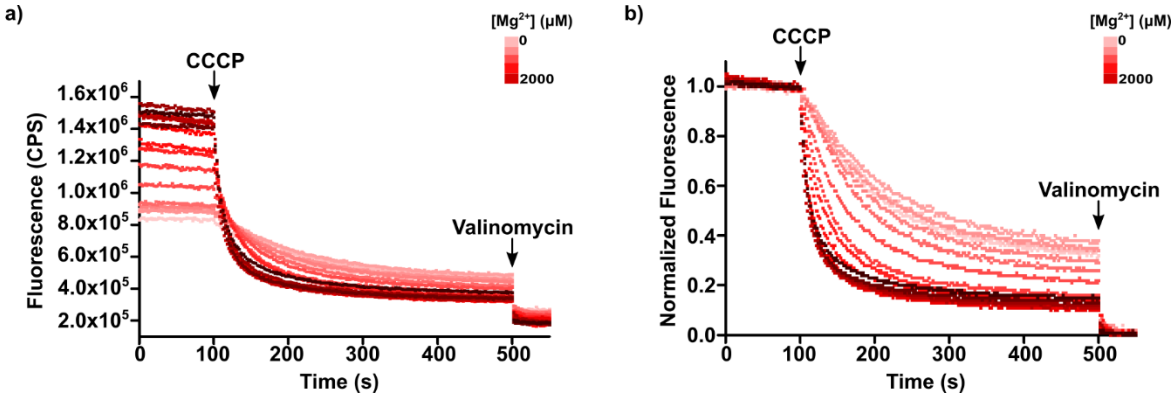

Figure 29: Fluorescence raw and normalized data from Mg^{2+} titration. a) Raw fluorescence data from representative titration. **b)** Same data after normalization to valinomycin quenching. Magnesium ion concentration increases with red color intensity from 0 to 2000 µM. In many of the thesis figures depicting flux assay experiments, the steady-state levels of fluorescence quenching curves are different from each other, as shown in b), when it would be expectable to have the same level. In most cases this resulted from the impact of the external solution conditions on the initial fluorescence value (before addition of CCCP), as shown in a), and from normalization using the fluorescence values after valinomycin addition, which change little across different experiments. We do not fully understand the reason for the differences in initial fluorescence but it appears that ACMA fluorescence is sensitive to the ionic strength of bathing solutions.

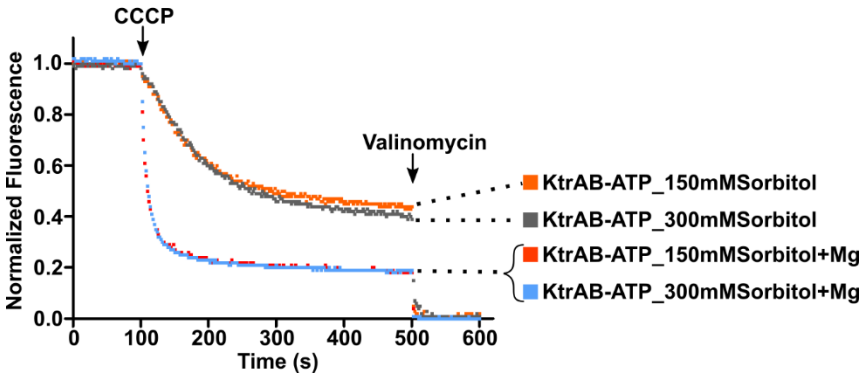

Figure 30: Effect of osmolarity in KtrAB flux. KtrAB-ATP proteoliposome flux assays with sorbitol at 150 or 300mM (matching the osmolarity of a 150 mM choline chloride solution) in the external solution, showing little impact of the osmolarity change on the function of KtrAB-ATP.

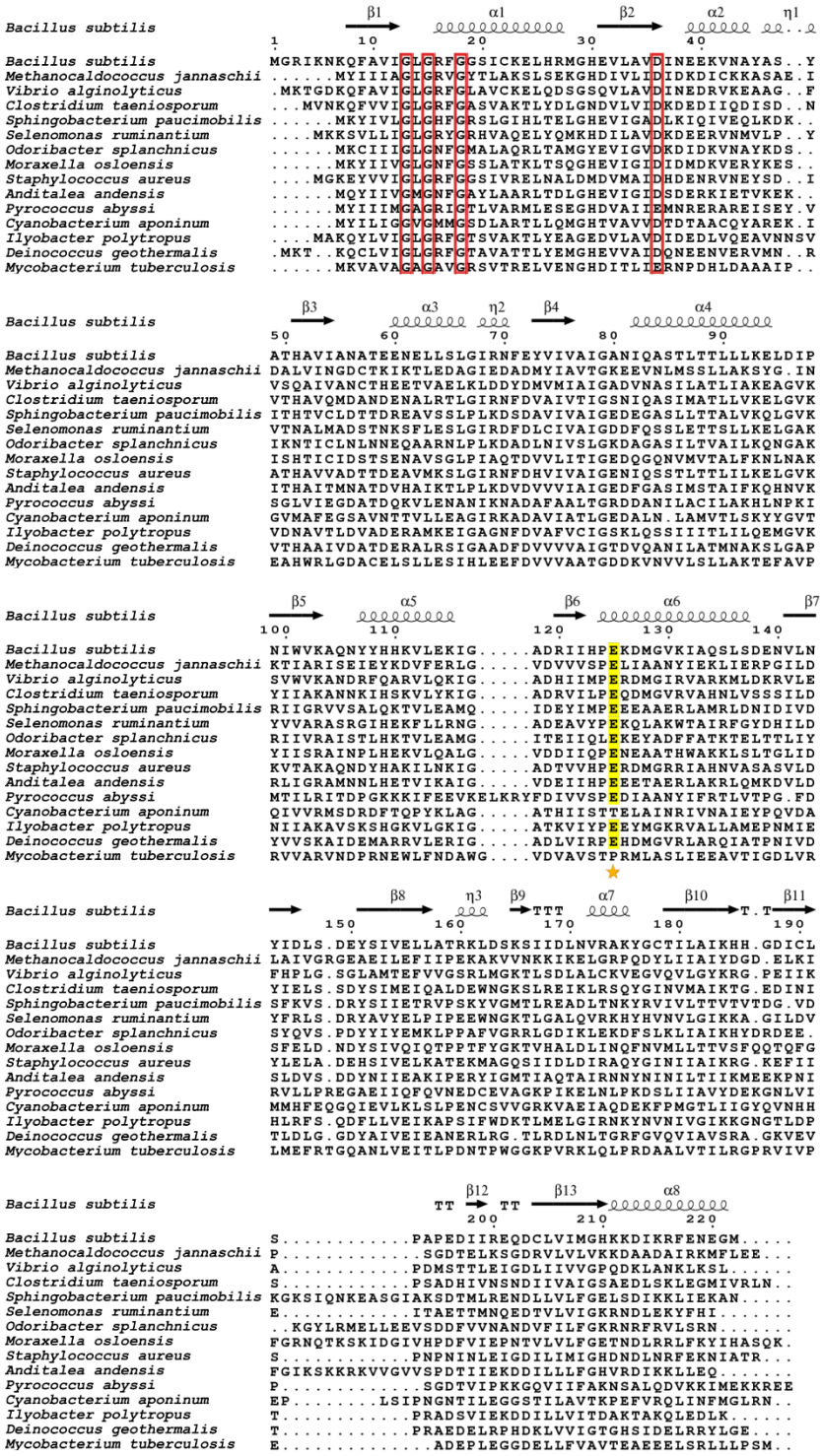

Figure 31: Sequence alignment of KtrA orthologs. Numbering and secondary structure features are from the first protein in the alignment. The position corresponding to the KtrA E125 is marked with a star. Conserved glutamates are highlighted in yellow and nucleotide binding motif positions are boxed in red.

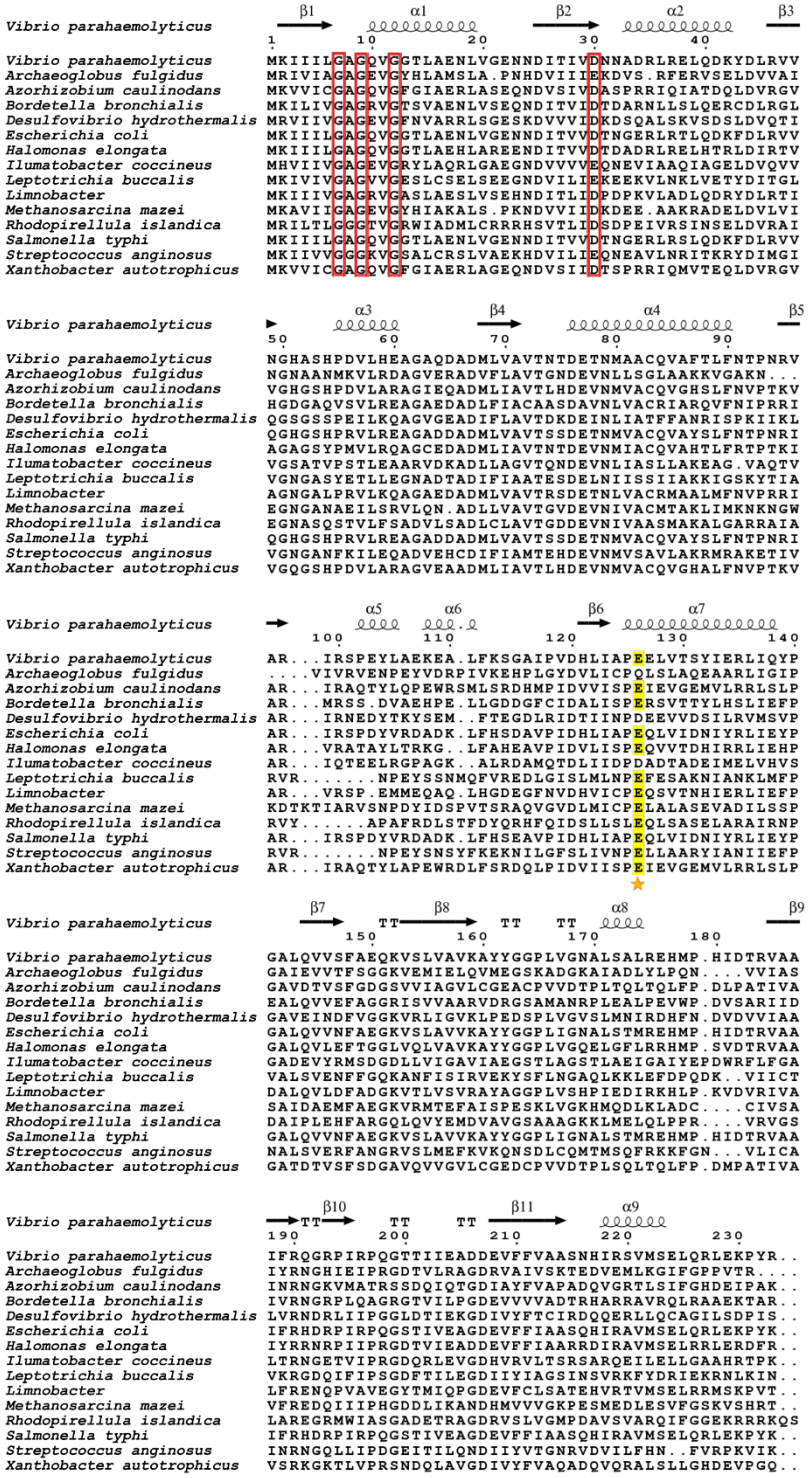

Figure 32: Sequence alignment of RCK1 domains from TrkA orthologs. Numbering and secondary structure features are from the first protein in the alignment. The position corresponding to the equivalent of KtrA E125 is marked with a star. Conserved glutamates are highlighted in yellow and nucleotide binding motif positions are boxed in red.

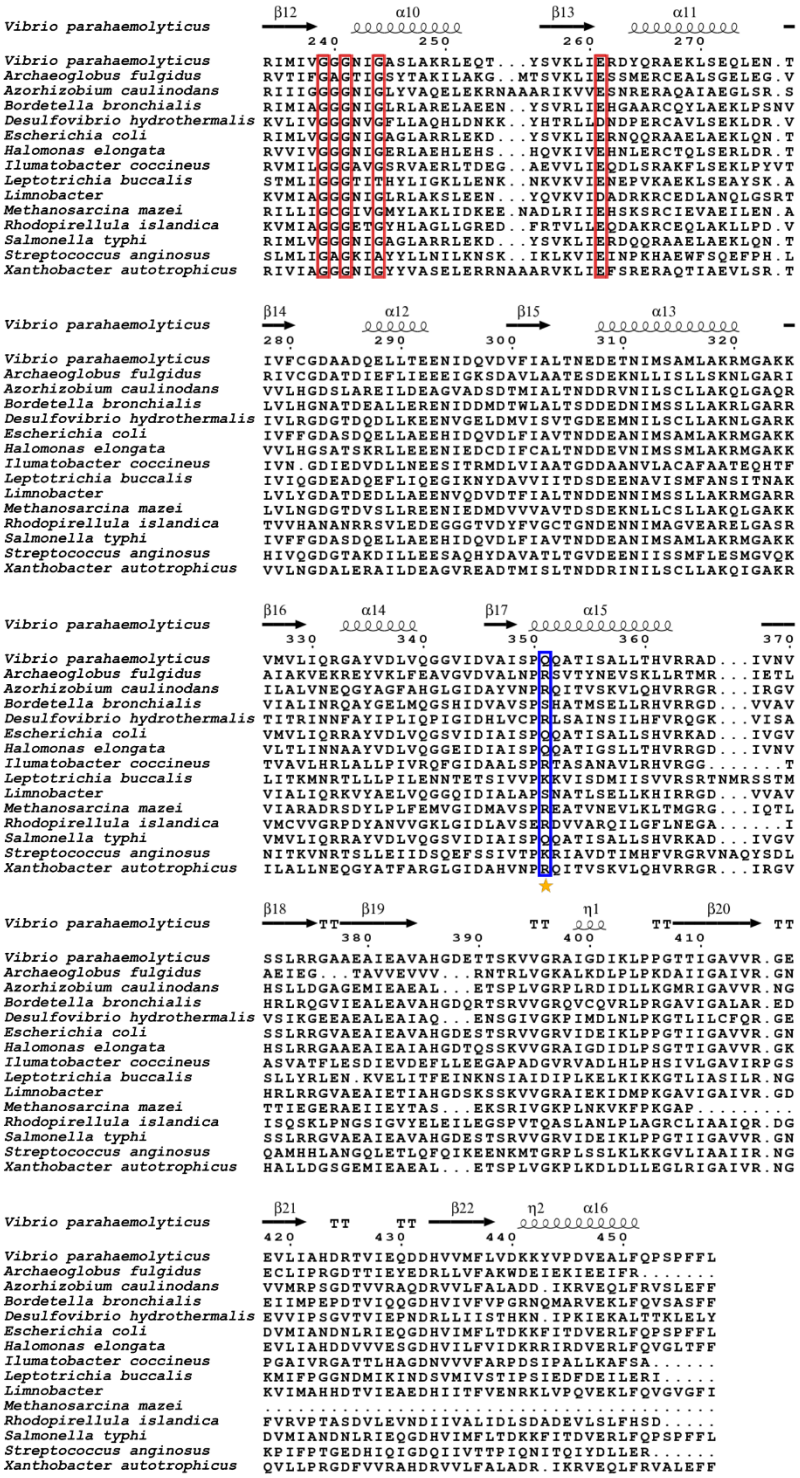

Figure 33: Sequence alignment of RCK2 domains from TrkA orthologs. Numbering and secondary structure features are from the first protein in the alignment. The position corresponding to the equivalent of KtrA E125 is marked with a star. Positions without conserved glutamates are boxed in blue and nucleotide binding motif positions are boxed in red.

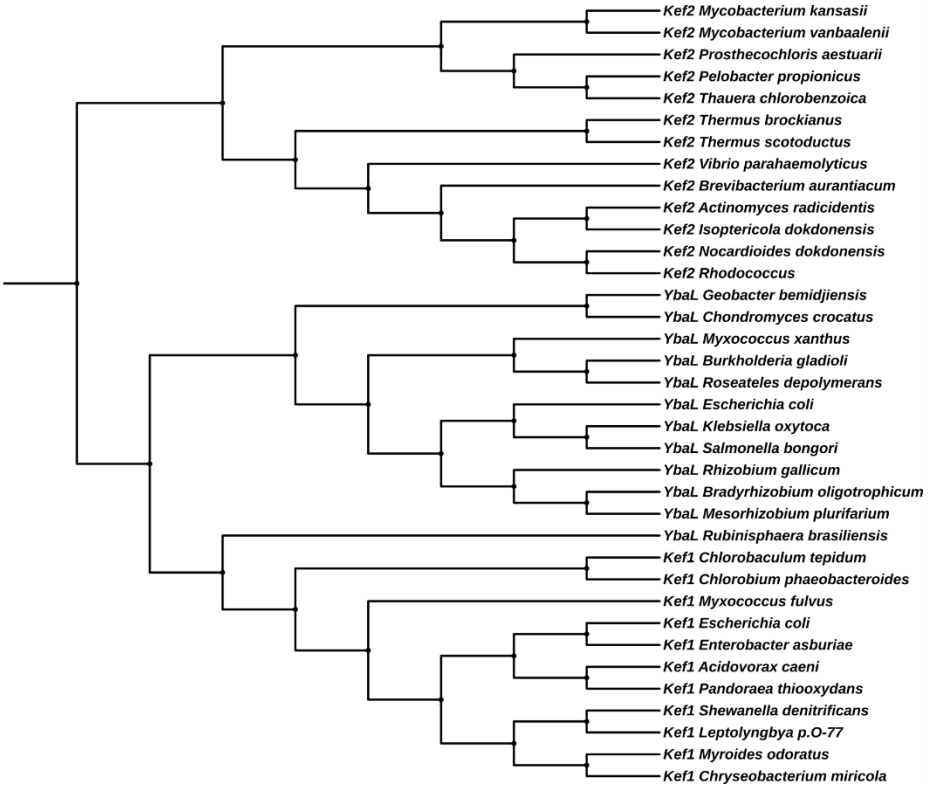

Figure 34: Phylogenetic tree of Kef-related proteins. Maximum-likelihood tree of sequence alignment of Kef-related proteins. The tree reveals three groups: Kef1 corresponds to KefC proteins, with at least 580 amino acids; Kef2 corresponds to KefC-like proteins, with less than 580 amino acids; and YbaL orthologs. Tree was generated using MEGA software (Tamura, et al., 2013).

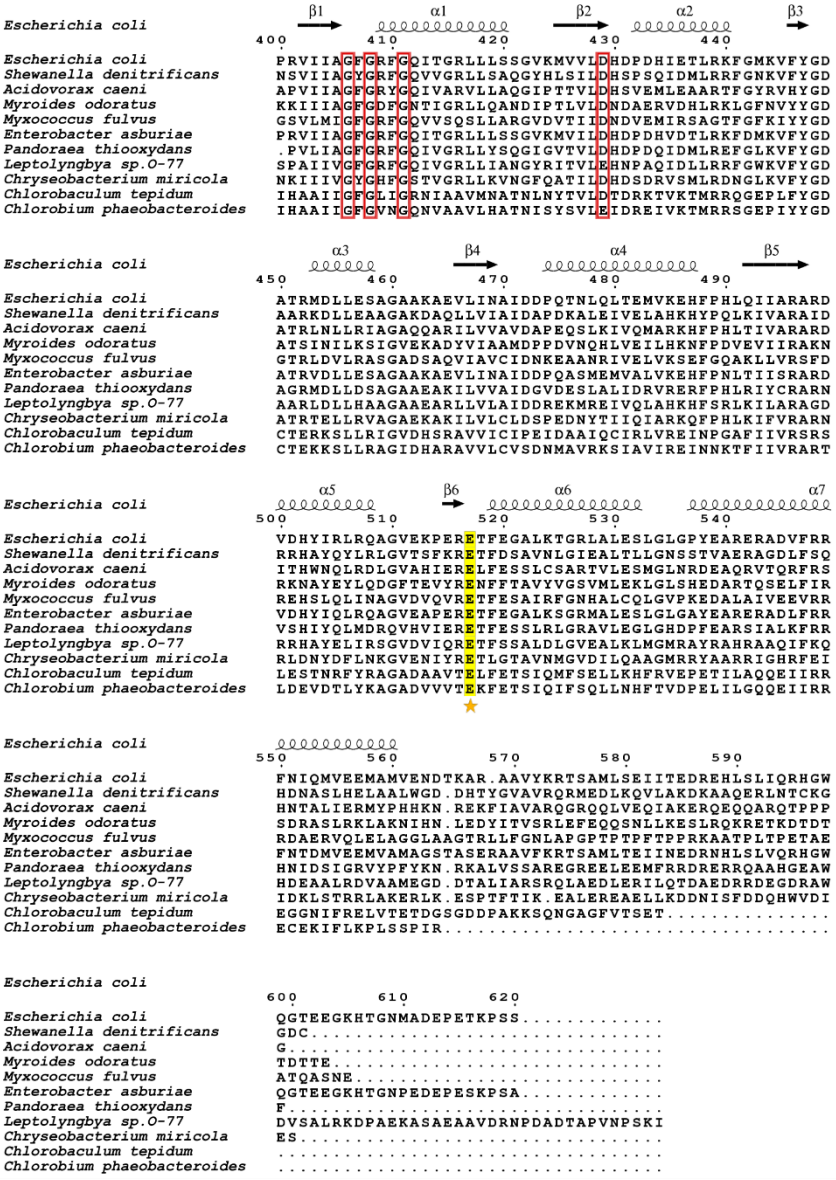

Figure 35: Sequence alignment of C-terminal domains from KefC orthologs. Numbering and secondary structure features are from the first protein in the alignment. The position corresponding to the equivalent of KtrA E125 is marked with a star. Conserved glutamates are highlighted in yellow and nucleotide binding motif positions are boxed in red.

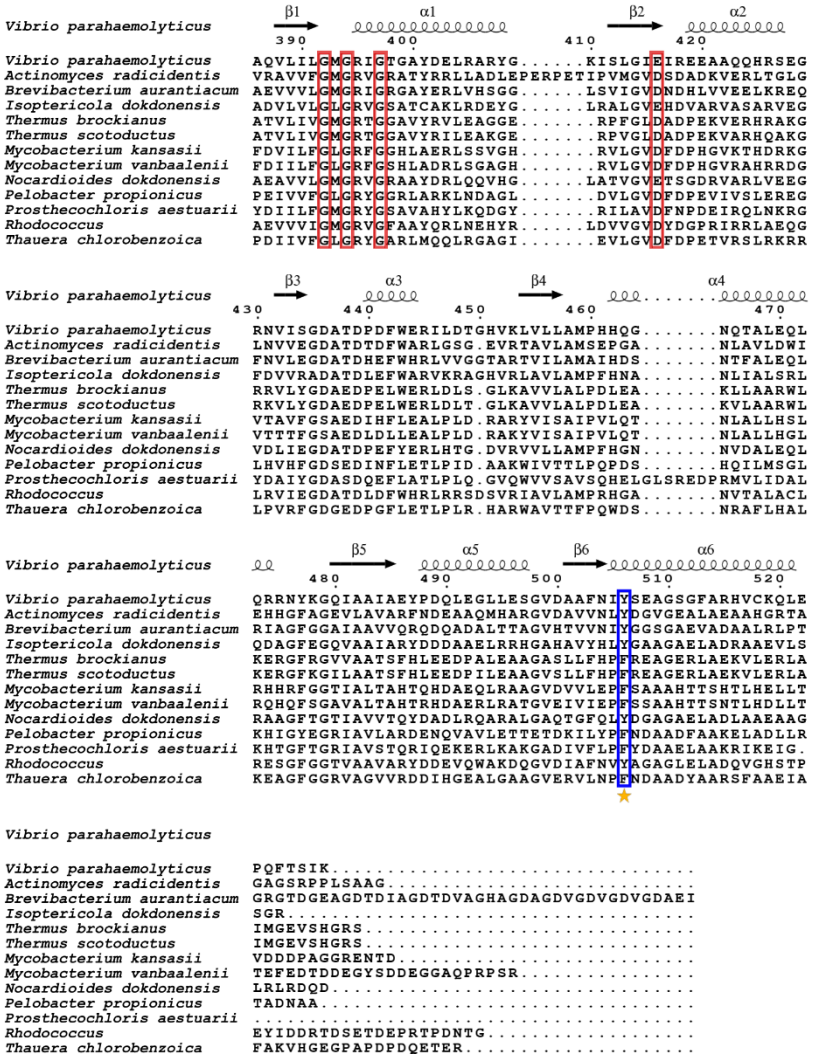

Figure 36: Sequence alignment of C-terminal domains from KefC-like orthologs. Numbering and secondary structure features are from the first protein in the alignment. The position corresponding to the equivalent of KtrA E125 is marked with a star. Positions without conserved glutamates are boxed in blue and nucleotide binding motif positions are boxed in red.

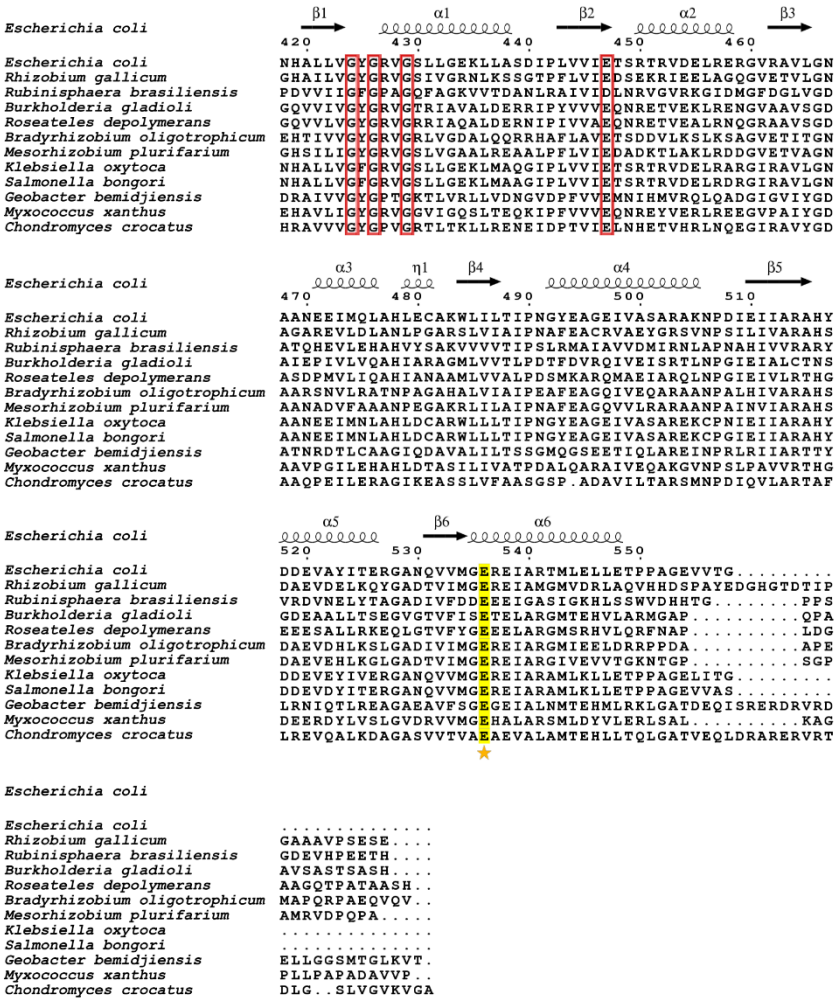

Figure 37: Sequence alignment of C-terminal domains from YbaL orthologs. Numbering and secondary structure features are from the first protein in the alignment. The position corresponding to the equivalent of KtrA E125 is marked with a star. Conserved glutamates are highlighted in yellow and nucleotide binding motif positions are boxed in red.

IV. REGULATION OF KtrA AND KtrC BY c-di-AMP

Some of the work presented in this chapter has been published in:

Rocha, R., Teixeira-Duarte, C. M., Jorge, J. M. P., & Morais-Cabral, J. H. (2019). Characterization of the molecular properties of KtrC, a second RCK domain that regulates a Ktr channel in Bacillus subtilis. J Struct Biol, 205(3), 34-43. doi: 10.1016/j.jsb.2019.02.002

INTRODUCTION

c-di-AMP is an essential second messenger in many bacteria that has a prominent role in the regulation of potassium homeostasis. This nucleotide was shown to regulate the activity of potassium channels and transporters by binding directly to their RCK regulatory domains and/or by controlling the protein expression level through interaction with a riboswitch and modulation of transcription.

c-di-AMP was shown to bind to KtrA orthologs and to regulate the expression of the *ktrAB* operon in *B. subtilis*. In particular, this nucleotide was shown to bind to the C-terminal domain of KtrA from *S. aureus* (R. M. Corrigan, et al., 2013). A structure of this RCK C-terminal domain bound to c-di-AMP was determined, revealing the details of the interaction with the nucleotide, and the ligand binding affinity was determined by ITC to be in the nM range (H. Kim et al., 2015). Importantly, this characterization did not explore the impact of the N-terminal ligands, ATP or ADP, in c-di-AMP binding. Furthermore, *S. aureus* only contains one Ktr RCK regulatory domain, while *B. subtilis* expresses two closely related orthologs, KtrA and KtrC. The differences in the c-di-AMP binding properties of these two proteins are not yet known.

In this chapter, we characterized the binding of c-di-AMP to the two *B. subtilis* RCK regulatory subunits, KtrA and KtrC. This was done using differential scanning fluorimetry (thermal shift assay) and isothermal titration calorimetry (ITC). Furthermore, we explored the role of this cyclic dinucleotide in the function of the KtrCB channel and used X-ray crystallography to obtain a structure of KtrCB-ATP in complex with c-di-AMP.

MATERIALS AND METHODS

Protein Expression and Purification

Tag-less wild-type KtrA and N-terminal Strep-tagged KtrB were expressed and purified as described previously, without EDTA addition.

Tag-less wild type KtrC, in a pET24a expression vector, was over-expressed in the *Escherichia coli* BL21 (DE3) strain. Cells transformed with the expression vector were grown at 37 ºC with agitation in LB medium supplemented with 50 mg/L kanamycin to an optical density at 600 nm (OD_{600}) of 0.7-0.8. At this point, cultures were placed in ice for 30 min (to induce cold-shock chaperones). Ethanol was then added dropwise to a final concentration of 1% (v/v) (to induce expression of heat-shock chaperones); IPTG was added to a final concentration of 0.5 mM for overnight induction at 20 ºC (14-16 h) and cells were harvested by centrifugation. Cell lysis was done in Buffer A (50 mM Tris-HCl pH 7.5, 50 mM KCl, 5 mM DTT) supplemented with protease inhibitors (1 mM PMSF, 1 µg/mL leupeptin, 1 µg/mL pepstatin A) using a cooled cell cracker Emulsiflex-C5 (Avestin). Lysate was cleared by centrifugation and the supernatant was loaded into an anion exchange column Hi-Trap Sepharose Q-HP (GE Healthcare). KtrC was eluted with a 50-1000 mM KCl gradient. Protein-containing fractions were pooled and incubated with an ATP-agarose resin (Immobilized γ-Aminophenyl-ATP C10-spacer from Jena Bioscience) overnight at 4 °C with gentle agitation. The resin was then washed thoroughly with Buffer H (50 mM Tris-HCl pH 8.0, 150 mM KCl, 5 mM DTT) and protein was eluted in Buffer H supplemented with 5 mM ADP or ATP (sodium salts). Protein was concentrated and further purified by size-exclusion chromatography in a Superdex-S200 (GE Healthcare) column equilibrated with Buffer I (50 mM Tris-HCl pH 8.0, 150 mM KCl, 5 mM DTT). Eluted KtrC was supplemented with 1 mM ATP or ADP. Protein concentration was determined using with a colorimetric assay (Bio-Rad).

The KtrCB complex was purified as previously described for KtrAB. EDTA was not added in any of the buffers. Briefly, N-terminal Strep-tagged KtrB was over-expressed in *Escherichia coli* BL21 (DE3) cells. Cells were lysed in Buffer D (50 mM Tris-HCl pH 8.0, 120 mM NaCl, 30 mM KCl) supplemented with protease inhibitors (1 mM PMSF, 1 µg/mL leupeptin, 1 µg/mL pepstatin A) using a cooled cell cracker Emulsiflex-C5 (Avestin). KtrB was extracted with 40 mM DDM (Sol-grade from Anatrace) overnight at 4 °C with gentle agitation. Spin-cleared lysate was loaded into a Strep-Tactin Sepharose resin (IBA Lifesciences) and washed with Buffer E (50 mM Tris-HCl pH 8.0, 120 mM NaCl, 30 mM KCl, 1 mM DDM, 5 mM DTT, 1 mM ATP). Purified KtrC-ATP was then

added to the resin and incubated for 30 min at 4 ºC with gentle agitation. The resin was thoroughly washed with Buffer E and KtrCB was eluted with Buffer E supplemented with 5 mM desthiobiotin. Eluted protein was dialysed overnight at 4 ºC in the presence of thrombin for KtrB tag cleavage, against Buffer J (20 mM Tris-HCl pH 8,0; 120 mM NaCl; 30 mM KCl; 0.5 mM DDM; 5 mM DTT) for crystallization or Buffer G (10 mM HEPES, 7 mM NMG (pH 8.0), 150 mM KCl, 0.5 mM DDM, 5 mM DTT), for proteoliposome reconstitution. Protein was further purified by size-exclusion chromatography in a Superdex-S200 (GE Healthcare) column using Buffer J, where 0.5 mM DDM was replaced by 1.5 mM Cymal-6, for crystallization or Buffer G for proteoliposome reconstitution. Eluted fractions corresponding to KtrCB were pooled, concentrated and used for crystallization trials or proteoliposome preparation. No nucleotide was added during dialysis and size-exclusion chromatography. Protein concentration was estimated by measuring absorbance at 280 nm on a NanoDrop ND-1000 Spectrophotometer (NanoDrop Technologies). KtrB alone was purified in the same manner as the KtrCB complex without the KtrC addition step.

Differential scanning fluorimetry

Thermal shift assays were performed as described by (Harley et al., 2012) with minor modifications. Wild-type KtrA and KtrC were purified as described in the Protein Expression and Purification section. Samples were prepared in 40 µL mixtures containing 1.5 µM protein and a 6-fold dilution of SYPRO Orange Protein Gel Stain (5,000X stock; Sigma-Aldrich) in Buffer C for KtrA and in Buffer I for KtrC. c-di-AMP, c-di-GMP and c-di-IMP (Biolog) were added to the mixtures when required, at 250 µM in KtrA assays and at 200 µM in KtrC assays. Mixtures were assembled in a 96-well PCR white plate (Bio-Rad) which was sealed and covered with aluminium foil to avoid light exposure. The plate was centrifuged for 1 min at 1500 rpm to ensure good mixing and the assay was performed in a iQ5 real-time PCR detection system (Bio-Rad) with the Cy3 optical filter for Sypro Orange detection (Excitation: 490; Emission: 575 nm). Temperature was varied in the 25 to 70 ºC range, with an increment of 0.5 ºC and a dwell time at each step of 30 seconds. Melting temperature (Tm) was estimated from the inflection point of the melting curve, by plotting the first derivative function. The data were analysed with the CFX Manager software (Bio-Rad). Assays with KtrC were performed by Rita Rocha (Structural Biochemistry Group, i3S).

Isothermal titration calorimetry

For ITC experiments, purified wild-type KtrA-ATP or KtrA-ADP was dialysed overnight at 4 ºC against Buffer K (50 mM HEPES-NaOH pH 7.5; 150 mM KCl; 1 mM TCEP; 0.5 mM ATP or ADP; 5 mM $MgCl_2$). Purified wild-type KtrC-ATP or KtrC-ADP was dialysed overnight at 4 ºC against Buffer L (50 mM HEPES-NaOH pH 8.0; 150 mM KCl; 1 mM TCEP; 0.5 mM ATP or ADP; 5 mM $MgCl_2$). All samples were centrifuged and thoroughly degassed. Protein concentrations were determined using a colorimetric assay (Bio-Rad). c-di-AMP concentration was determined by measuring absorbance at 259 nm and using the extinction coefficient ε_{259nm}= 27000 M^{-1} cm^{-1}. Experiments were performed using a VP-ITC calorimeter (MicroCal, LLC, Northampton, MA, USA) at 25 ºC for all samples and also at 15 ºC for KtrA-ATP. Protein samples were placed in the sample cell and c-di-AMP in the syringe. KtrA-ATP and KtrA-ADP, at 30 µM, were titrated with 400 µM c-di-AMP by injecting 5x8 µl and 24x10 µl of the ligand into the cell. KtrC-ATP and KtrC-ADP, at 10 µM, were titrated with 72 µM c-di-AMP by injecting 5x6 µl, 5x8 µl and 18x10 µl of the ligand into the cell. In all titration runs, the first injection had a volume of 2 µL and was discarded. Two to four independent experiments were performed for each case. Data were processed with the NITPIC software (Keller et al., 2012; Scheuermann & Brautigam, 2015) and analysed with a global fit protocol of the independent experiments using the SEDPHAT software (Chad A. Brautigam et al., 2016; Houtman et al., 2007; Zhao et al., 2015). Correction for the heat of dilution was performed during the fit in SEDPHAT, by refining a constant baseline contribution to all isotherm points. This refinement was performed for all experiments included in the global analysis. A single-site binding model ($\mathrm{A} + \mathrm{B} \leftrightarrow \mathrm{AB}$) was chosen for data fitting, with A representing a protein molecule and B a ligand. The error associated with the thermodynamic parameters was calculated using a 68.3% confidence interval. This interval corresponds to one standard deviation in a Gaussian curve and is reasonable for error estimation of biological data. In the KtrC-ATP titration case, a two-site macroscopic binding model $\mathrm{A} + 2\mathrm{B} \leftrightarrow \mathrm{AB} + \mathrm{B} \leftrightarrow \mathrm{ABB}$ was also attempted for data analysis. Plots were made using the GUSSI software (C. A. Brautigam, 2015). Assays with KtrC were performed by Rita Rocha (Structural Biochemistry Group, i3S).

Crystallization, data collection and refinement

KtrCB-ATP-c-di-AMP was purified as described previously, concentrated and dialysed overnight at 4 ºC using a 50 kDa molecular weight cut-off dialysis membrane (Spectra/Por 7) in order to remove empty detergent (Cymal-6) micelles. Cymal-6 was

the detergent used in the final purification step and crystallization trials due to its non-ionic nature and a small micelle size of ~32 kDa. At this point, no detergent screening was performed. Initial crystallization conditions were screened at 20 °C using a homemade screen. Sitting-drop vapour diffusion experiments were set up in 96 well plates (MRC 2, Swissci, Hampton Research) by mixing a 1:1 (v/v) ratio of protein mixture and reservoir solution, using an Oryx 4 crystallization robot (Douglas Instruments). Drops consisted of 300 nL of KtrCB-ATP-c-di-AMP (at 9.0 mg/mL) and 300 nL crystallization solution and were equilibrated against a 40 µL reservoir. Crystal forming conditions were optimized using fine screens around the hits in 24 or 48 well plates. 24 well plates (Cryschem, Hampton Research) were set up using 1 µL of protein and reservoir solution, equilibrated against a 500 µL reservoir. 48 well plates (MRC Maxi, Swissci, Hampton Research) were set up using 0.5 µL of protein and reservoir solution, equilibrated against a 150 µL reservoir. The best diffracting crystal formed in a 48-well plate in a crystallization condition containing 100 mM Tris-HCl pH 8.5, 700 mM KCl and 24% PEG 400. Before being flash-cooled in liquid nitrogen, the crystal was cryoprotected using 39% PEG 400 by adding 100 mM Tris-HCl pH 8.5, 700 mM KCl, 50% PEG 400, 1.5 mM Cymal-6, 0.5 mM ATP, 0.5 mM c-di-AMP, 0. 5mM $MgCl_2$ solution directly to the drop and equilibrating before freezing. A dataset was collected at the Proxima 2A beamline of the French National Synchrotron Source (SOLEIL) to 5.8 Å resolution. Data were processed using XDS (Kabsch, 2010) and AIMLESS (Evans & Murshudov, 2013) from the CCP4 program suite (Winn, et al., 2011). To solve the structure, a molecular replacement search was performed with Phaser (McCoy, et al., 2007) using a collection of search models that included the KtrB dimers from the KtrAB-ATP (PDB: 4J7C) and $KtrA_{\Delta C}$-ADP (PDB: 5BUT) structures, and RCK octameric rings with and without the C-terminal domains. Figures were created using PyMOL (Delano, 2002).

Preparation of proteoliposomes

ACMA-fluorescence-based K^+ flux assay

Proteoliposomes were prepared as previously described. Briefly, a lipid film of *E. coli* polar lipids (Avanti) was resuspended at 10 mg/mL lipid concentration in Internal Buffer (150 mM KCl, 10 mM HEPES, 7 mM NMG (pH 8.0), 0.1 mM ATP) using 4-6 cycles of sonication (15 s ON/ 15 s OFF on ice) in an ultrasonic bath Sonorex Digitec (Bandelin) and further solubilized by adding 40 mM DM (n-Decyl-β-D-Maltoside) (Sol-Grade from Anatrace) and 4-6 cycles of sonication. The lipid suspension was then incubated at

25 ºC for 2 h with gentle agitation. KtrB alone and KtrCB proteins were purified as described above, added to solubilized lipids at 1:100 (w:w) protein-to-lipid ratio and incubated for 30 min at room temperature. In control liposomes (empty), Internal Buffer was added to the lipids instead of protein. Detergent was removed using adsorbing SM-2 Biobeads (Bio-Rad): the protein-lipid mix was incubated twice with fresh Biobeads at 10:1 (w:w) bead-to-detergent ratio at room temperature for 1 h and then incubated overnight at 4 ºC at a 20:1 (w:w) bead-to-detergent ratio. Proteoliposomes were then flash-frozen in liquid nitrogen and stored at -80 ºC.

Pyranine-fluorescence-based K^+ flux assay

KtrCB proteoliposomes were prepared as for the ACMA K^+ flux assay. For encapsulation of pyranine (Lee et al., 2013; Wiedenmann et al., 2008), proteoliposomes were thawed in a 37 ºC water bath for 15 min and sonicated (3x5 s) in an ultrasound bath Sonorex Digitec (Bandelin). 100 µL of carefully resuspended proteoliposome samples were mixed with 50 µL of Internal Buffer (see above) containing 2.5 µL pyranine from a 60 mM stock (Cf= 1 mM). The mixture was then frozen in liquid nitrogen for 5 min, thawed in water and sonicated (2x10 s) in the ultrasound bath. The freeze/thaw/sonication procedure was repeated once. Non-incorporated pyranine was removed using size-exclusion chromatography, by loading the 150 µL samples into a 5 mL HiTrap Desalting column containing G-25 Superfine resin (GE Healthcare), pre-incubated with Internal Buffer. Proteoliposomes were collected from the void volume, concentrated by ultracentrifugation (30 min; 200.000 g; 4 ºC) in an Optima Max XP Tabletop Ultracentrifuge (Beckman Coulter) and resuspended in 50 µL of Internal Buffer. Samples were kept at 4 ºC.

ANTS fluorescence stopped-flow Tl^+ flux assay

To prepare the proteoliposomes for this assay, we followed the reconstitution protocol described by others (Posson et al., 2018) with some modifications. A lipid film of *E. coli* polar lipids (Avanti) was resuspended at 10 mg/mL lipid concentration in Reconstitution Buffer (100 mM KNO_3, 10 mM HEPES pH 8.0, 0.1 mM ATP, 1 mM MgAcetate) supplemented with 25 mM of 8-aminonaphthalene-1,3,6-trisulfonic acid (ANTS). Resuspension involved 5 cycles of sonication (15 s ON/ 30 s OFF) in an ultrasonic bath Sonorex Digitec (Bandelin) and addition of 40 mM DM (n-Decyl-β-D-Maltoside) (Sol-Grade from Anatrace), followed by 15 cycles of sonication. The lipid suspension was then incubated at 25 ºC for 30 min with gentle agitation. The KtrCB complex was purified

as described above, except for the size-exclusion chromatography step, which was done with Reconstitution Buffer supplemented with 0.5 mM DDM and 5 mM DTT. The protein was then added to solubilized lipids at a ratio of 10 µg of protein per mg of lipid and incubated for 30 min at room temperature. For the empty liposomes, Reconstitution Buffer was added to the lipids instead of the protein. Detergent was removed using adsorbing SM-2 Biobeads (Bio-Rad): the protein-lipid mix was incubated with fresh Biobeads at 30:1 (w:w) bead-to-detergent ratio at room temperature for 2 h. Non-incorporated ANTS was removed by diluting the proteoliposomes in Dilution Buffer (140 mM KNO_3, 10 mM HEPES pH 8.0, 0.1 mM ATP, 1 mM MgAcetate) and loading the sample into a PD-10 desalting column (Cytiva). Proteoliposomes were eluted in Dilution Buffer and stored at 12ºC.

ACMA-fluorescence-based K^+ flux assay

The assay was performed as previously described. Briefly, proteoliposomes were thawed in a 37 ºC water bath for 15 min, briefly sonicated (3x5 s) in an ultrasound bath Sonorex Digitec (Bandelin) and kept at room temperature until the experiment. The proteoliposomes were then diluted 100-fold (10 µL sample in 1 mL final volume) in Flux Buffer (10 mM HEPES and 7 mM NMG (pH 8.0), 150 mM choline chloride, 0.1 mM ATP; 2 mM $MgCl_2$) to establish the K^+ gradient. In experiments involving RCK additions to KtrB proteoliposomes, 10 µg of KtrA-ATP or KtrC-ATP were incubated for 10 min with the KtrB proteoliposomes before establishing the K^+ gradient. In the KtrCB-ATP titrations with c-di-AMP, the cyclic dinucleotide was included in the Flux buffer at the intended concentrations. ACMA was added to the proteoliposomes to a final concentration of 550 nM, from a 111 µM stock in DMSO. Fluorescence was monitored every 2 s (λ_{Ex}=410 nm, λ_{Em}=480 nm), using a 104F-QS 10 mm quartz cuvette (Hellma) with a small magnet in a Horiba FluoroMax 4 spectrofluorometer (Horiba Scientific). After measuring the initial baseline fluorescence during 100 s, the assay was initiated by adding 1 µM of the H^+ ionophore carbonyl cyanide m-chlorophenyl hydrazine (CCCP) from a 200 µM stock in HN Buffer (10 mM HEPES, 7 mM NMG (pH 8.0)) and the flux signal was monitored for 400 s (between ~101-500 s). For each experimental condition, one additional replica was performed in which, after baseline fluorescence measurement and CCCP addition, the K^+ ionophore valinomycin was quickly added 296 nM, from a 60 µM stock in DMSO, and flux signal was monitored for an additional 100s. This was performed to avoid valinomycin contamination of the cuvette between sample measurements and was done every day for each proteoliposome preparation.

Fluorescence quenching curves were normalized individually as follows:

$$NF = \frac{F - F_{val}}{F_{ini} - F_{val}}$$

NF is the normalized fluorescence, F is the measured fluorescence in arbitrary units, F_{ini} corresponds to the last baseline point measured before CCCP addition and F_{val} corresponds to the lowest point measured after valinomycin addition (501-600s). For c-di-AMP titrations, as well as c-di-GMP assays, normalization was also performed taking into account the steady-state of each curve instead of the fluorescence minimum obtained with valinomycin. In these cases, F_{val} was replaced in the previous expression by F_{ss} that corresponds to the average of the last 10 s of the assay (490-500 s). The flux rate constants were quantified as explained in the methods section of the previous chapter "Quantification of flux rate constants".

Pyranine-fluorescence-based K^+ flux assay

The assay was performed as described by others (Lee, et al., 2013; Wiedenmann, et al., 2008), with the required modifications for a 96-well plate format. Proteoliposomes were diluted 100-fold (2 µL sample in 200 µL final volume) in Assay Buffer (10 mM HEPES and 7 mM NMG (pH 8.0); 150 mM choline chloride; 0.1 mM ATP; 2 mM $MgCl_2$) to establish the K^+ gradient. Fluorescence was monitored every 12 s (λ_{Ex}=406 nm and 460nm, λ_{Em}=510 nm), in a Synergy MX plate reader (BioTek). After measuring the initial baseline fluorescence during 60 s, the assay was initiated by adding 1 µM of the H^+ ionophore carbonyl cyanide m-chlorophenyl hydrazine (CCCP) from a 205 µM stock in HN Buffer (10 mM HEPES, 7 mM NMG (pH 8.0)). CCCP enables H^+ entry into the liposomes to counterbalance the negative potential created by K^+ efflux, leading to quenching of pyranine fluorescence. Fluorescence was monitored for 300 s at which point 600 nM of the K^+ ionophore valinomycin was added from a 25 µM stock in DMSO and fluorescence was monitored for an additional 300 s. Valinomycin incorporates into all liposomes and mediates K^+ efflux, indicating the total flux of the liposome population. For normalization of the pyranine fluorescence changes, we made use of the isosbestic point in the pyranine excitation spectrum found at 406 nm.

The fluorescence curves were normalized individually as follows:

$$NF = \frac{F_{510\ (\text{excitation at } 406\text{nm})}}{F_{510\ (\text{excitation at } 460\text{nm})}}$$

NF is the normalized fluorescence, $F_{510\ (excitation\ at\ 406nm)}$ is the measured fluorescence in arbitrary units measured using an excitation wavelength of 406 nm and $F_{510\ (excitation\ at\ 460nm)}$ is the measured fluorescence in arbitrary units measured using an excitation wavelength of 460 nm. Due to this normalization, fluorescence increases upon potassium efflux due to channel activity, or valinomycin addition, and consequent proton influx through CCCP.

ANTS fluorescence stopped-flow Tl^+ flux assay

In this assay, proteoliposomes with encapsulated ANTS were diluted 10-fold in Dilution Buffer (140 mM KNO_3, 10 mM HEPES pH 8.0, 0.1 mM ATP, 1 mM MgAcetate) (150 µL proteoliposomes in 1.5 mL final volume). The assay was then performed using a manually controlled SFA 20 stopped flow device (Horiba Scientific) attached to a Horiba FluoroMax 4 spectrofluorometer (Horiba Scientific) with the following configuration:

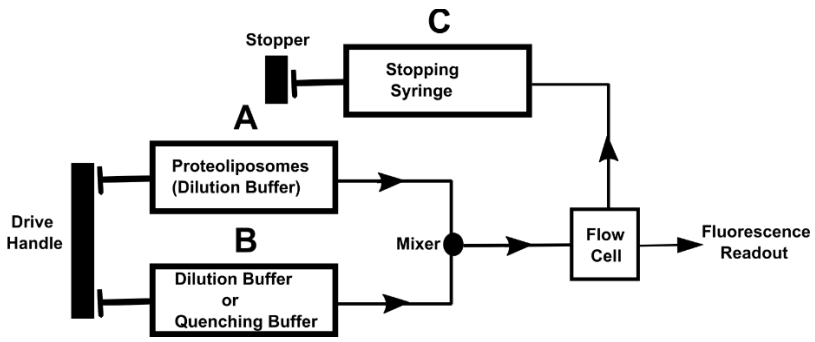

Syringes A and B were loaded with the intended solutions and the volume of the stopping syringe was adjusted to 200 µL. In each injection, upon manually pushing the drive handle, 100 µL of syringes A and B were mixed in the mixer and injected in a flow cell and then into the stopping syringe that halts liquid loading. The flow cell was inserted in a Horiba FluoroMax 4 spectrofluorometer (Horiba Scientific), allowing monitoring of fluorescence every 100 ms for 50 s (λ_{Ex}=360 nm, λ_{Em}=510 nm). The whole system was washed with H_20 and Dilution Buffer prior to starting the assays.

Each assay entailed two independent experiments. Each experiment consisted of 14 mixing injections of 100 µL from syringes A and B (200 µL final mixing volume in the flow cell). In the first experiment, proteoliposomes were loaded in syringe A and Dilution Buffer in syringe B. This experiment is used to obtain the maximum fluorescence signal of the sample in the absence of Tl^+ and used for data normalization. In the second

experiment, proteoliposomes were loaded in syringe A and Quenching Buffer (94 mM KNO_3; 50 mM $TlNO_3$; 10 mM HEPES pH 8.0, 0.1 mM ATP, 1 mM MgAcetate) in syringe B. In this experiment, an inward Tl^+ gradient is established and channel activity can be measured as a function of ANTS fluorescence quenching as Tl^+ accumulates inside the proteoliposomes. In each experiment the first seven injections were discarded since they were needed to completely fill the connecting tubes and flow cell with the mixed solution. The remaining seven were used for data analysis after discarding outliers.

Fluorescence was normalized as follows:

$$NF = \frac{F_{Quenching}}{F_{Dilution}}$$

NF is the normalized fluorescence, $F_{Dilution}$ is the averaged measured fluorescence in arbitrary units obtained in the first experiment (without Tl^+), $F_{Quenching}$ corresponds to the measured fluorescence in arbitrary units obtained in the second experiment (with Tl^+).

RESULTS

Characterization of c-di-AMP binding to *B. subtilis* KtrA and KtrC

c-di-AMP was very recently shown to bind to the two B.subtilis RCK proteins, KtrA and KtrC (Gundlach, et al., 2019). Nonetheless, the binding properties for these proteins have not yet been characterized, particularly in respect to the influence of the N-terminal ligands, ATP or ADP. To understand the molecular properties of c-di-AMP binding by the RCK proteins from *B. subtilis*, we started by evaluating c-di-AMP impact in protein thermal stability using differential scanning fluorimetry. KtrA and KtrC were purified in the presence of either ATP or ADP and supplemented with the cyclic dinucleotides c-di-AMP, c-di-GMP and c-di-IMP.

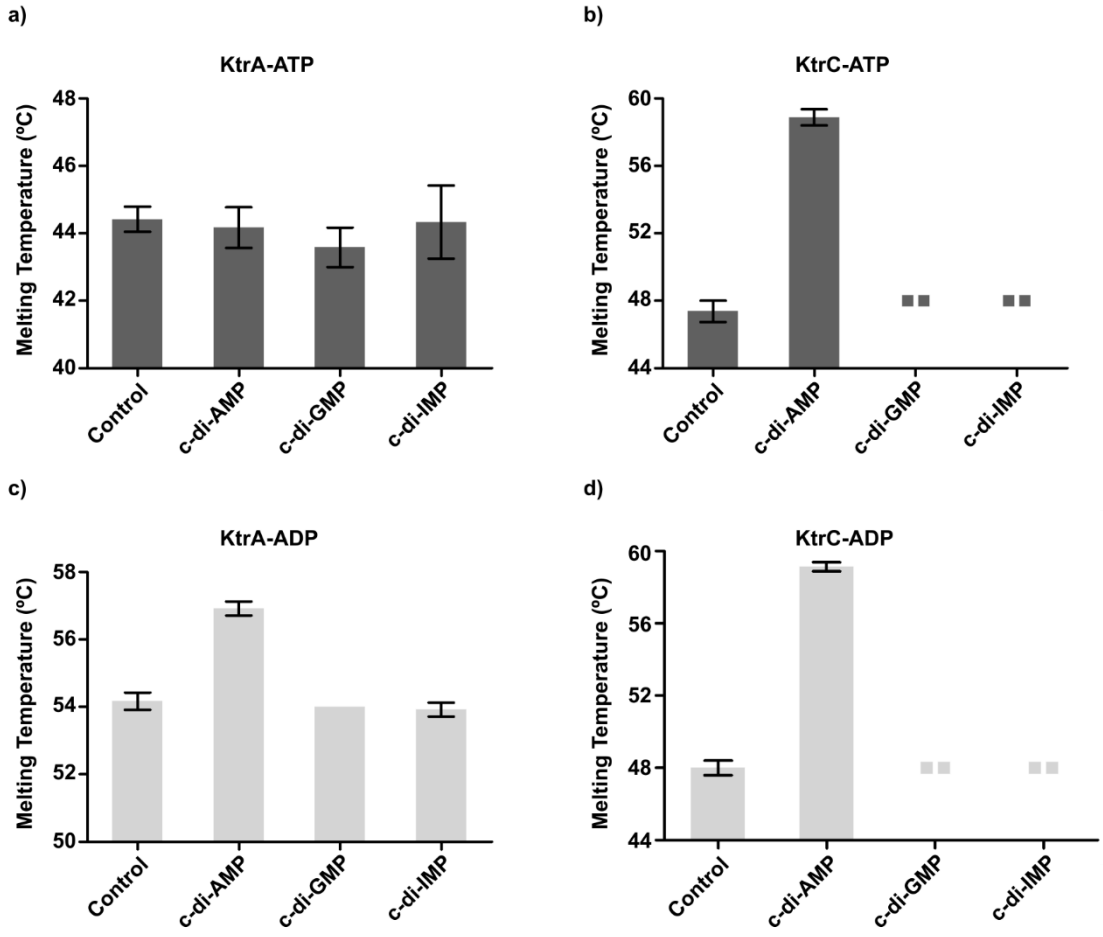

Figure 38: Impact of cyclic dinucleotides in the thermal stability of KtrA and KtrC. Plot of melting temperatures for: **a)** KtrA purified in the presence of ATP and incubated with 250 µM of different cyclic dinucleotides. Mean ± standard deviation is shown for n=6. **b)** KtrC purified in the presence of ATP and incubated with 200 µM of different cyclic dinucleotides. Mean ± standard deviation is shown for n=4. For c-di-GMP and c-di-IMP only 2 measurements were performed

and the individual values are plotted. **c)** KtrA purified in the presence of ADP and incubated with 250 µM of different cyclic dinucleotides. Mean ± standard deviation is shown for n=6. No error bar is shown for c-di-GMP, since the Tm value was 54 ºC for all six measurements. **d)** KtrC purified in the presence of ADP and incubated with 200 µM of different cyclic dinucleotides. Mean ± standard deviation is shown for n=4. For c-di-GMP and c-di-IMP only 2 measurements were performed and the individual values are plotted. Control corresponds to experiments without cyclic dinucleotide.

The melting temperatures obtained are shown in Figure 38 and Table 7. These assays revealed that, when KtrA is bound to ADP, c-di-AMP contributes to the stabilization of the protein, leading to a change in Tm (ΔTm) of ~ 3 ºC. Moreover, this effect is specific to this cyclic dinucleotide, since incubations with c-di-GMP and c-di-IMP did not result in meaningful changes of the melting temperature compared to the control (ΔTm< 1 ºC). In contrast, with KtrA bound to ATP, no cyclic dinucleotide caused a meaningful change in the melting temperature. In the case of KtrC, c-di-AMP greatly contributes to the thermal stability of the protein, resulting in a ΔTm of ~11 ºC for both the ATP and ADP-bound states. Like seen for KtrA, the c-di-AMP effect is specific, since incubations with c-di-GMP and c-di-IMP did not change the melting temperature in relation to the control (ΔTm<1 ºC).

Table 7: Melting temperature (Tm) values and respective standard deviations (SD) obtained in the thermal shift assay.

	KtrA				**KtrC**			
	ATP		**ADP**		**ATP**		**ADP**	
	Tm (ºC)	SD	Tm (ºC)	SD	Tm (ºC)	SD	Tm (ºC)	SD
Control	44.4	0.4	54.2	0.3	47.4	0.6	48.0	0.4
c-di-AMP	44.2	0.6	56.9	0.2	58.5	0.5	59.1	0.2
c-di-GMP	43.6	0.6	54.0	0.0	48.0/ 48.0	-	48.0/ 48.0	-
c-di-IMP	44.3	1.1	53.9	0.2	48.0/ 48.0	-	48.0/ 48.0	-

Values correspond to an n=6 for KtrA-ATP and KtrA-ADP and to an n=4 for KtrC-ATP and KtrC-ADP. In the KtrC case, no SD values are shown for c-di-GMP and c-di-IMP since only two experiments were performed with these nucleotides. In control experiments, the cyclic dinucleotides are absent.

In light of these results, it is clear that c-di-AMP is the only cyclic dinucleotide tested that significantly improves KtrA and KtrC thermal stability. Moreover, the influence of this

cyclic dinucleotide in the thermal stability is much greater for KtrC than for KtrA with ΔTm of 11 and 3 ºC, respectively. These results suggest that both KtrA and KtrC bind c-di-AMP.

In order to better characterize the binding of c-di-AMP to KtrA and KtrC, we performed isothermal titration calorimetry. Purified KtrA and KtrC bound to ATP or ADP where titrated with c-di-AMP (Figures 39 and 40 and Table 8). The c-di-AMP titration of KtrA-ADP at 25 ºC (Figure 39a), revealed an exothermic interaction (ΔH= -5.8 kcal/mol with a 68.3% confidence interval between -6.9 and -5.1 kcal/mol) and a binding dissociation constant (K_d) of 3.6 µM (with a 68.3% confidence interval between 2.7 and 4.7 µM). A similar titration of c-di-AMP into KtrA-ATP was performed, but no heat changes along the titration were observed (Figure 39b). We changed the temperature from 25 ºC to 15 ºC and repeated the titration, in order to try to increase the binding heat (Figure 39c). At 15 ºC, we detected binding of c-di-AMP to KtrA-ATP, with an exothermic interaction (ΔH= -6.2 kcal/mol with a 68.3% confidence interval between -10.0 and -4.7 kcal/mol) and a K_d of 11.0 µM (with a 68.3% confidence interval between 8.1 and 15.4 µM).

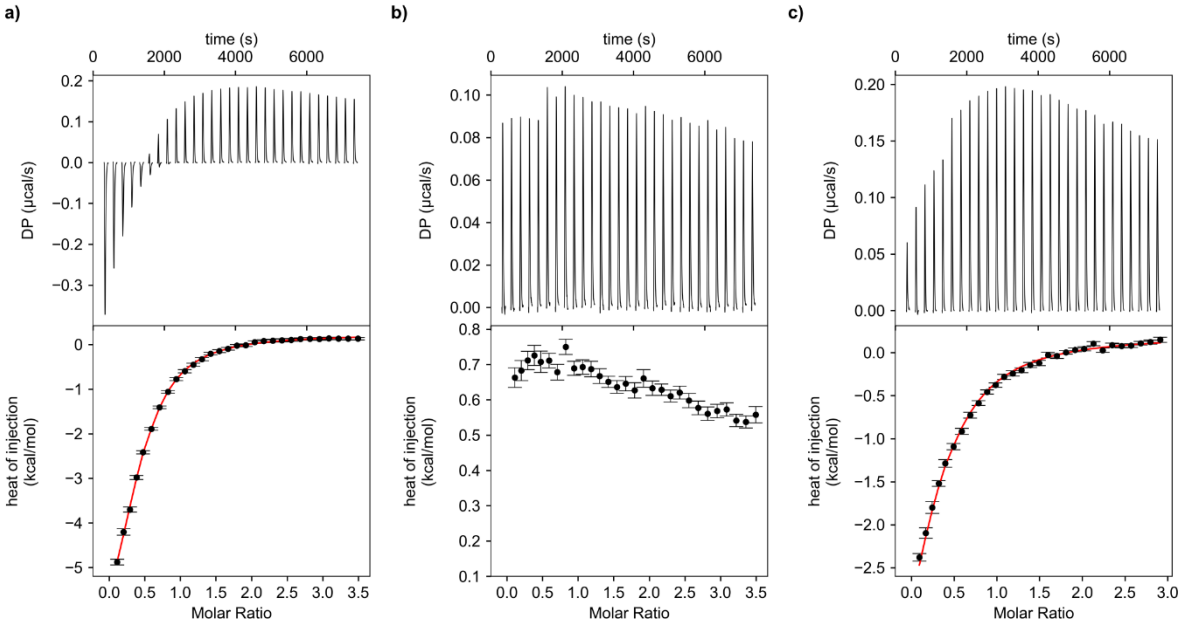

Figure 39: ITC titrations of c-di-AMP into KtrA. a) Example ITC titration of 400 µM c-di-AMP into 30 µM KtrA-ADP at 25 ºC. **b)** Example ITC titration of 400 µM c-di-AMP into 30 µM KtrA-ATP at 25 ºC. **c)** Example ITC titration of 400 µM c-di-AMP into 30 µM KtrA-ATP at 15 ºC. The top panel shows the thermogram depicting the raw heat released after each injection and the bottom panel shows the integrated heats of injection per mole of injectant.

The titration of c-di-AMP into KtrC-ADP (Figure 40a) revealed an exothermic interaction (ΔH= -12.7 kcal/mol with a 68.3% confidence interval between -13.0 and -12.3 kcal/mol) and a K_d of 31.5 nM (with a 68.3% confidence interval between 23.9 and 40.9 nM). The titration of c-di-AMP into KtrC-ATP also revealed an exothermic interaction but the shape of the binding curve suggested more than one binding event. We first attempted to fit the data with a single-site binding model as used for the other experiments (Figure 40b). Using this model, we obtained a ΔH= -14.5 kcal/mol (with a 68.3% confidence interval between -15.6 and -13.4 kcal/mol) and a K_d of 20.3 nM (with a 68.3% confidence interval between 10.1 and 36.5 nM).

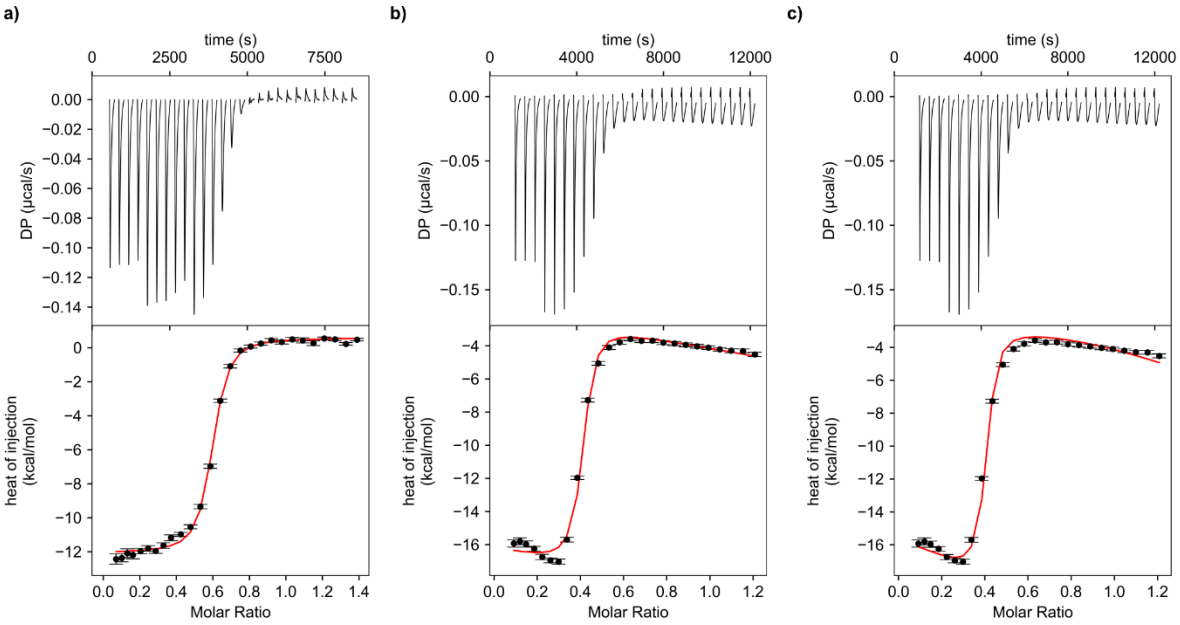

Figure 40: ITC titrations of c-di-AMP into KtrC. a) Example ITC titration of 72 µM c-di-AMP into 10 µM KtrC-ADP at 25 ºC. **b)** Example ITC titration of 72 µM c-di-AMP into 10 µM KtrC-ATP at 25 ºC and fitting with a single-site binding model. **c)** Example ITC titration of 72 µM c-di-AMP into 10 µM KtrC-ATP at 25 ºC and fitting with a two-site macroscopic binding model. The top panel shows the thermogram depicting the raw heat released after each injection and the bottom panel shows the integrated heats of injection per mole of injectant.

However, as depicted in the bottom panel of Figure 40b, the fit does not fully explain the first part of the titration curve. Therefore, we fitted the data with a two-site macroscopic binding model $(\mathrm{A} + 2\mathrm{B} \leftrightarrow \mathrm{AB} + \mathrm{B} \leftrightarrow \mathrm{ABB})$, where A is KtrC-ATP and B is c-di-AMP (Figure 40c). The following thermodynamic parameters were estimated: $K_d(1)$, which describes the binding of molecule B to molecule A and $K_d(2)$, which describes the binding of molecule B to the AB complex, along with the respective binding heats ΔH(1)

and ΔH(2). The global fit resulted in the following values: ΔH(1)= -18.5 kcal/mol (with a 68.3% confidence interval between -22.9 and -13.8 kcal/mol) and a K_d(1) of 7.8 nM (with a 68.3% confidence interval between 0.3 and 29.0 nM); ΔH(2)= -7.3 kcal/mol (with a 68.3% confidence interval higher limit of -3.3 kcal/mol) and a K_d(2) of 4.3 µM (with a 68.3% confidence interval lower limit of 1.7 µM). The lower limit for the 68.3% confidence interval of ΔH(2) and the higher limit for the 68.3% confidence interval of K_d(2) could not be estimated. This model seems to explain the data better, as shown in the lower panel of Figure 40c, revealing two events with exothermic interactions and different binding affinities. The first event involves a tight binding of c-di-AMP to KtrC-ATP with a K_d(1) of 7.8 nM. In the second event, the binding affinity of c-di-AMP decreases, with an estimated K_d(2) of 4.3 µM. However, we were not able to accurately estimate the 68.3% confidence intervals for the thermodynamic parameters related to the second binding event, ΔH(2) and K_d(2). This is an indication that the binding model is not appropriate (or is excessively parameterized) to use with the data and therefore, the parameters obtained with the single-site binding model were used for comparison with the other experiments.

Table 8: Thermodynamic parameters obtained for c-di-AMP titrations into KtrA and KtrC from global fitting of data with a single-site binding model.

Cell	K_d	68.3% Confidence interval for K_d	ΔH (kcal/mol)	68.3% Confidence interval for ΔH	ΔS (cal/mol*T)	incA	n
KtrA-ADP	3.6 µM	(2.7, 4.7)	-5.8	(-6.9, -5.1)	5.4	0.5	4
KtrA-ATP	10.9 µM	(8.1, 15.4)	-6.2	(-10.0, -4.7)	1.2	0.5	2
KtrC-ADP	31.5 nM	(23.9, 40.9)	-12.6	(-13.0, -12.3)	-8.1	0.5	3
KtrC-ATP	20.3 nM	(10.1, 36.5)	-14.5	(-15.6, -13.4)	-13.3	0.6	2

ΔS error estimation is not provided since it cannot be calculated in the software used for global fitting. incA corresponds to the incompetent fraction of molecule A (protein) and n corresponds to the number of independent titrations used for the global fit. T is the temperature in Kelvin.

The software employed for ITC data fitting, SEDPHAT, does not provide the binding stoichiometry of the reaction. Instead, it provides an estimation of the fraction of incompetent molecule A (protein), corresponding to the fraction of protein that appears not to contribute to the protein-ligand interaction. In most of these experiments, the

fraction of incompetent molecule A (KtrA or KtrC) was ~ 0.5 (Table 8). The value reflects that c-di-AMP binding occurs at the RCK C-lobe dimer interface, as seen in the structure of the KtrA ortholog from *S.aureus* (H. Kim, et al., 2015). Therefore, one molecule of c-di-AMP binds to a KtrA or KtrC dimer, resulting in a 0.5 binding stoichiometry relative to the RCK protein monomer.

The data analysis shows a very different affinity of KtrA (3.6-10.9 µM) and KtrC (20.3-31.5 nM) for c-di-AMP. c-di-AMP affinities determined for other RCK orthologs are intermediate between the values measured for the *B.subtilis* RCK proteins, with K_d values of 150 nM for the *S. pneumoniae* RCK and 664 nM for the *S. aureus* KtrA (Y. Bai, et al., 2014; H. Kim, et al., 2015). A previous characterization of the oligomeric properties of KtrA and KtrC showed that while KtrA forms an octamer in solution, KtrC exists in a dynamic equilibrium of different species, possibly octamer and tetramers. We have shown that the KtrC octamer is more prevalent with ADP than with ATP and that Mg^{2+} shifts the equilibrium towards the octameric species in the presence of ATP. Strikingly, c-di-AMP stabilizes the octamer, so that no other species are detected, both with ATP and ADP (Rocha, et al., 2019). The higher affinity of KtrC for c-di-AMP and the apparent existence of a more complex binding curve (Fig 40b and 40c) might be related to binding of the cyclic dinucleotide to different protein species. Alternatively, ITC studies performed with the *S. aureus* KtrA revealed that R169 and N175 are essential residues for c-di-AMP binding (H. Kim, et al., 2015). Both residues are conserved in KtrC, but in KtrA the asparagine is changed to a threonine. In the c-di-AMP-bound *S.aureus* KtrA C-lobe dimer structure, N175 is involved in interactions with c-di-AMP and at the dimeric interface of the RCK C-lobes. As such, the change in this residue in the *B.subtilis* KtrA might have an impact in c-di-AMP binding affinity. Importantly, there is currently no available data for the binding affinities of the KtrAB or KtrCB channels for c-di-AMP and therefore, it is still unclear if, in a full channel context, the difference in c-di-AMP binding affinity observed for KtrC and KtrA is still retained.

Overall, these results show that c-di-AMP binds to the *B. subtilis* RCK domain proteins, KtrA and KtrC, in good agreement with other work that employed a different technique (Gundlach, et al., 2019). c-di-AMP affinity for KtrC is higher than for KtrA and changes little with the N-terminal bound nucleotide, with K_d values of 3.6 µM and 10.9 µM for KtrA and of 31.5 nM and 20.3 nM for KtrC, in the ADP and ATP-bound states, respectively.

Impact of c-di-AMP in KtrCB activity

c-di-AMP has been proposed to inhibit the function of the Ktr channels but there is currently a lack of quantitative data that demonstrates a direct functional effect of c-di-AMP in the regulation of these channels. As stated previously, *B. subtilis* encodes two Ktr ion conducting subunits KtrB and KtrD, as well as two RCK regulatory subunits KtrA and KtrC. KtrA and KtrB are in the same operon while KtrC and KtrD are encoded separately. This has led to the proposal that two K^+ transport systems exist in this organism: KtrAB and KtrCD (Holtmann, et al., 2003).

Importantly, using an *E. coli* phenotype complementation assay, we have shown that KtrC and KtrA are functionally interchangeable. Both proteins are able to assemble functional complexes with KtrB (Rocha, et al., 2019). This functional property was confirmed using the ACMA-fluorescence-based K^+ flux assay. A single batch of KtrB proteoliposomes was incubated with equal amounts (10 µg) of purified KtrA-ATP or KtrC-ATP and flux was measured in an external solution containing 150 mM choline chloride and 2 mM magnesium (Figure 41). This external solution was chosen to ensure maximum channel activity, as previously measured for the KtrAB-ATP proteoliposomes. The two fluorescence quenching curves are very similar, with flux rates for two separate measurements of 0.098/0.096 s^{-1} for KtrB + KtrA-ATP and of 0.099/0.106 s^{-1} for KtrB + KtrC-ATP. These rates are comparable to the flux rates obtained for the KtrAB-ATP proteoliposomes under the same experimental conditions (0.079 ± 0.010 s^{-1}). This confirms that both RCK proteins assemble in a functional complex with KtrB, forming functional channels that display identical flux activities.

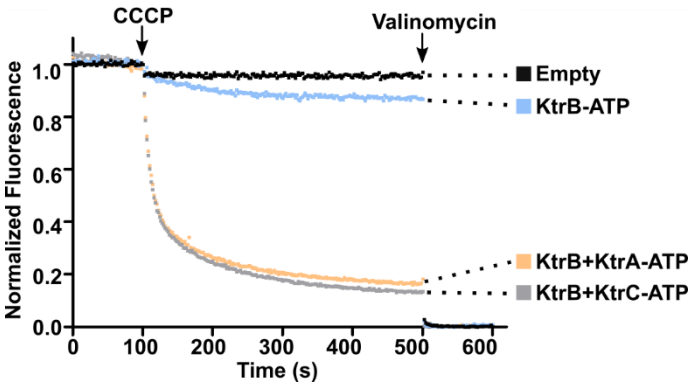

Figure 41: Comparison of KtrAB-ATP and KtrCB-ATP flux. Proteoliposome flux assay performed with KtrB proteoliposomes incubated with KtrA-ATP and KtrC-ATP, using a choline chloride external solution supplemented with magnesium. Representative fluorescence quenching curves are shown. Two measurements were performed for each condition, using a

single KtrB proteoliposome preparation. Empty liposomes were used as a control and KtrB-ATP proteoliposomes are shown for reference.

We then strived to characterize the role of c-di-AMP in the regulation of the KtrCB channel activity, since binding of the cyclic dinucleotide to KtrC was shown to be tighter than for KtrA.

We started by characterizing the biochemical properties of the KtrCB complex. We purified the KtrCB complex using the same methodology employed for the purification of the KtrAB complex. The size-exclusion chromatography profile revealed an elution peak that coincides with the one obtained for the KtrAB complex (Figure 42a). SDS-PAGE analysis of this elution peak showed the presence of both KtrC and KtrB, confirming that the peak corresponds to the KtrCB complex (Figure 42b). This suggests that the complex arrangement consists of two KtrB dimers that interact with a KtrC octameric ring, as previously described for KtrAB.

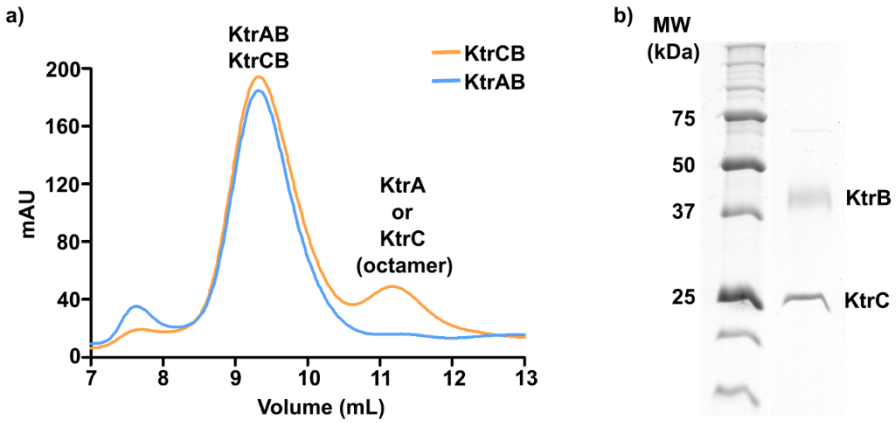

Figure 42: Size-exclusion chromatography elution profile of the KtrCB complex. a) Elution profiles of the KtrCB and KtrAB complexes. **b)** SDS-PAGE gel analysis of the KtrCB elution peak**.** Molecular weight markers (MW) are shown on the left. Bands corresponding to KtrB and KtrC are indicated.

The KtrCB-ATP complex was reconstituted into proteoliposomes, as previously described for KtrAB, and the impact of c-di-AMP on channel function was evaluated using the ACMA K^+ flux assay. An initial test was performed using two concentrations of c-di-AMP and c-di-GMP (Figure 43). We compared the flux of KtrCB-ATP with and without addition of c-di-AMP or c-di-GMP to an external solution containing 150 mM choline chloride and 2 mM magnesium. The flux rate of KtrCB-ATP is 0.054 s^{-1} and addition of c-di-GMP does not have an impact, with rate constants of 0.048 s^{-1} and 0.047 s^{-1} for 50 and 100 µM c-di-GMP, respectively. On the other hand, addition of 50 or 100

µM of c-di-AMP reduced KtrCB-ATP flux by ~1.5 fold and ~4 fold, respectively, with rate constants of 0.035 s^{-1} and 0.014 s^{-1} (Figure 43c). This effect is observed with both valinomycin and steady-state normalizations of the data (Figure 43a and 43b). This preliminary result is in good agreement with the thermal shift assay that indicated binding of c-di-AMP but not of c-di-GMP to KtrC. Furthermore, it shows that c-di-AMP inhibits KtrCB-ATP channel activity.

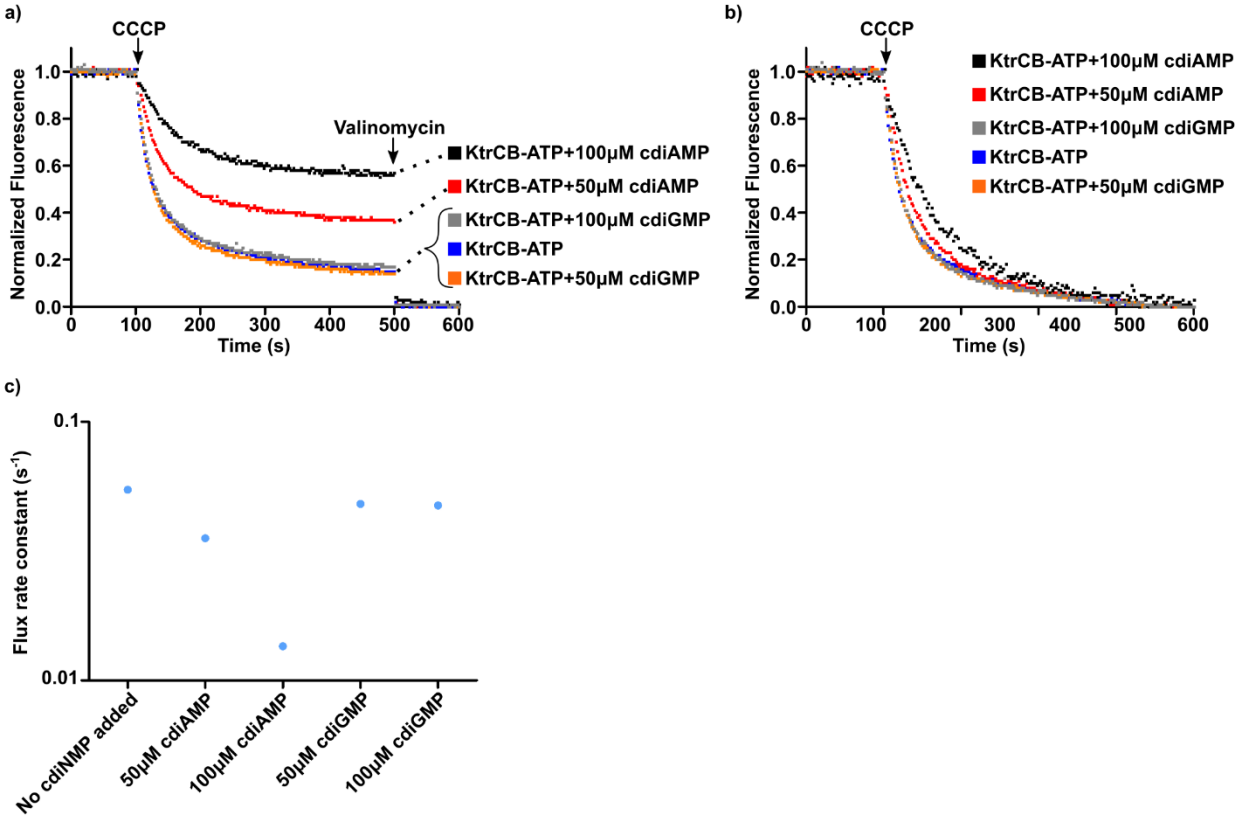

Figure 43: Impact of cdiAMP on KtrCB flux. a) and **b)** Proteoliposome flux assays performed with KtrCB-ATP in a choline chloride external solution supplemented with magnesium. Panels show fluorescence quenching curves normalized to the valinomycin signal in a) and normalized to steady-state in b). **c)** Plot of flux rate constants for conditions shown in a) and b). A single measurement was done for each condition in these initial tests, consequently no error bars are shown.

To better characterize the c-di-AMP effect in the KtrCB-ATP activity, we performed a titration of the cyclic dinucleotide using the flux assay (Figure 44). The titration shows that increasing concentrations of c-di-AMP result in a reduced flux rate (Figure 44a). Fitting the titrations with a Hill equation yielded a $K_{1/2}$ of inhibition of 65 ± 3 µM with a Hill coefficient of 3.8 ± 0.4, demonstrating a direct functional inhibitory effect of c-di-AMP in KtrCB-ATP activity (Figure 44b).

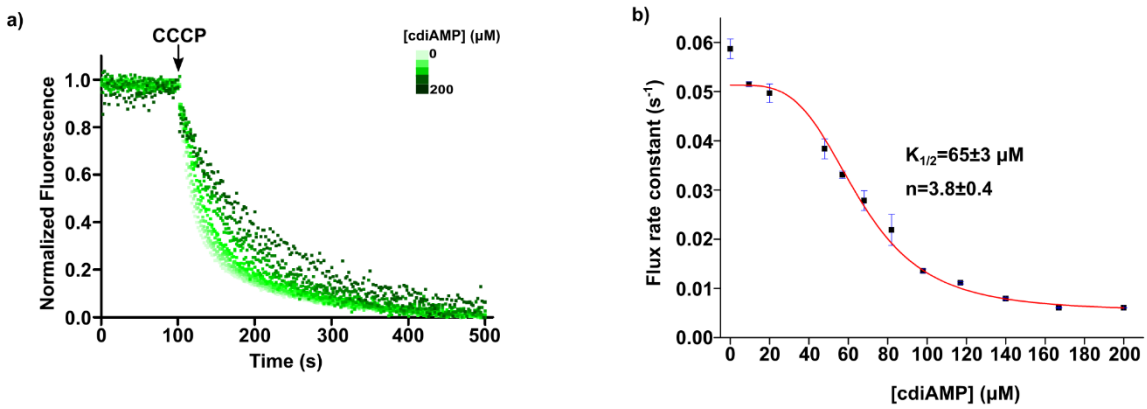

Figure 44: c-di-AMP titration of KtrCB-ATP. a) c-di-AMP titration of KtrCB-ATP using a proteoliposome flux assay performed with increasing amounts of c-di-AMP added to a 150 mM choline chloride external solution containing 2 mM magnesium. Panel shows representative fluorescence quenching titration curves normalized to their steady-state. c-di-AMP concentration increases with color intensity from 0 to 200 µM. Curves corresponding to the 167 and 200 µM concentrations are omitted due to high noise in signal normalization to the steady state. **b)** Plot of flux rate constants (mean ± SD, from 3 separate titrations) as a function of c-di-AMP concentration. Titrations were fitted with a Hill equation $= Start + (End - Start) \times \frac{x^n}{K_{1/2}^n + x^n}$. Mean ± SD of $K_{1/2}$ and of Hill coefficients (n) determined from fits to separate titrations are shown.

However, upon close inspection of the fluorescence quenching curves, it is apparent that we have an experimental issue, probably caused by interference of c-di-AMP with the ACMA fluorescent probe (Figure 45). We had previously noticed that ACMA fluorescence is affected by flux assay conditions. This was manifested by variations of the initial fluorescence value (before addition of CCCP), as previously exemplified for the KtrAB-ATP magnesium titration. We attributed this phenomenon to sensitivity of ACMA fluorescence to the ion composition of the bathing solutions. The c-di-AMP effect on the fluorescence quenching curves appears to be different. In the Mg^{2+} titration experiments, increasing the magnesium ion concentration in the external solution resulted in an increase of the initial fluorescence signal but had little effect in the final fluorescence values after valinomycin addition. This resulted in an increase of the signal window with the rise in magnesium concentration. In the KtrCB-ATP titration with c-di-AMP, an increase of nucleotide concentration had the opposite effect, leading to a decrease of the initial fluorescence signal (Figure 45). Moreover, it also increased the final fluorescence value after valinomycin addition. Overall, the signal window became progressively smaller with increasing amounts of cyclic dinucleotide (Figure 45a).

We analysed the curves of the initial tests with c-di-GMP and compared them with those from c-di-AMP at two different concentrations (Figure 45c). It is clear that, even though

c-di-GMP causes a decrease in the initial fluorescence signal, this effect is much smaller than with c-di-AMP for equal nucleotide concentrations and therefore, does not have a large impact in the signal window. These observations lead us to propose that c-di-AMP interferes directly with the fluorescence of ACMA, possibly reducing its sensitivity to a pH gradient across a membrane. c-di-AMP has already been shown to affect the fluorescence of other probes such as coralyne, a compound with structure similarities to ACMA (J. Zhou et al., 2014). Taking into account these observations, we concluded that the results obtained with the ACMA assay should be confirmed with other approaches.

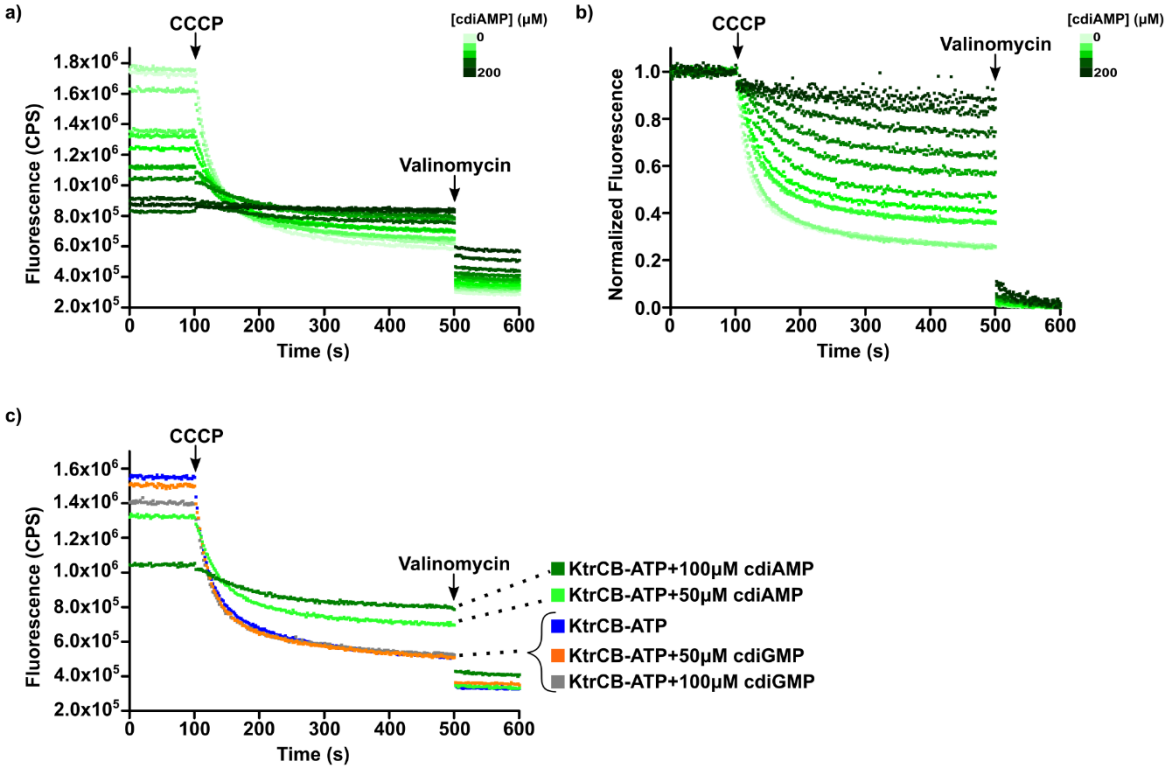

Figure 45: Fluorescence raw and normalized data from c-di-AMP titration. a) Raw fluorescence data from representative titration. **b)** Same data after normalization to valinomycin signal. c-di-AMP concentration increases with color intensity from 0 to 200 μM. **c)** Raw fluorescence representative curves of the impact of addition of increasing amounts of c-di-AMP and c-di-GMP on ACMA fluorescence quenching.

As alternatives to the ACMA flux assay, we attempted to implement other functional assays. First, we tried another proteoliposome K^+ flux assay using the hydrophilic pH-sensitive pyranine fluorescence probe (Lee, et al., 2013; Wiedenmann, et al., 2008). Unlike ACMA, pyranine is encapsulated inside the proteoliposomes and does not cross the membrane; therefore it will not interact with c-di-AMP added to the external solution.

In this assay, KtrCB proteoliposomes containing 150 mM KCl, and incorporated with 1 mM pyranine, were diluted in a low K^+ concentration solution in order to create a K^+ gradient. The assay was implemented in a plate format and initiated by addition of carbonyl cyanide m-chlorophenylhydrazone (CCCP, a H^+-ionophore), which builds-up a H^+ gradient across the membrane as potassium ions efflux through KtrCB. The pH decrease in the liposomal lumen results in quenching of pyranine fluorescence. The fluorescence signal is measured at a single emission wavelength of 510 nm, using two excitation wavelengths (406 nm and 460 nm). This allows the internal normalization of fluorescence, as excitation at 406 nm corresponds to an isosbestic point where the fluorescence signal is unchanged regardless of the pH, correcting for variations in the efficiency of pyranine encapsulation. The pH-dependent shift of the fluorescence signal is observed when exciting at 460 nm. Therefore, the final fluorescence signal, after normalization, corresponds to the ratio ($F_{510\ (excitation\ 406nm)}$ / $F_{510\ (excitation\ 460nm)}$) (Figure 46a). This ratio is expected to increase when the channel is active and mediates K^+ efflux. The K^+ ionophore valinomycin was added at the end of the assay to show the total possible flux from the liposome preparation.

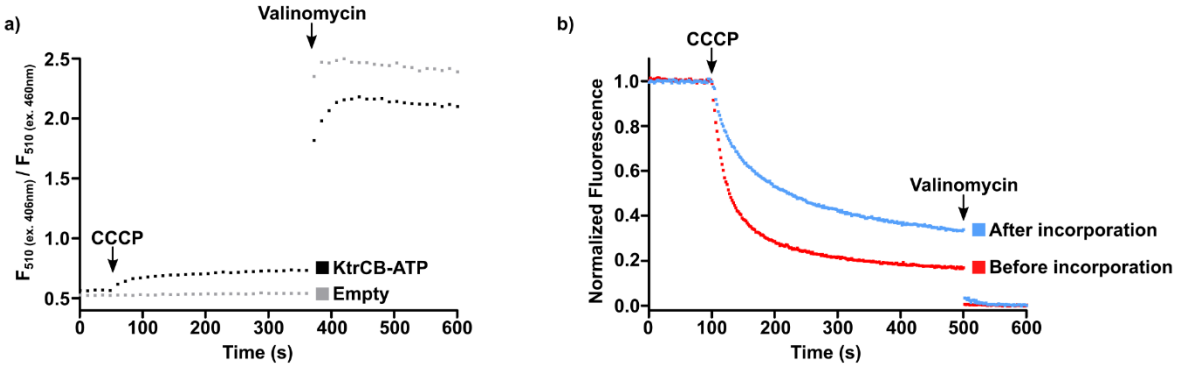

Figure 46: Normalized fluorescence data for KtrCB-ATP using the pyranine-K^+ flux assay. **a)** Normalized fluorescence data for a representative assay of KtrCB-ATP proteoliposomes incorporated with 1 mM pyranine. Empty liposomes incorporated with 1 mM pyranine were used as a control. Three measurements were performed for each condition. **b)** ACMA K^+ flux assay normalized fluorescence data for KtrCB-ATP proteoliposomes before and after the procedure for pyranine incorporation. For the KtrCB-ATP sample after incorporation, the procedure for incorporation was performed in the absence of the probe and the proteoliposomes were then tested using the ACMA-K^+ flux assay. A single measurement was performed for each condition.

Using this assay, we were only able to measure a small signal for KtrCB-ATP flux. The signal window corresponded to 11.0 ± 0.1 % (n=3) of the total signal from liposomes with incorporated pyranine, as estimated from the fluorescence signal after valinomycin addition (Figure 46a). This suggests that KtrCB is not fully active and we wondered if

the procedure for probe incorporation had disrupted in some way the KtrCB-ATP proteoliposomes, impairing channel function. In order to test this possibility, we mimicked the incorporation process in the absence of pyranine and tested the final KtrCB-ATP proteoliposome sample using the ACMA K^+ flux assay. Pyranine was not incorporated in these samples to avoid interferences in the fluorescence signal, due to the overlaps in the excitation and emission spectra of the two probes. The experiment shows that, even though flux was reduced relative to the values measured before incorporation (rate constant of 0.045 s^{-1} vs 0.054 s^{-1}), channels are active with flux curves reaching a steady-state value of ~83% and ~66% before and after the incorporation procedure, respectively (Figure 46b). As variation of several parameters, including K^+ gradient, CCCP concentration and pyranine concentration, did not improve the signal window and this was too small for a reliable quantification of c-di-AMP inhibition of channel activity, this assay was not pursued further.

Another alternative approach tested was a stopped-flow fluorometric ion flux assay that has been used to study the function of potassium channels (Ingólfsson & Andersen, 2010; Posson et al., 2015b; Posson, et al., 2018; Rusinova et al., 2014). This assay takes advantage of the permeability of K^+-conducting channels to thalium (Tl^+), using this cation to mimic K^+ flux. In this assay, the channel of interest is reconstituted in liposomes containing potassium and an encapsulated 8-Aminonaphthalene-1,3,6-Trisulfonic acid (ANTS) fluorophore. An inward gradient for Tl^+ is generated by using a stopped-flow mixing device and rapidly mixing the proteoliposomes with a solution containing Tl^+. When the channel is active, the Tl^+ ions will enter the proteoliposomes and quench the ANTS fluorescence. The increase in positive charges inside the liposomal lumen resulting from Tl^+ entrance is compensated by the efflux of K^+ ions. In conditions were the channel is fully active, the Tl^+ influx rate and respective ANTS fluorescence quenching is usually very fast (milliseconds).

To implement the assay, we reconstituted KtrCB-ATP in liposomes encapsulating 25 mM ANTS and 100 mM KNO_3. KtrCB channel reconstitution was confirmed by SDS-PAGE (Figure 47a). The proteoliposomes were then diluted 10-fold in an external solution containing 140 mM KNO_3 that was rapidly mixed with a solution containing 50 mM $TlNO_3$ using a stopped-flow mixing device coupled to a spectrofluorometer to register the fluorescence signal. All solutions contained 0.1 mM ATP and 1 mM MgAcetate to ensure full channel activity. An assay with empty liposomes reconstituted in the same manner was also performed as a control. Mixing of the diluted proteoliposome or empty liposome solutions with an external solution without thalium

was used to obtain the maximum fluorescence signal and normalize the data (Figure 47b).

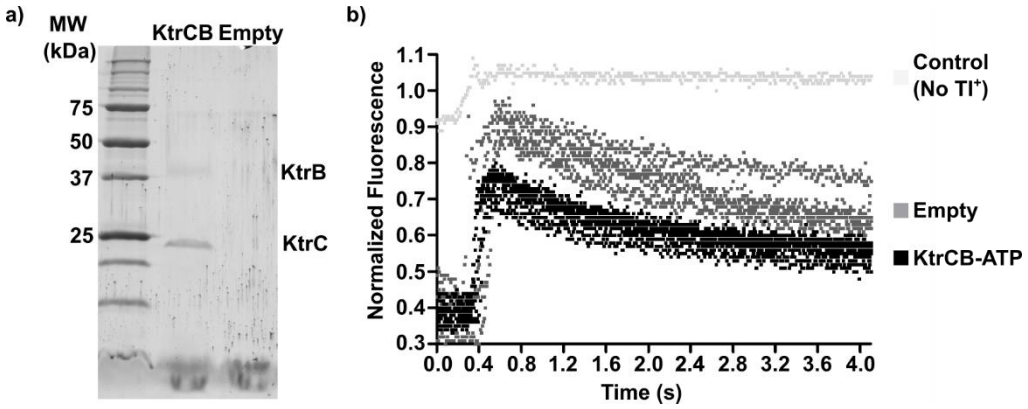

Figure 47: Normalized fluorescence data for KtrCB-ATP using the ANTS Tl^+ flux assay. a) SDS-PAGE gel showing the incorporation of KtrCB in the proteoliposomes. Empty liposome sample was also run to show there was no protein in this case. **b)** Normalized fluorescence data for the flux assays of KtrCB-ATP proteoliposomes with encapsulated ANTS. Empty liposomes also with encapsulated ANTS were used as a control. 4 replicas are shown for empty liposomes and 6 replicas are shown for the KtrCB-ATP proteoliposomes. A representative assay using KtrCB-ATP performed in the absence of Tl^+ is shown to indicate the maximum fluorescence signal obtained for this proteoliposome population. This signal was used for data normalization.

The data shows a jump in fluorescence during the mixing of the liposomes with the other solution. The baseline signal until the 0.4 s corresponds to the period before the mixing of the proteoliposome and thalium containing solutions, which occurs between 0.4 and 0.5 s. We were expecting to observe a rapid decrease in fluorescence after mixing with thallium in the samples reconstituted with KtrCB-ATP, relative to empty liposomes, indicating channel activity. Instead, the decay in fluorescence signal obtained for the KtrCB-ATP liposomes is similar to that obtained with empty liposomes, with a slow decay over the second time-scale from the maxima found after 0.4 s. Interestingly, we noticed that the normalized fluorescence signal at 0.5 s is consistently lower for the KtrCB-ATP proteoliposomes compared to the empty liposomes (Figure 47a). One possibility is that most of the quenching signal due to channel activity is hidden in the rising phase between the 0.4 and 0.5 s period. If this is the case, the quenching observed at 0.5 s could already be after the completion of the fast descending stage of the quenching curve. Unfortunately, this indicates that we have a limitation in our experimental setup as we do not have the necessary time-resolution with our stopped-flow mixing device. In studies of other K^+ conducting channels, this assay is performed

in a spectrofluorometer with an automated stopped-flow, making the process faster and more precise, with reported time constants of 4.9 and 12.1 milliseconds for the KcsA and MthK K^+ channels, respectively (Posson et al., 2015a; Rusinova, et al., 2014).

In light of these results, we have not yet been able to implement an assay that allows an accurate characterisation of the functional role of c-di-AMP in KtrCB activity. Other assays that do not require fluorescent probes will be tested in the future but no preliminary data is available at this time.

KtrCB-ATP-c-di-AMP channel structure determination

Results above demonstrate that c-di-AMP binds to the KtrA and KtrC RCK proteins from *B. subtilis*. Moreover, our results appear to confirm that this cyclic dinucleotide inhibits the function of the KtrCB-ATP channel. However, it is not known how binding of c-di-AMP affects the RCK octameric ring conformation and regulates channel activity. The structure of the C-terminal domain of a KtrA ortholog with bound c-di-AMP has been solved (H. Kim, et al., 2015) but, to date, the structure of a full-length KtrA or KtrC with bound c-di-AMP as not yet been determined. Despite our best efforts, we were unable to obtain well diffracting crystals of either KtrA or KtrC bound to cyclic-di-AMP, with either ATP or ADP bound at the N-terminal domain. Even though beautiful crystals were formed in multiple conditions for both proteins, the data sets obtained were limited to very low resolution (9 to 12 Å) and did not allow an evaluation of the impact of c-di-AMP in the conformation of the octameric ring or mapping of its binding site. Since KtrA and KtrC crystals in the absence of c-di-AMP diffract up to 2.9 and 2.0 Å, respectively, it is reasonable to assume that binding of the cyclic dinucleotide probably induces a conformational change that increases the flexibility of the proteins, resulting in poor diffracting crystals.

As an alternative approach, we attempted to determine the structure of KtrCB bound to ATP and c-di-AMP. We were hoping that association of the RCK octameric ring with the the membrane protein might confer additional rigidity that could result in better quality crystals than the ones obtained for the RCK domains alone. Since KtrC binds c-di-AMP with a higher affinity than KtrA, the KtrCB channel was chosen for the experiment instead of KtrAB.

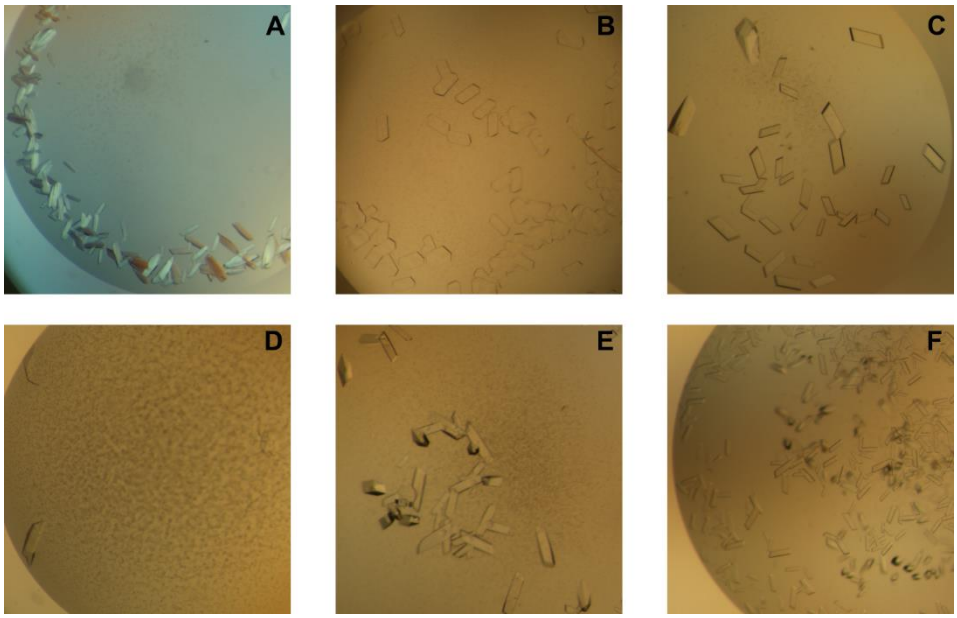

Figure 48: Representative crystals obtained for the KtrCB-ATP-c-di-AMP complex.

A- Crystals obtained in 100 mM Tris-HCl pH 8.5; 200 mM Ammonium sulfate and 25% PEG 400.

B- Crystals obtained in 100 mM ADA pH 6.5; 200 mM Ammonium sulfate and 20% PEG 400.

C- Crystals obtained in 100 mM Tris-HCl pH 8.5; 700 mM KCl and 24% PEG 400.

D- Crystals obtained in 100 mM HEPES-NaOH pH 7.5; 200 mM Ammonium sulfate and 10% PEG 4000.

E- Crystals obtained in 100 mM ADA pH 6.5; 800 mM Ammonium formate and 28% PEG 400.

F- Crystals obtained in 100 mM Tris-HCl pH 8.5; 1 M NaCl and 26% PEG 400.

For the crystallization trials, KtrCB was supplemented with 500 µM ATP, c-di-AMP and magnesium after the final purification step. Cymal-6 was the detergent used in this size-exclusion chromatography step for crystallization trials. At this point, no detergent screening was performed. Cymal-6 was chosen as a starting detergent since it is a mild non-ionic detergent and had been successfully used in the crystallization trials of the KtrAB complex. Initial crystallization conditions were obtained using a homemade screen and the sitting-drop vapour diffusion method at 20ºC. These conditions were further refined and the best crystals obtained are shown in Figure 48. These crystals were cryo-protected and X-ray diffraction data was collected at the Proxima 2A beamline of the SOLEIL synchrotron. A dataset was collected from a crystal diffracting up to 5.8 Å resolution, originating from the following crystallization condition: 100 mM Tris-HCl pH 8.5; 700 mM KCl and 24% PEG 400 (Figure 48c). The complex crystallized in space group $P2_1$, with unit cell dimensions 127.8, 143.7, 160.7 Å/90.0 112.4 90.0º. This space group is the same as the one obtained in the KtrAB-ATP structure (PDB: 4J7C) but with

different cell dimensions. The data is anisotropic, extending to 5.8 Å in the best direction and 6.5 Å in the worst direction.

To solve the structure, we performed molecular replacement searches using as search models a collection of KtrA octameric ring structures and two structures of KtrB dimers. The different models were used in order to cover a range of conformational arrangements of the KtrCB complex, facilitating the determination of the low resolution structure of the KtrCB-ATP-c-di-AMP complex. KtrA octameric rings without C-terminal domains were also used as search models, since the molecular replacement solutions with full-length rings showed that the density observed for those protein regions is poor, as shown in Figure 49.

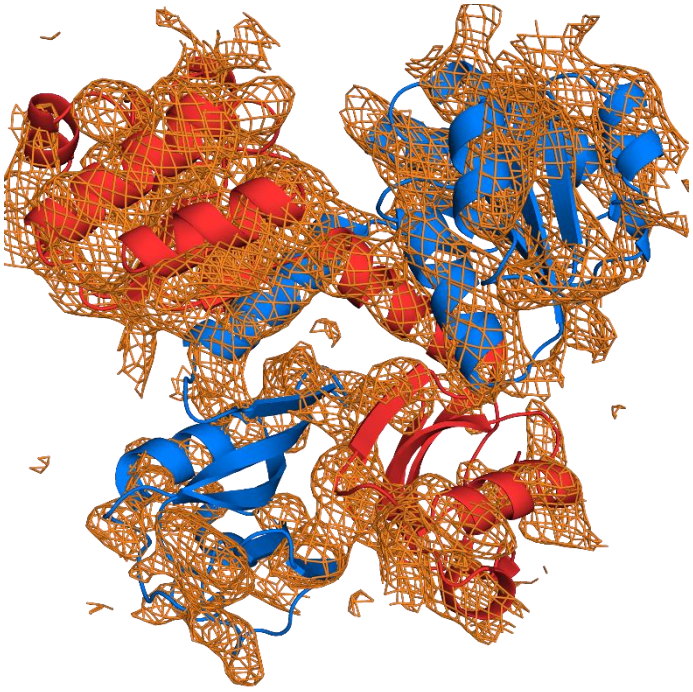

Figure 49: RCK dimer electron density in the KtrCB-ATP-c-di-AMP complex diffraction data. Representation of a KtrA dimer from the molecular replacement solution obtained using the KtrB dimer (ADP) + $KtrA_{E125Q}$-ADP_ring1 search model, showing the poor density available for the KtrA C-lobes. Electron density map 2Fo-Fc (in orange) is contoured at 1.0 σ and shown in mesh. KtrA subunits are colored blue and red.

We obtained several solutions with a packing of two membrane–protein dimers associated with opposing faces of an octameric RCK ring. Solutions were selected according to the value of the log-of-likelihood gain function (LLG), a measure of how well the structural model agrees with the experimental data. Representative combinations of the search models that resulted in higher LLG values are shown in Figure 50 and the full results are presented in Table 9.

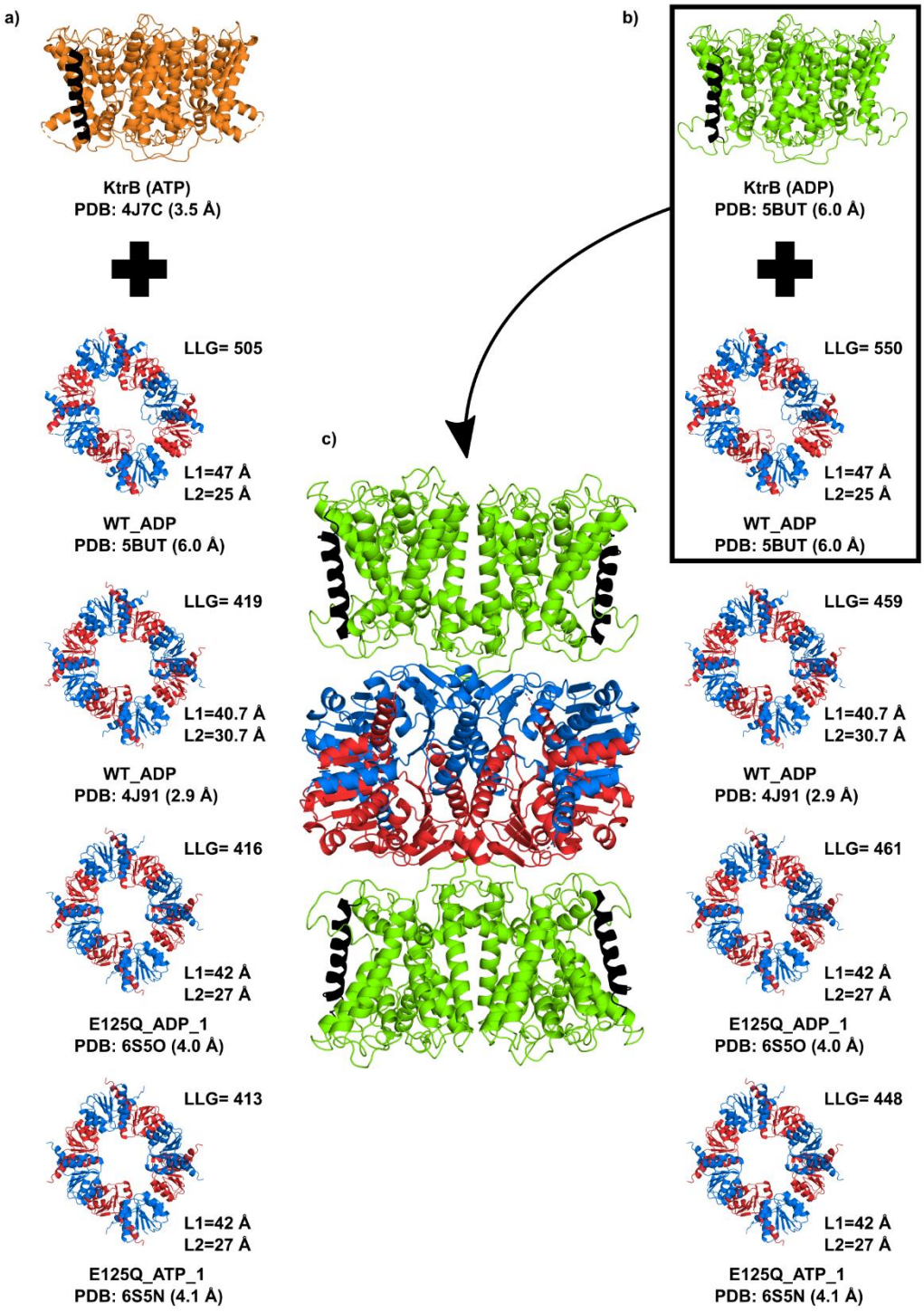

Figure 50: KtrCB-ATP-c-di-AMP complex molecular replacement. a) and **b)** Representative KtrA ring and KtrB dimer structures used as search models to determine the KtrCB-ATP-c-di-AMP structure. The KtrB dimer and KtrA ring combinations that resulted in higher LLG values are depicted, with the respective LLG value shown on the top right corner of each ring. For each KtrA ring, the L1 and L2 the pair of distances between the Cα of N38 residues located in opposite subunits across the ring are also shown to illustrate the differences in ring conformations. Subunits of the octameric rings are colored alternately blue and red. In the KtrB dimers, the

D2M1 helix is highlighted in black. **c)** Structure of the model corresponding to the best solution obtained with combinations of the KtrB dimers and KtrA rings.

Table 9: Log-of-likelihood gain (LLG) values obtained for the molecular replacement searches.

		RCK rings without C-terminal domains		RCK rings with C-terminal domains	
RCK ring	**PDB code**	**KtrB dimer (ATP) PDB: 4J7C**	**KtrB dimer (ADP) PDB: 5BUT**	**KtrB dimer (ATP) PDB: 4J7C**	**KtrB dimer (ADP) PDB: 5BUT**
Non-square conformations					
$KtrA_{WT}$-ADP	5BUT	505	550	#	#
$KtrA_{WT}$-ADP	4J91	419	459	386	426
$KtrA_{WT}$-ADP	2HMV	358	385	#	#
$KtrA_{WT}$-ATP	2HMU	358	386	#	#
$KtrA_{WT}$-NADH	2HMS	318	394	#	#
$KtrA_{WT}$-NADH	2HMT	363	388	#	#
$KtrA_{A80P}$-ADP	6S5G	308*	334*	292*	323*
$KtrA_{A80P}$-ATP	6S5E	307*	336*	296*	317*
$KtrA_{E125Q}$-ADP_ring1	6S5O	416	461	380	431
$KtrA_{E125Q}$-ADP_ring2	6S5O	319	385	311	362
$KtrA_{E125Q}$-ATP_ring1	6S5N	413	448	382	419
$KtrA_{E125Q}$-ATP_ring2	6S5N	308*	341	291*	334
$KtrA_{R16A}$-ADP_ring1	6S7R	325	369	297*	329*
$KtrA_{R16A}$-ADP_ring2	6S7R	342	381	327	369
$KtrA_{R16K}$-ADP	6S5B	313	345	294*	328*
Square conformations					
$KtrA_{WT}$-ATP	4J90	300*	342	287*	329*
$KtrA_{WT}$-ATP	2HMW	329	360	#	#
$KtrA_{WT}$-ATP-Ca	6S5C	298*	343	290*	331*
$KtrA_{R16A}$-ATP	6S5D	308	348	294*	331*
$KtrA_{R16K}$-ATP	6S2J	302*	341	288*	331*

* These solutions displayed incorrect packing and a translation function Z-score (TFZ) ≤ 8.0.

No LLG value is shown since these RCK ring structures do not contain the C-terminal domains.

As shown in Table 9, the search models containing RCK rings without C-terminal domains resulted in higher LLG values compared to their full-length ring counterparts. Furthermore, search models using RCK rings that adopt the square conformation resulted mainly in LLG values that are lower than the ones obtained with the RCK rings that adopt a non-square conformation. Also, the search models containing the KtrB dimer from the $KtrA_{\Delta C}B$-ADP structure resulted in higher LLG values than the ones containing the KtrB dimer from the KtrAB-ATP structure. The main difference in the KtrB dimer structures resides in the position of the D2M1 helix. In the $KtrA_{\Delta C}B$-ADP (PDB: 5BUT) structure, this helix was straightened with an outward movement of the cytosolic end, while in KtrAB-ATP structure (PDB: 4J7C) it is bent towards the cytosolic pore (Figure 50).

The best fit for the diffraction data corresponds to the combination of the KtrB dimers and RCK octameric ring from the $KtrA_{\Delta C}B$-ADP structure (PDB: 5BUT), with an LLG value of 550. Due to the low resolution of the data, no manual adjustments and subsequent refinements were performed at this stage. Nonetheless, the molecular replacement model clearly indicates that the KtrCB-ATP-c-di-AMP structure is similar to the $KtrA_{\Delta C}B$-ADP structure. We cannot confirm that the proteins in the crystal structure have either bound ATP or c-di-AMP, but KtrC was purified in the presence of ATP and the KtrCB complex was further supplemented with 500 µM of nucleotide. Thus, it is reasonable to assume that the KtrC ring contains bound ATP, as other higher-resolution structures of KtrA and KtrC solved in the lab have shown. As for c-di-AMP, the cyclic dinucleotide was supplemented at 500 µM, which is considerably higher than the $K_{1/2}$ of inhibition of 65 ± 3 µM determined for the KtrCB-ATP complex using the ACMA K^+ flux assay, and well above the c-di-AMP binding affinity estimated by ITC for KtrC (20 to 30 nM). Therefore this result suggests that c-di-AMP binding to the RCK protein destabilizes the square conformation (corresponding to the activated state of the octameric ring) giving rise to a non-square relaxed state that is identified with a low-activity state of a Ktr channel. This destabilization most likely involves a disruption of the interactions established by ATP and Mg^{2+} at the intra-dimer interface that tether the two ATP molecules and stabilize the two subunits in the RCK dimer close together. Furthermore, the conformational readjustment of the RCK ring seems to be propagated to the membrane protein, promoting an adjustment of the KtrB D2M1 helix.

V. GENERAL DISCUSSION

The KtrAB channel is formed by the assembly of a KtrB homodimer with an octameric ring of the nucleotide-dependent RCK protein KtrA. KtrA binds ATP and ADP at the N-terminal domain and nucleotide binding was shown to regulate the conformation of the octameric ring. The ATP-bound ring adopts a square conformation that results in high channel flux, while the ADP-bound ring adopts non-square conformations that result in a diminished flux. In this work, we have now established that the ATP-dependent activation mechanism involves divalent cations as cofactors. The divalent cation binds at the intra-dimer interface site of an ATP-bound KtrA dimer and stabilizes the octameric ring square conformation (Teixeira-Duarte et al., 2019). Furthermore, our data also strongly suggests that monovalent cations are also able to bind at the intra-dimer interface site and activate KtrAB, but with less affinity than the divalent cations.

The cyclic dinucleotide c-di-AMP was identified as an important regulator of K^+ homeostasis in many bacteria and its levels were shown to increase with K^+ concentration in *B.subtilis* (Gundlach, et al., 2017). Furthermore, this molecule binds to the C-terminal domain of KtrA orthologs (Y. Bai, et al., 2014; R. M. Corrigan, et al., 2013) and was also shown to regulate KtrAB protein expression in *B.subtilis* (Nelson, et al., 2013). We have now confirmed that c-di-AMP binds to both KtrA and KtrC and appears to inhibit KtrCB. Importantly, we revealed that this binding is not affected by ATP or ADP and that the c-di-AMP affinity for KtrC is higher than for KtrA. However, it is very possible that this affinity difference is altered in the Ktr complex. As c-di-AMP might have a central role in the regulation of the Ktr cation channels it is important to determine the binding affinities of c-di-AMP to the full Ktr channel complexes and study its functional impact.

Several questions about Ktr channel regulation and underlying molecular mechanisms remain unanswered. These include: What is the structure of an open Ktr channel? How are these channels regulated by different ligands (ATP, ADP and c-diAMP) in the cell? Does intracellular pH play a role in the activity of the channels? and What is the role of the two regulatory proteins?

The KtrB conformation adopted in the active state remains elusive. In the current KtrAB-ATP structure the pore remains occluded by the intramembrane loop, despite the adoption of the active square conformation by the KtrA ring (Vieira-Pires, et al., 2013). Therefore, a structure of the ATP-bound KtrAB complex portraying a KtrB fully open pore would provide important insights on channel conformational regulation. It was

proposed that the channel might not be able to adopt the fully open conformation in detergent (Vieira-Pires, et al., 2013). In order to overcome this limitation, an option would be to reconstitute the channel into nanodiscs and attempt to solve this structure by cryo-EM. The lipid bilayer provided by the nanodiscs creates an environment that resembles better the cellular membrane and may allow the stabilization of KtrB in the fully open pore conformation. Structural information is also required in order to understand the molecular mechanism of Ktr regulation by c-di-AMP. We have not been able to obtain a structure of c-di-AMP bound to KtrA or KtrC, but have determined a low-resolution structure of the KtrCB-ATP-c-di-AMP complex. This structure is similar to the previously determined $KtrA_{\Delta C}B$-ADP structure, with the KtrC ring adopting a non-square conformation. This suggests that c-di-AMP binding promotes a conformational change of the KtrC octameric ring, disrupting the active square conformation. A structure of the KtrCB-ATP complex is needed to confirm that KtrC-ATP adopts the square conformation in the absence of c-di-AMP and a higher resolution KtrCB-ATP-c-di-AMP structure will ensure that the ligands are present and reveal in more detail the conformational changes that occur in the channel upon c-di-AMP binding.

The regulation of the KtrAB channel by ATP, ADP and c-di-AMP in a physiological context remains unclear. The detergent solubilized *V.alginolyticus* KtrAB has similar affinities for ATP and ADP (K_d of 2.6 µM for ADP and 1.6 µM for ATP) (Diskowski, et al., 2017). In bacteria, the concentration of ATP is in the millimolar range and there is usually an excess of ATP over ADP, with the ATP/ADP ratio reported for *E.coli* ranging from ~8 to ~30, depending on the growth conditions and quantification methodology employed (Buckstein et al., 2008; Radchenko et al., 2010). In these conditions, KtrAB would be fully saturated with ATP and therefore fully active. Fluctuations of this ratio have been described in ammonium stress conditions, with the ATP/ADP ratio decreasing from ~ 8 to ~ 3 in an early phase after ammonium shock (Radchenko, et al., 2010). This fluctuation was shown to be sufficient to favor binding of ADP over ATP to the nucleotide regulated *E.coli* P_{II} protein, GlnK (Radchenko, et al., 2010). A similar effect might occur in response to situations where Ktr channel function has to be switched-off. It is worthwhile pointing-out that there is no available information on the effect of ATP/ADP ratio on the activity of the KtrAB channel. The functional and structural properties of the octameric ring, which contains eight N-terminal nucleotide binding sites, have only been studied in single nucleotide conditions. It would be interesting to test different nucleotide ratios in vitro, with the ACMA K^+ flux assay and possibly X-ray crystallography, in order to determine the fraction of ADP required for KtrA to adopt a non-square conformation and enable inactivation of the KtrAB channel.

c-di-AMP was proposed to signal the closure of Ktr channels in bacteria that produce this cyclic dinucleotide. This proposal results from complementation growth assays using bacterial strains that require a functional Ktr channel to grow in the tested conditions. In these assays, augmented levels of c-di-AMP production resulted in a non-growth phenotype (Y. Bai, et al., 2014; R. M. Corrigan, et al., 2013; Gibhardt, et al., 2019) but there is currently little direct functional evidence of Ktr channel inhibition by c-di-AMP. We studied the role played by this nucleotide in the regulation of the KtrCB-ATP channel function. Our *in vitro* study with the ACMA K^+ flux assay indicates a direct functional inhibitory effect of c-di-AMP in KtrCB activity. However, the assay is not ideal to study c-di-AMP due to interference of the nucleotide with ACMA. Unfortunately, we also failed to implement other functional assays using fluorescent probes to study the KtrCB channel activity. We will try to implement other flux assays in the lab, namely ion selective electrode-based assays, and characterize the effect of c-di-AMP in KtrCB and KtrAB channel activity. The role of c-di-AMP in the *in vivo* regulation of Ktr channel function can also be explored with *in vivo* growth assays in *B.subtilis*. These assays would show if there is a differential regulation of KtrA and KtrC by c-di-AMP and how this affects the bacterial growth phenotype. In particular, strains containing mutated versions of the RCK proteins in the c-di-AMP binding site can be used for this effect in growth contexts that require Ktr channel function, such as K^+ limitation and osmotic shock conditions.

Ktr channel activity is involved in the early K^+ uptake response to hyperosmotic shock. In parallel, K^+ uptake is a mechanism used to alkalinize the cytosol when bacterial cells are exposed to an acidic pH. Therefore, since most functional assays performed to date were done at neutral or alkaline pH, it would be interesting to see how channel activity responds to acidic pH and if pH affects complex formation.

A remarkable aspect still to be explored pertains to the diverse distribution of Ktr subunits across different organisms. For instance, *V.alginolyticus* possesses a single KtrAB channel (Nakamura, et al., 1998), while *S.aureus* contains two ion conducting subtunits, KtrB and KtrD, that appear to be regulated by one RCK regulatory subunit (Gries, et al., 2013). In *B.subtilis*, the Ktr channel system comprises two Ktr ion conduction subunits, KtrB and KtrD, as well as two RCK regulatory subunits, KtrA and KtrC. Since KtrA and KtrB are organized in the same operon and KtrC and KrD are encoded separately, the KtrAB and KtrCD complexes have been proposed to be the two Ktr channels. We have shown that both KtrA and KtrC are able to assemble in functional complexes with KtrB and KtrD (Rocha, et al., 2019). Furthermore, in this work

we demonstrated that the KtrCB-ATP complex is fully active *in vitro*. KtrA and KtrC appear to have very similar properties. This apparent redundancy is still largely unexplored. Why does *B. subtilis* have both KtrA and KtrC? Do these proteins have different roles? Our biochemical characterization of KtrC has already revealed different molecular properties relative to KtrA. While KtrA always assembles as a stable octamer, KtrC in solution exists in a dynamic oligomeric equilibrium that can be modulated by nucleotides, in particular c-di-AMP. Additional studies are needed to understand the impact of KtrA and KtrC in channel regulation. Our *in vitro* flux assays show that KtrAB-ATP and KtrCB-ATP display similar flux activities but no information is yet available regarding the KtrAD and KtrCD channels. Furthermore, *in vivo* assays using *B.subtilis* strains with targeted deletions in the Ktr channel system components are required to understand if KtrA and KtrC activity is redundant in this organism and to attempt to discern possible differential roles of the two RCK proteins. Growth of the *B.subtilis* strains in potassium limitation and osmotic stress conditions, such as salinity adaptation, might prove informative in this regard.

VI. REFERENCES

Abdul-Sater, A. A., Tattoli, I., Jin, L., Grajkowski, A., Levi, A., Koller, B. H., Allen, I. C., Beaucage, S. L., Fitzgerald, K. A., Ting, J. P., Cambier, J. C., Girardin, S. E., & Schindler, C. (2013). Cyclic-di-GMP and cyclic-di-AMP activate the NLRP3 inflammasome. *EMBO Rep, 14*(10), 900-906. doi: 10.1038/embor.2013.132

Abel, S., Bucher, T., Nicollier, M., Hug, I., Kaever, V., Abel zur Wiesch, P., & Jenal, U. (2013). Bi-modal Distribution of the Second Messenger c-di-GMP Controls Cell Fate and Asymmetry during the Caulobacter Cell Cycle. *PLOS Genetics, 9*(9), e1003744. doi: 10.1371/journal.pgen.1003744

Ablasser, A., Goldeck, M., Cavlar, T., Deimling, T., Witte, G., Röhl, I., Hopfner, K.-P., Ludwig, J., & Hornung, V. (2013). cGAS produces a 2′-5′-linked cyclic dinucleotide second messenger that activates STING. *Nature, 498*(7454), 380-384. doi: 10.1038/nature12306

Adams, P. D., Afonine, P. V., Bunkoczi, G., Chen, V. B., Davis, I. W., Echols, N., Headd, J. J., Hung, L. W., Kapral, G. J., Grosse-Kunstleve, R. W., McCoy, A. J., Moriarty, N. W., Oeffner, R., Read, R. J., Richardson, D. C., Richardson, J. S., Terwilliger, T. C., & Zwart, P. H. (2010). PHENIX: a comprehensive Python-based system for macromolecular structure solution. *Acta Crystallogr D Biol Crystallogr, 66*(Pt 2), 213-221. doi: 10.1107/S0907444909052925

Aggarwal, S. K., & MacKinnon, R. (1996). Contribution of the S4 segment to gating charge in the Shaker K+ channel. *Neuron, 16*(6), 1169-1177. doi: 10.1016/s0896-6273(00)80143-9

Alatossava, T., Jutte, H., Kuhn, A., & Kellenberger, E. (1985). Manipulation of intracellular magnesium content in polymyxin B nonapeptide-sensitized Escherichia coli by ionophore A23187. *J Bacteriol, 162*(1), 413-419.

Albright, R. A., Ibar, J. L., Kim, C. U., Gruner, S. M., & Morais-Cabral, J. H. (2006). The RCK domain of the KtrAB K+ transporter: multiple conformations of an octameric ring. *Cell, 126*(6), 1147-1159. doi: 10.1016/j.cell.2006.08.028

Albright, R. A., Joh, K., & Morais-Cabral, J. H. (2007). Probing the structure of the dimeric KtrB membrane protein. *J Biol Chem, 282*(48), 35046-35055. doi: 10.1074/jbc.M704260200

An, S.-Q., Chin, K.-H., Febrer, M., McCarthy, Y., Yang, J.-G., Liu, C.-L., Swarbreck, D., Rogers, J., Maxwell Dow, J., Chou, S.-H., & Ryan, R. P. (2013). A cyclic GMP-dependent signalling pathway regulates bacterial phytopathogenesis. *The EMBO journal, 32*(18), 2430-2438. doi: 10.1038/emboj.2013.165

Anderson, J. A., Huprikar, S. S., Kochian, L. V., Lucas, W. J., & Gaber, R. F. (1992). Functional expression of a probable *Arabidopsis thaliana* potassium channel in *Saccharomyces cerevisiae*. *Proc Natl Acad Sci U S A, 89*(9), 3736-3740. doi: 10.1073/pnas.89.9.3736

Armstrong, C. M. (1971). Interaction of tetraethylammonium ion derivatives with the potassium channels of giant axons. *J Gen Physiol, 58*(4), 413-437. doi: 10.1085/jgp.58.4.413

Armstrong, C. M. (1981). Sodium channels and gating currents. *Physiol Rev, 61*(3), 644-683. doi: 10.1152/physrev.1981.61.3.644

Ashman, D. F., Lipton, R., Melicow, M. M., & Price, T. D. (1963). Isolation of adenosine 3′,5′-monophosphate and guanosine 3′,5′-monophosphate from rat urine. *Biochemical and Biophysical Research Communications, 11*(4), 330-334. doi: https://doi.org/10.1016/0006-291X(63)90566-7

Atkinson, N. S., Robertson, G. A., & Ganetzky, B. (1991). A component of calcium-activated potassium channels encoded by the *Drosophila* slo locus. *Science, 253*(5019), 551-555. doi: 10.1126/science.1857984

Bai, Y., Yang, J., Eisele, L. E., Underwood, A. J., Koestler, B. J., Waters, C. M., Metzger, D. W., & Bai, G. (2013). Two DHH subfamily 1 proteins in *Streptococcus pneumoniae* possess cyclic di-AMP phosphodiesterase activity and affect bacterial growth and virulence. *J Bacteriol, 195*(22), 5123-5132. doi: 10.1128/jb.00769-13

Bai, Y., Yang, J., Zarrella, T. M., Zhang, Y., Metzger, D. W., & Bai, G. (2014). Cyclic di-AMP impairs potassium uptake mediated by a cyclic di-AMP binding protein in *Streptococcus pneumoniae*. *J Bacteriol, 196*(3), 614-623. doi: 10.1128/jb.01041-13

Bai, Y., Yang, J., Zhou, X., Ding, X., Eisele, L. E., & Bai, G. (2012). *Mycobacterium tuberculosis* Rv3586 (DacA) Is a Diadenylate Cyclase That Converts ATP or ADP into c-di-AMP. *PLOS ONE, 7*(4), e35206. doi: 10.1371/journal.pone.0035206

Bakker, E. P., & Mangerich, W. E. (1981). Interconversion of components of the bacterial proton motive force by electrogenic potassium transport. *J Bacteriol, 147*(3), 820-826.

Barker, J. R., Koestler, B. J., Carpenter, V. K., Burdette, D. L., Waters, C. M., Vance, R. E., & Valdivia, R. H. (2013). STING-Dependent Recognition of Cyclic di-AMP Mediates Type I Interferon Responses during *Chlamydia trachomatis* Infection. *MBio, 4*(3), e00018-00013. doi: 10.1128/mBio.00018-13

Bellamacina, C. R. (1996). The nicotinamide dinucleotide binding motif: a comparison of nucleotide binding proteins. *FASEB J, 10*(11), 1257-1269. doi: 10.1096/fasebj.10.11.8836039

Bernstein, J. (1902). Untersuchungen zur Thermodynamik der bioelektrischen Ströme. *Archiv für die gesamte Physiologie des Menschen und der Tiere, 92*(10), 521-562. doi: 10.1007/bf01790181

Berry, S., Esper, B., Karandashova, I., Teuber, M., Elanskaya, I., Rogner, M., & Hagemann, M. (2003). Potassium uptake in the unicellular cyanobacterium *Synechocystis sp*. strain PCC 6803 mainly depends on a Ktr-like system encoded by slr1509 (ntpJ). *FEBS Lett, 548*(1-3), 53-58. doi: 10.1016/s0014-5793(03)00729-4

Berthet, J., Rall, T. W., & Sutherland, E. W. (1957). The relationship of epinephrine and glucagon to liver phosphorylase. IV. Effect of epinephrine and glucagon on the reactivation of phosphorylase in liver homogenates. *J Biol Chem, 224*(1), 463-475.

Bezanilla, F., & Armstrong, C. M. (1977). Inactivation of the sodium channel. I. Sodium current experiments. *The Journal of general physiology, 70*(5), 549-566. doi: 10.1085/jgp.70.5.549

Blötz, C., Treffon, K., Kaever, V., Schwede, F., Hammer, E., & Stülke, J. (2017). Identification of the Components Involved in Cyclic Di-AMP Signaling in *Mycoplasma pneumoniae*. *Frontiers in microbiology, 8*, 1328-1328. doi: 10.3389/fmicb.2017.01328

Boch, J., Kempf, B., & Bremer, E. (1994). Osmoregulation in *Bacillus subtilis*: synthesis of the osmoprotectant glycine betaine from exogenously provided choline. *J Bacteriol, 176*(17), 5364-5371. doi: 10.1128/jb.176.17.5364-5371.1994

Bock, C. W., Kaufman, A., & Glusker, J. P. (1994). Coordination of water to magnesium cations. *Inorganic Chemistry, 33*(3), 419-427. doi: 10.1021/ic00081a007

Bossemeyer, D., Borchard, A., Dosch, D. C., Helmer, G. C., Epstein, W., Booth, I. R., & Bakker, E. P. (1989). K+-transport protein TrkA of *Escherichia coli* is a peripheral membrane protein that requires other *trk* gene products for attachment to the cytoplasmic membrane. *J Biol Chem, 264*(28), 16403-16410.

Botsford, J. L., & Drexler, M. (1978). The cyclic 3',5'-adenosine monophosphate receptor protein and regulation of cyclic 3',5'-adenosine monophosphate synthesis in *Escherichia coli*. *Mol Gen Genet, 165*(1), 47-56. doi: 10.1007/BF00270375

Bowman, L., Zeden, M. S., Schuster, C. F., Kaever, V., & Gründling, A. (2016). New Insights into the Cyclic Di-adenosine Monophosphate (c-di-AMP) Degradation Pathway and the Requirement of the Cyclic Dinucleotide for Acid Stress Resistance in *Staphylococcus aureus*. *J Biol Chem, 291*(53), 26970-26986. doi: 10.1074/jbc.M116.747709

Branda, S. S., Gonzalez-Pastor, J. E., Ben-Yehuda, S., Losick, R., & Kolter, R. (2001). Fruiting body formation by *Bacillus subtilis*. *Proc Natl Acad Sci U S A, 98*(20), 11621-11626. doi: 10.1073/pnas.191384198

Brass, E. P., & Vetter, W. H. (1993). Inhibition of Glucagon-Stimulated Glycogenolysis by S-Nitroso-N-acetylpenicillamine*. *Pharmacology & Toxicology, 72*(6), 369-372. doi: 10.1111/j.1600-0773.1993.tb01346.x

Braun, F., Thomalla, L., van der Does, C., Quax, T. E. F., Allers, T., Kaever, V., & Albers, S.-V. (2019). Cyclic nucleotides in archaea: Cyclic di-AMP in the archaeon *Haloferax volcanii* and its putative role. *MicrobiologyOpen, 8*(9), e00829-e00829. doi: 10.1002/mbo3.829

Brautigam, C. A. (2015). Calculations and Publication-Quality Illustrations for Analytical Ultracentrifugation Data. *Methods Enzymol, 562*, 109-133. doi: 10.1016/bs.mie.2015.05.001

Brautigam, C. A., Zhao, H., Vargas, C., Keller, S., & Schuck, P. (2016). Integration and global analysis of isothermal titration calorimetry data for studying macromolecular interactions. *Nature Protocols, 11*(5), 882-894. doi: 10.1038/nprot.2016.044

Brill, J., Hoffmann, T., Bleisteiner, M., & Bremer, E. (2011). Osmotically controlled synthesis of the compatible solute proline is critical for cellular defense of *Bacillus subtilis* against high osmolarity. *J Bacteriol, 193*(19), 5335-5346. doi: 10.1128/JB.05490-11

Buckstein, M. H., He, J., & Rubin, H. (2008). Characterization of nucleotide pools as a function of physiological state in *Escherichia coli*. *J Bacteriol, 190*(2), 718-726. doi: 10.1128/jb.01020-07

Burgering, B. M., Pronk, G. J., van Weeren, P. C., Chardin, P., & Bos, J. L. (1993). cAMP antagonizes p21ras-directed activation of extracellular signal-regulated kinase 2 and phosphorylation of mSos nucleotide exchange factor. *EMBO J, 12*(11), 4211-4220.

Buurman, E. T., McLaggan, D., Naprstek, J., & Epstein, W. (2004). Multiple paths for nonphysiological transport of K+ in *Escherichia coli*. *J Bacteriol, 186*(13), 4238-4245. doi: 10.1128/JB.186.13.4238-4245.2004

Cadoret, J. C., Rousseau, B., Perewoska, I., Sicora, C., Cheregi, O., Vass, I., & Houmard, J. (2005). Cyclic nucleotides, the photosynthetic apparatus and response to a UV-B stress in the Cyanobacterium *Synechocystis* sp. PCC 6803. *J Biol Chem, 280*(40), 33935-33944. doi: 10.1074/jbc.M503153200

Cao, Y., Jin, X., Huang, H., Derebe, M. G., Levin, E. J., Kabaleeswaran, V., Pan, Y., Punta, M., Love, J., Weng, J., Quick, M., Ye, S., Kloss, B., Bruni, R., Martinez-Hackert, E., Hendrickson, W. A., Rost, B., Javitch, J. A., Rajashankar, K. R., Jiang, Y., & Zhou, M. (2011). Crystal structure of a potassium ion transporter, TrkH. *Nature, 471*(7338), 336-340. doi: 10.1038/nature09731

Cao, Y., Pan, Y., Huang, H., Jin, X., Levin, E. J., Kloss, B., & Zhou, M. (2013). Gating of the TrkH ion channel by its associated RCK protein TrkA. *Nature, 496*(7445), 317-322. doi: 10.1038/nature12056

Carraretto, L., Formentin, E., Teardo, E., Checchetto, V., Tomizioli, M., Morosinotto, T., Giacometti, G. M., Finazzi, G., & Szabo, I. (2013). A thylakoid-located two-pore K+ channel controls photosynthetic light utilization in plants. *Science, 342*(6154), 114-118. doi: 10.1126/science.1242113

Cayley, S., Lewis, B. A., Guttman, H. J., & Record, M. T., Jr. (1991). Characterization of the cytoplasm of *Escherichia coli* K-12 as a function of external osmolarity. Implications for protein-DNA interactions in vivo. *J Mol Biol, 222*(2), 281-300. doi: 0022-2836(91)90212-O

Chen, Z.-h., & Schaap, P. (2012). The prokaryote messenger c-di-GMP triggers stalk cell differentiation in *Dictyostelium*. *Nature, 488*(7413), 680-683. doi: 10.1038/nature11313

Chin, K. H., Liang, J. M., Yang, J. G., Shih, M. S., Tu, Z. L., Wang, Y. C., Sun, X. H., Hu, N. J., Liang, Z. X., Dow, J. M., Ryan, R. P., & Chou, S. H. (2015). Structural Insights into the Distinct Binding Mode of Cyclic Di-AMP with SaCpaA_RCK. *Biochemistry, 54*(31), 4936-4951. doi: 10.1021/acs.biochem.5b00633

Cho, K. H., & Kang, S. O. (2013). Streptococcus pyogenes c-di-AMP phosphodiesterase, GdpP, influences SpeB processing and virulence. *PLOS ONE, 8*(7), e69425. doi: 10.1371/journal.pone.0069425

Cohen, D., Melamed, S., Millman, A., Shulman, G., Oppenheimer-Shaanan, Y., Kacen, A., Doron, S., Amitai, G., & Sorek, R. (2019). Cyclic GMP–AMP signalling protects bacteria against viral infection. *Nature, 574*(7780), 691-695. doi: 10.1038/s41586-019-1605-5

Commichau, F. M., & Stülke, J. (2018). Coping with an Essential Poison: a Genetic Suppressor Analysis Corroborates a Key Function of c-di-AMP in Controlling Potassium Ion Homeostasis in Gram-Positive Bacteria. *J Bacteriol, 200*(12). doi: 10.1128/jb.00166-18

Cook, S. J., & McCormick, F. (1993). Inhibition by cAMP of Ras-dependent activation of Raf. *Science, 262*(5136), 1069-1072. doi: 10.1126/science.7694367

Cordero-Morales, J. F., Cuello, L. G., Zhao, Y., Jogini, V., Cortes, D. M., Roux, B., & Perozo, E. (2006). Molecular determinants of gating at the potassium-channel selectivity filter. *Nat Struct Mol Biol, 13*(4), 311-318. doi: 10.1038/nsmb1069

Corrigan, R. M., Abbott, J. C., Burhenne, H., Kaever, V., & Gründling, A. (2011). c-di-AMP Is a New Second Messenger in *Staphylococcus aureus* with a Role in Controlling Cell Size and Envelope Stress. *PLOS Pathogens, 7*(9), e1002217. doi: 10.1371/journal.ppat.1002217

Corrigan, R. M., Campeotto, I., Jeganathan, T., Roelofs, K. G., Lee, V. T., & Gründling, A. (2013). Systematic identification of conserved bacterial c-di-AMP receptor proteins. *Proc Natl Acad Sci U S A, 110*(22), 9084-9089. doi: 10.1073/pnas.1300595110

Cuello, L. G., Romero, J. G., Cortes, D. M., & Perozo, E. (1998). pH-dependent gating in the *Streptomyces lividans* K+ channel. *Biochemistry, 37*(10), 3229-3236. doi: 10.1021/bi972997x

D T Clarkson, a., & Hanson, J. B. (1980). The Mineral Nutrition of Higher Plants. *Annual Review of Plant Physiology, 31*(1), 239-298. doi: 10.1146/annurev.pp.31.060180.001323

Davies, Bryan W., Bogard, Ryan W., Young, Travis S., & Mekalanos, John J. (2012). Coordinated Regulation of Accessory Genetic Elements Produces Cyclic Di-Nucleotides for *Vibrio cholerae* Virulence. *Cell, 149*(2), 358-370. doi: 10.1016/j.cell.2012.01.053

de Rooij, J., Zwartkruis, F. J., Verheijen, M. H., Cool, R. H., Nijman, S. M., Wittinghofer, A., & Bos, J. L. (1998). Epac is a Rap1 guanine-nucleotide-exchange factor directly activated by cyclic AMP. *Nature, 396*(6710), 474-477. doi: 10.1038/24884

Delano, W. L. (2002). The PyMOL Molecular Graphics System. http://www.pymol.org.

Deller, M. C., Johnson, H. A., Miller, M. D., Spraggon, G., Elsliger, M. A., Wilson, I. A., & Lesley, S. A. (2015). Crystal structure of a two-subunit TrkA octameric gating ring assembly. *PLOS ONE, 10*(3), e0122512. doi: 10.1371/journal.pone.0122512

Deng, Y., Schmid, N., Wang, C., Wang, J., Pessi, G., Wu, D., Lee, J., Aguilar, C., Ahrens, C. H., Chang, C., Song, H., Eberl, L., & Zhang, L.-H. (2012). Cis-2-dodecenoic acid receptor RpfR links quorum-sensing signal perception with regulation of virulence through cyclic dimeric guanosine monophosphate turnover. *Proceedings of the National Academy of Sciences, 109*(38), 15479-15484. doi: 10.1073/pnas.1205037109

Diner, Elie J., Burdette, Dara L., Wilson, Stephen C., Monroe, Kathryn M., Kellenberger, Colleen A., Hyodo, M., Hayakawa, Y., Hammond, Ming C., & Vance, Russell E. (2013). The Innate Immune DNA Sensor cGAS Produces a Noncanonical Cyclic Dinucleotide that Activates Human STING. *Cell Reports, 3*(5), 1355-1361. doi: https://doi.org/10.1016/j.celrep.2013.05.009

Dinnbier, U., Limpinsel, E., Schmid, R., & Bakker, E. P. (1988). Transient accumulation of potassium glutamate and its replacement by trehalose during adaptation of growing cells of *Escherichia coli* K-12 to elevated sodium chloride concentrations. *Arch Microbiol, 150*(4), 348-357. doi: 10.1007/bf00408306

Diskowski, M., Mehdipour, A. R., Wunnicke, D., Mills, D. J., Mikusevic, V., Barland, N., Hoffmann, J., Morgner, N., Steinhoff, H. J., Hummer, G., Vonck, J., & Hanelt, I. (2017). Helical jackknives control the gates of the double-pore K(+) uptake system KtrAB. *Elife, 6*. doi: 10.7554/eLife.24303

Dong, J., Shi, N., Berke, I., Chen, L., & Jiang, Y. (2005). Structures of the MthK RCK domain and the effect of Ca2+ on gating ring stability. *J Biol Chem, 280*(50), 41716-41724. doi: 10.1074/jbc.M508144200

Doyle, D. A., Morais Cabral, J., Pfuetzner, R. A., Kuo, A., Gulbis, J. M., Cohen, S. L., Chait, B. T., & MacKinnon, R. (1998). The structure of the potassium channel: molecular basis of K+ conduction and selectivity. *Science, 280*(5360), 69-77. doi: 10.1126/science.280.5360.69

Durell, S. R., Hao, Y., Nakamura, T., Bakker, E. P., & Guy, H. R. (1999). Evolutionary Relationship between K+ Channels and Symporters. *Biophysical journal, 77*(2), 775-788. doi: https://doi.org/10.1016/S0006-3495(99)76931-6

Dvir, H., Valera, E., & Choe, S. (2010). Structure of the MthK RCK in complex with cadmium. *Journal of structural biology, 171*(2), 231-237. doi: 10.1016/j.jsb.2010.03.020

Dworetzky, S. I., Trojnacki, J. T., & Gribkoff, V. K. (1994). Cloning and expression of a human large-conductance calcium-activated potassium channel. *Brain Res Mol Brain Res, 27*(1), 189-193. doi: 10.1016/0169-328X(94)90203-8

Emsley, P., Lohkamp, B., Scott, W. G., & Cowtan, K. (2010). Features and development of Coot. *Acta Crystallogr D Biol Crystallogr, 66*(Pt 4), 486-501. doi: 10.1107/S0907444910007493

Epstein, W., & Schultz, S. G. (1965). Cation Transport in *Escherichia coli*: V. Regulation of cation content. *J Gen Physiol, 49*(2), 221-234. doi: 10.1085/jgp.49.2.221

Evans, P. R., & Murshudov, G. N. (2013). How good are my data and what is the resolution? *Acta Crystallographica Section D, 69*(7), 1204-1214. doi: doi:10.1107/S0907444913000061

Fan, C., Sukomon, N., Flood, E., Rheinberger, J., Allen, T. W., & Nimigean, C. M. (2020). Ball-and-chain inactivation in a calcium-gated potassium channel. *Nature, 580*(7802), 288-293. doi: 10.1038/s41586-020-2116-0

Fesenko, E. E., Kolesnikov, S. S., & Lyubarsky, A. L. (1985). Induction by cyclic GMP of cationic conductance in plasma membrane of retinal rod outer segment. *Nature, 313*(6000), 310-313. doi: 10.1038/313310a0

Fujisawa, M., Kusumoto, A., Wada, Y., Tsuchiya, T., & Ito, M. (2005). NhaK, a novel monovalent cation/H+ antiporter of *Bacillus subtilis*. *Arch Microbiol, 183*(6), 411-420. doi: 10.1007/s00203-005-0011-6

Fujisawa, M., Wada, Y., & Ito, M. (2004). Modulation of the K+ efflux activity of *Bacillus subtilis* YhaU by YhaT and the C-terminal region of YhaS. *FEMS Microbiology Letters, 231*(2), 211-217. doi: 10.1016/s0378-1097(03)00959-5

Galperin, M. Y., Natale, D. A., Aravind, L., & Koonin, E. V. (1999). A specialized version of the HD hydrolase domain implicated in signal transduction. *J Mol Microbiol Biotechnol, 1*(2), 303-305.

Gangola, P., & Rosen, B. P. (1987). Maintenance of intracellular calcium in *Escherichia coli*. *J Biol Chem, 262*(26), 12570-12574.

Gao, P., Ascano, M., Wu, Y., Barchet, W., Gaffney, B. L., Zillinger, T., Serganov, A. A., Liu, Y., Jones, R. A., Hartmann, G., Tuschl, T., & Patel, D. J. (2013). Cyclic [G(2',5')pA(3',5')p] is the metazoan second messenger produced by DNA-activated cyclic GMP-AMP synthase. *Cell, 153*(5), 1094-1107. doi: 10.1016/j.cell.2013.04.046

Garthwaite, G., & Garthwaite, J. (1988). Cyclic GMP and cell death in rat cerebellar slices. *Neuroscience, 26*(1), 321-326. doi: https://doi.org/10.1016/0306-4522(88)90148-0

Gibhardt, J., Hoffmann, G., Turdiev, A., Wang, M., Lee, V. T., & Commichau, F. M. (2019). c-di-AMP assists osmoadaptation by regulating the *Listeria monocytogenes* potassium transporters KimA and KtrCD. *J Biol Chem, 294*(44), 16020-16033. doi: 10.1074/jbc.RA119.010046

Gries, C. M., Bose, J. L., Nuxoll, A. S., Fey, P. D., & Bayles, K. W. (2013). The Ktr potassium transport system in *Staphylococcus aureus* and its role in cell physiology, antimicrobial resistance and pathogenesis. *Mol Microbiol, 89*(4), 760-773. doi: 10.1111/mmi.12312

Gundlach, J., Herzberg, C., Kaever, V., Gunka, K., Hoffmann, T., Weiß, M., Gibhardt, J., Thürmer, A., Hertel, D., Daniel, R., Bremer, E., Commichau, F. M., & Stülke, J. (2017). Control of potassium homeostasis is an essential function of the second messenger cyclic di-AMP in *Bacillus subtilis*. *Sci Signal, 10*(475). doi: 10.1126/scisignal.aal3011

Gundlach, J., Krüger, L., Herzberg, C., Turdiev, A., Poehlein, A., Tascón, I., Weiss, M., Hertel, D., Daniel, R., Hänelt, I., Lee, V. T., & Stülke, J. (2019). Sustained sensing in potassium homeostasis: Cyclic di-AMP controls potassium uptake by KimA at the levels of expression and activity. *J Biol Chem, 294*(24), 9605-9614. doi: 10.1074/jbc.RA119.008774

Gundlach, J., Mehne, F. M., Herzberg, C., Kampf, J., Valerius, O., Kaever, V., & Stülke, J. (2015). An Essential Poison: Synthesis and Degradation of Cyclic Di-AMP in *Bacillus subtilis*. *J Bacteriol, 197*(20), 3265-3274. doi: 10.1128/jb.00564-15

Gundlach, J., Rath, H., Herzberg, C., Mäder, U., & Stülke, J. (2016). Second Messenger Signaling in *Bacillus subtilis*: Accumulation of Cyclic di-AMP Inhibits Biofilm Formation. *Front Microbiol, 7*, 804. doi: 10.3389/fmicb.2016.00804

H J Evans, a., & Sorger, G. J. (1966). Role of Mineral Elements with Emphasis on the Univalent Cations. *Annual Review of Plant Physiology, 17*(1), 47-76. doi: 10.1146/annurev.pp.17.060166.000403

Hallberg, Z. F., Wang, X. C., Wright, T. A., Nan, B., Ad, O., Yeo, J., & Hammond, M. C. (2016). Hybrid promiscuous (Hypr) GGDEF enzymes produce cyclic AMP-GMP (3', 3'-cGAMP). *Proc Natl Acad Sci U S A, 113*(7), 1790-1795. doi: 10.1073/pnas.1515287113

Hanelt, I., Lochte, S., Sundermann, L., Elbers, K., Vor der Bruggen, M., & Bakker, E. P. (2010). Gain of function mutations in membrane region M2C2 of KtrB open a gate controlling K+ transport by the KtrAB system from *Vibrio alginolyticus*. *J Biol Chem, 285*(14), 10318-10327. doi: 10.1074/jbc.M109.089870

Hanelt, I., Wunnicke, D., Muller-Trimbusch, M., Vor der Bruggen, M., Kraus, I., Bakker, E. P., & Steinhoff, H. J. (2010). Membrane region M2C2 in subunit KtrB of the K+ uptake system KtrAB from *Vibrio alginolyticus* forms a flexible gate controlling K+ flux: an electron paramagnetic resonance study. *J Biol Chem, 285*(36), 28210-28219. doi: 10.1074/jbc.M110.139311

Harding, M. M. (2001). Geometry of metal-ligand interactions in proteins. *Acta Crystallogr D Biol Crystallogr, 57*(Pt 3), 401-411. doi: 10.1107/s0907444900019168

Harley, C. A., Jesus, C. S. H., Carvalho, R., Brito, R. M. M., & Morais-Cabral, J. H. (2012). Changes in Channel Trafficking and Protein Stability Caused by LQT2 Mutations in the PAS Domain of the HERG Channel. *PLOS ONE, 7*(3), e32654. doi: 10.1371/journal.pone.0032654

Harms, C., Domoto, Y., Celik, C., Rahe, E., Stumpe, S., Schmid, R., Nakamura, T., & Bakker, E. P. (2001). Identification of the ABC protein SapD as the subunit that confers ATP dependence to the K+-uptake systems Trk(H) and Trk(G) from *Escherichia coli* K-12. *Microbiology, 147*(Pt 11), 2991-3003. doi: 10.1099/00221287-147-11-2991

He, J., Yin, W., Galperin, M. Y., & Chou, S.-H. (2020). Cyclic di-AMP, a second messenger of primary importance: tertiary structures and binding mechanisms. *Nucleic Acids Research, 48*(6), 2807-2829. doi: 10.1093/nar/gkaa112

Hecht, G. B., & Newton, A. (1995). Identification of a novel response regulator required for the swarmer-to-stalked-cell transition in *Caulobacter crescentus*. *J Bacteriol, 177*(21), 6223-6229. doi: 10.1128/jb.177.21.6223-6229.1995

Heginbotham, L., LeMasurier, M., Kolmakova-Partensky, L., & Miller, C. (1999). Single streptomyces lividans K(+) channels: functional asymmetries and sidedness of proton activation. *J Gen Physiol, 114*(4), 551-560. doi: 10.1085/jgp.114.4.551

Heginbotham, L., Lu, Z., Abramson, T., & MacKinnon, R. (1994). Mutations in the K+ channel signature sequence. *Biophysical journal, 66*(4), 1061-1067. doi: 10.1016/s0006-3495(94)80887-2

Hidalgo, P., & MacKinnon, R. (1995). Revealing the architecture of a K+ channel pore through mutant cycles with a peptide inhibitor. *Science, 268*(5208), 307-310. doi: 10.1126/science.7716527

Hille, B. (1970). Ionic channels in nerve membranes. *Prog Biophys Mol Biol, 21*, 1-32. doi: 10.1016/0079-6107(70)90022-2

Hille, B. (2001). *Ion channels of excitable membranes* (3rd ed. ed.): Sunderland (Mass.) : Sinauer associates.

Hodgkin, A. L., & Huxley, A. F. (1952a). The components of membrane conductance in the giant axon of Loligo. *J Physiol, 116*(4), 473-496. doi: 10.1113/jphysiol.1952.sp004718

Hodgkin, A. L., & Huxley, A. F. (1952b). Currents carried by sodium and potassium ions through the membrane of the giant axon of Loligo. *J Physiol, 116*(4), 449-472. doi: 10.1113/jphysiol.1952.sp004717

Hodgkin, A. L., & Huxley, A. F. (1952c). The dual effect of membrane potential on sodium conductance in the giant axon of Loligo. *J Physiol, 116*(4), 497-506. doi: 10.1113/jphysiol.1952.sp004719

Hodgkin, A. L., & Huxley, A. F. (1952d). A quantitative description of membrane current and its application to conduction and excitation in nerve. *J Physiol, 117*(4), 500-544. doi: 10.1113/jphysiol.1952.sp004764

Hodgkin, A. L., & Katz, B. (1949). The effect of sodium ions on the electrical activity of giant axon of the squid. *J Physiol, 108*(1), 37-77. doi: 10.1113/jphysiol.1949.sp004310

Hodgkin, A. L., & Keynes, R. D. (1955). The potassium permeability of a giant nerve fibre. *J Physiol, 128*(1), 61-88. doi: 10.1113/jphysiol.1955.sp005291

Holtmann, G., Bakker, E. P., Uozumi, N., & Bremer, E. (2003). KtrAB and KtrCD: two K+ uptake systems in *Bacillus subtilis* and their role in adaptation to hypertonicity. *J Bacteriol, 185*(4), 1289-1298. doi: 10.1128/jb.185.4.1289-1298.2003

Holtmann, G., & Bremer, E. (2004). Thermoprotection of *Bacillus subtilis* by exogenously provided glycine betaine and structurally related compatible solutes: involvement of Opu transporters. *J Bacteriol, 186*(6), 1683-1693. doi: 10.1128/jb.186.6.1683-1693.2004

Hoshi, T., Zagotta, W., & Aldrich, R. (1990). Biophysical and molecular mechanisms of Shaker potassium channel inactivation. *Science, 250*(4980), 533-538. doi: 10.1126/science.2122519

Hoshi, T., Zagotta, W. N., & Aldrich, R. W. (1991). Two types of inactivation in Shaker K+ channels: Effects of alterations in the carboxy-terminal region. *Neuron, 7*(4), 547-556. doi: 10.1016/0896-6273(91)90367-9

Houtman, J. C., Brown, P. H., Bowden, B., Yamaguchi, H., Appella, E., Samelson, L. E., & Schuck, P. (2007). Studying multisite binary and ternary protein interactions by global analysis of isothermal titration calorimetry data in SEDPHAT: application to adaptor protein complexes in cell signaling. *Protein Sci, 16*(1), 30-42. doi: 10.1110/ps.062558507

Huynh, T. N., Choi, P. H., Sureka, K., Ledvina, H. E., Campillo, J., Tong, L., & Woodward, J. J. (2016). Cyclic di-AMP targets the cystathionine beta-synthase domain of the osmolyte transporter OpuC. *Mol Microbiol, 102*(2), 233-243. doi: 10.1111/mmi.13456

Ignarro, L. J., Byrns, R. E., & Wood, K. S. (1987). Endothelium-dependent modulation of cGMP levels and intrinsic smooth muscle tone in isolated bovine intrapulmonary artery and vein. *Circulation Research, 60*(1), 82-92. doi: doi:10.1161/01.RES.60.1.82

Ingólfsson, H. I., & Andersen, O. S. (2010). Screening for small molecules' bilayer-modifying potential using a gramicidin-based fluorescence assay. *Assay and drug development technologies, 8*(4), 427-436. doi: 10.1089/adt.2009.0250

Jenny, H. C.-Y., Don, D., & Oger, J. (1985). Synthesis and Physical Characterization of Bis 3′→5′ Cyclic Dinucleotides (NpNp): RNA Polymerase Inhibitors. *Nucleosides and Nucleotides, 4*(3), 377-389. doi: 10.1080/07328318508056168

Jiang, Y., Lee, A., Chen, J., Cadene, M., Chait, B. T., & MacKinnon, R. (2002a). Crystal structure and mechanism of a calcium-gated potassium channel. *Nature, 417*(6888), 515-522. doi: 10.1038/417515a

Jiang, Y., Lee, A., Chen, J., Cadene, M., Chait, B. T., & MacKinnon, R. (2002b). The open pore conformation of potassium channels. *Nature, 417*(6888), 523-526. doi: 10.1038/417523a

Jiang, Y., Pico, A., Cadene, M., Chait, B. T., & MacKinnon, R. (2001). Structure of the RCK domain from the *E. coli* K+ channel and demonstration of its presence in the human BK channel. *Neuron, 29*(3), 593-601. doi: 10.1016/S0896-6273(01)00236-7

Jones, H. E., Holland, I. B., Baker, H. L., & Campbell, A. K. (1999). Slow changes in cytosolic free Ca2+ in *Escherichia coli* highlight two putative influx mechanisms in response to changes in extracellular calcium. *Cell Calcium, 25*(3), 265-274. doi: 10.1054/ceca.1999.0028

Kabsch, W. (2010). Xds. *Acta Crystallogr D Biol Crystallogr, 66*(Pt 2), 125-132. doi: 10.1107/S0907444909047337

Kalia, D., Merey, G., Nakayama, S., Zheng, Y., Zhou, J., Luo, Y., Guo, M., Roembke, B. T., & Sintim, H. O. (2013). Nucleotide, c-di-GMP, c-di-AMP, cGMP, cAMP, (p)ppGpp signaling in bacteria and implications in pathogenesis. *Chem Soc Rev, 42*(1), 305-341. doi: 10.1039/c2cs35206k

Kamb, A., Iverson, L. E., & Tanouye, M. A. (1987). Molecular characterization of Shaker, a *Drosophila* gene that encodes a potassium channel. *Cell, 50*(3), 405-413. doi: 10.1016/0092-8674(87)90494-6

Kamegaya, T., Kuroda, K., & Hayakawa, Y. (2011). Identification of a *Streptococcus pyogenes* SF370 gene involved in production of c-di-AMP. *Nagoya J Med Sci, 73*(1-2), 49-57.

Karaolis, D. K. R., Means, T. K., Yang, D., Takahashi, M., Yoshimura, T., Muraille, E., Philpott, D., Schroeder, J. T., Hyodo, M., Hayakawa, Y., Talbot, B. G., Brouillette, E., & Malouin, F. (2007). Bacterial c-di-GMP Is an Immunostimulatory Molecule. *The Journal of Immunology, 178*(4), 2171-2181. doi: 10.4049/jimmunol.178.4.2171

Kawasaki, H., Springett, G. M., Mochizuki, N., Toki, S., Nakaya, M., Matsuda, M., Housman, D. E., & Graybiel, A. M. (1998). A family of cAMP-binding proteins that directly activate Rap1. *Science, 282*(5397), 2275-2279. doi: 10.1126/science.282.5397.2275

Kellenberger, C. A., Wilson, S. C., Hickey, S. F., Gonzalez, T. L., Su, Y., Hallberg, Z. F., Brewer, T. F., Iavarone, A. T., Carlson, H. K., Hsieh, Y.-F., & Hammond, M. C. (2015). GEMM-I riboswitches from *Geobacter* sense the bacterial second messenger cyclic AMP-GMP. *Proceedings of the National Academy of Sciences of the United States of America, 112*(17), 5383-5388. doi: 10.1073/pnas.1419328112

Keller, S., Vargas, C., Zhao, H., Piszczek, G., Brautigam, C. A., & Schuck, P. (2012). High-precision isothermal titration calorimetry with automated peak-shape analysis. *Anal Chem, 84*(11), 5066-5073. doi: 10.1021/ac3007522

Ketchum, K. A., Joiner, W. J., Sellers, A. J., Kaczmarek, L. K., & Goldstein, S. A. (1995). A new family of outwardly rectifying potassium channel proteins with two pore domains in tandem. *Nature, 376*(6542), 690-695. doi: 10.1038/376690a0

Kim, B., Park, J.-S., Choi, H.-Y., Yoon, S. S., & Kim, W.-G. (2018). Terrein is an inhibitor of quorum sensing and c-di-GMP in *Pseudomonas aeruginosa*: a connection between quorum sensing and c-di-GMP. *Scientific Reports, 8*(1), 8617. doi: 10.1038/s41598-018-26974-5

Kim, H., Youn, S. J., Kim, S. O., Ko, J., Lee, J. O., & Choi, B. S. (2015). Structural Studies of Potassium Transport Protein KtrA Regulator of Conductance of K+ (RCK) C Domain in Complex with Cyclic Diadenosine Monophosphate (c-di-AMP). *J Biol Chem, 290*(26), 16393-16402. doi: 10.1074/jbc.M115.641340

Klein, D. J., Moore, P. B., & Steitz, T. A. (2004). The contribution of metal ions to the structural stability of the large ribosomal subunit. *RNA, 10*(9), 1366-1379. doi: 10.1261/rna.7390804

Kong, C., Zeng, W., Ye, S., Chen, L., Sauer, D. B., Lam, Y., Derebe, M. G., & Jiang, Y. (2012). Distinct gating mechanisms revealed by the structures of a multi-ligand gated K(+) channel. *Elife, 1*, e00184. doi: 10.7554/eLife.00184

Kopec, W., Kopfer, D. A., Vickery, O. N., Bondarenko, A. S., Jansen, T. L. C., de Groot, B. L., & Zachariae, U. (2018). Direct knock-on of desolvated ions governs strict ion selectivity in K(+) channels. *Nat Chem, 10*(8), 813-820. doi: 10.1038/s41557-018-0105-9

Kopfer, D. A., Song, C., Gruene, T., Sheldrick, G. M., Zachariae, U., & de Groot, B. L. (2014). Ion permeation in K(+) channels occurs by direct Coulomb knock-on. *Science, 346*(6207), 352-355. doi: 10.1126/science.1254840

Kraegeloh, A., Amendt, B., & Kunte, H. J. (2005). Potassium Transport in a Halophilic Member of the Bacteria Domain: Identification and Characterization of the K+ Uptake Systems TrkH and TrkI from *Halomonas elongata* DSM 2581T. *Journal of Bacteriology, 187*(3), 1036-1043. doi: 10.1128/jb.187.3.1036-1043.2005

Kratochvil, H. T., Carr, J. K., Matulef, K., Annen, A. W., Li, H., Maj, M., Ostmeyer, J., Serrano, A. L., Raghuraman, H., Moran, S. D., Skinner, J. L., Perozo, E., Roux, B., Valiyaveetil, F. I., & Zanni, M. T. (2016). Instantaneous ion configurations in the K+ ion channel selectivity filter revealed by 2D IR spectroscopy. *Science, 353*(6303), 1040-1044. doi: 10.1126/science.aag1447

Kroll, R. G., & Booth, I. R. (1981). The role of potassium transport in the generation of a pH gradient in *Escherichia coli. Biochem J, 198*(3), 691-698. doi: 10.1042/bj1980691

Kroll, R. G., & Booth, I. R. (1983). The relationship between intracellular pH, the pH gradient and potassium transport in *Escherichia coli*. *Biochem J, 216*(3), 709-716. doi: 10.1042/bj2160709

Kroning, N., Willenborg, M., Tholema, N., Hanelt, I., Schmid, R., & Bakker, E. P. (2007). ATP binding to the KTN/RCK subunit KtrA from the K+ -uptake system KtrAB of *Vibrio alginolyticus*: its role in the formation of the KtrAB complex and its requirement in vivo. *J Biol Chem, 282*(19), 14018-14027. doi: 10.1074/jbc.M609084200

Krüger, L., Herzberg, C., Warneke, R., Poehlein, A., Stautz, J., Weiß, M., Daniel, R., Hänelt, I., & Stülke, J. (2020a). Two ways to convert a low- to a high-affinity potassium channel: Control of *Bacillus subtilis* KtrCD by glutamate. *Journal of Bacteriology*, JB.00138-00120. doi: 10.1128/jb.00138-20

Krüger, L., Herzberg, C., Warneke, R., Poehlein, A., Stautz, J., Weiß, M., Daniel, R., Hänelt, I., & Stülke, J. (2020b). Two Ways To Convert a Low-Affinity Potassium Channel to High Affinity: Control of *Bacillus subtilis* KtrCD by Glutamate. *Journal of Bacteriology, 202*(12), e00138-00120. doi: 10.1128/jb.00138-20

Kulesekara, H., Lee, V., Brencic, A., Liberati, N., Urbach, J., Miyata, S., Lee, D. G., Neely, A. N., Hyodo, M., Hayakawa, Y., Ausubel, F. M., & Lory, S. (2006). Analysis of *Pseudomonas aeruginosa* diguanylate cyclases and phosphodiesterases reveals a role for bis-(3′-5′)-cyclic-GMP in virulence. *Proceedings of the National Academy of Sciences of the United States of America, 103*(8), 2839-2844. doi: 10.1073/pnas.0511090103

Kuo, M. M.-C., Baker, K. A., Wong, L., & Choe, S. (2007). Dynamic oligomeric conversions of the cytoplasmic RCK domains mediate MthK potassium channel activity. *Proceedings of the National Academy of Sciences, 104*(7), 2151-2156. doi: 10.1073/pnas.0609085104

Kuo, M. M., Haynes, W. J., Loukin, S. H., Kung, C., & Saimi, Y. (2005). Prokaryotic K(+) channels: from crystal structures to diversity. *FEMS Microbiol Rev, 29*(5), 961-985. doi: 10.1016/j.femsre.2005.03.003

Kuo, M. M., Maslennikov, I., Molden, B., & Choe, S. (2008). The desensitization gating of the MthK K+ channel is governed by its cytoplasmic amino terminus. *PLoS Biol, 6*(10), e223. doi: 10.1371/journal.pbio.0060223

Larsen, P. I., Sydnes, L. K., Landfald, B., & Strom, A. R. (1987). Osmoregulation in *Escherichia col*i by accumulation of organic osmolytes: betaines, glutamic acid, and trehalose. *Arch Microbiol, 147*(1), 1-7. doi: 10.1007/bf00492896

Lee, C., Kang, H. J., von Ballmoos, C., Newstead, S., Uzdavinys, P., Dotson, D. L., Iwata, S., Beckstein, O., Cameron, A. D., & Drew, D. (2013). A two-domain elevator mechanism for sodium/proton antiport. *Nature, 501*(7468), 573-577. doi: 10.1038/nature12484

Lenaeus, M. J., Burdette, D., Wagner, T., Focia, P. J., & Gross, A. (2014). Structures of KcsA in complex with symmetrical quaternary ammonium compounds reveal a hydrophobic binding site. *Biochemistry, 53*(32), 5365-5373. doi: 10.1021/bi500525s

Li, M., West, J. W., Numann, R., Murphy, B. J., Scheuer, T., & Catterall, W. A. (1993). Convergent regulation of sodium channels by protein kinase C and cAMP-dependent protein kinase. *Science, 261*(5127), 1439-1442. doi: 10.1126/science.8396273

Li , Y., Berke , I., Chen , L., & Jiang , Y. (2007). Gating and Inward Rectifying Properties of the MthK K+ Channel with and without the Gating Ring. *Journal of General Physiology, 129*(2), 109-120. doi: 10.1085/jgp.200609655

Liang, W., Silva, A. J., & Benitez, J. A. (2007). The cyclic AMP receptor protein modulates colonial morphology in *Vibrio cholerae*. *Applied and environmental microbiology, 73*(22), 7482-7487. doi: 10.1128/aem.01564-07

Liu, A. Y. (1982). Differentiation-specific increase of cAMP-dependent protein kinase in the 3T3-L1 cells. *J Biol Chem, 257*(1), 298-306.

Liu, J., Prindle, A., Humphries, J., Gabalda-Sagarra, M., Asally, M., Lee, D. Y., Ly, S., Garcia-Ojalvo, J., & Suel, G. M. (2015). Metabolic co-dependence gives rise to collective oscillations within biofilms. *Nature, 523*(7562), 550-554. doi: 10.1038/nature14660

Liu, S., Bayles, D. O., Mason, T. M., & Wilkinson, B. J. (2006). A cold-sensitive *Listeria monocytogenes* mutant has a transposon insertion in a gene encoding a putative membrane protein and shows altered (p)ppGpp levels. *Appl Environ Microbiol, 72*(6), 3955-3959. doi: 10.1128/aem.02607-05

Lori, C., Ozaki, S., Steiner, S., Böhm, R., Abel, S., Dubey, B. N., Schirmer, T., Hiller, S., & Jenal, U. (2015). Cyclic di-GMP acts as a cell cycle oscillator to drive chromosome replication. *Nature, 523*(7559), 236-239. doi: 10.1038/nature14473

Loukin, S. H., Kuo, M. M., Zhou, X. L., Haynes, W. J., Kung, C., & Saimi, Y. (2005). Microbial K+ channels. *J Gen Physiol, 125*(6), 521-527. doi: 10.1085/jgp.200509261

Lowrie, D. B., Jackett, P. S., & Ratcliffe, N. A. (1975). Mycobacterium microti may protect itself from intracellular destruction by releasing cyclic AMP into phagosomes. *Nature, 254*(5501), 600-602. doi: 10.1038/254600a0

Lubin, M., & Ennis, H. L. (1964). On the Role of Intracellular Potassium in Protein Synthesis. *Biochim Biophys Acta, 80*, 614-631. doi: 10.1016/0926-6550(64)90306-8

Lundberg, M. E., Becker, E. C., & Choe, S. (2013). MstX and a putative potassium channel facilitate biofilm formation in *Bacillus subtilis*. *PLOS ONE, 8*(5), e60993. doi: 10.1371/journal.pone.0060993

Luo, Y., & Helmann, J. D. (2012). Analysis of the role of *Bacillus subtilis* σ(M) in β-lactam resistance reveals an essential role for c-di-AMP in peptidoglycan homeostasis. *Mol Microbiol, 83*(3), 623-639. doi: 10.1111/j.1365-2958.2011.07953.x

Macallum, A. B. (1926). THE PALEOCHEMISTRY OF THE BODY FLUIDS AND TISSUES. *Physiological Reviews, 6*(2), 316-357. doi: 10.1152/physrev.1926.6.2.316

MacKinnon, R. (1991). Determination of the subunit stoichiometry of a voltage-activated potassium channel. *Nature, 350*(6315), 232-235. doi: 10.1038/350232a0

MacKinnon, R. (2004). Nobel Lecture. Potassium channels and the atomic basis of selective ion conduction. *Biosci Rep, 24*(2), 75-100. doi: 10.1007/s10540-004-7190-2

MacKinnon, R., & Miller, C. (1989). Mutant potassium channels with altered binding of charybdotoxin, a pore-blocking peptide inhibitor. *Science, 245*(4924), 1382-1385. doi: 10.1126/science.2476850

Makman, R. S., & Sutherland, E. W. (1965). Adenosine 3',5'-Phosphate in *Escherichia Coli*. *J Biol Chem, 240*, 1309-1314.

Marden, J. N., Dong, Q., Roychowdhury, S., Berleman, J. E., & Bauer, C. E. (2011). Cyclic GMP controls *Rhodospirillum centenum* cyst development. *Molecular Microbiology, 79*(3), 600-615. doi: 10.1111/j.1365-2958.2010.07513.x

Matsuda, N., Kobayashi, H., Katoh, H., Ogawa, T., Futatsugi, L., Nakamura, T., Bakker, E. P., & Uozumi, N. (2004). Na+-dependent K+ uptake Ktr system from the cyanobacterium *Synechocystis* sp. PCC 6803 and its role in the early phases of cell adaptation to hyperosmotic shock. *J Biol Chem, 279*(52), 54952-54962. doi: 10.1074/jbc.M407268200

McCoy, A. J., Grosse-Kunstleve, R. W., Adams, P. D., Winn, M. D., Storoni, L. C., & Read, R. J. (2007). Phaser crystallographic software. *J Appl Crystallogr, 40*(Pt 4), 658-674. doi: 10.1107/S0021889807021206

McFarland, A. P., Luo, S., Ahmed-Qadri, F., Zuck, M., Thayer, E. F., Goo, Y. A., Hybiske, K., Tong, L., & Woodward, J. J. (2017). Sensing of Bacterial Cyclic Dinucleotides by the Oxidoreductase RECON Promotes NF-κB Activation and Shapes a Proinflammatory Antibacterial State. *Immunity, 46*(3), 433-445. doi: 10.1016/j.immuni.2017.02.014

McKee, R. W., Mangalea, M. R., Purcell, E. B., Borchardt, E. K., & Tamayo, R. (2013). The second messenger cyclic Di-GMP regulates *Clostridium difficile* toxin production by controlling expression of sigD. *Journal of Bacteriology, 195*(22), 5174-5185. doi: 10.1128/jb.00501-13

McLaggan, D., Naprstek, J., Buurman, E. T., & Epstein, W. (1994). Interdependence of K+ and glutamate accumulation during osmotic adaptation of *Escherichia coli*. *J Biol Chem, 269*(3), 1911-1917.

McWhirter, S. M., Barbalat, R., Monroe, K. M., Fontana, M. F., Hyodo, M., Joncker, N. T., Ishii, K. J., Akira, S., Colonna, M., Chen, Z. J., Fitzgerald, K. A., Hayakawa, Y., & Vance, R. E. (2009). A host type I interferon response is induced by cytosolic sensing of the bacterial second messenger cyclic-di-GMP. *J Exp Med, 206*(9), 1899-1911. doi: 10.1084/jem.20082874

Merighi, M., Lee, V. T., Hyodo, M., Hayakawa, Y., & Lory, S. (2007). The second messenger bis-(3'-5')-cyclic-GMP and its PilZ domain-containing receptor Alg44 are required for alginate biosynthesis in *Pseudomonas aeruginosa*. *Mol Microbiol, 65*(4), 876-895. doi: 10.1111/j.1365-2958.2007.05817.x

Merkel, T. J., Barros, C., & Stibitz, S. (1998). Characterization of the bvgR locus of *Bordetella pertussis*. *J Bacteriol, 180*(7), 1682-1690. doi: 10.1128/jb.180.7.1682-1690.1998

Meury, J. (1988). Glycine betaine reverses the effects of osmotic stress on DNA replication and cellular division in *Escherichia coli*. *Arch Microbiol, 149*(3), 232-239. doi: 10.1007/bf00422010

Meury, J., Robin, A., & Monnier-Champeix, P. (1985). Turgor-controlled K+ fluxes and their pathways in *Escherichia coli*. *Eur J Biochem, 151*(3), 613-619. doi: 10.1111/j.1432-1033.1985.tb09148.x

Mikusevic, V., Schrecker, M., Kolesova, N., Patino-Ruiz, M., Fendler, K., & Hanelt, I. (2019). A channel profile report of the unusual K(+) channel KtrB. *J Gen Physiol, 151*(12), 1357-1368. doi: 10.1085/jgp.201912384

Milkman, R. (1994). An *Escherichia coli* homologue of eukaryotic potassium channel proteins. *Proc Natl Acad Sci U S A, 91*(9), 3510-3514. doi: 10.1073/pnas.91.9.3510

Mitchell, P. (1966). Chemiosmotic coupling in oxidative and photosynthetic phosphorylation. *Biol Rev Camb Philos Soc, 41*(3), 445-502. doi: 10.1111/j.1469-185x.1966.tb01501.x

Moncany, M. L., & Kellenberger, E. (1981). High magnesium content of *Escherichia coli* B. *Experientia, 37*(8), 846-847. doi: 10.1007/bf01985672

Morais-Cabral, J. H., Zhou, Y., & MacKinnon, R. (2001). Energetic optimization of ion conduction rate by the K+ selectivity filter. *Nature, 414*(6859), 37-42. doi: 10.1038/35102000

Moscoso, J. A., Schramke, H., Zhang, Y., Tosi, T., Dehbi, A., Jung, K., & Gründling, A. (2016). Binding of Cyclic Di-AMP to the *Staphylococcus aureus* Sensor Kinase KdpD Occurs via the Universal Stress Protein Domain and Downregulates the Expression of the Kdp Potassium Transporter. *J Bacteriol, 198*(1), 98-110. doi: 10.1128/jb.00480-15

Mulkidjanian, A. Y., Bychkov, A. Y., Dibrova, D. V., Galperin, M. Y., & Koonin, E. V. (2012). Origin of first cells at terrestrial, anoxic geothermal fields. *Proc Natl Acad Sci U S A, 109*(14), E821-830. doi: 10.1073/pnas.1117774109

Munro, A. W., Ritchie, G. Y., Lamb, A. J., Douglas, R. M., & Booth, I. R. (1991). The cloning and DNA sequence of the gene for the glutathione-regulated potassium-efflux system KefC of *Escherichia coli*. *Mol Microbiol, 5*(3), 607-616. doi: 10.1111/j.1365-2958.1991.tb00731.x

Nakamura, T., & Gold, G. H. (1987). A cyclic nucleotide-gated conductance in olfactory receptor cilia. *Nature, 325*(6103), 442-444. doi: 10.1038/325442a0

Nakamura, T., Yuda, R., Unemoto, T., & Bakker, E. P. (1998). KtrAB, a new type of bacterial K(+)-uptake system from *Vibrio alginolyticus*. *J Bacteriol, 180*(13), 3491-3494.

Nanatani, K., Shijuku, T., Takano, Y., Zulkifli, L., Yamazaki, T., Tominaga, A., Souma, S., Onai, K., Morishita, M., Ishiura, M., Hagemann, M., Suzuki, I., Maruyama, H., Arai, F., & Uozumi, N. (2015). Comparative analysis of kdp and ktr mutants reveals distinct roles of the potassium transporters in the model cyanobacterium *Synechocystis* sp. strain PCC 6803. *J Bacteriol, 197*(4), 676-687. doi: 10.1128/jb.02276-14

Naslund, P. H., & Hultin, T. (1970). Effects of potassium deficiency on mammalian ribosomes. *Biochim Biophys Acta, 204*(1), 237-247. doi: 10.1016/0005-2787(70)90507-1

Naslund, P. H., & Hultin, T. (1971). Structural and functional defects in mammalian ribosomes after potassium deficiency. *Biochim Biophys Acta, 254*(1), 104-116. doi: 10.1016/0005-2787(71)90117-1

Nelson, J. W., Sudarsan, N., Furukawa, K., Weinberg, Z., Wang, J. X., & Breaker, R. R. (2013). Riboswitches in eubacteria sense the second messenger c-di-AMP. *Nat Chem Biol, 9*(12), 834-839. doi: 10.1038/nchembio.1363

Nelson, J. W., Sudarsan, N., Phillips, G. E., Stav, S., Lünse, C. E., McCown, P. J., & Breaker, R. R. (2015). Control of bacterial exoelectrogenesis by c-AMP-GMP. *Proc Natl Acad Sci U S A, 112*(17), 5389-5394. doi: 10.1073/pnas.1419264112

Nissen, P., Hansen, J., Ban, N., Moore, P. B., & Steitz, T. A. (2000). The structural basis of ribosome activity in peptide bond synthesis. *Science, 289*(5481), 920-930. doi: 10.1126/science.289.5481.920

Ochrombel, I., Ott, L., Kramer, R., Burkovski, A., & Marin, K. (2011). Impact of improved potassium accumulation on pH homeostasis, membrane potential adjustment and survival of *Corynebacterium glutamicum*. *Biochim Biophys Acta, 1807*(4), 444-450. doi: 10.1016/j.bbabio.2011.01.008

Ogunniyi, A. D., Paton, J. C., Kirby, A. C., McCullers, J. A., Cook, J., Hyodo, M., Hayakawa, Y., & Karaolis, D. K. R. (2008). c-di-GMP is an effective immunomodulator and vaccine adjuvant against pneumococcal infection. *Vaccine, 26*(36), 4676-4685. doi: https://doi.org/10.1016/j.vaccine.2008.06.099

Okabayashi, T., Ide, M., & Yoshimoto, A. (1963). Excretion of adenosine-3',5'-phosphate in the culture broth of *Brevibacterium liquefaciens*. *Arch Biochem Biophys, 100*, 158-159. doi: 10.1016/0003-9861(63)90046-8

Oppenheimer-Shaanan, Y., Wexselblatt, E., Katzhendler, J., Yavin, E., & Ben-Yehuda, S. (2011). c-di-AMP reports DNA integrity during sporulation in *Bacillus subtilis*. *EMBO Rep, 12*(6), 594-601. doi: 10.1038/embor.2011.77

Padan, E., Zilberstein, D., & Rottenberg, H. (1976). The proton electrochemical gradient in *Escherichia coli* cells. *Eur J Biochem, 63*(2), 533-541. doi: 10.1111/j.1432-1033.1976.tb10257.x

Papazian, D. M., Schwarz, T. L., Tempel, B. L., Jan, Y. N., & Jan, L. Y. (1987). Cloning of genomic and complementary DNA from Shaker, a putative potassium channel gene from *Drosophila*. *Science, 237*(4816), 749-753. doi: 10.1126/science.2441470

Parfenova, L. V., Abarca-Heidemann, K., Crane, B. M., & Rothberg, B. S. (2007). Molecular architecture and divalent cation activation of TvoK, a prokaryotic potassium channel. *J Biol Chem, 282*(33), 24302-24309. doi: 10.1074/jbc.M703650200

Parfenova, L. V., Crane, B. M., & Rothberg, B. S. (2006). Modulation of MthK potassium channel activity at the intracellular entrance to the pore. *J Biol Chem, 281*(30), 21131-21138. doi: 10.1074/jbc.M603109200

Pau, V. P., Abarca-Heidemann, K., & Rothberg, B. S. (2010). Allosteric mechanism of Ca2+ activation and H+-inhibited gating of the MthK K+ channel. *J Gen Physiol, 135*(5), 509-526. doi: 10.1085/jgp.200910387

Pau, V. P., Smith, F. J., Taylor, A. B., Parfenova, L. V., Samakai, E., Callaghan, M. M., Abarca-Heidemann, K., Hart, P. J., & Rothberg, B. S. (2011). Structure and function of multiple Ca2+-binding sites in a K+ channel regulator of K+ conductance (RCK) domain. *Proc Natl Acad Sci U S A, 108*(43), 17684-17689. doi: 10.1073/pnas.1107229108

Paul, K., Nieto, V., Carlquist, W. C., Blair, D. F., & Harshey, R. M. (2010). The c-di-GMP binding protein YcgR controls flagellar motor direction and speed to affect chemotaxis by a "backstop brake" mechanism. *Mol Cell, 38*(1), 128-139. doi: 10.1016/j.molcel.2010.03.001

Paul, R., Weiser, S., Amiot, N. C., Chan, C., Schirmer, T., Giese, B., & Jenal, U. (2004). Cell cycle-dependent dynamic localization of a bacterial response regulator with a novel di-guanylate cyclase output domain. *Genes & development, 18*(6), 715-727. doi: 10.1101/gad.289504

Pearson, W. L., Dourado, M., Schreiber, M., Salkoff, L., & Nichols, C. G. (1999). Expression of a functional Kir4 family inward rectifier K+ channel from a gene cloned from mouse liver. *J Physiol, 514 (Pt 3)*, 639-653. doi: 10.1111/j.1469-7793.1999.639ad.x

Peng, X., Zhang, Y., Bai, G., Zhou, X., & Wu, H. (2016). Cyclic di-AMP mediates biofilm formation. *Mol Microbiol, 99*(5), 945-959. doi: 10.1111/mmi.13277

Peterkofsky, A., & Gazdar, C. (1971). Glucose and the metabolism of adenosine 3':5'-cyclic monophosphate in *Escherichia coli*. *Proc Natl Acad Sci U S A, 68*(11), 2794-2798. doi: 10.1073/pnas.68.11.2794

Petersen, S., & Young, G. M. (2002). Essential Role for Cyclic AMP and Its Receptor Protein in *Yersinia enterocolitica* Virulence. *Infection and Immunity, 70*(7), 3665-3672. doi: 10.1128/iai.70.7.3665-3672.2002

Pham, H. T., Nhiep, N. T. H., Vu, T. N. M., Huynh, T. N., Zhu, Y., Huynh, A. L. D., Chakrabortti, A., Marcellin, E., Lo, R., Howard, C. B., Bansal, N., Woodward, J. J., Liang, Z. X., & Turner, M. S. (2018). Enhanced uptake of potassium or glycine betaine or export of cyclic-di-AMP restores osmoresistance in a high cyclic-di-AMP *Lactococcus lactis* mutant. *PLoS Genet, 14*(8), e1007574. doi: 10.1371/journal.pgen.1007574

Pietrobon, M., Zamparo, I., Maritan, M., Franchi, S. A., Pozzan, T., & Lodovichi, C. (2011). Interplay among cGMP, cAMP, and Ca2+ in Living Olfactory Sensory Neurons In Vitro and In Vivo. *The Journal of Neuroscience, 31*(23), 8395-8405. doi: 10.1523/jneurosci.6722-10.2011

Pittenger, C., Huang, Y. Y., Paletzki, R. F., Bourtchouladze, R., Scanlin, H., Vronskaya, S., & Kandel, E. R. (2002). Reversible inhibition of CREB/ATF transcription factors in region CA1 of the dorsal hippocampus disrupts hippocampus-dependent spatial memory. *Neuron, 34*(3), 447-462. doi: 10.1016/s0896-6273(02)00684-0

Pliotas, C., Grayer, S. C., Ekkerman, S., Chan, A. K. N., Healy, J., Marius, P., Bartlett, W., Khan, A., Cortopassi, W. A., Chandler, S. A., Rasmussen, T., Benesch, J. L. P., Paton, R. S., Claridge, T. D. W., Miller, S., Booth, I. R., Naismith, J. H., & Conway, S. J. (2017). Adenosine Monophosphate Binding Stabilizes the KTN Domain of the *Shewanella denitrificans* Kef Potassium Efflux System. *Biochemistry, 56*(32), 4219-4234. doi: 10.1021/acs.biochem.7b00300

Pongs, O., Kecskemethy, N., Muller, R., Krah-Jentgens, I., Baumann, A., Kiltz, H. H., Canal, I., Llamazares, S., & Ferrus, A. (1988). Shaker encodes a family of putative potassium channel proteins in the nervous system of *Drosophila*. *EMBO J, 7*(4), 1087-1096.

Posson, D. J., Rusinova, R., Andersen, O. S., & Nimigean, C. M. (2015a). Calcium ions open a selectivity filter gate during activation of the MthK potassium channel. *Nature communications, 6*, 8342-8342. doi: 10.1038/ncomms9342

Posson, D. J., Rusinova, R., Andersen, O. S., & Nimigean, C. M. (2015b). Calcium ions open a selectivity filter gate during activation of the MthK potassium channel. *Nature Communications, 6*(1), 8342. doi: 10.1038/ncomms9342

Posson, D. J., Rusinova, R., Andersen, O. S., & Nimigean, C. M. (2018). Stopped-Flow Fluorometric Ion Flux Assay for Ligand-Gated Ion Channel Studies. *Methods in molecular biology (Clifton, N.J.), 1684*, 223-235. doi: 10.1007/978-1-4939-7362-0_17

Price-Whelan, A., Poon, C. K., Benson, M. A., Eidem, T. T., Roux, C. M., Boyd, J. M., Dunman, P. M., Torres, V. J., & Krulwich, T. A. (2013). Transcriptional profiling of *Staphylococcus aureus* during growth in 2 M NaCl leads to clarification of physiological roles for Kdp and Ktr K+ uptake systems. *MBio, 4*(4). doi: 10.1128/mBio.00407-13

Prince, W. S., & Villarejo, M. R. (1990). Osmotic control of proU transcription is mediated through direct action of potassium glutamate on the transcription complex. *J Biol Chem, 265*(29), 17673-17679.

Prindle, A., Liu, J., Asally, M., Ly, S., Garcia-Ojalvo, J., & Suel, G. M. (2015). Ion channels enable electrical communication in bacterial communities. *Nature, 527*(7576), 59-63. doi: 10.1038/nature15709

Quintana, I., Espariz, M., Villar, S. R., González, F. B., Pacini, M. F., Cabrera, G., Bontempi, I., Prochetto, E., Stülke, J., Perez, A. R., Marcipar, I., Blancato, V., & Magni, C. (2018). Genetic Engineering of *Lactococcus lactis* Co-producing Antigen and the Mucosal Adjuvant 3' 5'- cyclic di Adenosine Monophosphate (c-di-AMP) as a Design Strategy to Develop a Mucosal Vaccine Prototype. *Front Microbiol, 9*, 2100. doi: 10.3389/fmicb.2018.02100

Quintana, I. M., Gibhardt, J., Turdiev, A., Hammer, E., Commichau, F. M., Lee, V. T., Magni, C., & Stülke, J. (2019). The KupA and KupB Proteins of *Lactococcus lactis* IL1403 Are Novel c-di-AMP Receptor Proteins Responsible for Potassium Uptake. *J Bacteriol, 201*(10). doi: 10.1128/jb.00028-19

Radchenko, M. V., Thornton, J., & Merrick, M. (2010). Control of AmtB-GlnK complex formation by intracellular levels of ATP, ADP, and 2-oxoglutarate. *J Biol Chem, 285*(40), 31037-31045. doi: 10.1074/jbc.M110.153908

Rall, T. W., & Sutherland, E. W. (1958). Formation of a cyclic adenine ribonucleotide by tissue particles. *J Biol Chem, 232*(2), 1065-1076.

Ranganathan, R., Lewis, J. H., & MacKinnon, R. (1996). Spatial localization of the K+ channel selectivity filter by mutant cycle-based structure analysis. *Neuron, 16*(1), 131-139. doi: 10.1016/s0896-6273(00)80030-6

Rapoport, R. M., & Murad, F. (1983). Agonist-induced endothelium-dependent relaxation in rat thoracic aorta may be mediated through cGMP. *Circulation Research, 52*(3), 352-357. doi: doi:10.1161/01.RES.52.3.352

Rhoads, D. B., Waters, F. B., & Epstein, W. (1976). Cation transport in *Escherichia coli*. VIII. Potassium transport mutants. *J Gen Physiol, 67*(3), 325-341. doi: 10.1085/jgp.67.3.325

Rickman, L., Scott, C., Hunt, D. M., Hutchinson, T., Menéndez, M. C., Whalan, R., Hinds, J., Colston, M. J., Green, J., & Buxton, R. S. (2005). A member of the cAMP receptor protein family of transcription regulators in *Mycobacterium tuberculosis* is required for virulence in mice and controls transcription of the rpfA gene coding for a resuscitation promoting factor. *Molecular Microbiology, 56*(5), 1274-1286. doi: 10.1111/j.1365-2958.2005.04609.x

Ringer, S. (1882a). Concerning the Influence exerted by each of the Constituents of the Blood on the Contraction of the Ventricle. *J Physiol, 3*(5-6), 380-393. doi: 10.1113/jphysiol.1882.sp000111

Ringer, S. (1882b). Regarding the Action of Hydrate of Soda, Hydrate of Ammonia, and Hydrate of Potash on the Ventricle of the Frog's Heart. *J Physiol, 3*(3-4), 195-202 196. doi: 10.1113/jphysiol.1882.sp000095

Ringer, S. (1883a). A further Contribution regarding the influence of the different Constituents of the Blood on the Contraction of the Heart. *J Physiol, 4*(1), 29-42 23. doi: 10.1113/jphysiol.1883.sp000120

Ringer, S. (1883b). A third contribution regarding the Influence of the Inorganic Constituents of the Blood on the Ventricular Contraction. *J Physiol, 4*(2-3), 222-225. doi: 10.1113/jphysiol.1883.sp000127

Robert, X., & Gouet, P. (2014). Deciphering key features in protein structures with the new ENDscript server. *Nucleic Acids Res, 42*(Web Server issue), W320-324. doi: 10.1093/nar/gku316

Rocha, R., Teixeira-Duarte, C. M., Jorge, J. M. P., & Morais-Cabral, J. H. (2019). Characterization of the molecular properties of KtrC, a second RCK domain that regulates a Ktr channel in *Bacillus subtilis*. *J Struct Biol, 205*(3), 34-43. doi: 10.1016/j.jsb.2019.02.002

Rodriguez-Navarro, A. (2000). Potassium transport in fungi and plants. *Biochim Biophys Acta, 1469*(1), 1-30. doi: 10.1016/s0304-4157(99)00013-1

Roosild, T. P., Castronovo, S., Healy, J., Miller, S., Pliotas, C., Rasmussen, T., Bartlett, W., Conway, S. J., & Booth, I. R. (2010). Mechanism of ligand-gated potassium efflux in bacterial pathogens. *Proc Natl Acad Sci U S A, 107*(46), 19784-19789. doi: 10.1073/pnas.1012716107

Roosild, T. P., Castronovo, S., Miller, S., Li, C., Rasmussen, T., Bartlett, W., Gunasekera, B., Choe, S., & Booth, I. R. (2009). KTN (RCK) domains regulate K+ channels and transporters by controlling the dimer-hinge conformation. *Structure, 17*(6), 893-903. doi: 10.1016/j.str.2009.03.018

Roosild, T. P., Miller, S., Booth, I. R., & Choe, S. (2002). A mechanism of regulating transmembrane potassium flux through a ligand-mediated conformational switch. *Cell, 109*(6), 781-791. doi: 10.1016/s0092-8674(02)00768-7

Ross, P., Weinhouse, H., Aloni, Y., Michaeli, D., Weinberger-Ohana, P., Mayer, R., Braun, S., de Vroom, E., van der Marel, G. A., van Boom, J. H., & Benziman, M. (1987). Regulation of cellulose synthesis in *Acetobacter xylinum* by cyclic diguanylic acid. *Nature, 325*(6101), 279-281. doi: 10.1038/325279a0

Rossmann, M. G., Moras, D., & Olsen, K. W. (1974). Chemical and biological evolution of nucleotide-binding protein. *Nature, 250*(463), 194-199. doi: 10.1038/250194a0

Rozov, A., Khusainov, I., El Omari, K., Duman, R., Mykhaylyk, V., Yusupov, M., Westhof, E., Wagner, A., & Yusupova, G. (2019). Importance of potassium ions for ribosome structure and function revealed by long-wavelength X-ray diffraction. *Nat Commun, 10*(1), 2519. doi: 10.1038/s41467-019-10409-4

Rubin, B. E., Huynh, T. N., Welkie, D. G., Diamond, S., Simkovsky, R., Pierce, E. C., Taton, A., Lowe, L. C., Lee, J. J., Rifkin, S. A., Woodward, J. J., & Golden, S. S. (2018). High-throughput interaction screens illuminate the role of c-di-AMP in cyanobacterial nighttime survival. *PLoS Genet, 14*(4), e1007301. doi: 10.1371/journal.pgen.1007301

Rusinova, R., Kim, D. M., Nimigean, C. M., & Andersen, O. S. (2014). Regulation of ion channel function by the host lipid bilayer examined by a stopped-flow spectrofluorometric assay. *Biophysical journal, 106*(5), 1070-1078. doi: 10.1016/j.bpj.2014.01.027

Russell, M. H., Bible, A. N., Fang, X., Gooding, J. R., Campagna, S. R., Gomelsky, M., & Alexandre, G. (2013). Integration of the Second Messenger c-di-GMP into the Chemotactic Signaling Pathway. *MBio, 4*(2), e00001-00013. doi: 10.1128/mBio.00001-13

Sambanthamoorthy, K., Sloup, R. E., Parashar, V., Smith, J. M., Kim, E. E., Semmelhack, M. F., Neiditch, M. B., & Waters, C. M. (2012). Identification of Small Molecules That Antagonize Diguanylate Cyclase Enzymes To Inhibit Biofilm Formation. *Antimicrobial Agents and Chemotherapy, 56*(10), 5202-5211. doi: 10.1128/aac.01396-12

Savage, C. R., Arnold, W. K., Gjevre-Nail, A., Koestler, B. J., Bruger, E. L., Barker, J. R., Waters, C. M., & Stevenson, B. (2015). Intracellular Concentrations of *Borrelia burgdorferi* Cyclic Di-AMP Are Not Changed by Altered Expression of the CdaA Synthase. *PLOS ONE, 10*(4), e0125440-e0125440. doi: 10.1371/journal.pone.0125440

Scheuermann, T. H., & Brautigam, C. A. (2015). High-precision, automated integration of multiple isothermal titration calorimetric thermograms: New features of NITPIC. *Methods, 76*, 87-98. doi: https://doi.org/10.1016/j.ymeth.2014.11.024

Schlosser, A., Kluttig, S., Hamann, A., & Bakker, E. P. (1991). Subcloning, nucleotide sequence, and expression of trkG, a gene that encodes an integral membrane protein involved in potassium uptake via the Trk system of *Escherichia coli*. *J Bacteriol, 173*(10), 3170-3176. doi: 10.1128/jb.173.10.3170-3176.1991

Schlosser, A., Meldorf, M., Stumpe, S., Bakker, E. P., & Epstein, W. (1995). TrkH and its homolog, TrkG, determine the specificity and kinetics of cation transport by the Trk system of *Escherichia coli*. *J Bacteriol, 177*(7), 1908-1910. doi: 10.1128/jb.177.7.1908-1910.1995

Schrempf, H., Schmidt, O., Kummerlen, R., Hinnah, S., Muller, D., Betzler, M., Steinkamp, T., & Wagner, R. (1995). A prokaryotic potassium ion channel with two predicted transmembrane segments from *Streptomyces lividans*. *EMBO J, 14*(21), 5170-5178.

Schultz, S. G., & Solomon, A. K. (1961). Cation transport in *Escherichia coli*. I. Intracellular Na and K concentrations and net cation movement. *J Gen Physiol, 45*, 355-369. doi: 10.1085/jgp.45.2.355

Schuster, C. F., Bellows, L. E., Tosi, T., Campeotto, I., Corrigan, R. M., Freemont, P., & Gründling, A. (2016). The second messenger c-di-AMP inhibits the osmolyte uptake system OpuC in *Staphylococcus aureus*. *Sci Signal, 9*(441), ra81. doi: 10.1126/scisignal.aaf7279

Schwartz, D. A., & Rubin, C. S. (1983). Regulation of cAMP-dependent protein kinase subunit levels in Friend erythroleukemic cells. Effects of differentiation and treatment with 8-Br-cAMP and methylisobutyl xanthine. *J Biol Chem, 258*(2), 777-784.

Sentenac, H., Bonneaud, N., Minet, M., Lacroute, F., Salmon, J. M., Gaymard, F., & Grignon, C. (1992). Cloning and expression in yeast of a plant potassium ion transport system. *Science, 256*(5057), 663-665. doi: 10.1126/science.1585180

Severin, G. B., Ramliden, M. S., Hawver, L. A., Wang, K., Pell, M. E., Kieninger, A. K., Khataokar, A., O'Hara, B. J., Behrmann, L. V., Neiditch, M. B., Benning, C., Waters, C. M., & Ng, W. L. (2018). Direct activation of a phospholipase by cyclic GMP-AMP in El Tor *Vibrio cholerae*. *Proc Natl Acad Sci U S A, 115*(26), E6048-E6055. doi: 10.1073/pnas.1801233115

Shioi, J. I., Matsuura, S., & Imae, Y. (1980). Quantitative measurements of proton motive force and motility in *Bacillus subtilis*. *J Bacteriol, 144*(3), 891-897.

Siemen, D., Loupatatzis, C., Borecky, J., Gulbins, E., & Lang, F. (1999). Ca2+-activated K channel of the BK-type in the inner mitochondrial membrane of a human glioma cell line. *Biochem Biophys Res Commun, 257*(2), 549-554. doi: 10.1006/bbrc.1999.0496

Simm, R., Morr, M., Kader, A., Nimtz, M., & Römling, U. (2004). GGDEF and EAL domains inversely regulate cyclic di-GMP levels and transition from sessility to motility. *Mol Microbiol, 53*(4), 1123-1134. doi: 10.1111/j.1365-2958.2004.04206.x

Slonczewski, J. L., Rosen, B. P., Alger, J. R., & Macnab, R. M. (1981). pH homeostasis in *Escherichia coli*: measurement by 31P nuclear magnetic resonance of methylphosphonate and phosphate. *Proc Natl Acad Sci U S A, 78*(10), 6271-6275. doi: 10.1073/pnas.78.10.6271

Smith, F. J., Pau, V. P., Cingolani, G., & Rothberg, B. S. (2012). Crystal structure of a Ba(2+)-bound gating ring reveals elementary steps in RCK domain activation. *Structure, 20*(12), 2038-2047. doi: 10.1016/j.str.2012.09.014

Smith, F. J., Pau, V. P., Cingolani, G., & Rothberg, B. S. (2013). Structural basis of allosteric interactions among Ca2+-binding sites in a K+ channel RCK domain. *Nat Commun, 4*, 2621. doi: 10.1038/ncomms3621

Smith, W. M., Pham, T. H., Lei, L., Dou, J., Soomro, A. H., Beatson, S. A., Dykes, G. A., & Turner, M. S. (2012). Heat resistance and salt hypersensitivity in *Lactococcus lactis* due to spontaneous mutation of llmg_1816 (gdpP) induced by high-temperature growth. *Applied and environmental microbiology, 78*(21), 7753-7759. doi: 10.1128/aem.02316-12

Stewart, L. M., Bakker, E. P., & Booth, I. R. (1985). Energy coupling to K+ uptake via the Trk system in *Escherichia coli*: the role of ATP. *J Gen Microbiol, 131*(1), 77-85. doi: 10.1099/00221287-131-1-77

Stone, T. W., & Taylor, D. A. (1977). Microiontophoretic studies of the effects of cylic nucleotides on excitability of neurones in the rat cerebral cortex. *The Journal of physiology, 266*(3), 523-543. doi: 10.1113/jphysiol.1977.sp011780

Su, J., Gong, H., Lai, J., Main, A., & Lu, S. (2009). The Potassium Transporter Trk and External Potassium Modulate *Salmonella enterica* Protein Secretion and Virulence. *Infection and Immunity, 77*(2), 667-675. doi: 10.1128/iai.01027-08

Su, Z., Brown, E. C., Wang, W., & MacKinnon, R. (2016). Novel cell-free high-throughput screening method for pharmacological tools targeting K+ channels. *Proc Natl Acad Sci U S A, 113*(20), 5748-5753. doi: 10.1073/pnas.1602815113

Suelter, C. H. (1970). Enzymes activated by monovalent cations. *Science, 168*(3933), 789-795. doi: 10.1126/science.168.3933.789

Sun, L., Wu, J., Du, F., Chen, X., & Chen, Z. J. (2013). Cyclic GMP-AMP Synthase Is a Cytosolic DNA Sensor That Activates the Type I Interferon Pathway. *Science, 339*(6121), 786-791. doi: 10.1126/science.1232458

Sureka, K., Choi, P. H., Precit, M., Delince, M., Pensinger, D. A., Huynh, T. N., Jurado, A. R., Goo, Y. A., Sadilek, M., Iavarone, A. T., Sauer, J. D., Tong, L., & Woodward, J. J. (2014). The cyclic dinucleotide c-di-AMP is an allosteric regulator of metabolic enzyme function. *Cell, 158*(6), 1389-1401. doi: 10.1016/j.cell.2014.07.046

Sutherland, E. W., & Rall, T. W. (1958). Fractionation and characterization of a cyclic adenine ribonucleotide formed by tissue particles. *J Biol Chem, 232*(2), 1077-1091.

Sutherland, L., Cairney, J., Elmore, M. J., Booth, I. R., & Higgins, C. F. (1986). Osmotic regulation of transcription: induction of the proU betaine transport gene is dependent on accumulation of intracellular potassium. *J Bacteriol, 168*(2), 805-814. doi: 10.1128/jb.168.2.805-814.1986

Szabo, I., Bock, J., Jekle, A., Soddemann, M., Adams, C., Lang, F., Zoratti, M., & Gulbins, E. (2005). A novel potassium channel in lymphocyte mitochondria. *J Biol Chem, 280*(13), 12790-12798. doi: 10.1074/jbc.M413548200

Szollosi, A., Vieira-Pires, R. S., Teixeira-Duarte, C. M., Rocha, R., & Morais-Cabral, J. H. (2016). Dissecting the Molecular Mechanism of Nucleotide-Dependent Activation of the KtrAB K+ Transporter. *PLoS Biol, 14*(1), e1002356. doi: 10.1371/journal.pbio.1002356

Tagliabue, L., Antoniani, D., Maciąg, A., Bocci, P., Raffaelli, N., & Landini, P. (2010). The diguanylate cyclase YddV controls production of the exopolysaccharide poly-N-acetylglucosamine (PNAG) through regulation of the PNAG biosynthetic pgaABCD operon. *Microbiology, 156*(Pt 10), 2901-2911. doi: 10.1099/mic.0.041350-0

Takeuchi, K., Takahashi, H., Kawano, S., & Shimada, I. (2007). Identification and characterization of the slowly exchanging pH-dependent conformational rearrangement in KcsA. *J Biol Chem, 282*(20), 15179-15186. doi: 10.1074/jbc.M608264200

Tal, R., Wong, H. C., Calhoon, R., Gelfand, D., Fear, A. L., Volman, G., Mayer, R., Ross, P., Amikam, D., Weinhouse, H., Cohen, A., Sapir, S., Ohana, P., & Benziman, M. (1998). Three cdg operons control cellular turnover of cyclic di-GMP in *Acetobacter xylinum*: genetic organization and occurrence of conserved domains in isoenzymes. *J Bacteriol, 180*(17), 4416-4425. doi: 10.1128/jb.180.17.4416-4425.1998

Tamura, K., Stecher, G., Peterson, D., Filipski, A., & Kumar, S. (2013). MEGA6: Molecular Evolutionary Genetics Analysis version 6.0. *Mol Biol Evol, 30*(12), 2725-2729. doi: 10.1093/molbev/mst197

Tang, Q., Luo, Y., Zheng, C., Yin, K., Ali, M. K., Li, X., & He, J. (2015). Functional Analysis of a c-di-AMP-specific Phosphodiesterase MsPDE from *Mycobacterium smegmatis*. *Int J Biol Sci, 11*(7), 813-824. doi: 10.7150/ijbs.11797

Tascón, I., Sousa, J. S., Corey, R. A., Mills, D. J., Griwatz, D., Aumüller, N., Mikusevic, V., Stansfeld, P. J., Vonck, J., & Hänelt, I. (2020). Structural basis of proton-coupled potassium transport in the KUP family. *Nature Communications, 11*(1), 626. doi: 10.1038/s41467-020-14441-7

Teixeira-Duarte, C. M., Fonseca, F., & Morais-Cabral, J. H. (2019). Activation of a nucleotide-dependent RCK domain requires binding of a cation cofactor to a conserved site. *Elife, 8*, e50661. doi: 10.7554/eLife.50661

Tempel, B. L., Jan, Y. N., & Jan, L. Y. (1988). Cloning of a probable potassium channel gene from mouse brain. *Nature, 332*(6167), 837-839. doi: 10.1038/332837a0

Tester, M., & Blatt, M. R. (1989). Direct measurement of k channels in thylakoid membranes by incorporation of vesicles into planar lipid bilayers. *Plant Physiol, 91*(1), 249-252. doi: 10.1104/pp.91.1.249

Tholema, N., Bakker, E. P., Suzuki, A., & Nakamura, T. (1999). Change to alanine of one out of four selectivity filter glycines in KtrB causes a two orders of magnitude decrease in the affinities for both K+ and Na+ of the Na+ dependent K+ uptake system KtrAB from *Vibrio alginolyticus*. *FEBS Lett, 450*(3), 217-220. doi: 10.1016/s0014-5793(99)00504-9

Tholema, N., Vor der Bruggen, M., Maser, P., Nakamura, T., Schroeder, J. I., Kobayashi, H., Uozumi, N., & Bakker, E. P. (2005). All four putative selectivity filter glycine residues in KtrB are essential for high affinity and selective K+ uptake by the KtrAB system from *Vibrio alginolyticus*. *J Biol Chem, 280*(50), 41146-41154. doi: 10.1074/jbc.M507647200

Thompson, A. N., Posson, D. J., Parsa, P. V., & Nimigean, C. M. (2008). Molecular mechanism of pH sensing in KcsA potassium channels. *Proc Natl Acad Sci U S A, 105*(19), 6900-6905. doi: 10.1073/pnas.0800873105

Tischler, A. D., & Camilli, A. (2004). Cyclic diguanylate (c-di-GMP) regulates *Vibrio cholerae* biofilm formation. *Mol Microbiol, 53*(3), 857-869. doi: 10.1111/j.1365-2958.2004.04155.x

Tischler, A. D., & Camilli, A. (2005). Cyclic diguanylate regulates *Vibrio cholerae* virulence gene expression. *Infect Immun, 73*(9), 5873-5882. doi: 10.1128/iai.73.9.5873-5882.2005

Torgersen, K. M., Vang, T., Abrahamsen, H., Yaqub, S., & Tasken, K. (2002). Molecular mechanisms for protein kinase A-mediated modulation of immune function. *Cell Signal, 14*(1), 1-9. doi: 10.1016/s0898-6568(01)00214-5

Vieira-Pires, R. S., Szollosi, A., & Morais-Cabral, J. H. (2013). The structure of the KtrAB potassium transporter. *Nature, 496*(7445), 323-328. doi: 10.1038/nature12055

Vlamakis, H., Aguilar, C., Losick, R., & Kolter, R. (2008). Control of cell fate by the formation of an architecturally complex bacterial community. *Genes Dev, 22*(7), 945-953. doi: 10.1101/gad.1645008

Voet, D., Voet, J. G., & Pratt, C. W. (2006). *Fundamentals of Biochemistry: Life at the molecular level* (Second Edition ed.): Wiley.

Volckmar, J., Knop, L., Stegemann-Koniszewski, S., Schulze, K., Ebensen, T., Guzmán, C. A., & Bruder, D. (2019). The STING activator c-di-AMP exerts superior adjuvant properties than the formulation poly(I:C)/CpG after subcutaneous vaccination with soluble protein antigen or DEC-205-mediated antigen targeting to dendritic cells. *Vaccine, 37*(35), 4963-4974. doi: 10.1016/j.vaccine.2019.07.019

Walsh, D. A., Perkins, J. P., & Krebs, E. G. (1968). An adenosine 3',5'-monophosphate-dependant protein kinase from rabbit skeletal muscle. *J Biol Chem, 243*(13), 3763-3765.

Whatmore, A. M., Chudek, J. A., & Reed, R. H. (1990). The effects of osmotic upshock on the intracellular solute pools of *Bacillus subtilis*. *J Gen Microbiol, 136*(12), 2527-2535. doi: 10.1099/00221287-136-12-2527

Whatmore, A. M., & Reed, R. H. (1990). Determination of turgor pressure in *Bacillus subtilis*: a possible role for K+ in turgor regulation. *J Gen Microbiol, 136*(12), 2521-2526. doi: 10.1099/00221287-136-12-2521

Whiteley, A. T., Eaglesham, J. B., de Oliveira Mann, C. C., Morehouse, B. R., Lowey, B., Nieminen, E. A., Danilchanka, O., King, D. S., Lee, A. S. Y., Mekalanos, J. J., & Kranzusch, P. J. (2019). Bacterial cGAS-like enzymes synthesize diverse nucleotide signals. *Nature, 567*(7747), 194-199. doi: 10.1038/s41586-019-0953-5

Whiteley, A. T., Garelis, N. E., Peterson, B. N., Choi, P. H., Tong, L., Woodward, J. J., & Portnoy, D. A. (2017). c-di-AMP modulates *Listeria monocytogenes* central metabolism to regulate growth, antibiotic resistance and osmoregulation. *Mol Microbiol, 104*(2), 212-233. doi: 10.1111/mmi.13622

Wiedenmann, A., Dimroth, P., & von Ballmoos, C. (2008). Δψ and ΔpH are equivalent driving forces for proton transport through isolated F0 complexes of ATP synthases. *Biochimica et Biophysica Acta (BBA) - Bioenergetics, 1777*(10), 1301-1310. doi: https://doi.org/10.1016/j.bbabio.2008.06.008

Winn, M. D., Ballard, C. C., Cowtan, K. D., Dodson, E. J., Emsley, P., Evans, P. R., Keegan, R. M., Krissinel, E. B., Leslie, A. G., McCoy, A., McNicholas, S. J., Murshudov, G. N., Pannu, N. S., Potterton, E. A., Powell, H. R., Read, R. J., Vagin, A., & Wilson, K. S. (2011). Overview of the CCP4 suite and current developments. *Acta Crystallogr D Biol Crystallogr, 67*(Pt 4), 235-242. doi: 10.1107/S0907444910045749

Withers, D. J., Bloom, S. R., & Rozengurt, E. (1995). Dissociation of cAMP-stimulated mitogenesis from activation of the mitogen-activated protein kinase cascade in Swiss 3T3 cells. *J Biol Chem, 270*(36), 21411-21419. doi: 10.1074/jbc.270.36.21411

Witte, C. E., Whiteley, A. T., Burke, T. P., Sauer, J.-D., Portnoy, D. A., & Woodward, J. J. (2013). Cyclic di-AMP Is Critical for *Listeria monocytogenes* Growth, Cell Wall Homeostasis, and Establishment of Infection. *MBio, 4*(3), e00282-00213. doi: 10.1128/mBio.00282-13

Witte, G., Hartung, S., Büttner, K., & Hopfner, K.-P. (2008). Structural Biochemistry of a Bacterial Checkpoint Protein Reveals Diadenylate Cyclase Activity Regulated by DNA Recombination Intermediates. *Molecular Cell, 30*(2), 167-178. doi: 10.1016/j.molcel.2008.02.020

Woodward, J. J., Iavarone, A. T., & Portnoy, D. A. (2010). c-di-AMP secreted by intracellular *Listeria monocytogenes* activates a host type I interferon response. *Science, 328*(5986), 1703-1705. doi: 10.1126/science.1189801

Wu, Y., Yang, Y., Ye, S., & Jiang, Y. (2010). Structure of the gating ring from the human large-conductance Ca(2+)-gated K(+) channel. *Nature, 466*(7304), 393-397. doi: 10.1038/nature09252

Xia, P., Wang, S., Xiong, Z., Zhu, X., Ye, B., Du, Y., Meng, S., Qu, Y., Liu, J., Gao, G., Tian, Y., & Fan, Z. (2018). The ER membrane adaptor ERAdP senses the bacterial second messenger c-di-AMP and initiates anti-bacterial immunity. *Nat Immunol, 19*(2), 141-150. doi: 10.1038/s41590-017-0014-x

Yang, J., Bai, Y., Zhang, Y., Gabrielle, V. D., Jin, L., & Bai, G. (2014). Deletion of the cyclic di-AMP phosphodiesterase gene (cnpB) in *Mycobacterium tuberculosis* leads to reduced virulence in a mouse model of infection. *Mol Microbiol, 93*(1), 65-79. doi: 10.1111/mmi.12641

Ye, M., Zhang, J. J., Fang, X., Lawlis, G. B., Troxell, B., Zhou, Y., Gomelsky, M., Lou, Y., & Yang, X. F. (2014). DhhP, a cyclic di-AMP phosphodiesterase of *Borrelia burgdorferi*, is essential for cell growth and virulence. *Infect Immun, 82*(5), 1840-1849. doi: 10.1128/iai.00030-14

Ye, S., Li, Y., Chen, L., & Jiang, Y. (2006). Crystal structures of a ligand-free MthK gating ring: insights into the ligand gating mechanism of K+ channels. *Cell, 126*(6), 1161-1173. doi: 10.1016/j.cell.2006.08.029

Ye, S., Li, Y., & Jiang, Y. (2010). Novel insights into K+ selectivity from high-resolution structures of an open K+ channel pore. *Nature Structural & Molecular Biology, 17*(8), 1019-1023. doi: 10.1038/nsmb.1865

Yellen, G., Jurman, M., Abramson, T., & MacKinnon, R. (1991). Mutations affecting internal TEA blockade identify the probable pore-forming region of a K+ channel. *Science, 251*(4996), 939-942. doi: 10.1126/science.2000494

Yuan, P., Leonetti, M. D., Pico, A. R., Hsiung, Y., & MacKinnon, R. (2010). Structure of the human BK channel Ca2+-activation apparatus at 3.0 A resolution. *Science, 329*(5988), 182-186. doi: 10.1126/science.1190414

Zadek, B., & Nimigean, C. M. (2006). Calcium-dependent gating of MthK, a prokaryotic potassium channel. *J Gen Physiol, 127*(6), 673-685. doi: 10.1085/jgp.200609534

Zagotta, W., Hoshi, T., & Aldrich, R. (1990). Restoration of inactivation in mutants of Shaker potassium channels by a peptide derived from ShB. *Science, 250*(4980), 568-571. doi: 10.1126/science.2122520

Zarrella, T. M., Yang, J., Metzger, D. W., & Bai, G. (2020). Bacterial Second Messenger Cyclic di-AMP Modulates the Competence State in *Streptococcus pneumoniae*. *J Bacteriol, 202*(4). doi: 10.1128/jb.00691-19

Zhang, H., Pan, Y., Hu, L., Hudson, M. A., Hofstetter, K. S., Xu, Z., Rong, M., Wang, Z., Prasad, B. V. V., Lockless, S. W., Chiu, W., & Zhou, M. (2020). TrkA undergoes a tetramer-to-dimer conversion to open TrkH which enables changes in membrane potential. *Nat Commun, 11*(1), 547. doi: 10.1038/s41467-019-14240-9

Zhang, L., & He, Z.-G. (2013). Radiation-sensitive gene A (RadA) targets DisA, DNA integrity scanning protein A, to negatively affect cyclic Di-AMP synthesis activity in *Mycobacterium smegmatis*. *The Journal of biological chemistry, 288*(31), 22426-22436. doi: 10.1074/jbc.M113.464883

Zhang, L., Li, W., & He, Z.-G. (2013). DarR, a TetR-like transcriptional factor, is a cyclic di-AMP-responsive repressor in *Mycobacterium smegmatis*. *The Journal of biological chemistry, 288*(5), 3085-3096. doi: 10.1074/jbc.M112.428110

Zhao, H., Piszczek, G., & Schuck, P. (2015). SEDPHAT--a platform for global ITC analysis and global multi-method analysis of molecular interactions. *Methods (San Diego, Calif.), 76*, 137-148. doi: 10.1016/j.ymeth.2014.11.012

Zheng, C., Ma, Y., Wang, X., Xie, Y., Ali, M. K., & He, J. (2015). Functional analysis of the sporulation-specific diadenylate cyclase CdaS in *Bacillus thuringiensis*. *Front Microbiol, 6*, 908. doi: 10.3389/fmicb.2015.00908

Zheng, H., Chruszcz, M., Lasota, P., Lebioda, L., & Minor, W. (2008). Data mining of metal ion environments present in protein structures. *J Inorg Biochem, 102*(9), 1765-1776. doi: 10.1016/j.jinorgbio.2008.05.006

Zhou, J., Sayre, D. A., Zheng, Y., Szmacinski, H., & Sintim, H. O. (2014). Unexpected Complex Formation between Coralyne and Cyclic Diadenosine Monophosphate Providing a Simple Fluorescent Turn-on Assay to Detect This Bacterial Second Messenger. *Analytical Chemistry, 86*(5), 2412-2420. doi: 10.1021/ac403203x

Zhou, X. L., Vaillant, B., Loukin, S. H., Kung, C., & Saimi, Y. (1995). YKC1 encodes the depolarization-activated K+ channel in the plasma membrane of yeast. *FEBS Lett, 373*(2), 170-176. doi: 10.1016/0014-5793(95)01035-d

Zhou, Y., Morais-Cabral, J. H., Kaufman, A., & MacKinnon, R. (2001). Chemistry of ion coordination and hydration revealed by a K+ channel-Fab complex at 2.0 A resolution. *Nature, 414*(6859), 43-48. doi: 10.1038/35102009

Zhu, Y., Pham, T. H., Nhiep, T. H. N., Vu, N. M. T., Marcellin, E., Chakrabortti, A., Wang, Y., Waanders, J., Lo, R., Huston, W. M., Bansal, N., Nielsen, L. K., Liang, Z.-X., & Turner, M. S. (2016). Cyclic-di-AMP synthesis by the diadenylate cyclase CdaA is modulated by the peptidoglycan biosynthesis enzyme GlmM in *Lactococcus lactis*. *Molecular Microbiology, 99*(6), 1015-1027. doi: 10.1111/mmi.13281

Zulkifli, L., Akai, M., Yoshikawa, A., Shimojima, M., Ohta, H., Guy, H. R., & Uozumi, N. (2010). The KtrA and KtrE subunits are required for Na+-dependent K+ uptake by KtrB across the plasma membrane in *Synechocystis* sp. strain PCC 6803. *J Bacteriol, 192*(19), 5063-5070. doi: 10.1128/jb.00569-10